Dissipative anchor devices for the seismic retrofit of heritage buildings

Paganoni, Sara

Award date:
2016

Awarding institution:
University of Bath

DISSIPATIVE ANCHOR DEVICES FOR THE SEISMIC RETROFIT OF HERITAGE BUILDINGS

Volume 1 of 1

Sara Paganoni

A thesis submitted for the degree of Doctor of Philosophy

University of Bath

Department of Architecture and Civil Engineering

September 2015

TABLE OF CONTENTS

TABLE OF FIGURES

TABLE OF TABLES

ACKNOWLEDGEMENTS

I acknowledge my supervisors Dr. D'Ayala, for her precious guidance and sharp technical insight, which have so much contributed to the development of this research project and Mr. Wilson Jones, for looking after the final stages of the writing up process.

I also wish to acknowledge Cintec International Ltd. for being a long term, reliable partner and for their continuous technical and commercial feedback.

Finally, I acknowledge the KTP and FP7-NIKER projects, which were not only my main sources of funding, but also two inspirational environments that nurtured and challenged me as a researcher.

ABSTRACT

In the last decades, considerable improvements have been achieved in the seismic design of buildings thanks to the implementation of concepts such as ductility and energy dissipation. Consequently, new structures are not only able to perform better during seismic events, but are also more efficient in terms of balance between life safety and costs.

Conversely, historic centres are still considerably affected by earthquakes. To understand the extent of seismic-related damage in historic centres, it may suffice to think that the ICOMOS World Report 2008-2010 on Monuments and Sites in Danger reports no less than five earthquakes, Chile 2010, Sichuan 2008, Haiti 2010, L'Aquila 2009 and Christchurch 2010, all of which impacted and endangered heritage buildings and assets.

The lack of good quality connections among structural elements greatly affects the dynamic performance of heritage masonry structures and is the cause of out-of-plane failures of masonry panels, which are most frequently recurring, most dangerous in terms of human lives and most damaging from the point of view of conservation.

Although it is recognised that the strengthening of connections is of capital importance for damage reduction and prevention, ad-hoc solutions are missing from the technical literature. Furthermore, design codes are vague when it comes to define the assessment and design procedures to be followed when implementing innovative strengthening system in historic structures.

This dissertation aims to tackle such technical gaps by developing a new strengthening system and compiling a draft protocol for its validation and design.

Two typologies of dissipative devices are designed to address the out-of-plane mechanisms of wall panels and limit cracking in the historic substratum, in accordance with both the principles of multilevel performance design and of the preservation of historic assets. The prototypes are validated through experimental assessment, on-site application to a case study and computational modelling. The recurring structural features and issues surveyed in the aftermaths of major seismic events feed into the validation process; the weakness of historic structural connections, the characteristics of original materials, traditional construction techniques as much as current practice are all taken in due consideration.

Throughout the validation process, great importance is given to the relevance of experimental and computational results to the task of creating a systematic process, which can provide guidance to those facing the challenge of creating and implementing innovative structural solutions through a broad variety of methodologies.

The research project contributes to the collection of quantitative data and, even more importantly, it amounts to a first step towards the development of validation and

design procedures. These, although not exhaustive of the broad variety of scenarios typical of heritage structures, constitute the basis for further developments and research challenges, as highlighted in the conclusions.

Ultimately the thesis aims to address the missing link between research, market and practice. In spite of the peculiarities and limits of each case, research should indeed strive to provide targeted, yet flexible solutions that end users will be able to apply in compliance with the requirements of current codes.

"[..] tremit vibratque. Hiatus vero alias remanet ostendens quae sorbuit, alias occultat ore conpresso rursusque ita inducto solo, ut nulla vestigia exstent, urbibus plerumque devoratis agrorumque tractu hausto [..]"

"(The earth) quivers and shakes. The crack sometimes remains wide open, showing what it has swallowed, sometimes hides everything, shutting its mouth and covering everything with ground, so that no trace is left: whole cities are often buried and countries swallowed. [..]"

Pliny the Elder, On Opinions and Causes of Earthquakes,

Natural History – Naturalis Historia (77 A.D.)

1 INTRODUCTION

1.1 THE PRESERVATION OF HISTORIC STRUCTURES IN SEISMIC PRONE AREAS

The Oxford dictionary defines heritage as “Property that is or may be inherited; an inheritance”, although the terms has also come to mean: “Valued objects and qualities, such as historic buildings and cultural traditions, that have been passed down from previous generations” and “[…] denoting or relating to things of special architectural, historical, or natural value that are preserved for the nation”.

The word heritage indicates an entity, for instance a building, as valuable as an inheritance, valuable to the point that a nation, or the whole humankind, wishes to preserve it and hand it over to the future generations.

However, the preservation of heritage buildings is no easy task, as many hazards endanger their survival: pollution, traffic, atmospheric agents and natural disasters - only to name a few. While some of these phenomena occur over time and can be tackled before their effects become irreversible, others, like earthquakes, have a highly destructive power and can reduce buildings to ruins within fractions of a minute.

Therefore, the careful implementation of prevention measures such as structural repair and upgrading are the current means whereby the risk of heritage loss can be reduced. However, seismic protection is a work in progress, far from being successfully completed. Suffice it to mention the emblematic case of the seismic sequence of the 2010 Darfield and 2011 Christchurch earthquakes in New Zealand: in a country that rightly prides itself for its seismic design codes and preparedness, a large majority of heritage buildings were damaged beyond repair.

The continuous research of safer, more efficient structural solutions for the prevention of seismic-related damage and protection of human lives is a hot topic, a priority point in the agenda of heritage preservation.

This thesis offers a contribution in such sense; in the specific, it tries to address the existing gap between new built and existing structures. Why are the improvements obtained with new structures so slow to follow in the field of retrofit, especially for historic structures? What are the specific requirements of heritage buildings? Can these be met by a strengthening system that is at the same time readily implemented and reliable?

These are the questions that gave the impetus to the research described in the following pages.

1.2 OBJECTIVES OF RESEARCH

The research aims in the first instance to address the paucity of performance-based strengthening systems for the seismic protection of heritage structures. Accordingly, it focuses on the development of a set of devices that match specific requirements, such as: reduction of seismic-related damage, control of displacement and acceleration,

increase of ductility and energy dissipation in the structural system, but also reduction of the intervention intrusiveness, optimisation of materials and structural elements. At the same time, site and financial constraints, as much as ease of use and installation are taken into account.

Emphasis is given not only to the devices as final products, but to the whole proof concept, namely the procedure that covers the development of the strengthening system, including its validation and writing up of implementation guidelines.

The development process is carried out through a number of stages involving, in a first phase, a typical prototyping process; an initial concept is developed through design and testing into one or more physical objects, in compliance with a set of requirements. In a second phase, the prototypes are further tested through experimental campaigns, numerical simulations and a pilot implementation to verify their field of applicability, reliability, and need for further development. Throughout this process, a constant concern has been to adhere as much as possible to the current performance based design framework, so that the prototypes are in line with current seismic design standards and practices.

In pursuing this approach, it has become apparent that the current gap between new-built and heritage structures has also much to do with the lack of operative design guidelines: prescriptions and recommendations for historic structures are mainly qualitative and offer little support to end users wishing to look for alternatives to well-established systems. Therefore, the second main objective of the thesis is to show how the characterisation of a strengthening system can be implemented in an analytical process so as to link new results, code prescriptions and technical literature.

The process is conceived as a flexible, open flow chart, which can be enlarged through further testing, different case studies and a larger sample of analysed buildings; in spite of the specific features that characterise the dissipative devices described herein, it aspires to provide a first example towards the development of more efficient structural solutions and more comprehensive design codes.

1.3 CONTENT OF THE THESIS

Besides this first introductory chapter, the thesis consists of six chapters, plus a chapter of conclusions and suggestions for further work, and a bibliography.

Chapter 2 introduces the rationale of the research. Having established the need for an innovative product that can tackle the issues typical of historic structures and current strengthening techniques, the chapter reviews advantages and limitations of existing strengthening devices as reported in literature, how these are currently assessed and what types of requirements should control the development of new products and rule their design.

In light of this review, Chapter 3 defines the framework of the research project. Two prototypes are described, discussing the reasons for the technical choices made during

the concept design phases. The chapter also outlines the validation process that is detailed point by point in the following three chapters.

Chapter 4 overviews the experimental part the of the validation process, namely the campaigns carried out on the isolated devices, as well as on a number of masonry specimens where the devices were embedded. Tests allow for the characterisation of the structural behaviour depending on the sample layout, geometry and material properties, and are a first means to create a set of analytical models for predicting the performance of the devices.

After gaining insight into the response of the prototypes to a range of inputs, one device is instrumented and installed in an earthquake-damaged structure, so as to be able to observe additional phenomena that might have not been included in the experimental campaign and yet might affect the anchor performance. Chapter 5 compares the records taken during on site validation with previous results, critically analysing the performance of the prototype in a realistic, complex environment.

Drawing on laboratory and site evidence, a set of numerical models is developed, as described in Chapter 6. Finite Element models are calibrated on the basis of previous output, searching for a compromise between simplification and accurateness; in the process, the definition of the main parameters controlling the behaviour of the devices is checked and refined.

The outcome of Chapters 4, 5 and 5 feeds into the development of the design procedure presented in Chapter 7, which exemplifies how the gathered results can inform the design, sizing and checks of the whole strengthening intervention, how they can be benchmarked against code requirements and be complemented through other sources. The methodology is summarised through tables and flow charts, thus providing a systematic example for further developments.

The main achievements, further challenges and possible improvements of the research conclude the thesis.

2 RESEARCH RATIONALE AND BACKGROUND

2.1 ROLE AND DAMAGE OF STRUCTURAL CONNECTIONS IN HERITAGE STRUCTURES UNDERGOING SEISMIC EVENTS

The global response of a structure to earthquakes is influenced by the performance of each structural component as well by their relative interactions, which are determined by the typology and quality of structural connections.

The importance of connections with respect to buildings' seismic behaviour has been long acknowledged. Indeed, Eurocode 8 (EN 1998:2005-1) states that: "Floor systems and the roof should be provided with in-plane stiffness and resistance and with effective connection to the vertical structural systems". This rule is also applicable to interventions on existing structures (EN 1998:2005-1): "The connection between the floors and walls shall be provided by steel ties or reinforced concrete ring beams" and specifically to masonry: "Non-ductile lintels should be replaced, inadequate connections between floor and walls should be improved, out-of-plane horizontal thrusts against walls should be eliminated".

Code prescriptions are motivated by the fact that well-connected bearing walls ensure the box-like behaviour of masonry structures, so that rather than detaching one from the others, walls transmit horizontal loads thus ensuring that seismic forces are distributed among structural members according to their relative stiffness (Tomaževič, 1999). As this is hardly the case in historic buildings, structural connections have become the object of studies aiming to determine their influence on the type and extent of earthquake- induced damage.

D'Ayala and Speranza (2003) developed an analytical model by means of an extensive database of on-site observations collected in the aftermath of main seismic events. The model is able to identify likely damage mechanisms as consequence of building geometry, materials and connections. Indeed, the poor quality of connections between walls or part of them determines the partial or total overturning of the façade, which is recurrently observed in heritage buildings. Conversely, when well-built quoins are present, the façade doesn't behave as a free-standing masonry wall, and overturning involves part of the side walls, also depending on the quality of the masonry and on the layout of openings and perpendicular load-bearing walls.

The analytical model developed by de Felice and Giannini (2001) can also predict both these out-of-plane mechanisms – simple overturning of facade or out-of-plane involving side walls – through a limit approach that considers wall geometry and connections to surrounding elements.

Arch mechanisms are observed in presence of steel cross ties located at the top and along the sides of a façade and causing the masonry panel to respond to horizontal forces as a plate (D'Ayala and Paganoni, 2011). Continuous and efficient connections prevent out-of-plane mechanisms, so that the shear capacity of the masonry is activated instead and in-plane damage takes place (D'Ayala and Paganoni, 2011).

Giuffrè (1993) distinguishes overturning mechanisms, the so called first mode mechanism, from in-plane – second mode – mechanisms; the boundary conditions determining the occurrence of the first rather than the latter are similar to those mentioned by D'Ayala and Speranza (2003). Giuffrè's limit model for the calculation of damage mechanism has been applied by Valluzzi et al. (2004) to the study of vulnerability of historic centres. The method is based on the equilibrium analysis of kinematic mechanisms of macroelements, which are identified by looking, among the others, at the typology and quality of connections between structural elements. Such methodology leads to better results in respect to modelling techniques that do not acknowledge the importance of effective connections and the frequent lack thereof, such for instance models that assume a box-like behaviour of buildings.

Similarly to residential buildings and palaces, the seismic response of religious buildings is also influenced by connections. The outward movement and eventually overturning of the front façade of churches, which is a common damage mechanism (Doglioni et alt., 1994), is caused by a number of factors: the high mass of decorative elements, the lack of connection to horizontal structures at floor levels, which are missing from the typical church layout, and the poor connection with side walls. The latter might be due to previous collapses and reconstructions, but also to changes and substitutions for the purpose of adjusting the building appearance to the dominant architectural style.

Even in the case of religious buildings, mechanical models are able to predict satisfactorily the modes of damage (da Porto et al., 2012), so that, not only the importance of structural connections of historic buildings has been ascertained, but the consequences of their lack or poor quality can be foreseen and quantified. However, while it is common practice to strengthen single structural elements in order to achieve a better overall structural performance, not as much work has been carried out specifically on the strengthening of connections in historic buildings. This is an existing technical gap that this dissertation aims at tackling.

The development of adequate strengthening techniques for structural connections of heritage buildings in seismic-prone areas faces the main challenge of the choice of an adequate design philosophy/methodology. The last decades have been characterised by a shift in the principles guiding seismic design, yet the transition between new and old approach in the field of heritage structures has not been clear-cut and an array of different methodologies is being currently used.

As seismic events have highlighted pros and cons of existing retrofit systems that were applied in historic building through the years, it is becoming progressively clearer which systems offer the best results and what issues still need addressing. Nevertheless, the task of collecting and interpreting such know-how and translating it into a viable concept design is not trivial, this being the reason for innovative techniques being applied less than in the case of new structures. A newly developed strengthening technique must not only feature the positive aspects of current strengthening systems and address the existing pitfalls, but it also needs to comply

with current design codes, it has to be in line with the latest engineering concepts and findings and, last but not least, must meet the set of stringent requirements typical of conservation engineering.

The main reference when dealing with historic buildings are the ICOMOS' Venice Charter (1964) and, more recently, the ICOMOS/ISCARSAH Recommendations for the Analysis and Restoration of Architectural Heritage (ICOMOS/ISCARSAH, 2005) and the Annex on Heritage Structures of the latest ISO Standard on the assessment of existing structures (ISO/TC 98/SC2, 2010). These documents list a set of main requirements for interventions on heritage structures, such as:

1. Respect for structural authenticity. The restoration of monuments must focus on preserving the original features of the structure, causing as little alteration as possible. This not only applies to geometry and materials, but also to the structural response and governing mechanisms;
2. Structural reliability. Human safety is of capital importance and heritage structures are no exceptions, although it should also be remembered that in case of seismic loading, the attainment of the same performance level as a new structure is not required if this entails heavy interventions, which cannot comply with the other requirements in the list (DPCM 2011);
3. Minimal intervention. ISO/TC 98/SC2 (2010) defines a minimal intervention as "an intervention that balances the safety requirements with the protection of character-defining elements, ensuring the least harm to heritage values";
4. Compatibility. The ICOMOS/ISCARSAH Recommendations (2005) state that "The characteristics of materials used in restoration work and their compatibility with existing materials should be fully established. In any case, it has to be clear that compatibility is a necessary but not sufficient condition to accept a product, because its benefit has to be demonstrated. This must include long-term effects, so that undesirable side effects are avoided".
5. Non-intrusiveness. "[..] the choice between "traditional" and "innovative" techniques should be determined on a case-by-case basis with preference given to those that are least invasive and most compatible with heritage values, consistent with the need for safety and durability" (ICOMOS/ISCARSAH, 2005).
6. Non-obtrusiveness: Obtrusiveness refers to the quality of being undesirably noticeable. The Venice Charter (1964) states that "replacements of missing parts must integrate harmoniously with the whole, but at the same time must be distinguishable from the original so that restoration does not falsify the artistic or historic evidence. Additions cannot be allowed except in so far as they do not detract from the interesting parts of the building, its traditional setting, the balance of its composition and its relation with its surroundings".
7. Durability and reversibility.
8. Ease of monitoring, control and maintenance.

All considerations and requirements outlined above must translate into a set of design parameters that feed into the concept design of the strengthening system, are used as benchmark in the validation process and finally inform the structural design in case of implementation. The in-depth study of the state of the art is an important step in the process of identification and collection of these parameters.

2.2 FROM CAPACITY-BASED TO PERFORMANCE-BASED DESIGN: THE SHIFT OF PHILOSOPHY IN STRUCTURAL DESIGN

Presently, seismic engineering pursues the protection of structures through a variety of solutions, which can be classified depending on the principle that underlies their design and function.

A first category includes techniques that are based on the increase of structural capacity, i.e. the improvement of strength and the limitation of deformation for the purpose of enhancing the structural performance. Such approach was typical of early seismic design codes; in the following paragraphs, the Italian seismic code is taken as example, as Italy is not only a seismic-prone country, but it has also a large number of heritage buildings and sites, making it a representative case in the study of the seismic protection of historic structures.

Early codes dating back to the period between 1960 and 1980 (e.g. Legge 64/74) only require the design to be carried out for large magnitude earthquakes (i.e. for what today would be considered the Ultimate Limit State) according to the admissible tension method and by studying the response of an elastic system equivalent to the building in analysis. The ductile resources of the structural system are neither accounted for nor exploited.

This approach, although valid for static problems, is not always viable for seismic applications, partly because of the high margin of the uncertainties inherent to the nature of earthquakes, partly because of limitations such as materials properties and costs of realisation (Miller, 1998; Wen, 2001).

For this reason, other strengthening techniques have been developed drawing on the energy balance equation, which states that the seismic demand energy, E_{SD}, is equal to the sum of elastic energy, E_E, and total energy dissipated by the structures, E_D (Aiken et al., 1993; Castellano et al., 2001; Symans et al., 2008):

2-1) $$E_{SD} = E_E + E_D = (E_S+E_K) + (E_\mu+E_\xi)$$

where:

E_S is the recoverable strain energy stored in the structure
E_K is the kinetic energy of the moving mass
E_μ is the unrecoverable energy dissipated hysteretically
E_ξ is the viscous damping energy.

Traditional and conventional strengthening techniques, as much as early design codes, satisfy the balance expressed in Eq. (2-1) by increasing the elastic energy, E_E. Alternatively, the seismic demand E_{SD} can be reduced or the dissipated energy E_D can be increased. The reduction of seismic demand is obtained limiting the energy input into the structure through seismic isolation techniques, while energy dissipation can be pursued either enhancing the ductility of the structure itself or by additional dissipative devices (Constantinou et al., 1998; Symans et al., 2008).

Accordingly, E_μ and E_ξ can be written in the form:

2-2) $$E_\mu = E_{\mu,Structure} + E_{\mu,Devices}$$

2-3) $$E_\xi = E_{\xi,Structure} + E_{\xi,Devices}$$

In Eq. (2-2) $E_{\mu,Structure}$ represents the part of hysteretic energy dissipated by main structural elements while $E_{\mu,Devices}$ is dissipated by added energy devices. In Eq. (2-3) the viscous damping energy is divided into inherent damping of the structural materials, $E_{\xi,Structure}$, and damping provided by specific additional devices, $E_{\xi,Devices}$.

Seismic isolation and additional damping are relatively innovative techniques: their methodical development and use in contemporary times started approximately two decades ago, after earthquakes such as Kobe, Japan, 1995, highlighted the unreliability of highly stiff structures and shifted engineers' attention towards ductility-based design methods (Bruneau, 1996; Chandler and Lam, 2001; Peng et al., 2005, Robinson, 1982).

In line with this shift in design philosophy, the second generation seismic codes in Italy (CNR-GNDT, 1984; P.C.M., 2003) are characterised by the use of the semi-probabilistic method of the Limit States. Two performance levels, i.e. Service (SLS) and Ultimate Limit State (ULS), corresponding to seismic events with a returning period of 95 and 475 years respectively, must be considered. Although a strength approach is followed at ULS, energy dissipation and ductility are explicitly considered and can be implemented in the design strategy. The structural demand is indeed reduced in function of the ductility of the system, expressed as by appropriate coefficients (e.g. q factor of EN 1998:2005).

One can choose whether ductility is achieved by means of additional elements, i.e. dampers ($E_{\mu,Devices}$ or $E_{\xi,Devices}$), or by exploiting the dissipative capacity of the structural system instead ($E_{\mu,Structure}$). This is done by choosing a number of adequate "sacrificial" locations and making sure that the remaining "non-dissipative" structural elements are designed following a capacity hierarchy that ensures that no damage will occur. The criterion of weak beams-strong columns for frame structures well represents this concept of capacity design.

A further evolution of codes consist in the Performance Based Design (PBD), which was developed in response to the need of optimising the performance of structures for multiple seismic action levels, i.e. several limit states, so as to minimise the costs

connected to damage and repair. For instance, the DM 14/01/2008 defines two service limit states (Operational Limit State, SLO, and Damage Limit State, SLD) and two ultimate limit states (Life Safety Limit State, SLV, and Collapse Limit State, SLC), thus allowing the refinement of seismic design down to the level of non-structural elements and services. More specifically to heritage structures, DPCM 2011 also defines a limit state for artistic assets (SLA), which are most sensitive to dynamic actions.

It is worth noticing that the level of performance expected by heritage structures is not necessarily the same as per new structures: DPCM 2011 states that the performance of heritage structures must be assessed in the existing configuration and compared with the seismic demand, so as to establish the urgency and extent of strengthening interventions in light of the expected service life. Once the need for an upgrade has been ascertained, the benefits of possible upgrade interventions in terms of seismic performance must be compared with the impact on the original aesthetic and functioning of the building. Even though human safety must be given the priority, the document acquiesces to a lower safety margin with the aim of limiting the interventions, in line with the ICOMOS principles of minimal intervention.

In the context of PBD, damping and isolation systems (Aiken et al., 1993; Hanson, 1993) present many advantages, as they allow a considerable level of control on the structural performance; hence, they are gradually substituting other well-established techniques and are included in design codes (EN 1998:2005, FEMA 450). The application of techniques involving ductility and energy dissipation is recommended even for the repair and strengthening of heritage structures (California Historical Building Code, 2007; DPCM, 2011).

Yet, strength-only systems, such as RC or steel ring beams and jacketing are still allowed for, in spite of the extent of interventions necessary to meet the expected performance level.

This can be explained considering that:

- The enhancement of the dissipation by the structure itself ($E_{\mu,Structure}$) is not always feasible in heritage structures. For instance, the formation of plastic hinges that dominates the performance of steel structures doesn't apply to historic masonry, which dissipates energy through damage, which is an undesirable effect;
- At the same time, not all the innovative systems (E_{SD}, $E_{\mu,Devices}$ or $E_{\xi,Devices}$) can be easily applied to existing structures – for example, seismic isolation is seldom viable, especially in the case of heritage buildings;
- Moreover, conventional techniques are able to remedy the poor constructive methods typical of some historical buildings. For instance, the strengthening of a weak substratum by injections is a widely applied methodology, even before proceeding to seismic retrofit with dampers (Castellano et al., 2001);

- Additionally, a fairly high number of damping devices have such size and shape that cannot be integrated in a structure without affecting its aesthetic. Although it was not possible to source information regarding the exact geometry of the devices reviewed in §2.5, many are normally employed in frame structures in series with the beams or the braces and their size is proportional to that of other structural members. Even when available in reduced dimensions, they are designed to suit the damage mechanisms typical of frame structures (Rodgers et al., 2007) and cannot be easily adapted to and implemented in masonry buildings.
- Finally, the use of innovative techniques, which is regarded as an additional option in respect to the increase of ductility, is methodically regulated only in the case of applications to new constructions or retrofit of modern structural systems; on the contrary, specific regulations for the retrofit of heritage building are missing. Indeed, code requirements and prescriptions are mainly qualitative (EN 1998:2005). End users are left with the difficult decision of how to dimension strengthening elements and where to source the values to use in the design process. Much of the current practice relies on engineers' know-how and "rule of thumb"; this is neither systematic, nor viable for innovative techniques and complex structural solutions.

Consequently, strength-only techniques are still widely applied, in spite of a number of drawbacks. Tie-columns, for instance, have a significantly positive effect on the seismic performance of a masonry structure, but only when RC tie beams are built too, as shown by Karantoni and Fardis (1992). However, the construction of concrete elements hinders the original aesthetic and functionality of the building and it is in sharp contrast with the criterion of minimum intervention that should be pursued in the retrofit of heritage structures.

Moreover, experimental studies performed on masonry structures reinforced by strength-only systems show that the difference in mechanical properties between original materials and additional elements can lead to collateral effects. For instance, Benedetti et al. (1998) observe that shear failure of masonry might occur at the level of steel hoops if the strengthening elements are not able to redistribute the horizontal loads. Drawbacks observed in the controlled environment of testing facilities have further-reaching consequences in historic city centres experiencing major seismic events (D'Ayala and Paganoni, 2011). Poorly designed connections between masonry walls and concrete ring beams, which are hardly compatible with a historic substratum due to excessive mass and stiffness, frequently determine tragic collapses (Fig. 2-1).

Far better performance is instead observed for strengthening systems that restore the box-like behaviour of buildings without increasing the overall mass. Cross ties installed at the intersection of perpendicular sets of walls are able to prevent the overturning of whole façades without interfering with the original structural lay-out (Tomaževič, 1999). The only pitfall of cross-ties is the possibility of pull-out damage at the head of the anchorage due to the different deformability of metal and masonry.

Fig. 2-1: Examples of collapses due to r.c. ring beam/ roof structures at top level of masonry buildings. Onna, L'Aquila, Italy, January 2010 – Eight months after L'Aquila earthquake, 2009. Author's own

The use of high-ductility systems recommended by codes would overcome this issue, thus achieving the objective of protecting culturally valuable finishes and preserving life and safety. Notwithstanding their appeal, innovative, high-ductility systems only feature in a few high-profile case studies or research projects (Mandara and Mazzolani, 1994; Bonci et al., 2001; Benedetti, 2004 and 2007).

In light of these considerations, it is clear that a gap between design codes and practice, technological development and feasibility, conventional and innovative still exists in the field of the seismic protection of heritage structures. The extent of such discrepancy and whether it can be remedied will be investigated in the following chapters, so as to provide further insight in a topic that has serious implications on the preservation of both human lives and unique heritage assets.

The thesis specifically focuses on connections among sets of perpendicular walls, as these are common weak points in heritage structures and their strengthening is beneficial to all categories of buildings, including those that are less influenced by the diaphragm action of floors and hence by the connection between vertical and horizontal structures, like churches.

2.3 UNREINFORCED AND REINFORCED CONNECTIONS IN HERITAGE STRUCTURES LOCATED IN SEISMIC-PRONE AREAS

Since ancient times, populations living in seismic prone areas had to deal with the problem of protection of buildings from earthquake-related damage. The process of improvement of structures probably relied on a process of trial and error, which led to the selection of a number of techniques that then became part of the standard constructive practice. Hence, beside unreinforced structural elements, various reinforcement typologies were adopted and handed down from generation to generation. However, the process was neither systematic nor standardised.

Constructors were able to grasp the importance of well realised connections to improve the distribution of vertical and horizontal load. Therefore, connections between sets of perpendicular walls in seismic prone areas often feature specific

detailing, such as better quality blocks (typical set-up of stone quoins in brickwork buildings) or corner-shaped elements. In other cases, additional elements, such as metallic and timber ties (Fig. 2-2a and b), were added either at the time of construction or at a later stage, in the aftermath of a damaging earthquake or for prevention purposes.


a)


b)

Fig. 2-2: Example of a) metal and b) timber cross-ties (D'Ayala Paganoni, 2010 and Carocci and Lagomarsino, 2009 respectively)

Complex techniques involving additional elements were also in use: Turkish hatil and himiş buildings (Doğangün et al., 2006), Indian and Kashmiri Dhajji-dewari (Fig. 2-3) and Taq structures (Langenbach, 1990; Paikara and Rai, 2006), Bathar constructions and complex timber plates in adobe buildings (Tolles and Krawinkler, 1988; Schacher, 2007), Greek timber-laced systems (Tsakanika, 2006; Vintzileou, 2008) all involve the use of timber elements placed at different locations of the building to connect together wall panels, horizontal structures and masonry wythes, providing continuity to materials, redistributing horizontal loads and ensuring box-like behaviour. Other positive side effects of timber elements are that they have a Young modulus comparable with masonry so that they work well together in the elastic range and that they are able to dissipate part of the seismic energy by deformation and friction against the masonry material.

Although in general beneficial, traditional systems are frequently affected by a number of issues that might hinder their robustness and reliability (Fig. 2-4). For instance, a survey by NTUA/EPPO (2005) on timber tied structures revealed that common pitfalls of these structures are the quality of connection between timber elements and the splicing of ties, which are not always as carefully realised as they should be, and the deterioration of timber as consequence of weather conditions or ageing. Similarly, cross-ties have a positive effect on the three-dimensional response of a structure, although poor maintenance resulting in corrosion, decay, or connection rod/plate becoming loose can compromise such performance (Modena et al., 2010).

It is worth highlighting that at the time of construction little was the awareness of the mechanics governing the structural behaviour and, therefore, the reasons behind certain structural choices were easily lost through the years. This explains the lack of

maintenance and in certain cases the voluntary alteration of reinforcement elements. It's only in more recent centuries that systematic awareness of seismic damage developed and that seismic reinforcement started becoming methodical: in 1781, Milizia suggested the use of wooden floors and timber ties through the entire thickness of masonry walls to achieve earthquake-resistant structures.

Fig. 2-3: Dhajji-dewari system (Paikara and Rai, 2006)

Fig. 2-4: poor performance of timber tie (D'Ayala Paganoni, 2011)

The traditional reinforcement systems described above become a feature integrated with the structure at the time of construction and hence can be regarded as unstrengthened connections; strengthening, on the contrary, involves the modification of the original structure to increase its performance level; this being a concept typical of contemporary seismic and conservation engineering.

Indeed, in the last decades, several strengthening systems have been developed to solve the issues related to the drawbacks of traditional reinforcement as well as with the more general goal of increasing the capacity of structures in respect to their original configuration. This upgrade can be necessary because of new legal obligations, as consequence of a change of use of the building, or simply to protect historic buildings and their occupants from seismic hazard.

Strengthening is implemented through a variety of systems, so much so that it would be hard to review all the existing. A short overview of the most common follows so as to provide the reader with a picture of the state of the art and of the rationale for the research project described herein.

2.4 TECHNIQUES FOR THE SEISMIC STRENGTHENING OF HERITAGE STRUCTURES

Nowadays, strengthening draws on the same principles that were at the basis of the construction of reinforced connections in the past. If vertical elements, horizontal structures and vaults are efficiently connected, loads are better distributed, out-of-plane mechanisms of damage reduced and, hence, major failures can be avoided.

When connections lack adequate capacity, further elements can be added to the original structure to achieve the desired performance. However, this task is not as straightforward as for engineered structures, since issues such as compatibility between chemical and mechanical properties of the strengthening system and of the parent material need to be taken into account.

In respect to the past, strengthening systems for structural connections today rely on a more accurate design, and innovative and more durable materials, like for example stainless steel or titanium, which substituted iron and mild steel in cross-ties, with considerable advantages in terms of issues related to material deterioration (e.g. cracking and spalling due to the expansion of corroded material, failures due to reduced resisting section).

Nevertheless, many strengthening techniques, after an initial success, have proved to not perform at the required level and showed drawbacks when undergoing dynamic loading. This is for instance the case of reinforced concrete ring beams, which were frequently used in the recent past and are now seldom implemented because of their well-known incompatibility with unreinforced, weak masonry. Failures connected to excessive mass and stiffness have been documented by a number of authors (e.g. Spence and D'Ayala, 1999; D'Ayala and Paganoni, 2010). As result, alternative options are being developed; an example is the masonry ring beam made by layers of bricks and laminates embedded within a polymeric matrix or a cementitious grout (Borri et al., 2007; Borri et al., 2009) (Fig. 2-5 and Fig. 2-6).

Fig. 2-5: Construction process of reinforced masonry beam (Blasi et al., 1999)

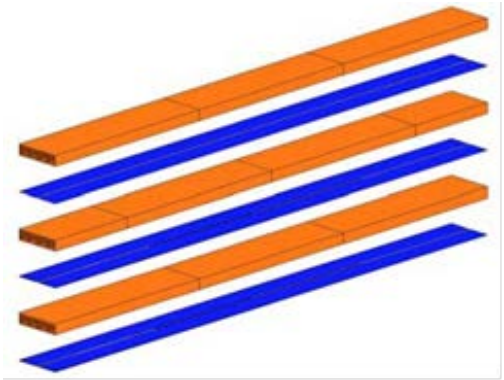

Fig. 2-6: Assembly of LATLAM ring-beam, (Borri et al. 2007)

Metallic elements can also be applied to achieve the same effect as a ring beam. The Italian DPCM (2011) suggests the use of:

- A trussed frame made of plates and angular elements jointed together and anchored to the masonry walls;
- A set of plates positioned on the inner and outer surfaces along the top part of the masonry walls and connected by anchors embedded in the masonry and running throughout its thickness.

Either way, the masonry in the intervention and surrounding areas should be consolidated by resins or grouting so as to offer a sufficiently solid substratum (DPCM, 2011).

Several other strengthening systems consist of metallic anchors for the connection of perpendicular sets of walls. Metallic anchors can either be grouted (Gigla, 2004; Elingehausen et al., 2006) or simply installed without any binder or embedment. In the former, the transmission of loads is ensured by bond and shear along the contact surface between the binder, grout or resin, and the parent material. The latter feature a front plate or peg that distributes the tension load experienced by the metallic rod to a portion of masonry; plates can be variously shaped and depending on their size feature stiffening elements, which prevent out-of-plane bending.

Another family of strengthening systems relies on the application of a thin, continuous layer or material that creates a “hoop” action around the building, thus confining the wall against outward detachment, indirectly improving the behaviour at the corner connections. The materials used vary depending on local availability and mechanical properties of the original materials, which need to be matched as closely as possible to avoid localised failures. Some examples are: geotextiles (Blondet and Aguilar, 2007; Torrealva, 2008; Torrealva et al., 2009; Torrealva, 2009), metallic mesh (San Bartolomé et al., 2004 and 2008), and polypropylene mesh (Mayorca and Meguro, 2004; Macabuag et al., 2009). These materials have been mainly applied to earthen buildings, but wrapping is also possible in brickwork masonry: Italian guidelines for strengthening by fibre composites (CNR-DT 200 R1/2012) mention carbon, steel and glass fibres, while recent commercial development also include basalt and organic fibres (Fidia, 2014).

All the above mentioned techniques pertain to the category of capacity designed systems. Although some can provide a certain level of ductility to the structure where they are installed, ductility and energy dissipation are not the main parameters that control their design and functioning. This of course doesn’t mean that they cannot improve the performance of a building. However, they do have drawbacks connected to high stiffness in respect to the existing parent materials and are not in line with the recommendations of design codes. In fact, they are in open contrast with the current trend in seismic engineering design.

A sample of how this is pursued and implemented in new structures will be presented in the following, so as to clarify the difference between design approaches and give insight into available techniques.

2.5 DISSIPATIVE DEVICES AND DAMPERS IN CURRENT ENGINEERING PRACTICE

As mentioned in §2.1, a variety of systems for the enhancement of energy dissipation have been designed in the last decades. In the following a brief overview of commercially available systems will be given, so as to investigate the reasons why these systems have seen limited implementation in the strengthening of heritage

buildings and which would have the potential of being implemented in historic masonry structures.

According to this goal, some systems will be omitted, as there is strong evidence to rule them out of the summary. For instance, isolation systems will not be discussed, as their applicability to heritage structures is limited due to the difficulties connected to working on buildings with highly irregular, weak foundations. It should however be noticed that some exceptions do exist (Johnson, 2005) and that scientific research is already exploring the possibility of adapting this method to historic buildings (Clemente et al., 2012).

Velocity-displacement dampers, i.e. viscous dampers and viscoelastic (VE) solid dampers are also not considered, although for different reasons. In fact, viscous dampers have already been applied in heritage structures and are also already patented; moreover they require complex mechanical design and detailing. Hence, it has been decided not to explore this specific technique to the purpose of developing another, similar prototype. Nevertheless, given their relevance to the topic, existing case studies with viscous dampers will be discussed in §2.5.4.

This implies that the review will only cover displacement-dependent damping devices, namely those systems where the dissipation of energy is proportional to the deformation experienced by the damper as consequence of yielding of metal or controlled sliding among mechanical parts.

2.5.1 Yielding Dampers

In conventionally designed frame systems, dissipation is produced by inelastic actions at beam-column connections (EN 1998:2005). As dissipation involves cyclic plastic deformations of metallic elements and eventually damage and collapse, it is preferable to increase the contribution of $E_{\mu,Devices}$ (Eq.2-2) by shifting the dissipation from primary structural elements, $E_{\mu,Structure}$, to “sacrificial” elements.

Such elements are metallic dissipating devices and are generally divided in two categories (Constantinou et al., 1998; Symans et al., 2008): Buckling Restrained Braces (BRB) and Added Damping and Stiffness (ADAS) Dampers.

A BRB (Fig. 2-7a) system consists of a steel brace with a cruciform cross section surrounded by a stiff steel tube; the space between the tube and brace is filled with a concrete-like material. A special coating prevents the concrete from bonding to the brace, so that this can experience large deformations even in compression without risk of buckling (Coffman Engineers Inc., 2005). This overcomes the pitfall of traditional bracing, which can only work in tension.

ADAS (Fig. 2-7b) dampers consist of a series of steel plates wherein the bottom of the plates are attached to the top of a chevron bracing arrangement and the top of the plates are attached to the floor level above the bracing. The geometrical configuration of the plates is such that the bending moments induced by the lateral deformation of

the floor with respect to the bracing produce a uniform flexural stress distribution, and hence inelastic action, over the height of the plates (Constantinou et al., 1998).

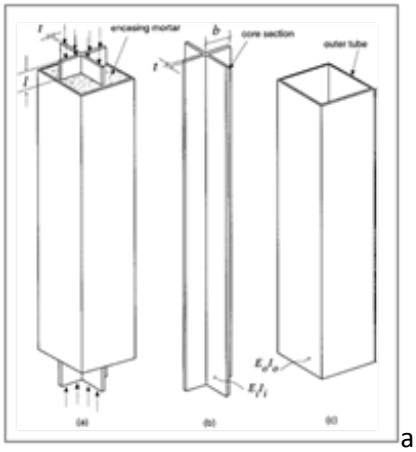

a)

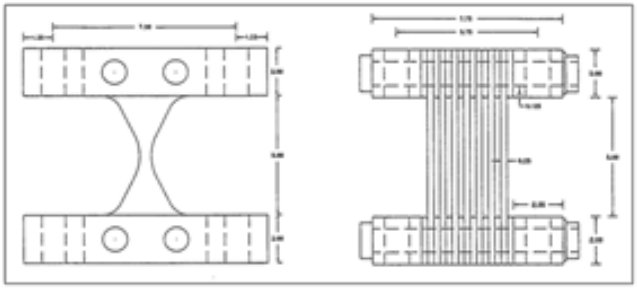

b)

Fig. 2-7: Typologies of yielding dampers: a) BRB (Black et al., 2004), b) ADAS (Aiken et al., 1993)

Currently a number of application cases featuring the use of this type of dampers are available in literature, both for retrofit and new construction (Black et al., 2004). The success of metallic dampers is partly due to the fact that their behaviour is familiar to practising engineers and, even if non-linear analysis is necessary, theoretical models are available and show good agreement with experimental results (Black et al., 2004; Constantinou et al., 1998). Furthermore yielding dampers are reliable as their properties are not substantially influenced by temperature and their hysteretic behaviour is stable.

On the other hand, plastic deformation is not completely reversible and therefore yielding devices may need replacing after demanding seismic events.

Buckling is another possible drawback: despite the shape of the dampers, which are designed to not be affected by sudden instability (Ibrahim et al., 2007), and the use of systems such as the encasing for BRB, phenomena such as torsional buckling have been pointed out and modelled (Black et al., 2004).

The majority of applications to existing building and experimental case studies (Aiken et al., 1993; Black et al., 2004) are relevant to steel frames, but examples of retrofit of concrete frames with masonry infill are not uncommon (Fip Industriale, 2006).

2.5.2 Friction Dampers

Friction dampers dissipate energy via sliding friction across the interface between two solid bodies; the mechanism can be modelled by the idealized Coulomb law for friction (Constantinou, 1998):

2-4) $$F_{//}=\mu F_{\perp}$$

where $F_{//}$ is the slip load, $F_{\perp}$ is the normal force at the sliding interface and μ is the coefficient of friction, which is variable depending not only upon the selection of sliding materials, but also on the condition of the sliding surfaces.

One of the main advantages of friction devices is the rectangular shape of hysteresis loops that dissipate a large amount of energy. As such, friction devices have many applications and are thoroughly studied (Pall and Marsh, 1982; Ciampi et al., 1995; Dimova et al., 1995; Colajanni and Papia, 1997; Mualla and Belev, 2002; Soong and Spencer, 2002; Moreschi and Singh, 2003; Rojas et al. 2005; Christopoulos et al., 2008). Currently, available devices can be divided in two main categories: bolted-slotted and uniaxial.

The functioning principle behind bolted-slotted dampers is fairly simple: the pressure applied by bolts on a series of metallic profiles defines the slip load at which the device starts its relative movement. The steel plates are generally treated to obtain a reliable friction coefficient. One major producer of such devices is Pall Dynamics Limited, whose catalogue includes solutions for long slender tension-only cross bracing, single diagonal tension-compression bracing (Fig. 2-8) and chevron bracing. Friction surfaces are brake lining pads (Pall, 2004). Pall's dampers have been used for several applications, both in the field of new structures and for the retrofit of existing steel frames buildings (Chang et al., 2006; Pall, 2004).

Uniaxial friction devices are composed by an assembly where the compressive force developed by a spring acts on wedges and provokes a normal force on the internal surface of a cylinder, which also work as the outer case of the device assembly.

Fig. 2-8: Single bracing Pall's friction damper (Chang et al., 2006)

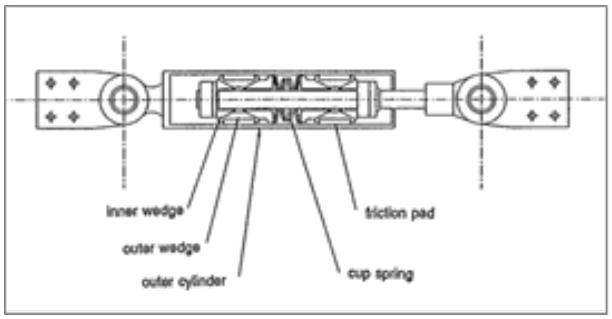

Fig. 2-9: Sumitomo uniaxial friction damper (Aiken et al., 1993)

In the device designed and developed by Sumitomo Metal Industries Ltd. (Fig. 2-9), Japan, the force exerted by the spring is converted through the action of inner and outer wedges (Constantinou et al., 1998). The Energy Dissipating Restraint (EDR) produced by Fluor Daniel Inc. (Fig. 2-10a), works on a similar concept; however, in this case the length of the internal spring is controlled by stops and compression/tension gaps that create load-displacement cycles slightly different from the classical

rectangular-shaped friction loops (Nims et al., 1993). This has the interesting advantage that the device can be set to generate self-centring loops, thus avoiding the presence of residual deformation, which are a considerable problem after major earthquakes (Fig. 2-10b).

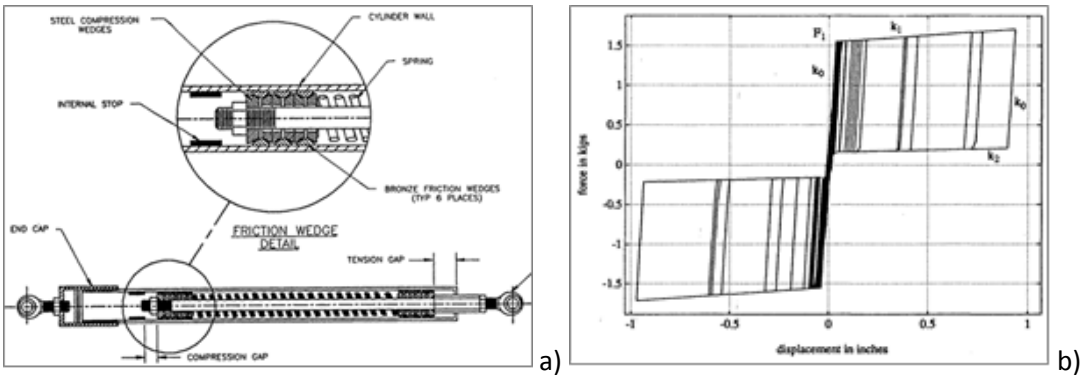

Fig. 2-10: Fluor Daniel's EDR (Nims et al., 1993): a) device, b) self-centring loops

Besides tests on commercially available friction devices, such as Pall's (Aiken et al., 1988; Black et al., 1993), Sumitomo's (Aiken et al., 1998) or Fluor's (Nims et al., 1993), several testing campaigns have been performed within the framework of research projects. Among others, it is worth mentioning prototypes such as the friction-slip device tested at the University of Berkley, California, (Aiken et al., 1993), the ring spring damper tested by Filiatrault et al. (2000), and the device developed by Morgen and Kurama (2008) that exploits the formation of gaps at the joints between precast beam and column members to generate slip displacements at the friction interfaces.

Great attention needs to be paid to the coupling of different materials at the frictional interfaces, as this may affect positively the friction coefficient but trigger corrosion via galvanic contact. Indeed the choice of most suitable materials is investigated by Constantinou et al., 1998 and Morgen and Kurama, 2008.

2.5.3 Phase Transformation Dampers

Shape Memory Alloys (SMAs) are metallic alloys that, due to a reversible transformation between two crystalline configurations, show a peculiar mechanical property, the so called superelasticity, i.e. the capacity of reaching high levels of strains – up to the 6% of the ultimate – with almost no residual deformation.

For some alloys, the phase transformation is temperature-correlated, while for others, such as Nitinol (NiTi SMA), the phase change can be stress-induced at room temperature.

Shape Memory Alloy Devices (SMADs) consisting of metallic profiles in series with groups of SMA wires were developed within the framework of the ISTECH project (Indirli et al., 2001) by Fip Industriale, Padova, Italy, which now owns the patent. SMADs are able to provide large displacements, recover deformations and after the first ductile plateau can be designed to have one or more increases in stiffness

followed by further ductile plateaus (Fig. 2-11a and b), meaning that they can be conveniently designed for several limit states. As such, they have been implemented in rehabilitation projects on heritage buildings (Bonci et al., 2001; Castellano et al., 2001). Their use has also been theoretically studied for application to other typologies of structures such as bridges (DesRoches and Delemont, 2002).

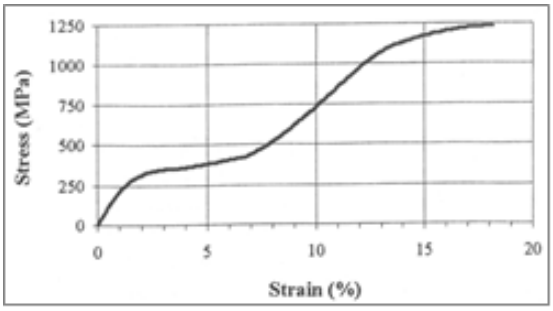

a)

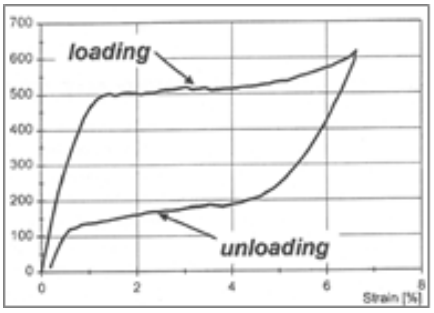

b)

Fig. 2-11: NiTi SMA wire (Indirli and Catellano, 2008): a) monotonic tension test up to failure, b) cyclic tension test in the super-elastic range

2.5.4 Damping Devices Applied to Heritage Structures

All the typologies of dampers mentioned above find wide application in the field of new construction and of the retrofit of steel/concrete frames. Only a small number of case studies on historic structures appear in the technical literature and all are worth mentioning, as to date they constitute important examples of the attempts done to apply the concept of energy dissipation in the field.

The interventions carried out in the S. Giovanni Battista Church in Carife, Italy (Mandara and Mazzolani, 1994) and in the New Library of Federico II University of Naples, Italy (Mazzolani, 2001) are the first cases of seismic upgrading of heritage constructions carried out by means of viscous dissipative devices.

Viscous dampers, or Shock Transmission Units (STUs), consist of a hollow cylinder filled with fluid, typically silicone based, and a piston. As the piston moves, the fluid is forced to flow through orifices either around or through the piston head. The resulting difference in pressure across the piston head can produce very large forces that resist the relative motion of the damper; input energy is dissipated in form of heat due to friction between the piston head and fluid particles flowing at high velocity. Conversely, since these devices are velocity-dependent, slow movements, such as thermal expansions, are allowed.

In the case of S.Giovanni Battista, a set of oleodynamic devices were coupled to a new roof structure made of steel trusses pinned to an r.c. ring beam cast on top of the masonry walls. The oleodynamic devices resist dynamic loads performing like pins, i.e. allowing relative rotation at the joint wall/roof structure, yet preventing relative movements, thus ensuring the connection between roof and walls, while the roof structure behaves like a rigid diaphragm, aiding the redistribution of horizontal loads among the different walls. At the same time, the devices can accommodate

temperature cycles by behaving like sliding bearings, thus avoiding the degradation of the historic materials as result of thermal-induced stresses.

Interestingly, the authors (Mandara and Mazzolani, 2001) also investigated two different methods for dimensioning the devices, thus not only addressing the problem of what technology to use, but also how to design it. In the Plastic Threshold Approach (PTA), devices are conceived and sized to limit the magnitude of force transmitted across connected members to a maximum value, determined according to the design resistance of structural elements involved. Beyond this threshold, hysteretic energy dissipation takes place, while below the threshold the behaviour of dampers is virtually rigid; as such it ensures the maximum degree of redundancy of the structure under serviceability conditions. According to the Optimal Viscous Approach (OVA), the interaction between connected members is ruled by the viscous properties of the devices, which are dimensioned so as to minimise the magnitude of the force acting on them independently from its value. Contrary to PTA, the connection between elements is never fully rigid, so that energy can be dissipated under moderate intensity earthquakes too.

Tolles et al. (2002) also propose the use of a light steel frame and a series of viscous dampers at roof level in the case study of Las Cruces Adobe. However, no experimental evidence regarding this system, a rare example of viscous dampers being applied to earthen structures, is provided.

The seismic retrofit interventions of the Upper Basilica of S. Francis in Assisi, San Feliciano cathedral in Foligno and San Serafino Church in Montegranaro, Italy were carried out instead by Fip Industriale's SMADs. These churches were damaged by the 1997 Umbria-Marche earthquake, whereby the out-of-plane mechanism with detachment of their front facade from the rest of the building was triggered to different extent. In the case of S. Francis, the pounding action between tympanum and concrete roof beams (inserted in the 1960's) had also caused the collapse of the transept vault. Post-earthquake interventions, described by Indirli and Castellano (2008), and Bonci et al. (2001), aimed to restore the connection between roof and façade providing a mean to control the relative displacement and transmission of loads between the elements. As mentioned in §2.5.3, shape memory alloys have properties that result particularly favourable when pursuing these goals.

Strengthening interventions were carried out in San Serafino and San Pietro churches in Feletto, Italy, with similar configurations. However, the size and capacity of SMADs largely varied depending on the case study, with the load capacity of each device ranging between 2 to 52 kN and the maximum allowable displacement varying between ±8 to ±25 mm.

Benedetti (2004, 2007) addresses the problem of out-of-plane failures through different typologies of hysteretic devices: the RAG energy absorber, for instance, consists of four arms hinged at their end so as to form a square element. Hinges are made of lead cylinders press-fitted into the arms. When two (or four) of the corners of

the device, which are connected to the masonry wall via metallic rods, displace relatively one from the other as a consequence of damage in the parent material, the hinges deform plastically in torsion or bending. Conversely, the arms are made of a stiffer material so as to not undergo plastic deformations. Drawing on the same principle, Benedetti (2007) designed a rotation amplifying absorber, which is conceived to be installed at the inner corner between two perpendicular walls. This works thanks their relative rotation, which induces torsion in the lead pin located at the connection between the two L-shaped arms of the device. Benedetti (2004, 2007) also developed a "continuous" energy absorber, which overcomes the problem of identifying a-priori the location of damage. The concept largely draws on the concept of metallic mesh confinement, as recently revised and further developed by Borri et al. (2008) and Dolce et al. (2001), but in this case the mesh, which is called RETE, is made of lead, so that yielding of the threads occurs at an early stage (for elongations of about 0.2 mm). The mesh is applied as a continuous layer on the structure and it is therefore able to "capture" relative displacements and deformations occurring at any point.

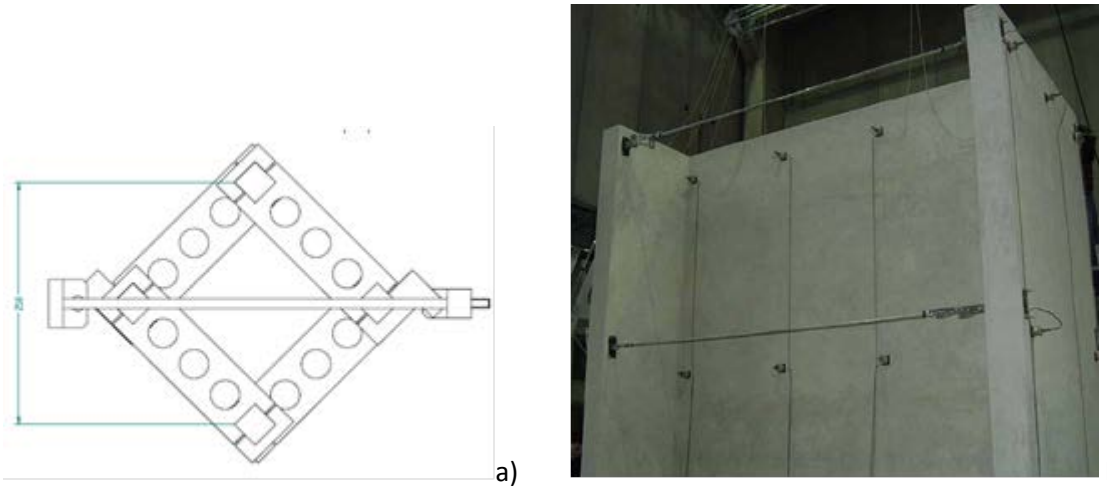

a) b)

Fig. 2-12: RAG energy absorber: a) prototype (Benedetti, 2007); b) setup in series with metallic cross-tie installed on a masonry specimen, (Benedetti, 2007)

Finally, a rocking-damper system, the DIS-CAM (DISsipative Active Confinement of Masonry) was developed within the framework of the restoration project of the drum of the dome of S. Nicolò church in Catania (Di Croce et al., 2010). The system is made of metallic elements placed at the top and bottom of the masonry panels of the dome; during earthquakes the panels rock rigidly in their plane, forming flexional cracks at their extremities. The devices control such relative motion, prevent the complete crushing at the corners of the masonry panels and dissipate energy, without interfering with the recentring capacity of the panels.

In spite of the variety of dissipative systems specifically designed for heritage structures, to the author's knowledge, only Mandara and Mazzolani's STUs and Fip's SMADs have been applied in practice; Benedetti's dissipators have been extensively

characterised in a laboratory environment, but never applied in practice, and the DIS-CAM system is at the stage of computational validation.

Overall it is clear that the concept of energy dissipation and ductility can be applied to heritage structures; on the other hand, it is also clear that this is seldom done in practice. Indeed, dissipative systems remain within the domain of scientific research, without much guidance being provided to end users who wished to implement such systems in real case studies. Hence, it is necessary to look further in depth at design prescriptions, so as to understand where the missing link is.

2.6 SEISMIC DESIGN OF RETROFIT INTERVENTIONS FOR HERITAGE STRUCTURES

Although European and national codes (e.g. DPCM, 2011) provide for the use of various systems for the strengthening of connections (§2.4), such as for example ring beams, no detailed reference is made to specific procedures for the dimensioning of these structural elements. The only indication in this sense can be found in section 6.1 “Retrofit Design Procedure” for existing building of Eurocode 8 (EN 1998-3:2005), which states that the design process should cover:

- Selection of techniques and/or materials, as well as of type and layout of intervention;
- Preliminary sizing of additional structural parts;
- Preliminary calculation of stiffness of strengthened elements;
- Analysis of strengthened structure by linear or non-linear analysis. The typology of analysis is chosen depending on the level of knowledge regarding the geometry detailing and materials of the structure;
- Safety verifications for existing, modified and new structural elements carried out by checking that the demand at three different limit states – Damage Limitation, Significant Damage and Near Collapse - is lower than the structural capacity.

In the safety verifications, mean values of mechanical properties of existing materials derived from in-situ tests, available documentation or relevant sources shall be used, taking into account the confidence factors (CFs) specified in 3.5 of Eurocode 8 (EN 1998-3:2005). Conversely, for new materials, nominal properties shall be used without modification by confidence factor. The code also states that in case the structural system, meaning both existing and new structural elements, fulfils the requirements of EN1998-12004, the verifications may be carried out in accordance with the provisions of the material specific codes.

This implies that for systems such as RC ring beams or corner ties, reference can be made to the specifications for RC members in the relevant sections of EC8 and other Eurocodes. However, this leaves the problem of quantifying the interaction between original and additional structural elements open; hence, the assessment of the global seismic performance of the strengthened structure will still be affected by a large number of uncertainties. For instance, Giuffrè (1993) suggests performing a check for

sliding shear on the horizontal surface underneath the area of masonry to which the ring beam is connected by metallic fixings. This seems a logical check considering that failure involving ring beams are caused by the concrete element sliding off its supports; however, the recommendation derives from the author's expertise rather than from provisions in the codes.

Other strengthening systems hardly feature in codes. This could be due to the fact that the sizing of the element itself, e.g. steel cross-tie with end plate, is fairly straightforward and established in the current technical know-how; furthermore, formulas can be drawn from those of other structural members, e.g. axial capacity of steel elements. Still, designers are left to their own devices at the moment of assessing the interaction between old and new, since this affects the global performance of the strengthened building.

For instance, a large number of failures were observed on heritage buildings in the aftermaths of the second Christchurch quake (Canterbury earthquake, February 2011). As reported by Wilkinson et al. (2013), several bonded anchors for the connection between horizontal structures and walls failed as consequence of insufficient dimensioning, width of spacing and disregard for the properties of the materials in which they were embedded. This clearly shows that, even in a country at the forefront of earthquake protection like New Zealand, gaps still exist in the regulations regarding the design of seismic strengthening for structural connections, and this might have serious repercussions on buildings' performance.

A lack of standardisation is also the result of the recent development of techniques, as well as the high level of expertise and financial resources required for their application. Innovative technologies have yet to be extensively applied and validated in real-life situations, and the retrofit of a complex, precious building by means of unconventional systems is a difficult task that goes beyond standard conservation practice. Quantitative data is in fact missing even for basic techniques.

Furthermore, the characteristics of historic masonry are a major source of uncertainty, this meaning that the application of guidelines written for similar structural systems is not a viable solution. For instance, the performance of metallic anchors embedded in concrete has been extensively studied (Elingehausen et al., 2006) and European design guidelines published (EOTA 2006, DD CEN/TS 1992-4-1:2009). Conversely, anchors embedded in masonry lack specifically dedicated codes or recommendations. One could try to derive modes of failure and hence the design procedure from the guidelines for concrete; however, these rely on a series of parameters, such as bond strength or minimum distance to edge, that should be either provided by the anchor producer or derived experimentally case by case.

Whichever the case - quantitative data feeding into code prescriptions, design values provided by producers for their standard and innovative products, experimental assessment carried out for specific case studies - it would be expected that the methodology and testing procedure are standardised so as to ensure repeatability and

reliability of results. However, this does not occur either at national or international level, to the author's knowledge, and hence represents an important gap in the correct practice for the strengthening of structural connections in heritage buildings.

2.7 EXPERIMENTAL ASSESSMENT OF STRENGTHENING TECHNIQUES FOR THE SEISMIC PROTECTION OF HISTORIC CONNECTIONS

As discussed above, a wide variety of materials and products for the strengthening of historic structures can be found in literature and current practice. At the same time, the experimental assessment of strengthening techniques is a well-established practice both in the scientific community and among commercial producers.

It is therefore surprising that the experimental assessment of connections in unreinforced and strengthened configuration as such is rarely performed and very few codes of practice deal with this topic.

Currently, strengthening products are generally tested either at a local scale, i.e. for the repair and upgrade of a single structural element, or at a global scale by shaking table tests. Yet, tests performed on a single structural element are insufficient to describe how the strengthening system works when it is used at the connection between two or more parts. For instance FRPs, which can be applied to strengthen corner connections and to restrain out-of-plane failure of walls (CNR-DT 200 R1/2012), are most often tested for the wrapping of single columns (Corradi et al., 2007; Di Ludovico et al., 2010) and confinement/strengthening of wall panels (Ehsani and Saadatmanesh, 1996; Tan and Patoary, 2004). On the other hand, when a strengthening system is used for global scale applications, it may be hard to monitor its specific influence on connections, even more so if other techniques have been applied to the structure, this being the common set-up for shaking table tests.

Nevertheless, a few publications do focus on the experimental assessment of structural connections, both in unreinforced and strengthened configurations, by shaking table tests. Experimental campaigns are either performed on subassemblies including one or more walls or on mock-ups of the whole structure where only one strengthening system is implemented at the time.

Subassemblies generally consist of a masonry panel loaded in the out-of-plane direction and, in some cases, two side wall returns, which are either fully connected to the front wall or detached so as to simulate pre-existing damage and connected by means of strengthening, such as cross ties. An example of the typical set-up is shown in Fig. 2-13.

However, materials, geometry of the front and wing walls, and strengthening systems greatly vary from author to author: for instance, Al Shawa et al. (2009) performed a set of shaking table tests on three C-shaped brick strengthened by different techniques. Dowling and Samali (2006) also investigated various strengthening techniques by using C-shaped specimens; however, these were built in adobe. Benedetti (2007) carried out the experimental validation of his energy absorbers by using H-shaped full scale walls,

while Zuccarello et al. (2009) tested a set of simple brick masonry walls; the influence of side walls on the out-of-plane response was simulated by varying the boundary conditions. Similarly, Indirli and Castellano (2008) carried out a set of shaking table tests on brick walls simulating a portion of a church façade connecting it to a stiff steel frame representing the rest of the structure; different strengthening elements were used at the interface between the two. An overview of tests showing the range of methodologies and set-up features is provided in Table 2-1.

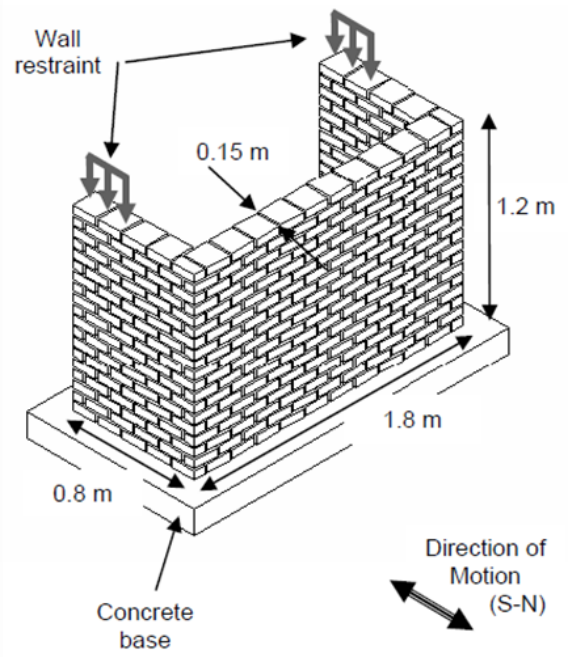

Fig. 2-13: Typical set-up of test on subassembly (Dowling and Samali, 2006)

Each of the above testing campaign explores the behaviour of connections by focussing on different aspects of the unreinforced structure and of the effect of the specific strengthening systems. For instance, the analyses of the experimental campaigns conducted by Benedetti (2004, 2007) and by Indirli and Castellano (2008) aim to validate the performance of new strengthening systems. As such, great relevance is given to the increase in PGA that specimens can withstand without damage thanks to the dissipative elements: 50% for structural connections strengthened by SMADs in respect to specimens strengthened by conventional anchor ties (Indirli and Castellano, 2008), 50% for specimens with energy absorbers (Benedetti, 2004) in respect to unreinforced specimens. Benedetti (2004) also carries out an extensive analysis of damping, dissipated energy and maximum displacements of the specimens, while Dowling and Samali (2006) mainly focus on the typology of damage mechanism displayed by the specimens and whether this is a truthful representation of the response of real buildings. The improvement of dynamic behaviour as consequence of strengthening is quantified through the level of amplification of the input signal at collapse (75% for unreinforced, 125% for strengthened specimens), the level of cracking and the displacements of the walls.

Table 2-1: Comparison of experimental assessment of connections as carried out by various authors

Sample		Scale	Materials	Connection configuration	Strengthening system	Load input	Source
Geometry	No						
C-shaped walls, 330 x 250 cm in plan, 344 cm high, 25 cm thick	3	1:1	Stone blocks and lime mortar	Unreinforced (scarce brick overlapping) and undamaged/ unreinforced and damaged (vertical crack and front wall tilted outwards)/ strengthened	Metallic cross-ties	Recorded Italian earthquakes scaled for increasing amplitudes	Al Shawa et al. (2009)
C-shaped walls, 184 x 83 cm in plan, 120 cm high, 15 cm thick. Openings are present	10	1:2	Adobe	Unreinforced/ strengthened	Corner ties, chicken wire (internal or external), timber ring beam, bamboo pegs and combinations of the above	El Salvador, 2011, scaled to match input frequency content and sample natural frequencies	Dowling and Samali (2006)
H-shaped walls, 570 x 125 cm in plan, 550 cm high, 25 cm thick. Openings are present	5	1:1	Brickwork with poor mortar	Unreinforced/ strengthened	Energy absorbers (RAG, SER and RETE)	Artificially generated dynamic input according EC8	Benedetti (2004)
H-shaped walls, 570 x 125 cm in plan, 550 cm high, 25 cm thick. Openings are present	5	1:1	Brickwork with poor mortar	Strengthened	Energy absorbers (RAG and RETE)	Artificially generated dynamic input according EC8	Benedetti (2007)
Masonry panels, 100 x 100 x 4 cm	9	1:3	Solid bricks without mortar	Unreinforced. Boundary conditions vary	-	Increasing monotonic point load	Zuccarello et al. (2009)
Masonry panels, 99 x 403 x 36.5 cm	2	1:1	Brickwork masonry with mortar	Strengthened by various systems	Steel ties, SMADs	Seismic input	Indirli and Castellano (2008)

Al Shawa et al. (2009) and Zuccarello et al. (2009) discuss experimental results in light of the correspondence with the numerical analysis developed on the basis of the shaking table test.

Even though all the publications above serve the purpose of experimental assessment and provide interesting results, the lack of any standard both in the test set-up and how the results are presented is a pitfall. Indeed, tests might be hardly applicable to other scenarios and do not allow for a direct comparison between different systems. Furthermore, it remains unclear how experimental results can be implemented in practice and incorporated in a design procedure.

Similar observations can be drawn by looking at shaking table tests on small-scale models of whole buildings, although in this case the variability in terms of the sample geometry is limited by the capacity of testing apparatus, which limit the weight and hence typology of tested mock-ups. Yet, a number of other testing parameters can be varied (e.g. input signal, materials, similitude laws), so that a considerable scattering is still present.

Among the studies that most focus on the characterisation of structural connections, it is worth mentioning the experimental campaign by Tomaževič et al. (1996) on four models of simple two-storey brickwork houses strengthened by cross-ties or by substituting the timber floor structure with reinforced concrete. Interestingly, the study shows that both cross-ties and r.c. slab have a positive effect on the global behaviour of the structure, which can be quantified by the increase of 2-2.5 times of the input energy by the shaking table and required to attain the same level of damage as for the unreinforced structure.

However, tests also show that the slab can have detrimental side-effect, especially when connection between the concrete element and the masonry wall are not sufficient. Indeed, damage due to the sliding motion of the r.c. slab was detected at the top level of the model.

Tomaževič and Klemenc (1997a) also carried out an experimental campaign on a four-storey brickwork structure to the purpose of investigating the effect of joint use of RC slabs and column-ties. Although the performance of the strengthened system exceeded the expected target, such technique is highly invasive and hardly applicable in a large number of historic structures.

A particularly extensive testing campaign of shaking table tests was performed by Benedetti et al. (1998) on a number of brick and stonework masonry specimens; specimens were first tested to damage and then repaired and strengthened by various systems of common use in current practice. Test models were specifically designed to reproduce two aspects critical to determine the response of masonry buildings to strong motions, namely the corner connections between orthogonal walls and the connection of the floor structure to the supporting walls. Again, experimental results show that traditional techniques, and in particular cross- ties coupled with load spreading elements, can be highly successful in enhancing the seismic behaviour of

masonry structures. Lateral resistance is increased by 1.2 after repair, input signals with peak accelerations double as high as for the unreinforced samples can be withstood, and the ductility of the structural system, as expressed by the coefficient q, is fully recovered after strengthening and in some cases improved. Most importantly, failure by overturning mechanisms is fully prevented, both in the case of brickwork and stonework specimens.

2.8 FINAL REMARKS

Structural connections are crucial to understand, predict and control the response of buildings to seismic excitation; indeed, it has been observed that damage and failure of historic structures during main earthquakes are related to discontinuous or low-quality connections among structural elements. The poor quality of original constructive techniques, as well as the deterioration due to weathering and previous seismic events, or the architectural modifications that are frequently carried out on monumental and residential buildings are among the main reasons for such weakness.

On-site findings are corroborated by analytical models, which correlate the boundary conditions of masonry panels to observed damage modes, thus ascertaining the link between connections and seismic-induced damage. Insufficient, weak connections lead to out-of-plane damage and overturning of parts of or whole masonry panels, which constitute a risk for safety and human lives, but also seriously endanger unique heritage assets.

Accordingly, current design codes recommend the strengthening of connections in heritage buildings with the purpose of improving the overall structural response. However, while the use of strengthening systems that enhance ductility is encouraged, strength-only elements are not only still allowed, but widely applied in practice. Whereas some, like r.c. ring beams, are being eventually abandoned in light of the reduced compatibility with historic materials, others, like metallic cross ties, are currently implemented and influence positively the dynamic response of structures, as they restore connections without increasing the mass. Yet, even these systems are not completely exempt from drawbacks, such as, for instance, pull-out failures.

These pitfalls could be avoided by using strengthening techniques able to provide a higher level of ductility; this would not only solve the problems connected to fragile failures, but would also allow a higher level of control on the performance of the strengthening elements, and hence the application of a performance-based approach. PBD aims to ensure a reliable, yet cost-efficient structural response for various levels of seismic excitation; dampers and dissipative elements allow controlling displacements and accelerations and can therefore be integrated in a multilevel design methodology in order to optimise the structural design.

In spite of the advantages they offer and of the success they enjoy in new structures, ductility and energy dissipation systems have gained little success in the field of conservation engineering. Few of these systems match the requirements specific to heritage buildings; furthermore, clear indications on how to test and design

strengthening systems for historic structural connections are missing from codes, even more so in the case of innovative techniques.

In the attempt to tackle such technical gap, two innovative anchoring devices have been developed and validated in the framework of conservation and performance based design, namely aiming to comply with the ICOMOS' principle of minimum intervention and the requirements of a multiple limit state approach.

The devices are designed as an add-on for metallic cross ties, and provide steel rods with extra ductility. In the following, the experimental, on site and computational validation of devices is described; besides the discussion of achieved results, importance is given to the description of the procedures whereby these are obtained. This not only ensures that the development of devices falls in line with the initial set of requirements, but also provides an explicit example of how an innovative strengthening system can be characterised and developed. Quantitative data as well as testing and modelling protocols are collated and commented, so as to create the basis for further modifications to the devices, for their validation under different boundary conditions, but also for the application of the same procedure to other strengthening systems.

To complete the validation process, a design procedure for the implementation of the devices is developed with the intent of providing both a practical tool and an example of the methodology through which experimental, computational and on-site data feed into structural design, in compliance with current design codes.

3 RESEARCH METHODOLOGY: DESIGN AND VALIDATION OF THE DISSIPATIVE DEVICES

3.1 INTRODUCTION

In the last decades, increasing knowledge and awareness of the effect of structural connections on the seismic behaviour of heritage buildings have been achieved through post-earthquake surveys and analytical studies. Accordingly, public and experts' attention has moved towards the development and application of strengthening techniques that might improve the performance of connection, thus protecting historic structures and their inhabitants from earthquake actions.

Traditional systems have been improved and, most importantly, innovative techniques that rely on ductility and energy dissipation have been tested and implemented in a number of case studies. Nonetheless, as it has been discussed in Chapter 2, the clear-cut that has characterised the shift from capacity-based to performance-based design of new structures has not affected to the same extent the research and the implementation in heritage buildings.

Indeed, very few dissipative systems are specifically designed for heritage buildings; as such, a large number don't comply with the criteria of minimal intervention, which are the very basis of modern conservation engineering (ICOMOS, 2003) and essential when dealing with historic structures. In fact, the main goal of the development of a dissipative device should not be the creation of something completely new, but rather the improvement of an existing strengthening techniques, which is already widely applied, familiar to the professional figures operating in the field of conservation engineering, cost-effective and in line with the current conservation practice.

As mentioned in §2.3, metallic cross ties have been successfully applied for many centuries, so much so that their modern counterparts still draw on the same principles (§2.4): reconnecting horizontal and vertical structures by means of thin metallic elements, thus restoring the box-like behaviour without adding excessive mass (Fig. 3-1). Beside the positive structural influence, metallic anchors have a number of other advantages, such as:

- Low aesthetic impact. As anchors have been used for centuries, new ones can be easily designed so as to match the appearance of those already on site or to clearly differentiate later interventions. Certain typologies rely on grouted elements rather than end plates and as such, they can be fully concealed in the masonry. Whichever the conservation approach, cross-ties are a common architectural element, which doesn't disrupt the aesthetic of the building;
- Readily available and inexpensive material. Steel is a common construction material and fairly inexpensive in comparison with others, like fibres.

Furthermore, steel is a material familiar to conservation engineering experts and this facilitates its use and success;

- If stainless steel is used, cross ties offer a good level of durability. If metallic elements are fully embedded in the masonry, they are in pseudo-passive conditions, protected from harsh environmental conditions. In case of elements with exposed parts, regular maintenance can be carried out easily and at a limited cost.

In spite of many positive features, metallic anchors can suffer local failures due to the higher stiffness of steel in respect to the surrounding historic material, so that punching and pull-out failures are not uncommon (D'Ayala and Paganoni, 2011), (Fig. 3-1). Localised failures are a considerable drawback, partly because they might hinder almost completely the positive effect that ties have on the structural response, but also because damage should be avoided as much as possible in historic substrata, so as to protect the original finishes and materials.

In light of the observation above, metallic anchors are taken as a starting point for further developments that aim to rectify typical pitfalls by use of ductility and energy dissipation (Fig. 3-1). The description of the selected type of anchor, among the various typologies available on the market, and the discussion of the reasons for this choice are presented in §3.2. The dissipative system to be coupled to the metallic anchors is chosen among the displacement-dependent systems described in Chapter 2, which are compared in terms of compliance with a set of requirements concerning structural dynamics as well as conservation issues.

The main design concept of the dissipative devices is that they should be able to accommodate small displacements between a masonry wall and the structural elements to which this is connected via the cross-ties. Such relative displacements are the consequence of out-of-plane excitation and frequently occur in heritage structures, as reported by various authors (da Porto et al., 2012; D'Ayala and Benzoni, 2012; Ingham and Griffith, 2011; Lagomarsino, 2012) and discussed in the previous chapters. In particular, the prevalence of out-of-plane damage mechanisms as surveyed by the author in the historic centre of L'Aquila after the 2009 earthquake (D'Ayala and Paganoni, 2011) gave impetus to the design of devices able to both address and exploit out-of-plane mechanisms.

It is worth highlighting that the strengthening of connections by standard systems is also a means to prevent out-of-plane failures and improve structural response; however, even leaving aside the problem of localised failures, "strong" connections are not exempt from drawbacks. Indeed, when overturning and tilting of walls is prevented and horizontal forces efficiently distributed, the in-plane resistance of walls is activated and in-plane cracking becomes the means whereby energy dissipation occurs (Senaldi et al., 2014; Magenes et al., NTUA shaking table tests as reported in WP9, NIKER, www.niker.eu). By doing so structural capacity and safety increase, thus making this option preferable to that of having "weak" connections; nevertheless, the resulting damage is not negligible, especially when preservation of architectural

features is pursued. This is one main reason for allowing a certain degree of ductility at the corner connections of masonry structures, rather than only proceeding to restoring/creating a box-like behaviour, at least for demanding seismic events. Prevention of local damage to the anchorage and the historic material is another desirable effect deriving from a ductile, instead of a highly stiff, connection.

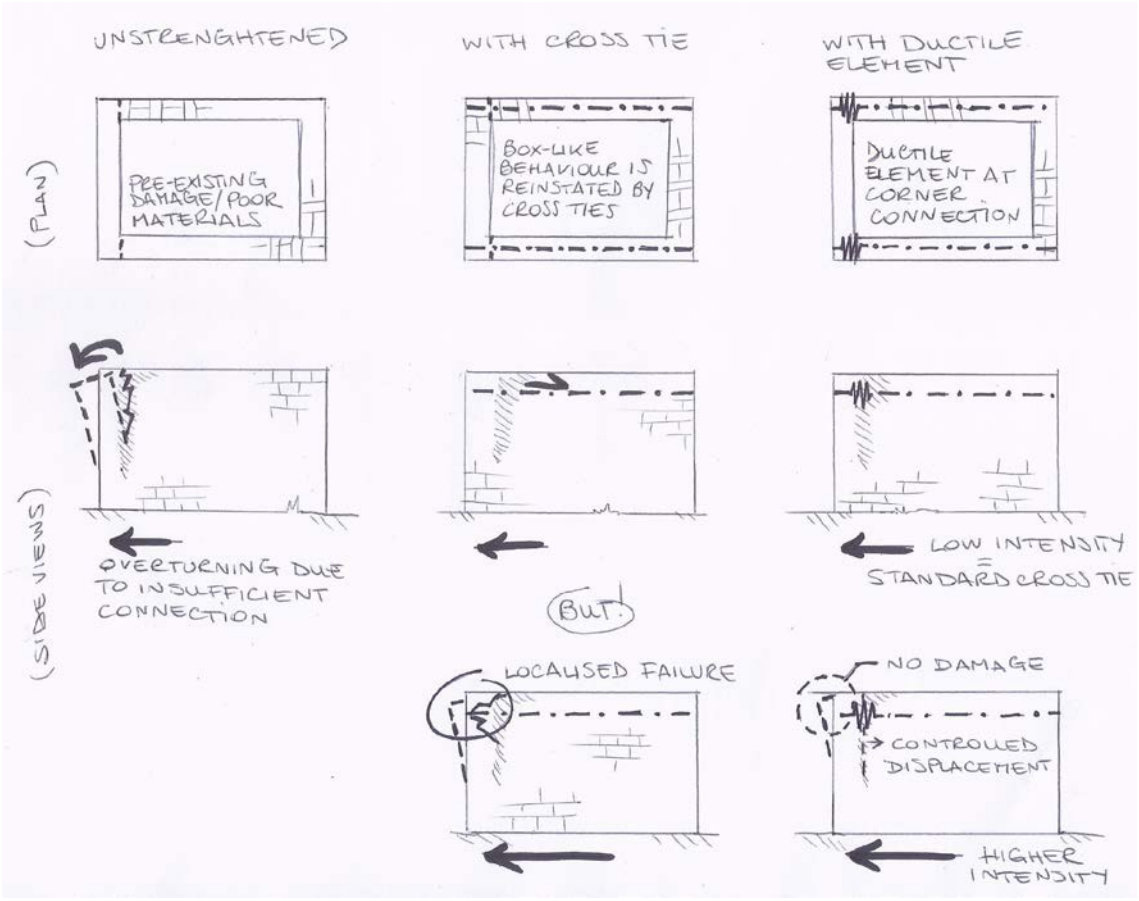

Fig. 3-1: Concept design of anchor dissipative device on the basis of damage typical of unstrengthened and strengthened by cross-tie masonry structures

The first requirement for the dissipative anchoring devices is the capacity to meet an attended level of allowable displacement and protect the structure in case of unexpected actions.

For yielding dampers, permitted displacements are bounded to a maximum value, depending on the shape of hysteretic loops and ultimate capacity of the device (Constantinou et al., 1998). Such restriction is not equally limiting in the case of SMAs, as superelasticity widens the range of allowable displacements and allows for a further increase of stiffness after the first plateau (Indirli et al., 2001 and 2008). Friction devices also offer a more flexible design, provided that the mechanical parts of the device and other structural elements are designed for the load associated to the target displacement.

The limitation of allowable displacements for yielding dampers could be overcome through the use of a series rather than a single device; nevertheless the increase in stiffness beyond yielding would remain the only safety margin offered to the structure in case of stronger earthquakes or after-shocks.

Furthermore, for yielding devices the amount of dissipated energy is directly proportional to displacements, i.e. to strains, which are connected to the length of devices. However, slenderness is also a cause of buckling. Conversely, friction devices can be designed to have an activation threshold lower than their buckling critical load, while SMADs can be assembled so that wires work in tension even when the device is in compression.

Another main requirement for the dissipative devices regards the optimisation and the stability of the supplied level of damping.

SMAs provide high damping and their hysteretic loops present a decreasing inclination of the unloading branch for larger displacements so that the dissipation of energy improves for larger amplitudes of movement (DesRoches and Delemont, 2002). However, for a certain level of displacements, subsequent cycles show a decreasing area; “training” of wires is indeed needed to ensure stable loops (Indirli et al., 2008). Friction devices are satisfactorily efficient since their behaviour is independent from the amplitude of cycles (Morgen and Kurama, 2008) and rectangular loops dissipate more energy than yielding cycles for the same amplitude and load peak (Constantinou et al., 1998; Pall, 2004). Nonetheless, a sufficient level of stability of the coefficient of friction for increasing number of cycles must be ensured.

SMADs are the only displacement-dependent dampers that naturally present self-centring properties (Indirli et al., 2008), whilst the other typologies have to rely on additional elements such as springs to avoid residual deformations (Constantinou et al., 1998; Nims et al., 1993).

However, SMAs are costly[1]: a kilogram of Nitinol alloy bars is worth roughly $78/125 or more, against the approximately $1.5/7 for stainless steel grade 304 bars. Furthermore, the complex physical behaviour of these alloys has not been much modelled as far as their structural application and performance go, so that few specific software can be used for numerical analysis involving SMAs. These two issues cannot be overlooked when attempting to develop a strengthening system that should be both readily available and such that conservation engineering professionals feel comfortable using it.

Therefore, yielding and friction devices are eventually selected for this project: a frictional element seemed the most promising in terms of achievable performance and the most viable in terms of realisation and use. On the other hand, the hysteretic device offer the advantage of being less complex and therefore a good term of

[1] Figures are taken from commercial website Alibaba.com as reference to exemplify the rough difference in prices at the time when the webpage was last accessed (20/01/2015)

comparison to assess the behaviour of the frictional device, also in respect to a standard anchor.

In the following the design and development process of both devices will be shortly outlined. As prototypes are still under development and one typology is protected by patent (James et al., 2012), descriptions are limited to the level of detailing sufficient to provide a background to the results that will be presented later on. A brief overview of the steel anchor used as starting point for the development of the devices is also provided, as this is also essential to comprehend the design of the devices.

3.2 THE GROUTED STAINLESS STEEL ANCHOR

At the current state of the art, different types of metallic structural anchors are available on the market: products range from coil profiles to steel elements embedded in grout or resin.

This research project has been carried out selecting one specific type of anchor, by involving Cintec International Ltd, Newport, a company that manufactures, distributes and installs anchors, in a joint venture with the University of Bath and by seeking funding through two research grants: a Knowledge Transfer Partnership (Partnership No 6842) and a FP7 project (the NIKER project, Grant Agreement No 244123, http://www.niker.eu).

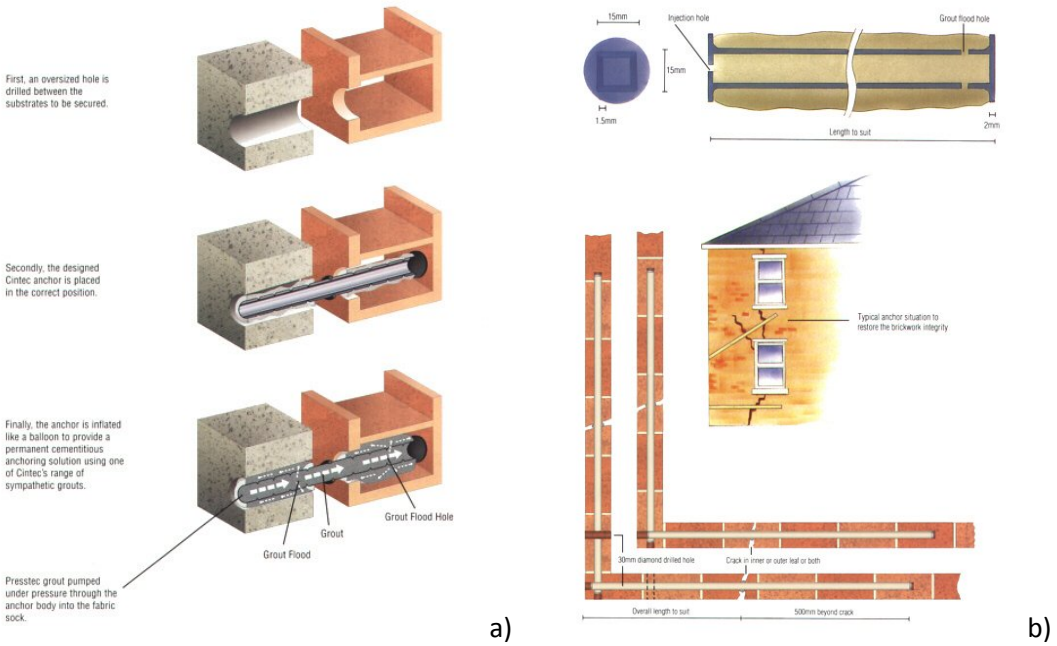

a) b)

Fig. 3-2: Cintec's anchors: a) grout injection and bond development; b) layout. Courtesy of Cintec Ltd.

Cintec's production consists of a range of patented anchoring systems made of a stainless steel profile installed within a cavity drilled in the wall and embedded in grout. The company's patented system includes, beside the steel section, a mesh fabric sleeve. The sleeve is wrapped loosely around the steel rod and expands as grout is

injected into it under low pressure, thus moulding into the shape and spaces within the walls, providing a mechanical as well as chemical bond (Fig. 3-2a).

Metallic end plates are attached at the end of the metallic profile, so as to increase the pull-out capacity of the steel element in respect to the grouted element.

Cintec's anchors are used for the repair of a variety of structures, damaged as a result of subsidence, earthquake or general wear and tear. Short anchors can be used to connect the wythes of masonry in the direction perpendicular to the wall plane, whereas long anchors are embedded along the length of the wall (Fig. 3-2b), thus strengthening corner connections and stitching wall cracks.

This typology of anchors doesn't need front plates, like in the case of standard cross-ties, as load is transferred by shear and bond at the interfaces steel/grout and grout/masonry rather than through the compressive action of the front plate. Additionally, the fabric sleeve restrains the flow of grout preventing leakage that might affect paintings or other precious architectural features.

The system is highly flexible as:

- Steel sections can be chosen among a wide variety: the company catalogue offers square and circular hollow sections, rebars and studded bars. This gives the opportunity of creating different types of connections to any extra element, such as brackets, turnbuckles or the dissipative devices;
- Although anchors are generally grouted along their whole length, the geometry and layout of the fabric sleeves can be changed so that only parts of the anchors are embedded in grout, while others are left dry. This is an important characteristic for two reasons:
    - Flexible grouting allows for the transfer of forces between device and parent material to occur at the locations and over the lengths chosen by the designer. This is an important feature when working with multileaf masonry, with different level of cohesion and shear capacity
    - The relative displacements that the dissipative devices will experience during seismic action are not compatible with the fact of having a full grout embedment;
- Moreover, the possibility of modifying the layout of fabric sleeves means that the system can still have a front plate and work like a standard cross tie, thus adjusting to different conservation approaches and to the needs of diverse applications;
- On the other hand, the fact that the anchor is grouted reduces the deflection length, thus decreasing the likelihood of instability phenomena, which might interfere with the functioning of the dissipative devices beyond the small-strain regime. Hence it does not require post-tensioning.

In light of these characteristics, Cintec's anchors were selected for coupling with the dissipative devices. In particular, it was decided to use threaded bars for the ease of

substitution in case of damage and the availability of off-shelf connectors and adaptors to accommodate different size bars and dissipative devices.

The company installs threaded bars with sizes between M10 and M42; M16 are taken as reference for the development of the devices as, in the company's experience, this is one of the most common bar sizes for interventions on masonry buildings in seismic prone areas. Bars are AISI 304 (EN 1.4301) stainless steel, class 70 (yield proof stress 450 MPa, ultimate tensile strength 700 MPa).

3.3 THE HYSTERETIC DEVICE

The hysteretic device consists of a hollow stainless steel profile (Fig. 3-3) and was carefully devised so as to have a lower capacity in the central portion, where tensile stresses concentrate, thus bringing the section to yielding. The ends of the device are instead designed to have a higher capacity, so as to avoid failure at the connections with the anchor threaded rods.

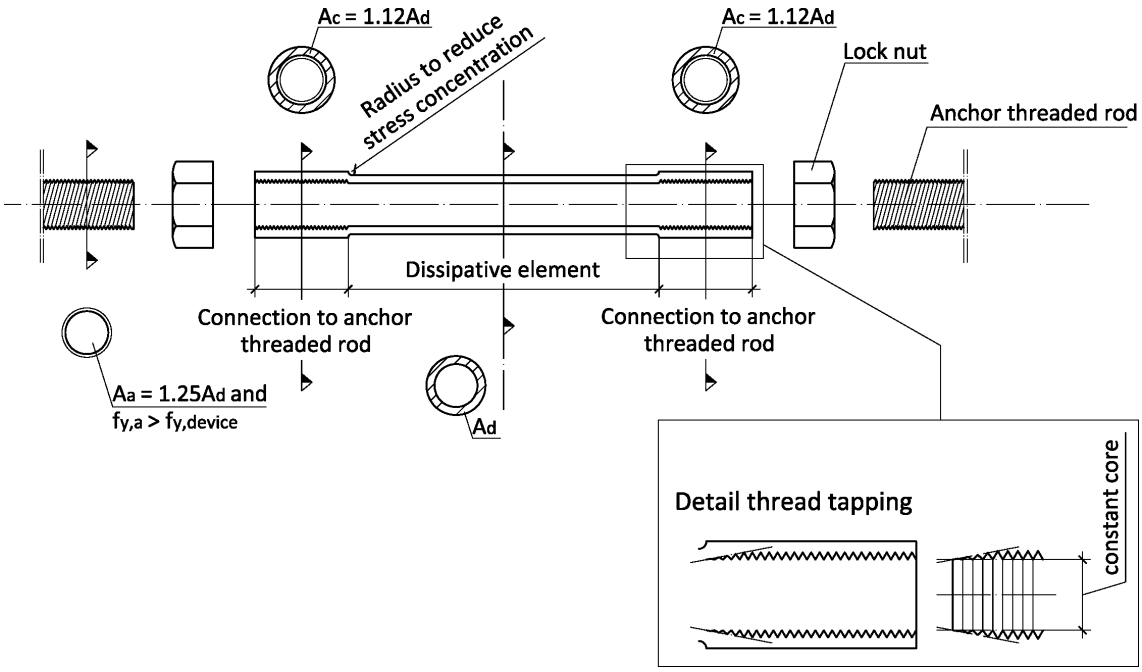

Fig. 3-3: Geometry of hysteretic dissipative device

Such difference in capacities is achieved both by controlling the ratio between the cross sectional areas of the various parts of the assembly as well as by using different steel classes for the dissipative element and the anchor rods.

The walls of the central part of the dissipative element are cut thinner, so that the cross sectional areas is lower than that of the connections, even though these are internally threaded. Furthermore, the hysteretic device is made of stainless steel AISI 304, class 50 (yield proof stress 210 MPa, ultimate tensile strength 500 MPa) and has therefore a yielding strength 40% lower than the threaded rods. Stainless steel is used

both for the anchor and for the dissipative device, so as to ensure high durability and avoid corrosion issues triggered by the coupling of different metals.

The use of a hollow section, rather than a solid section, ensures a higher buckling load, for the same direct tension yielding capacity, hence increasing the safety against buckling and a wider equivalent range of capacity.

The final design of the device, as presented in Fig. 3-3, is the result of a number of trial tests (Paganoni, 2009), which are not reported herein for expedition reasons, but were functional to refining geometry and design details, such as radiuses and tapping, class of materials, and anodization. During the design development and trial tests various systems aiming at perfecting the coupling of the two parts were investigated, taking in due care the differences in material capacity as well the modest flexibility in the geometry of the parts.

3.4 THE FRICTIONAL DEVICE

The design of the frictional device draws on the well-known Coulomb equation of friction (Fig. 3-4): a perpendicular force, $F_{\perp}$, applied to a stack of plates, generates friction among the parts when these move relative to each other. Plates are able to slide one onto the others only when the applied force acting in their own plane, $F_{//}$, exceeds the static friction force. Once motion has been initiated, the reaction force in the restrained plates is equal to the applied $F_{//}$ minus the kinetic friction force.

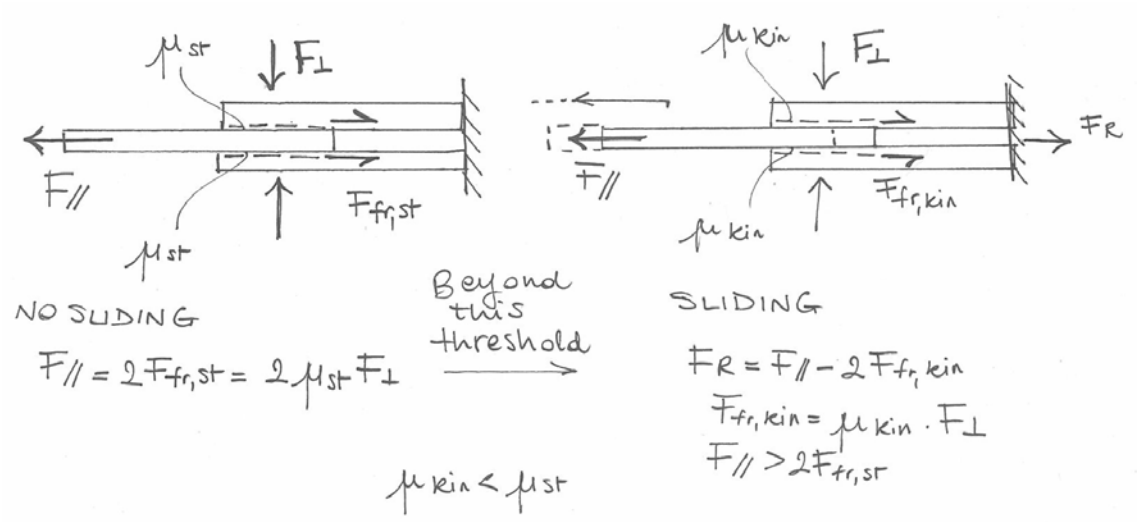

Fig. 3-4: Physical principle of frictional device

In practice, this is achieved by means of three steel plates (Fig. 3-5): two are coupled by means of a steel block, which also acts as connection to the anchor threaded rod. This pair of plates acts in compression on a sliding element, thus generating friction; the level of perpendicular force, $F_{\perp}$, is controlled by means of a set of bolts. Even in this case, the detailing of the device is the result of a number of design iterations informed by trial tests; for instance, the slots of the frictional plates aim to maintain

the alignment of parts and have been designed in response to the mechanical buckling observed during the initial development phases.

The whole frictional device is made of the same stainless steel of the anchor rods. The large majority of frictional dampers and isolators available on the market feature an additional layer of material, which has the specific purpose of improving the frictional behaviour by stabilising the value of the coefficient of friction and avoiding issues connected with the fast wearing of materials, mechanical locking and so forth.

During the development of the frictional device, the option of adding a coat or layer of frictional material was considered, but eventually ruled out, at the current stage, on the basis of the following motivations:

- The higher risk of corrosion deriving from coupling different metals, like a thin layer of metal with higher friction coefficient (e.g. copper or lead) between the stainless steel frictional plates and the sliding element;
- The higher machining complexity, and hence higher costs, involved in sourcing, designing, and machining a device including a layer of graphite or polytetrafluorethylene (PTFE), which are frequently used because stable under a large number of cycles.

This choice does not hinder the proof of the concept, which is the main goal of the project; nevertheless, its impact will be discussed in detail on the basis of the experimental results presented in Chapter 4.

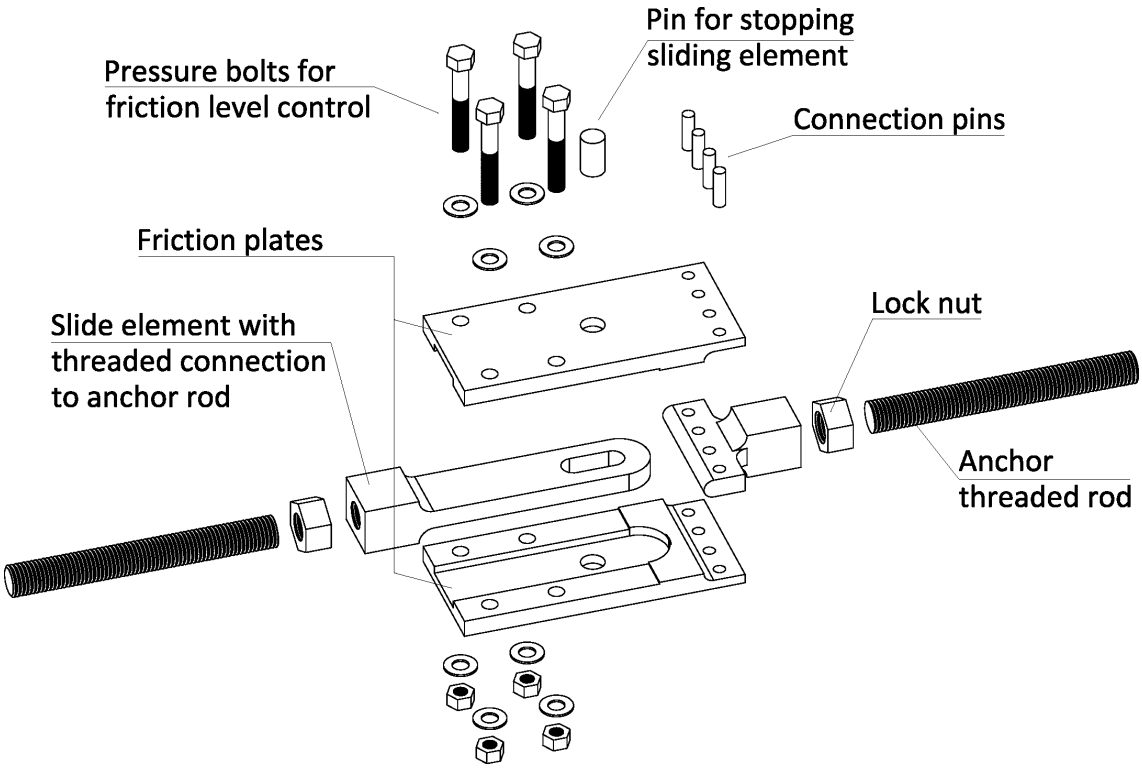

Fig. 3-5: Geometry of frictional device as patented by Cintec International Ltd.

3.5 VALIDATION METHODOLOGY

The overall validation process, although functional to the creation of devices that might be later on refined and commercialised, mainly aims to prove that the concept of a dissipative element in series with a metallic cross ties is feasible and can target a number of issues typical of currently available strengthening systems.

Furthermore, the process in itself provides a reference point for the development and validation of strengthening systems in general; indeed, in spite of the peculiarities of the dissipative anchoring devices, the implemented procedure refers to concepts, guidelines and methodologies that are generally applicable in the field of conservation and seismic engineering, although not fully standardised and codified.

As already stated in the introductory chapter, what miss from the field of conservation engineering is not only innovative, ad-hoc strengthening techniques, but also clear guidelines ruling how these systems should be validated and designed. Therefore, aside the novelty of the concept proposed herein, the thesis strives to fully investigate a validation and design methodology. What is needed to characterise a strengthening system? How is information obtained and collected in fashion useful to further elaborations? How are the stages of the validation process interconnected? How can the output of the validation process be linked with code prescriptions and implemented in a design procedure? Giving an answer to these questions is one main goal that will be pursued in the following chapters.

The description, as well as presentation of an example of the procedure for the design of the dissipative anchoring devices is the conclusion of the thesis, and most importantly, the completion of the whole process that is the object of the dissertation. Providing design guidelines is, firstly, the proof that the dissipative devices have a potential for being implemented in real case studies, since they comply with code requirements both from a conservation point of view and in terms of structural performance and life safety. Secondly, the procedure represents the merging point of the assessment process, where the output of the validation stages eventually feeds.

The preliminary tests that brought to the final design of the dissipative devices are reported in previous publications (Paganoni and D'Ayala, 2009); the three validation steps:

1. Experimental tests;
2. On-site application to a case study;
3. Numerical modelling.

are firstly outlined in the following, and then analysed by discussing its outcomes in the relevant chapters.

3.5.1 Experimental Validation

As discussed in Chapter 2, experimental validation is a first, and highly crucial, step that researchers and producers follow to assess the performance of current and

innovative techniques for structural strengthening, and to tune products' performance to code requirements or ad-hoc specifications.

It has also been discussed how a considerable gap exists between products for new-built and for already existing structures, especially if these fall in the category of heritage buildings. The technical gap regards the standardisation of both the product requirements, and the procedures for their assessment and design, but it affects various types of strengthening systems to different extents. For instance, in spite of its relatively recent application to the field of civil engineering, fibre reinforcement has already been investigated to the point that design guidelines for the retrofit of both c.a. and masonry have already been published, and are periodically reissued to ensure that prescriptions match the latest market developments (CNR-DT 200/2004, CNR-DT 200 R1/2012). Far more traditional systems, like cross-ties, are less considered at code level and dimensioning is generally left to the rule of thumb and to the design skills of practitioners.

The dissipative devices developed in this research project constitute an ambiguous case: on the one hand the technique relies on standard grouted anchors, which are not thoroughly regulated at least as far as masonry substrata are concerned. On the other hand, the devices are comparable to dampers, these being provided for by both the European prescriptions for anti-seismic devices (BS EN 15129:2009) and Part 3 of Eurocode 8 (EN 1998-3:2005). It is therefore debatable how the devices should be tested and what protocol should be followed.

In fact, neither EN 15129 nor Eurocode 8 specifically addresses the issue of dissipative and ductile systems for the strengthening of heritage buildings: the former regulates the validation process needed for the production and sale of anti-seismic devices, the latter provides qualitative indications for their applications in structures.

Nevertheless, the use of codified and standard experimental procedures is of capital importance to ensure repeatability of tests through several sets of specimens and to achieve results that can be comparable to other typologies of specimens and strengthening systems. Accordingly, the approach followed herein is to apply existing guidelines as far as possible, and integrate missing parts by relying on the technical literature and creating a parallel with similar case studies.

As far as the characterisation of the devices in the isolated configuration is concerned, procedures described by EN 15129 are relevant and generally applicable. The testing protocol is adapted to the specific needs of the research project, which pursues the full characterisation of the devices, rather than the extensive validation of devices designed to meet a set of requirements for a specific commercial application. The modified procedure, as well as the experimental outcome, are detailed in §4.2 of Chapter 4.

Tests in the isolated configuration, however useful in tuning the response to different scenarios, cannot represent the behaviour of devices when embedded in a masonry substratum. Historic parent materials generally feature low mechanical properties and,

therefore, tend to be the weak link when retrofit by new construction materials is carried out.

Additionally, the experimental characterisation of the dissipative devices embedded in a masonry sample can be meaningful only if an adequate term of comparison is used. As stated in the introduction, dissipative devices aim at tackling the drawbacks typical of standard steel anchors; the extent of this improvement can be quantified only when the performance of standard and dissipative anchors is tested in similar conditions. Furthermore, considering the complexity of the behaviour of historic materials, testing standard anchors allows for checking that the chosen experimental procedures are suitable. Indeed, common mechanisms of failure of standard anchors are known from the literature; if the testing set-up can recreate those, the validity of the assumptions used in the laboratory environment is also substantiated.

Accordingly, pull-out and cyclic tests are carried out to analyse the behaviour of a connection between two vertical elements, i.e. walls, strengthened by steel anchors. The focus is on the performance of the connection element, namely the anchor, as stand-alone or coupled with the dissipative devices, and the damage of masonry panels as consequence of horizontal loading.

Pull-out tests offer the advantage that only one structural element of the two present in a connection, i.e. only one of the two walls, has to be built; this simplifies the test set-up, the loading apparatus and measuring equipment. Accordingly, they are suitable for the first assessment of the devices in presence of a substratum.

Specific design codes for anchors in masonry substrata are completely missing from the existing technical literature; therefore, for the sake of homogeneity with the current code of practice, the same principles as pull-out test of anchors in concrete substrata (EN 1881:2006) and of masonry bed-joint reinforcement (EN 846-2:2000) are applied. However, greater attention is given to phenomena and requirements specific to historic masonry, such as the influence of a non-homogeneous substratum on the modes of failure and the importance of damage limitation. Indeed, it is worth noticing that historic masonry is frequently composed by various materials and different wythes, which might or might not be interlocked and may contain loose infill. This contributes to give historic masonry a far more complex behaviour than homogeneous materials like concrete, and should be taken in due consideration when dealing with heritage structures. The influence of the substratum and of the type of anchors chosen for the testing campaign, experimental results and possible amendments suggested for the improvement of the procedure are described in §0 of Chapter 4.

As the pull-out test set-up doesn’t reproduce a full corner connection, it can only partially represent the overall response of a strengthened masonry subsystem. Moreover, pull-out tests are carried out in monotonic load regime, this clearly being a considerable simplification in respect to the load input experienced by a structure during an earthquake.

Hence, cyclic tests on subassembly of T-shaped masonry connection are carried out to supplement the outcome of pull-out tests. No code prescription exists for similar tests, which are therefore devised drawing on the experience acquired during the pull-out campaign and on the technical literature, as described in §4.4.

The three testing sessions are performed with the objective of fully assessing the performance of the devices, as well as of identifying a set of parameters useful for the development of the design procedure that will be extensively discussed in Chapter 7. Results presented in the relevant chapter are commented in the light of such goals, although attention is also given to the details of the test set-ups, which are provided to the purpose of exemplifying how to proceed to the methodical assessment of strengthening systems for heritage structures in case prescriptions are missing from current codes.

It is worth highlighting that experimental validation as reported in the technical literature frequently includes large scale testing, i.e. shaking table tests on a full structure or at least on a structural sub-assembly, while these are missing from this research project. In fact, an ad hoc European-funded project was set up to carry out dynamic test on a scaled model of masonry building, in both the unreinforced and strengthened configurations (Paganoni and D'Ayala, 2012). Unfortunately, due to a number of technical and financial reasons, the project has not brought sufficient results to contribute to the thesis. Nonetheless, thanks to the positive outcome of on-site and computational validation, missing experimental information is otherwise sourced. Whether the lack of shaking table tests has impacted on the validation process and to what extent will be commented in Chapter 8.

3.5.2 On-Site Validation

Following the experimental assessment described in Chapter 4, one prototype of the dissipative anchors underwent on site validation by installation in a case study building within the framework of the FP7 NIKER project.

The on-site validation aims to provide further insight into the performance of the anchor in the uncontrolled environment of a real heritage structure. While laboratory assessment offers the opportunity of choosing a set of meaningful loading inputs to study the response of the devices, their implementation in a case study gives a full picture of the unforeseen parameters that might affect their performance and hence their suitability as a strengthening technique for heritage structures.

The prototype is installed in a purposely chosen location where pre-existing damage and site conditions are likely to cause small relative movements at the connection between two structural elements. These should trigger a response in the anchor, thus allowing the assessment of its behaviour in a number of real-life scenarios. In particular, the case study is selected to feature clear out-of-plane damage of one wall of a corner connection, as this is the typology of damage mechanism that the dissipative anchoring device mainly aims to prevent and control. Furthermore, the connection is chosen so that the damage has dimensions and extent compatible with

the implementation of one single anchoring device. It is expected that the anchor behaves in a fashion similar to that observed during the experimental campaign, depending on the intensity of the forces acting on it.

Adequate instrumentation must be implemented to quantify and record environmental and physical parameters influencing the structural connection as well as the anchor performance. Therefore, the in-situ validation must combine two different aspects: strengthening by a dissipative anchor device and monitoring of the device and surrounding structure.

Structural Health Monitoring (SHM) is normally defined as a set of techniques and methodologies to quantify damage and observe its evolution during time. It is traditionally divided in global and local monitoring (Chang et al., 2003). Global monitoring aims to determine whether damage has occurred and at what rate it is progressing by working on macro-elements or on the building in its totality. Local monitoring studies damage at specific locations.

Long-term global monitoring of pseudo-static phenomena, such as temperature gradients and stress concentrations as result of static loads, is implemented in historic-valuable buildings to check their health on a continuous basis and decide whether strengthening is required (Binda et al., 1997). This type of monitoring can be carried out by means of fairly simple devices, e.g. extensometers placed in correspondence of main cracks, and with a low acquisition rate.

However, global SHM is also crucial when dealing with dynamic phenomena or damage scenarios where the identification and screening of damage are not as straightforward. In new built, global monitoring aims to pinpoint damage and to follow its evolution by identifying variations in natural frequencies, modal shapes and curvature of the modal shapes as consequence of long and short term damage (Chang et al., 2003; Doebling et al., 1996; Rainieri et al., 2011). To this purpose, recordings of the vibrations induced in a structure by ambient vibrations, seismic tremors or artificially applied excitations must be acquired through high-rate sensors. The output of the dynamic structural identification can feed into the development of complex computational models, which are then used to simulate further scenarios, e.g. future seismic events likely to occur in the area.

This methodology is currently applied to study the evolution of damage in historic buildings too (Antunes et al., 2012; De Stefano and Clemente, 2006; Ramos et al., 2010), especially in seismic areas (Jaishi et al., 2003) and in the aftermaths of major seismic events (Gattulli et al., 2013; Russo, 2013) so as to establish the damage mechanisms and inform restoration and repair works. One main difficulty of SHM of heritage structures is that, while civil engineering structures such as modern bridges or tall buildings, can be described as an elastic continuum, with a clear set of fundamental period and higher harmonics, which determine a clear set of vibration modes, the same cannot always be said for historic structures, where local modes might be more important than global modes, due to poor connections among macroelements, thus

considerably complicating the task of analysing the structural response (De Stefano and Clemente, 2006). Towers and large domes or vaults, because of their regular, simple shape, constitute an exception, as their deformability is well captured by dynamic identification (Ceriotti et al., 2009; Gentile and Saisi, 2006).

As global monitoring mainly provides an overview of the structural behaviour, but doesn't define localised phenomena, a number of other techniques, such as ultrasonic waves or eddy current techniques, can be used to study in detail damage patterns, construction technique and materials (Chang et al., 2003). This information is also essential to complement and support the dynamic identification of buildings through monitoring; for instance mechanical characterisation of material is critical to the development of reliable FEMs. Non-destructive (Binda et al., 2003; Binda et al., 2007; Valle et al., 1998), slightly destructive (ASTM C1196, 2009; ASTM C1197, 2009; Binda et al., 2000) and destructive techniques (Baronio et al., 1999; EN 1052, 1999; Müller and Weise, 2008) can all be applied to investigate materials and stress fields.

As highlighted by de Stefano and Clemente (2006), only the joint use of a number of global and local techniques can overcome the uncertainties intrinsic to heritage structural systems, such as the irregularity of materials and complexity of damage patterns. Techniques must be chosen case by case, so as to accommodate both the necessity to collect sufficient data and the need to avoid invasive interventions and sampling.

The on-site validation of the yielding dissipative anchor device also requires a mixed approach in terms of monitoring techniques. As on-site measurements aim to quantify the behaviour of an anchor device embedded in a specific position of a historic building, the monitoring focuses on localised phenomena. However, the investigated parameters are not only specific to the quality of the masonry and its mechanical properties, but also relate to the pseudo-static and dynamic phenomena occurring at the structural connection of a historic building. Both low and high-rate phenomena can be critical: long term evolution of cracking as result of variations in temperature as much as rapid movements due to tremors can affect the structural system and hence trigger a response in the anchor device. Furthermore, although the monitoring can provide information regarding the evolution of damage, the main goal is to determine whether the device is performing as expected. Therefore monitoring must focus on the strengthening itself, this being unusual for HSM, where more attention is normally paid to the global performance of an unstrengthened/strengthened structure.

The instrumentation and monitoring system implemented on site have been designed so as to be comparable to the instrumentation used during the experimental validation and to allow for cross-correlation of results. This means placing a number of sensors that can record strains and loading of the dissipative device components, in a pattern consistent with the instrumentation used in the laboratory tests.

At the same time, the instrumentation set-up draws on the current know-how in the field of SHM as reported by the technical literature, so as to be functional to the goal

of detecting the structural events that determine the response of the dissipative device. Foreseeable events include, for instance, settlements and microtremors; hence, the system needs to include a number of sensors able to record relative movements – vertical and horizontal, out-of-plane and in-plane– typical of kinematic mechanisms resulting from such events. This can be achieved by complementing the information coming from the sensors located directly on the anchors with other sensors that detect accelerations and movements in different directions and are installed on the masonry adjacent the anchoring device.

It is worth highlighting that, if the pilot installation proves successful, the instrumented prototype could be further developed as integrated system for both strengthening and monitoring damaged connections in the aftermaths of seismic events. Such a technique could provide precious information for devising the repair/intervention strategy and at the same time could offer a strengthening system, even just temporary, for damaged connections. The concept is not fully developed herein, yet its feasibility is probed on the basis of the results of the installation of the first prototype.

As much as experimental validation, Chapter 5, which deals with on-site assessment, aims to identify a set of meaningful parameters that control the response of the anchoring devices and quantify them so as to inform the development of a design procedure, which is extensively discussed in Chapter 7.

3.5.3 Computational Validation

Experimental and on-site validations allow gaining insight into the mechanics of the dissipative devices and studying their response to a range of artificial and environmental inputs. In the framework of a validation process finalised to the development of a design procedure, results discussed in Chapter 4 and 5 contribute to identify and quantify the parameters that control the device performance and that can be varied to find the correct balance between structural demand and capacity.

Nevertheless, experimental and on-site assessment cannot be regarded as exhaustive. In order to define structural actions as well as to fine-tune the design of a strengthening intervention, structural codes such as DPCM 2011 require analysing the dynamic performance of a structure both before and after the implementation of the chosen strengthening system, so as to optimise the intervention and minimising its impact. Such task is not trivial and the support of computational models is unavoidable, especially when one wants to properly accounts for load and material non-linearity typical of heritage structures undergoing seismic actions.

Numerical simulations offer the possibility of carrying out parametric studies and vary a large number of boundary conditions, materials and inputs, so as to efficiently compare a number of scenarios, as required when performing a multilevel performance design. However, computational modelling of a whole structure implies the ability of simulating the response of the strengthening system and its interaction with the construction materials/structural elements.

From the point of view of the dissipative devices, this means that, although their performance is known through the research described above, their implementation in heritage structures still depends on the possibility of predicting their influence on a specific structure undergoing seismic actions. As the thesis aims to complete the validation process by defining a design procedure for the devices, it is crucial to develop a suitable numerical model to simulate and predict realistic scenarios.

Different modelling approaches are suggested by DPCM 2011, as well as by Eurocode 8 (EN 1998:2005); indeed, both provide for linear as well as non-linear modelling techniques. Prescriptions are detailed and well-articulated: section 4.3 of EN 1998-1-1:2005 gives guidance on the input to use, the applicability of each method, the procedure to follow and so forth. DPCM 2011 even describes a set of simplified models for the preliminary large-scale assessment of heritage structures depending on their typology.

However, codes mainly deal with models of whole structures and do not give as much insight into subassemblies and connections between them. For instance, DPCM 2011 acquiesces to limiting modelling to macroelements or parts of the structure when strengthening is applied only to a defined portion of the building. However, the code doesn't specifically refer to connections, or to boundary conditions. This means that, if one wished to assess a connection in the existing configuration and compare it against the response in the strengthened set-up, boundary conditions would have to be derived from a larger model including the entire building.

Additionally, the fact that the code prescribes the use of numerical models entails that the designer already possesses all the input data necessary to run the analysis purely relying on the output of the model. This of course requires expertise on part of the designer and possibly a number of other case studies or data from the literature that can be used to aid the process. However, the occurrence of these conditions is not given, especially considering the variability intrinsic to historic materials.

Accordingly, experimental work is generally the preparatory step whereby input data, such as material properties, is sourced and modelling hypotheses are verified. Indeed this is the case for some of the experimental work referenced in §2.7 and other publications (e.g. Tomaževič and Klemenc, 1997b; Cuomo et al., 2006).

The same methodology is adopted in Chapter 6: a set of Finite Element models is developed by Autodesk Autodesk Algor Simulation Simulation © software. Modelling proceeds from lower to higher level of complexity, i.e. at first only considering the strengthening elements and then progressively incorporating more and more elements of the connection and of the structure, in line with the methodology followed during experimental and on-site assessment. This process aims to create robust models, but also to identify a satisfactory level of approximation, whereby the behaviour of the devices is correctly simulated, but the computational burden is kept within limits. While undergoing calibration, models are able to provide additional information

regarding phenomena that were not measured during the previous phases of validation, such as the overall distribution of strains in the devices.

Upon completion of modelling, it is possible to collate all results in a design procedure, and prove by computational analysis that devices are suitable for the strengthening of heritage structures in seismic prone and that the assessment methodology illustrated in the thesis can be used as guideline for the validation of new strengthening systems for structural connections.

4 EXPERIMENTAL VALIDATION

4.1 INTRODUCTION

As already outlined in the previous chapter, the experimental validation of the anchoring devices consists of three experimental campaigns.

The first focuses on the dissipative devices as isolated elements and investigates their response to a number of loading input. The campaign draws on the prescription for damping devices of EN 15129 and aims to identify and quantify all the parameters that control the performance of the devices.

A second experimental campaign deals with the behaviour of stainless steel anchors embedded in a masonry wall and undergoing a pull-out load. Such set up reproduces one half of a corner connection experiencing horizontal loading and allows observing the performance of anchors, both in the standard lay-out and in series with the anchoring devices, when coupled to a weak, historic-like substratum.

Finally, anchors and anchoring devices are installed in a set of T-shaped walls and are tested under pseudo-static, cyclic load, so as to simulate the behaviour of a full connection and complement the results of the pull-out tests.

Experimental campaigns are presented and commented giving relevance to the test set-up as well as to the relevance of results to the goal of creating a design procedure.

4.2 TESTS ON ISOLATED DEVICES

4.2.1 Experimental Procedure and Test Set-Up

For the characterisation of the dissipative elements in the isolated configuration, specimens of the devices connected to threaded bars screwed at both ends are inserted in a push and pull apparatus and undergo a number of loading sessions, according to the programme summarised in Table 4-1.

Besides monotonic and cyclic tests, displacement time-histories are used as input for tests on both types of devices (Table 4-1). The input signal is generated via a simplified Finite Element (FE) model of a two-storey masonry residential building created with Audodesk Autodesk Algor Simulation Simulation ©. By doing so, the following phenomena can be taken into account:

- Anchor ties are used at the upper level of buildings; therefore, they are subjected to the amplifications of the structure responding to the ground motion.
- Anchoring devices are installed at the connections of perpendicular walls, where damage is likely to occur or already exists. Cracking causes adjacent structural elements to behave independently, so that the cross-tie experiences a push-and-pull action proportional to the relative

displacements of the two structural elements rather than to the earthquake motion.

Table 4-1: Summary of testing campaign

		Hysteretic	**Friction**
Monotonic		Static tensile test to failure	Impact tensile test to failure
Pseudo-static cyclic	**Type of input signal**	Sinusoidal	Sinusoidal
	Frequency [Hz]	0.01	0.01
	Amplitude [mm]	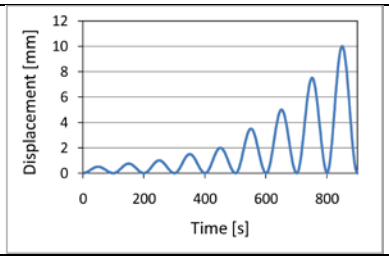	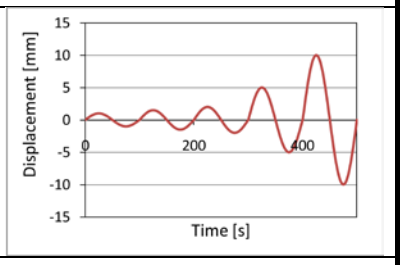
	Number of cycles	One per amplitude	One per amplitude
Dynamic cyclic	**Type of input signal**	Sinusoidal	Sinusoidal
	Frequency [Hz]	0.1, 0.5, 1	0.1, 0.5, 1
	Amplitude [mm]	0/+1.25	-5/+5
	Number of cycles	10 per frequency	10 per frequency
Time-history	**Type of input signal**	FE output: relative displacement at top of corner connection of masonry structure undergoing L'Aquila 2009 earthquake (ITACA)	FE output: relative displacement at top of corner connection of masonry structure undergoing L'Aquila 2009 earthquake (ITACA)
	Frequency content	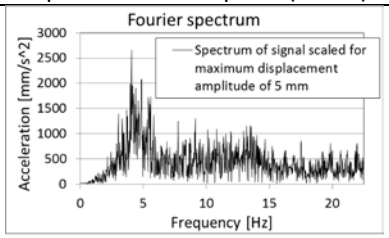 E.g. of signal frequency content	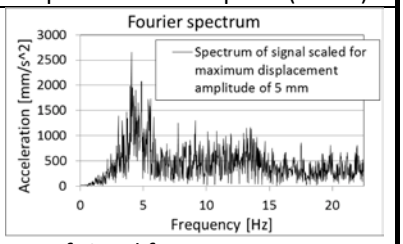 E.g. of signal frequency content
	Amplitude [mm]	FE signal is scaled to maximum amplitude of 1.25, 2.5 and 5 mm	FE signal is scaled to maximum amplitude of 1.25, 2.5, 5 and 10 mm
Fatigue	**Type of input signal**	-	Sinusoidal
	Frequency [Hz]	-	0.5
	Amplitude [mm]	-	-5/+5
	Number of cycles	-	300

Geometry, distribution of mass and stiffness, and material properties of the FE model (Table 4-2, Fig. 4-1) are chosen so as to be representative of a class of historic residential buildings. The structure is assumed to damage by detachment of the top halves of the solid walls from the side walls, according to on-site observation of recurring out-of-plane damage mechanisms (D'Ayala and Paganoni, 2010). Cracking is simulated by disconnecting the sets of walls along a vertical line and defining a cylindrical hinge at half height of the solid walls. The input signal used is L'Aquila 2009 mainshock, as recorded at the station of L'Aquila - Valle Aterno - Centro Valle, station code AQV (ITACA http://itaca.mi.ingv.it/ItacaNet/CadmoDriver). The recorded signal is applied in the direction perpendicular to the solid walls. The difference between the displacements experienced at the top of the two disconnected walls is scaled for different magnitudes of peak displacement (e.g. max. 5 mm as shown in Fig. 4-1) and used as input for tests; time is also scaled so as to maintain acceleration within the limits of the testing apparatus.

Table 4-2: Summary of geometry and material properties of building prototype modelled by FE

Building prototype dimensions						
	Width	6.15	m			
	Depth	8.27				
	Height	9,92				
Windows	Width	1.2				
	Height	1.54				
Doors	Width	1.2				
	Height	2.94				
	Floor structure:	Timber beams and boards				
	Roof structure:	Timber truss				
	Dead load	1,519.48	kN	GF	728.49	kN
				1^{st}F	790.99	kN
	Live load	25.07	kN			
	Total load	1544.55	kN			
	Masonry mechanical properties					
	Young modulus	4000	MPa			
	Poisson's coefficient	0.2				
	Cohesion	1	MPa			
	Angle of friction	0.4	rad			

Specimens are instrumented as following (Fig. 4-2 to Fig. 4-5):

- Hysteretic devices have: pairs of strain gauges placed at diametrically opposite points along the main axis on device and connectors. Load and total displacements are read from the actuator;

- Frictional devices have: four washer plate pressure cells that read the tension in the bolts that apply a perpendicular pressure to the device frictional plates, two LVDTs that read the relative displacements within the assembly and two strain gauges. Strain gauges are placed in proximity of the sliding element, so as to verify that no plastic deformation occurs in the device. Load and displacement are logged directly from the actuator. Moreover, two thermal gauges are placed on the sliding element of the device to check temperature gain during tests with accelerograms.

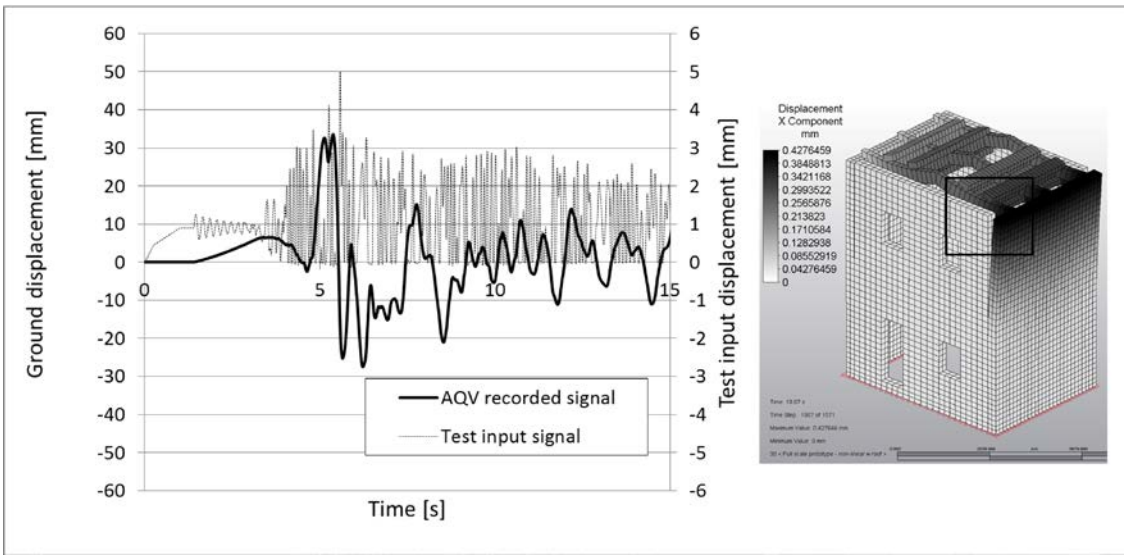

Fig. 4-1: Recorded AQV signal and FEM relative corner displacements, scaled for 5 mm max. amplitude

4.2.2 Hysteretic Anchoring Devices – Results

The dissipative anchoring device is designed to have variable cross sectional area and lower yielding strength than the one of the threaded bar forming the standard anchor the device is coupled with. This means that, according to Saint-Venant equation for axial loads, for a given level of axial force acting on the assembly, different sections feature different stress levels, but only the dissipative element undergoes yielding.

Pseudo static tests show that cycles of increasing amplitude smoothly define hysteresis loops, mildly hardening and consistent with the monotonic curve obtained by direct tensile tests (Fig. 4-2). Yielding is concentrated in the dissipative element, whereas the connections and the threaded bars remain in the elastic field (Fig. 4-2). The dissipated energy is calculated by considering the area below the envelope curve of the displacement-load cycles in the positive quadrant of the graph, as shown in Fig. 4-2. Assuming a maximum displacement of 3.5 mm, as seen in Fig. 4-2, the energy dissipated in the positive part of the cycle is equal to 98 J. An element with the same stiffness as the dissipative device, but working in the elastic field only, would achieve the same strain energy for 1.85 mm elongation and a force of 106 kN, namely double the peak load of the dissipative device. For the elastic element to achieve the same

elongation as the dissipative device, the force peak should be increased up to about 200 kN, i.e. five times the maximum load in the hysteretic device. Even though the strain energy would grow to 350 J, the acting load would be hardly withstood by a historic substratum; this being the reason for using a ductile rather than an elastic element.

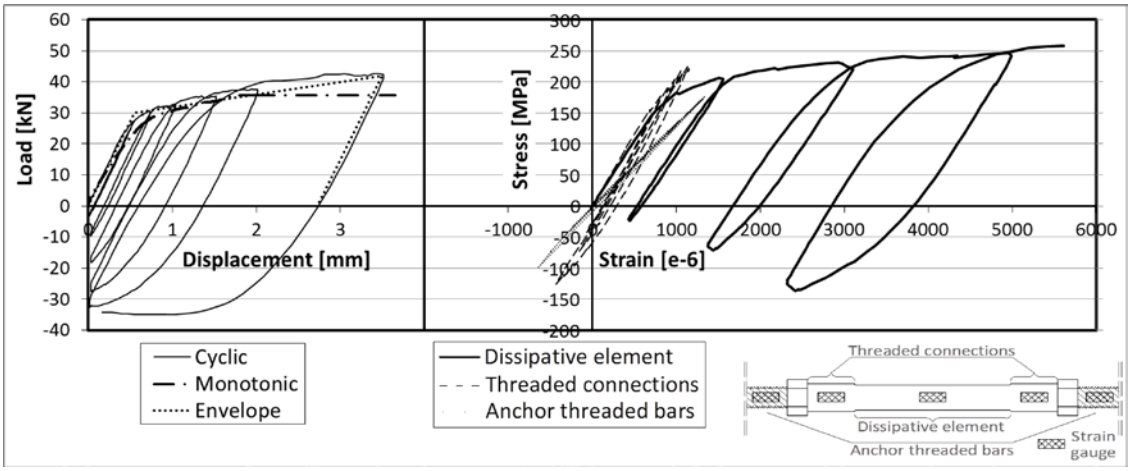

Fig. 4-2: Load-displacement and σ-ε curves of hysteretic device undergoing monotonic and cyclic load

Imposed cyclic displacements are in the tension field only, as it is assumed that when two wall panels connected by the device come into contact, the device only goes back to its initial configuration and compression is prevented. Nevertheless, the force required to bring the specimen back to the initial position is sufficient to trigger buckling when larger displacements are involved. After buckling, which occurs for -31 kN, cycling is continued up to 10 mm total displacement and cycles repeated until failure of the specimen (Fig. 4-3). The purpose is to observe whether the post-buckling behaviour is stable and cycles have a regular shape as well as to determine the influence of buckling on the failure mode.

As it could be expected, buckling has a negative effect on the shape and dimension of the hysteresis loops, nonetheless repeatability is observed and failure only occurs after 10 cycles at maximum amplitude, namely 10 mm. Such behaviour shows that the performance of the hysteretic device can be defined as a function of the elongation of the dissipative elements.

In the range 0-0.5% of elongation of the dissipative element (0-46% of maximum load capacity), the device is in the elastic field, meaning that the behaviour is the same as a standard anchors. In the interval 0.5-5% of elongation (46-72% of maximum load capacity) the device works in the non-linear range, with the upper boundary being the design ultimate displacement capacity before buckling. Beyond 5% elongation, further increase in load can be withstood and the device can achieve deformation of up to 10%, determining a safety factor of 2. In terms of force the coefficient of safety is lower, namely 1.6; nonetheless, this is greater than the standard safety factor of 1.2

and the minimum partial material factor of 1.1 prescribed for displacement-dependent anti-seismic devices (BS EN 15129:2009).

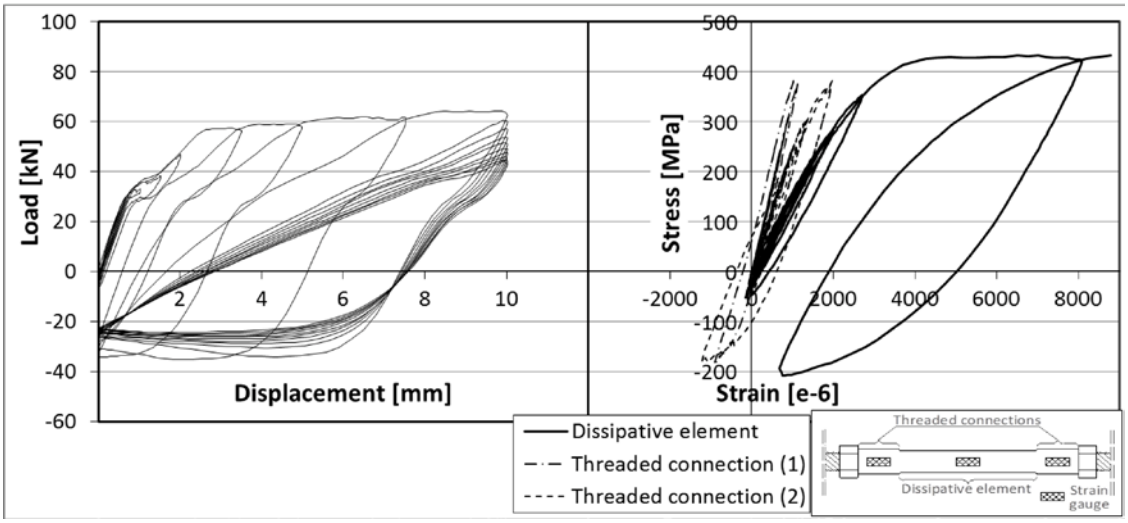

Fig. 4-3: Load-displacement and σ-ε curves of hysteretic device beyond buckling point

Failure occurs at the point where buckling heightens the necking phenomenon under cycles at maximum displacement. Normally, only few large amplitude peaks are present in an earthquake signal; the fact that failure of the device only occurs after ten cycles at maximum amplitude constitutes a further margin of safety.

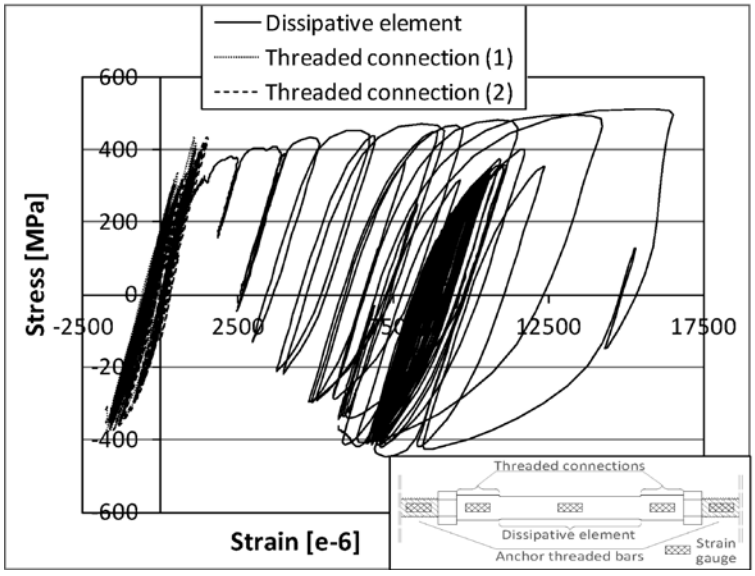

Fig. 4-4: σ-ε curve of hysteretic device undergoing FEM-generated signal scaled to a max. amplitude of 2.5 mm

Moreover, since the threaded connections of the device remain undamaged throughout testing, the device could be substituted after a seismic event by removing the end plate on the façade or by over-drilling the front portion of the grouted anchor.

This has great importance in terms of durability and ease of maintenance, and also responds to the requirements of BS EN 15129:2009, which prescribes that connections of dampers remain undamaged even at the ultimate limit state.

Increasing frequency cycles show repeatable loops, with little kinetic hardening and deformation localised in the dissipative element. Similarly, the specimen undergoing the dynamic signal derived from the AQV accelerogram has a robust performance, with linear behaviour for small displacements and regular hysteresis loop for peak displacements (Fig. 4-4). Large deformations remain localised in the dissipative element.

Fig. 4-4 shows the example of with the input signal scaled for a maximum of 2.5 mm, as this offers the clearest example in terms of resulting graph. Tests for larger scaled amplitude, i.e. 5 mm, although successful, are more difficult to read as the strain gauges are at times out of scale, so that load-displacement curves are not continuous.

4.2.3 Frictional Anchoring Devices - Results

The constitutive law for the prediction of the performance of the frictional device is defined through the Coulomb friction equation:

4-1) $$F_{//}=n\cdot\Phi\cdot F_{\perp}$$

where:

$F_{//}$ is the slip load at which friction is overcome and sliding movement begins;
n is the number of frictional surfaces, in the specific case equal to 2;
$F_{\perp}$ is the perpendicular pressure imposed on the device.

In a standard Coulomb friction equation, the ratio between $F_{//}$ and $F_{\perp}$ is expressed through the coefficient of friction, μ, which is a property typical of the materials that come into contact under the action of the perpendicular force $F_{\perp}$. In this case though, μ is substituted with Φ to account for the fact that, due to the peculiarity of the device assembly, the ratio between $F_{//}$ and $F_{\perp}$ is influenced by a number of factors. As the test-set up does not allow quantifying separately the influence of each parameter, it is deemed appropriate to use a different symbol to represent these combined effects. Φ is calculated as average over each cycle on the basis of the recorded values of $F_{//}$ and $F_{\perp}$.

Fig. 4-5a, shows good performance of the device, with loops of rectangular shape, regardless of the amplitude and frequency of exciting cycles; the slip load is proportional to the imposed level of perpendicular pressure, as expected for a friction-controlled sliding device. Such behaviour is observed both for sinusoidal cycling and in case of earthquake-like input, as shown in Fig. 4-5b.

It is worth pointing out that the asymmetry of cycles for the lowest level of $F_{\perp}$ (Fig. 4-5) depends on an imprecision in the setting up of the testing apparatus, rather than on any issue with the device itself, as it can be seen from the other curves.

The frictional device is tested for a number of cycles higher than those experienced during one seismic event. This is done because, conversely to the hysteretic device, the frictional device neither fails nor requires substitution; therefore it could be left in place to withstand successive shakings, as long as its performance is sufficiently stable and well known, namely as long as the frictional plates wear off or the pins fail.

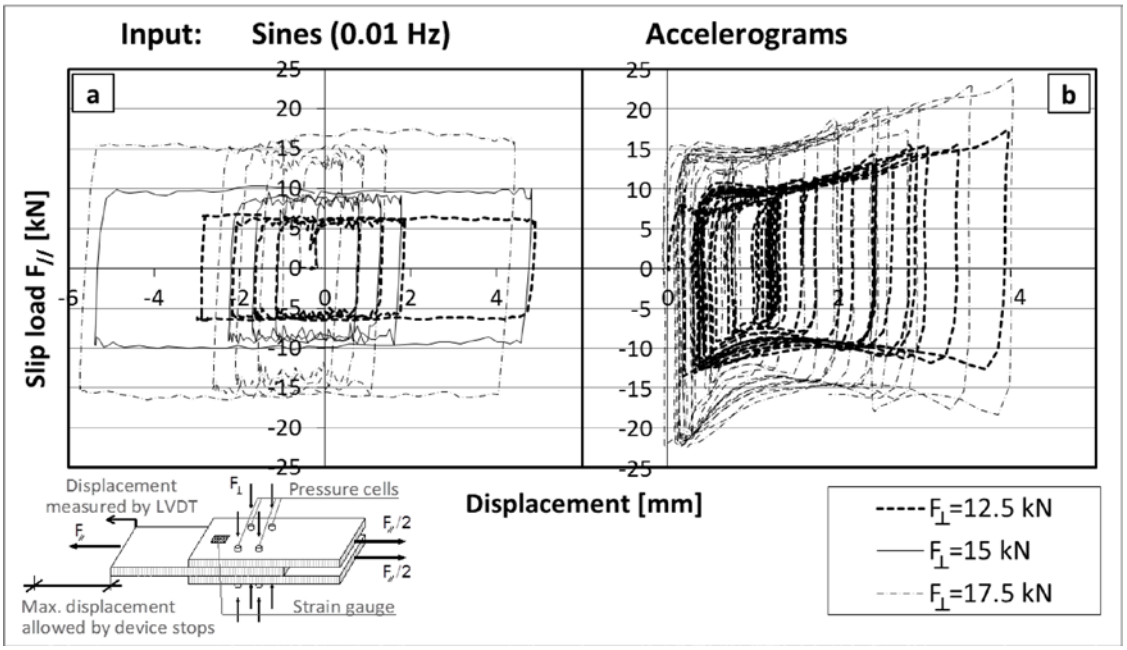

Fig. 4-5: Load-displacement curves of frictional device for increasing levels of amplitude and F⊥

A change in slip load, supposedly due to the progressive wear of the frictional surfaces, is observed throughout the dynamic and fatigue testing sessions; accordingly, a correlation between Φ and the number of cycles is sought.

The values of Φ calculated from slip load and perpendicular pressure are plotted against the cumulative number of cycles (Fig. 4-6). For dynamic tests, Φ is calculated at each cycle, whereas for the fatigue test, results are plotted for 5 cycles every 50, as Φ variation is smooth. The values of F⊥ used in the calculation are those recorded by the pressure cells and therefore are real time values that may differ from the initial value imposed by providing a nominal torque to the pressure bolts at the beginning of tests.

Up to 50 cycles, Φ tends to increase from the initial value of 0.15 to then progressively settle on the value of 0.55; the initial value is calculated as average of Φ values at the first cycle experienced by each specimen, whereas 0.55 is taken as average over the Φ values calculated for each specimen for cycles beyond the fiftieth. Between these two values, Φ increases with a linear trend.

The observed variation in Φ can be ascribed to a number of factors: firstly, the repeated rubbing of the frictional plates, which provokes wearing of the surfaces and enhances the material roughness, thus increasing friction. Secondly, the number of cycles also affects the perpendicular pressure, which increases from the initial nominal

value imposed. This could be due to the effect of repeated cycles on the locking of tension bolts and to the presence of debris between the friction plates: metal dust created by the wearing of the friction surfaces might remain within the assembly, thus creating additional pressure.

Additionally, mechanical locking, which is likely due to the machining of specimens, occurs in a random manner only affecting some loading cycles throughout tests, thus provoking a variation in $F_{//}$ unrelated to the perpendicular pressure. This means that mechanical locking creates scattering in the proportion between $F_{//}$ and $F_{\perp}$, i.e. in the values of Φ.

A logarithmic regression curve can be used to express the correlation for dynamic tests:

4-2) $$\Phi=0.0880\cdot ln(n_c)+0.1511$$

where n_c is the number of cycles that the frictional anchor device has undergone.

The trend changes during the fatigue test (Fig. 4-6) when, beyond the interval included between 50 and 150 cycles, Φ drops as consequence of further wear and tear of the frictional surfaces, which, after the initial roughening, become smoother as cycling continues. The negative trend recorded beyond 50 cycles is not well captured by the regression curve.

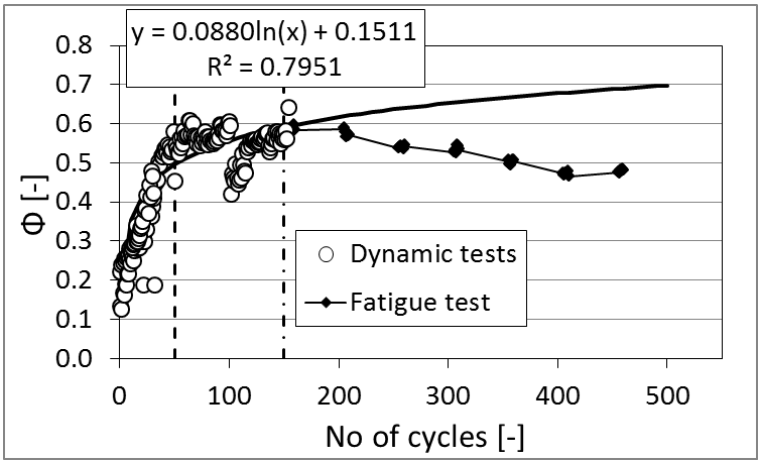

Fig. 4-6: Variation of Φ as function of the number of cycles experienced by the friction device specimens

Thanks to the regular shape of cycles, the dissipated energy can be expressed as:

4-3) $$E=F_{//}\cdot u=n\cdot\Phi\cdot F_{\perp}\cdot d$$

where

$F_{//}$, n, Φ and $F_{\perp}$ are the same as per equation (4-1);
d is the total displacement of the sliding plates per cycle.

The energy dissipated assuming a cycle of amplitude equal to 3.5 mm is calculated through equation (4-3), considering a whole rectangular cycle. Results are reported in Table 4-3 considering the case of Φ=0.15, namely a device with pristine friction plates, and the case of Φ=0.55, i.e. frictional plates that have already undergone a sufficient number of cycles to reach the plateau of Fig. 4-6. The two values of Φ represent the lowest and highest achievable value of $F_{//}$ and hence dissipated energy; they can therefore be considered as the lower and upper bound which identify the performance range of the device according to BS EN 15129:2009.

As it can be seen in Table 4-3, where the energy dissipated by the hysteretic device for a cycle of the same amplitude is also reported, the energy dissipated by the frictional devices is far lower, in certain cases down to a tenth of the hysteretic device. However, it should also be considered that the axial force necessary to obtain energy dissipation is also considerably lower, this being a main advantage as it means that lower stresses are transmitted to the weak parent material. Furthermore, the frictional device has a more favourable ratio between dissipated energy and applied axial load, as it can be seen from the last but one column of Table 4-3.

It's also worth pointing out that the dissipation of energy occurs for a small dynamic input, as shown by the ratio between the cycle maximum load and the ultimate load capacity of the threaded rod of a standard anchor – see last column of Table 4-3.

Table 4-3: Energy dissipated for a cycle of 3.5 mm amplitude by hysteretic and frictional device

		Perpendicular force $F_{\perp}$ [kN]	**Load $F_{//}$ [kN]**	**Dissipated energy, E_d [J]**	**Ratio $F_{//}/E_d$ [kN/J]**	**Ratio F/F_u standard anchor [%]**
Friction	Φ=0.15	12.5	3.8	13.1	3.5	3.5
		15.0	4.5	15.8	3.5	4.1
		17.5	5.3	18.4	3.5	4.8
	Φ=0.55	12.5	13.8	48.1	3.5	12.6
		15.0	16.5	57.8	3.5	15.0
		17.5	19.3	67.4	3.5	17.6
Hysteretic		N/A	42.7	121.0	2.8	38.9

Temperature is not influential to the performance of the devices: the duration of the shaking and the thermal inertia of the steel parts are such that, at room temperature, the device starts warming up after the motion has already stopped.

The monotonic tensile test to failure shows the behaviour of the device in the case of an impact tensile load: the frictional mechanism is activated after reaching the slip load, sliding occurs until the plates reach the end of their run and then the device undergoes tension. The connection pins yields for a load of about 80 kN and the assembly eventually fails at 100 kN, when the pins are pulled out of their holes. Such

loads are higher than the yielding load of the threaded rod of a standard anchor (70.7 kN). This is a positive feature: although yielding of the pins is also ductile, the risk of pull-off must be avoided, as it determines a sudden failure of the device; it is therefore preferred that the anchor rod yields at lower levels.

4.3 PULL-OUT TESTS

4.3.1 Test Set-Up

When a strengthened corner- or T-connection between walls undergoes a seismic loading, the panel perpendicular to the direction of the main shock will tend to overturn as consequence of its low flexural stiffness. The phenomenon can be triggered by the thrust of horizontal structures and is generally accentuated by pre-existing damage or by the onset of new cracks caused by the poor material quality and scarce overlapping of masonry units at the joint between the masonry panels; indeed, metallic anchors are purposely installed to restore the box-like behaviour of the buildings and facilitate the distribution of horizontal loads according to the stiffness of structural elements. The tilting action of one panel will be transmitted to the metallic element, and hence to the wall within which this runs, through the grouted interface. Because of the lower embedment length and larger experienced deformations, the part of the anchorage grouted in the wall acted upon in the direction perpendicular to its plane is the most likely to fail, whereas, for the sake of simplicity, the remaining part of the anchor can be assumed almost undisturbed.

Accordingly, the test set-up consists of the portion of stainless steel anchor embedded in a masonry panel perpendicular to the main seismic action, while the pulling action of the testing apparatus simulates the reaction of the anchor lying within the wall parallel to the main shock direction (Fig. 4-7).

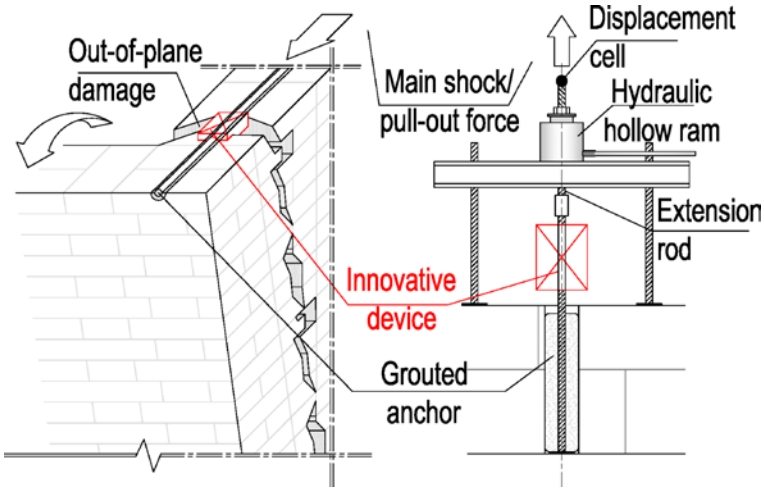

Fig. 4-7: On-site layout and laboratory set-up of pull-out tests

When dissipative devices are used, they are positioned at the interface between the two orthogonal walls, so that any relative displacement between panels can be

exploited to dissipate energy. Accordingly, during tests, devices are installed as add-on elements (marked in red in Fig. 4-7) in series with the anchor grouted in the wall and the pull-out jack.

4.3.2 Materials and Samples

Following the prescriptions of EN 846-2 (2000) for testing of ancillary components for masonry, anchors are positioned in free-standing panels. The relative distance between anchors must be sufficient to avoid interaction effects between adjacent anchors or between anchor and wall edges. As already explained before, a code specifically dealing with anchors in masonry is missing from the technical literature. The minimum distance centre to centre of two diameters that determines a group effect in the case of piles is taken as reference (BOCA, 1993).

The positioning of the anchors in respect to bed joints, head joints and masonry units is intentionally left random, so that results can be representative of the average behaviour of anchors in an irregular substratum, although care is taken that at least one joint is included in the area of coring (so as to avoid performing a pull-out from a single brick).

A vertical load is applied throughout tests; the code (EN 846-2:2000) prescribes the use of a load apt to create a stress between 0.05 and 0.1 MPa, which simulates the typical compression stress field perpendicular to bed joints.

Two different values of loads are applied to three out of the six tested standard anchors, each group being installed in a different wall panel. The use of different levels of vertical compression allows for the analysis of the influence of the vertical load on the performance of anchors. A first panel undergoes a load creating a pressure of 0.07 MPa, thus reproducing the standard case scenario according to code, whereas a pressure of 0.7 MPa is applied to the second panel. The latter vertical load represents the limit case scenario of application of anchors installed in bell towers or buildings with heavy horizontal structures like vaults.

In the case of anchors in series with the dissipative devices, only the value of 0.07 MPa is used for the vertical compression of panels. As the shear strength of masonry depends on the vertical compression applied on it and a pulling action of a bonded anchor is transmitted to the surrounded material by shear, the case of low compressive strength represents the most unfavourable scenario in terms of parent material resistance. Hence it is taken as reference to validate the dissipative anchoring devices.

Masonry panels are built using recycled Victorian bricks and natural hydraulic lime mortar (Fig. 4-8a). Masonry units are fired bricks, sized 220 x 110 x 70 mm, with 20 vertical holes.

Characterisation of materials is carried out according to relevant Eurocodes (EN 772:2000 - Masonry Units, EN 1015:1999 –Mortar, EN 1052:1999 – Masonry), repeating the tests at 28 days and at the age when pull-outs are performed, namely 60

days, this period including the curing of masonry, the installation of anchors – coring and grouting – and curing of grout. The mechanical properties of materials at age of testing are summarised in Table 4-4, whilst the overall set-up in shown in Fig. 4-8.

Anchors are made of threaded M16 bar, AISI 304 stainless steel (UNI 14301) class 70 (yield proof stress 450 MPa, ultimate tensile strength 700 MPa), 400 mm long and are installed in 80 mm diameter diamond-drilled holes passing through the wall. A 60 mm diameter end plate closes the 350 mm long fabric sleeve for the grouting (Fig. 4-8c). Compressive strength of grout as stated by the producer is 50 MPa

Table 4-4: Mechanical properties of materials used for test samples

Recycled Victorian bricks (220x110x70 mm) with 20 vertical holes		
Compressive strength	27.3 (CoV 19%)	[MPa]
NHL 5 lime mortar		
Mix proportions lime to sand	1:2	b.v.
Flexural strength	0.3 (CoV 29%)	[MPa]
Compressive strength	1.0 (CoV 13%)	[MPa]
Masonry panels (1.4x0.35 m, 1.5 m high), English bond		
Compressive strength	6.7 (CoV 1%)	[MPa]
Bond strength (by wrench test)	0.67 (CoV 15%)	[MPa]

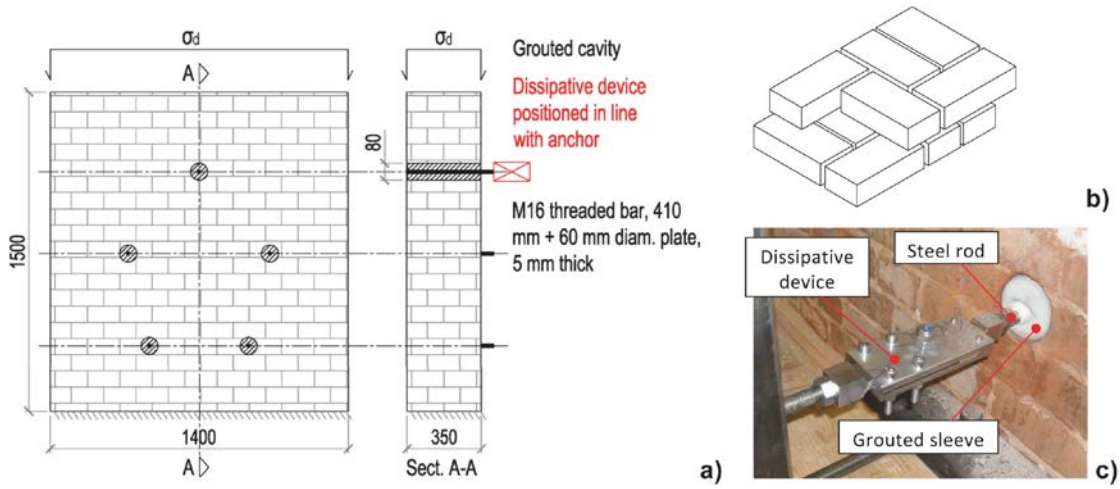

Fig. 4-8: a) Set-up of masonry panels for pull-out tests; b) Detail of English cross bond; c) Detail of frictional device in series with the anchor

4.3.3 Testing Procedure and Instrumentation

Tests are performed in load control mode, with pull-out load being applied by a hydraulic jack in steps of 2 kN. Load is increased, maintained constant for 1 minute and then increased again. This pause between increments ensures that relaxation of the material at the interface and slippage, if any take place before the following load increment. Vertical load is kept constant throughout the test.

Total displacements are measured by the dial gauge located in series with the pulling apparatus (Fig. 4-7), while relative displacements of the grouted sleeve and the parent material around the grouted hole are measured by displacement transducers.

At the end of the test the load is released down to 2 kN to read the residual deformation. The test is considered complete when either the parent material presents damage, this being clearly detectable by visual inspection or by inability of further increasing the load, or when the target displacement of 10 mm is reached. Limitation of damage to finishes, and hence to the substratum in general, is indeed a main requirement of strengthening systems for heritage structures and should therefore be accounted for during tests. The limit displacement criterion is set considering that a 10 mm displacement is comparable with the maximum allowable drift for damage limitation, d_r=0.003, taken from Circolare 02/02/2009 N. 617 (2009); this code, unlike EN 1998:2004, specifically refers to ordinary masonry buildings when stating drift limits for masonry walls and is therefore deemed more suitable in the case of historic masonry structures. This limit is also in line with the expected drift stated in FEMA 356 (2000) for unreinforced masonry buildings at the limit state of Immediate Occupancy.

In the case of friction anchors, if the device activates successfully and no damage is detected at the end of the test, the whole procedure is repeated for a higher level of vertical pressure on the friction devices ($F_{\perp}$), which in turn determines a higher value of slip load of the friction plates ($F_{//}$) and hence different response of the anchor assembly.

4.3.4 Experimental Results

For the testing set-up described above, one may expect failure of standard anchors to occur (Fig. 4-9 and Table 4-5):

1. For bond failure:
    a. Between the steel profile and the grout;
    b. Between the grouted element and the parent material;
    c. Between adjoining bricks;
2. For tensile failure:
    a. Of masonry units;
    b. Of steel profile by yielding and eventually fracture;
3. By a mixed mode, including any of the above.

Possible failure modes are listed on the basis of on-site observations and comparison with the typologies of failure that have been collated for the case of anchors in concrete (EOTA, 2006; DD CEN/TS 1992:2009, ACI 318-11).

Of these failures, types 1a and 2b rarely occur in practice, as:

- The crests of the anchor rod ensure a good bond between the metallic bar and the surrounding grout. Failure 1a could possibly occur if grouting is not carried out according to the producers' recommendation, i.e. when incorrect

grout mixing and wrong injection pressure lead to presence of voids within the sock or to reduced grout strength. This is hardly the case when anchors are installed by qualified personnel in the controlled environment of laboratories and left to cure for the prescribed time. Additionally, the chosen typology of anchors feature an end plate at the rear of the anchor rod, which works in compression, thus preventing the pull-out of the bar and shifting the failure to the surrounding material, as also observed by Subramanian and Cook (2004).

- Steel normally has the highest capacity among the elements of the assembly, so that failure 2b hardly occurs unless the steel profile is substantially under-dimensioned.

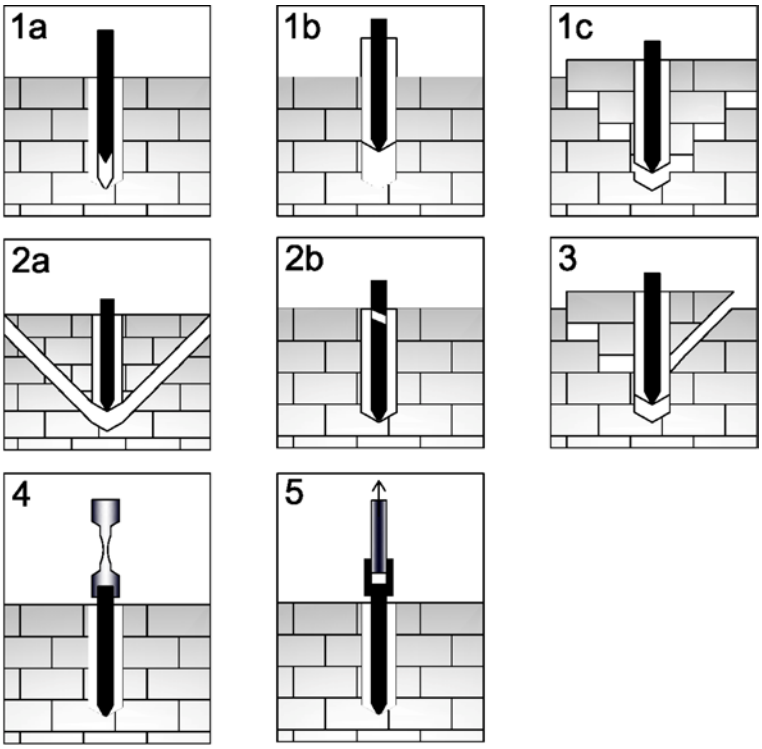

Fig. 4-9: Possible modes of failure of axially loaded anchors grouted in masonry substratum

Table 4-5: Summary of possible modes of failures as shown in Fig. 4-9

Failure modes			
1	**a**	Bond failure between	steel profile and grout
	b		grouted element and parent material
	c		adjoining bricks
2	**a**	Tensile failure of	masonry units
	b		masonry mortar joints
	c		steel profile
3		Mixed mode	Combination of others
4		Yielding	Yielding located in the hysteretic dissipative device
5		Sliding	Frictional sliding occurring in the frictional device

When designing the anchor assembly for the specimens, the geometry was chosen so as to avoid failure 1a and 2b; such design allows both to reproduce the standard behaviour of anchors, and to focus on the capacity of the parent material and of its interface with the anchor assembly.

Yielding of hysteretic device (mechanism type No 4) and activation of the friction device (mechanism type No 5=sliding of friction plates) in series with the standard anchors aim to prevent the remaining failures (Fig. 4-9).

For standard anchors tested in this campaign, failure at the bond between the grouted sleeve and the parent material (1b) is the main mode of failure for standard anchors and the first to occur, then followed in some cases by a further increase in stiffness and cracking of other elements of the assembly according to other failure types (Fig. 4-10 and Table 4-6).

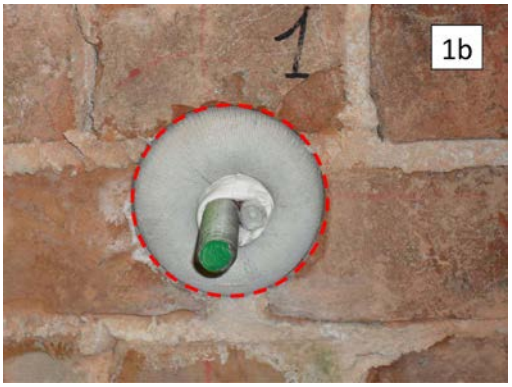

a)

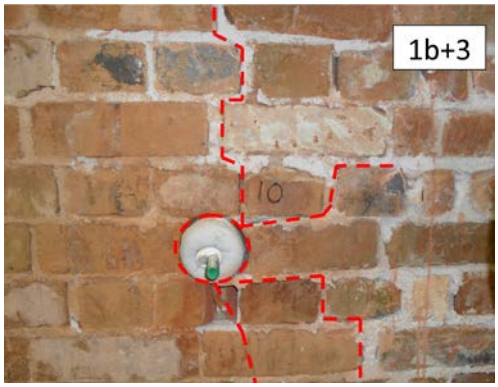

b)

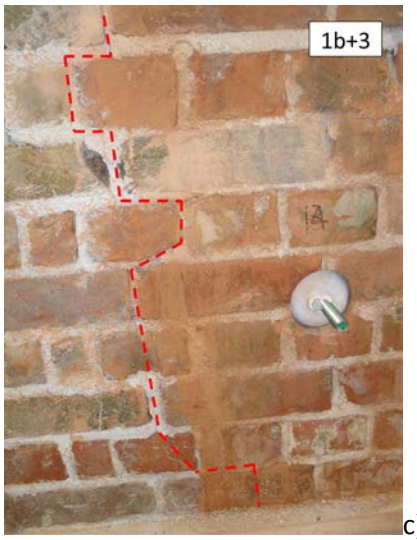

c)

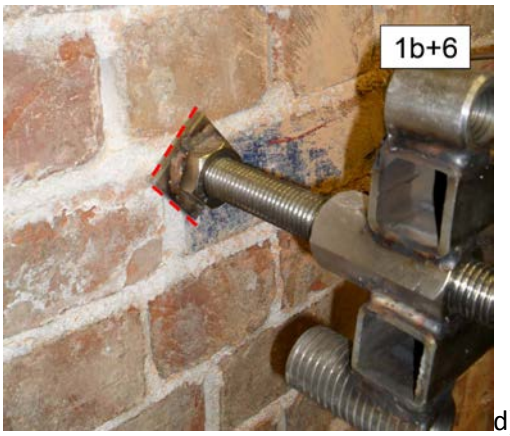

d)

Fig. 4-10: Standard anchors – Modes of failure observed during tests: bond failure (1b), in many cases followed by other failures: (1b + 3) bond failure in the mortar joints, or (1b + 6) crushing of masonry

Failure type 3 features pseudo-vertical cracks developing either in the head joints or in those bricks where the holes of the masonry units provide a weak pattern. This type of

failure is likely to be caused by the mechanical locking of the anchors within the parent material. Whereas a homogeneous material would behave similarly to the idealised modes of failure shown in Fig. 4-9, irregularities, which are typical of historic masonry, provoke concentration of high shear stresses, so that cracking randomly radiates from the hole to the parent material, thus affecting the shape of the failure surface.

Table 4-6: Standard anchor – Summary of failure modes of pull-out tests

Sample No	**Failure type**	
a	1b	Bond failure grouted element/ parent material
b	1b + 6	Bond failure grouted element/ parent material followed by failure due to testing apparatus (masonry crushing at the pulling rig footing)
c	1b + 6	Bond failure grouted element/ parent material followed by failure due to testing apparatus (masonry crushing at the pulling rig footing)
d	1b + 3	Bond failure grouted element/ parent material followed by a mixed mode
e	1b + 3	Bond failure grouted element/ parent material followed by a mixed mode
f	1b + 3	Bond failure grouted element/ parent material followed by a mixed mode

Accidental crushing of masonry at the support of the pulling apparatus occurs in a few cases due to the test set-up (failure due to test set-up, type No 6); the issue is addressed in the sequent tests by using metallic plates to spread the pressure at the foot of the loading apparatus on a larger bearing area.

The overall response of anchors can be observed by looking at the curves in the graph of Fig. 4-11, which show the readings both at loading and after the minute during which load is maintained constant, so as to highlight any variation in the anchor assembly behaviour.

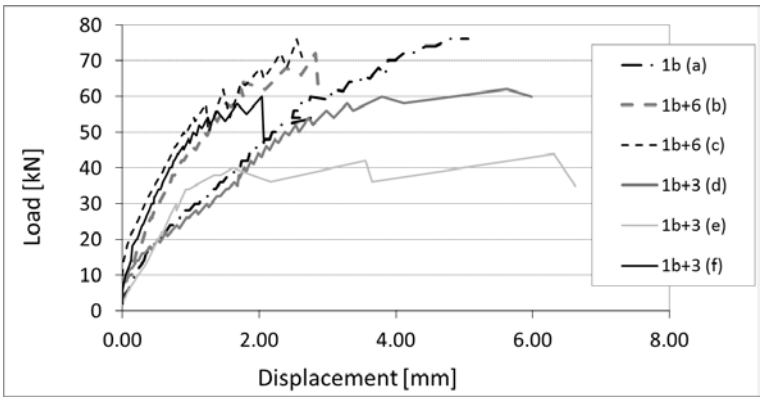

Fig. 4-11: Standard anchors – Load-displacement graph. For a summary of samples and failure modes refer to Table 4-6

While curves start off smoothly, they tend to become jagged (Fig. 4-11): this saw-like appearance is due to the fact that, as an anchor fails, it keeps moving outwards without the need for a further increase in pulling force. Such movement is recorded during the minute elapsing between two load increments and involves a drop in the jack pressure, as the anchor cannot offer resistance to the load. Hence, the curve jaggedness, as well as a major drop in the curve stiffness, identifies the maximum load capacity of the anchor, as measured experimentally.

Looking in details at load-displacement curves, other aspects emerge. Each curve presents indeed more than one change in stiffness, thus identifying: the first appearance of relative movement (point A), the achievement of maximum load (point B), the achievement of maximum displacement under sustained load (point C) and the ultimate failure (point D) (Fig. 4-12a). In some cases, further stiffness is attained (E), beyond the plateau B-C. These four threshold points identify an idealised curve that approximates the experimental behaviour (Table 4-7).

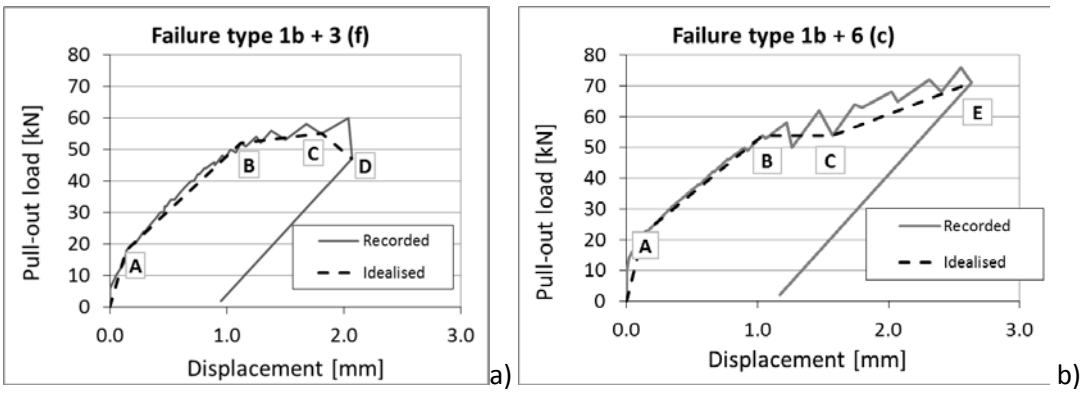

Fig. 4-12: Standard anchors – Idealised curves of experimental load-displacement curves

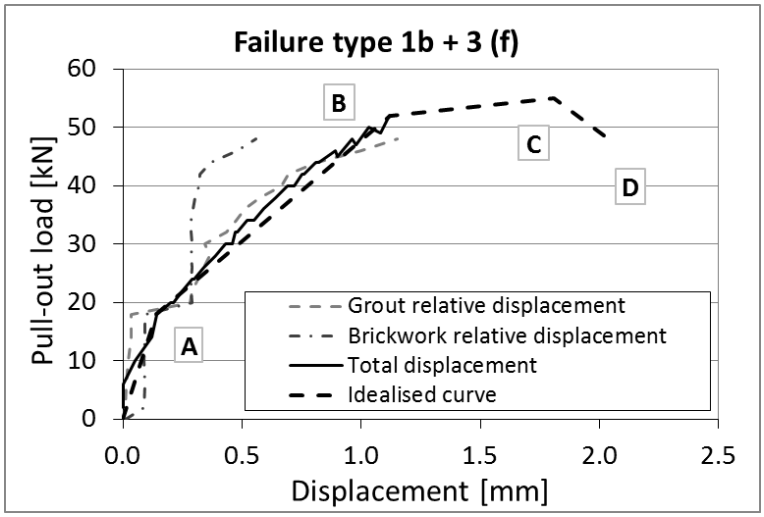

Fig. 4-13: Standard anchor – Comparison between idealised load-displacement curve of the whole assembly with the curves showing relative displacements of the various components

The first change in stiffness, point A, can be identified with precision by looking at the displacements of the single components of the assembly. Indeed, the measurements recorded at the surface of grout and brick clearly show when the first relative movements occur and allow the correlation with the variation in steepness of the idealised curve (Fig. 4-13).

It is considered that the peak capacity is reached at point B, as this is the point that identifies a major change in stiffness, after which pseudo-constant load determines continuous movement. In the majority of cases, load capacity eventually drops beyond point C and the anchor reaches its ultimate capacity.

Some anchors, after the load plateau between B and C, have a further increase in stiffness (Fig. 4-12b) identified as point E. It is believed that this further increase in stiffness is related to the phenomenon of mechanical locking, namely the mechanical resistance offered by the "bumps" of the grouted element that are engrained in the irregularities of masonry and resist the pulling load working in compression.

The influence of the bearing mechanism of the irregularities of the grouted sock on the capacity of the anchor is similar to the effect of the thread on a steel anchor embedded in concrete; threaded bars mainly rely on the compressive strength of concrete, which is act upon by the crests of the thread. According to various authors, as reported and commented by Lowes (1999), only when the concrete around the thread crushes and sliding is initiated, friction becomes the main controlling phenomenon. One can assume that because of the similarity of relative stiffness between steel/concrete and grout/masonry, grouted anchors embedded in the masonry behave in a similar way. Nevertheless, while the threads of a steel bar are regular in shape and spacing, this doesn't apply to the grouted sock, which fills the random cavities within the masonry. This means that:

- The bearing mechanism is not necessarily the first mechanism to occur. Sliding could be possible before mechanical locking is activated and the anchor resists the pull load by bearing on the substratum;
- The bearing mechanism is difficult to quantify as the presence of voids in the substratum and the degree of grout penetration is not known "a priori".

Hence, mechanical locking is a further "source" to resist a pulling force, but it is hardly predictable, this being the reason for using the conservative approach of not considering its influence at all and taking B as the ultimate load capacity of the anchor assembly.

Nonetheless, load-displacement curves are not perfectly horizontal between point B and C, thus meaning that further sliding of the anchor requires an additional load increase to overcome friction between the sliding surfaces. This behaviour provides a certain measure of ductility at peak capacity, which makes this type of anchors particularly suitable for applications in seismic prone areas.

Upon completion of the experimental campaign, recorded values of load capacity of the anchors are compared with theoretical calculated values, so as to identify a suitable analytical model to predict the anchor response. As bond failure is most influential to the anchor behaviour, analytical models of the failure at the interface binder/parent material are taken in consideration.

Table 4-7: Standard anchors – Summary of points defining the idealised load-displacement curves

Anchor ID	**A**		**B**		**C**		**D**		**E**	
	kN	mm	kN	mm	kN	mm	kN	mm	kN	mm
a	16	0.34	60	2.75	66	3.84			76	5.05
b	18	0.22	64	1.77	62	2.09			72	2.82
c	22	0.13	54	1.04	54	1.57			71	2.63
d	10	0.06	58	3.29	60	5.98	-	-		
e	10	0.93	38	1.08	35	6.62	-	-		
f	18	0.14	52	1.12	55	1.81	47	2.07		
Av.	16	0.19	54	1.84	55	3.65			73	3.5
CoV [%]	31	52	17	52	47	61			4	38

Similarly to adhesive anchors installed in concrete (Cook et al., 2007), the bond capacity binder/substratum of anchors grouted in the masonry can be thought influenced by adhesion as well as interlocking. Accordingly, a model similar to that described and discussed by Cook (1993) can be adopted:

4-4) $$N_{u,m} = \tau_0 \pi d_0 h_{ef}$$

where d_0 and h_{ef} are respectively diameter and embedment length of the grouted anchor and a uniform failure stress, τ_0, is assumed on the whole embedment length, as such simplification doesn't impair the correctness of the model (Cook, 1993).

This same model is proposed by various authors (McVay et al., 1996; Marti, 1993) and current codes refer to it too. Indeed, the complex formulation presented by ACI 318 for single anchor:

4-5) $$N_a = \frac{A_{Na}}{A_{Na,0}} \psi_{ed,Na} \psi_{cp,Na} N_{ba}$$

ultimately refers to a pull-out capacity calculated as

4-6) $$N_{ba} = \lambda_a \tau_{cr} \pi d_a h_{ef}$$

where τ_{cr} is the 5% fractile of results of bond slip tests according to ACI 355.4. Other terms appearing in Eq. (4-5) express the fact that the anchor load capacity is reduced in proximity of edges ($\Psi_{ed,\,Na}$), in conditions other than uncracked concrete with extra reinforcement to prevent splitting ($\Psi_{cp,\,Na}$) and whenever the presence of edges or

other anchors might influence the failure surface (this being expressed by the ratio of failure surfaces $A_{Na}/A_{Na,0}$).

To check whether the models of the equations above match the experimental load capacities, the bond strength between binder and parent material, τ_0 or τ_{cr}, must be known. While in the case of anchors embedded in concrete, literature and commercial specifications provide a plethora of values, this is not quite the case for anchors embedded in masonry, also in view of the high variability of substrata and hence in bond strength.

One approach is to test anchors in a situation where boundary conditions ensure the full development of load capacity (e.g. far away from edges and other anchors) and calculate the bond strength by reversing equation (4-4). This value of strength can be then input in equation (4-5) to check whether calculated capacities match experimental results.

However, it should be considered that for the tested anchors the phenomenon of mechanical locking could be, in certain cases, prevalent, inasmuch the presence of the fabric sock, the type and irregularities of masonry and hence the roughness of the drilled cavity all contribute to create considerable locking surface, far more than what is normally present in an homogeneous material as concrete.

Hence, it might be difficult to identify by testing an average value of bond strength that does not depend on the peculiarities of the substratum. It should also be considered that on-site testing for heritage structures can only be very limited, with destructive testing being discouraged, if allowed at all, and that the task of reproducing a historic substratum in a laboratory environment is not an easy one.

In view of these observations, one could speculate whether another value, such for instance the shear strength of masonry, could be used in the analytical models listed above and could provide a reasonable approximation. Shear strength represents a lower bond in respect to the bond strength of grout to masonry, and values are available in the technical literature, can be calculated by relying on codes or by correlation with other parameters that are determined by non-destructive testing (e.g. compressive strength determined by flat jack tests). Therefore, its use, if justified, would be beneficial in terms of identifying a general model for the prediction of the behaviour of anchors.

The model suggested by Gigla and Wenzel (2000) offers another option to bypass the direct measurement of the bond strength at the interface grout/parent material; in this model load capacity is indeed expressed by:

4-7) $$N = \tau_u \frac{A_B}{A_{g,d}} A_{A,d}$$

where A_B is the contact area grout/masonry blocks, i.e. the contact area grout/mortar joints is excluded, $A_{g,d}$ is the total surface area at the interface grout/parent material and $A_{A,d}$ is the area of the interface anchor rod/grout. Bond strength is calculated by:

4-8) $$\tau_u = \Phi_J \left(\frac{f_{G,c}^2}{500} + X_{B,W} \right)$$

where Φ_J is the reduction factor for bed or head joints (=0.5), $f_{G,c}$ is the compressive strength of grout and $X_{B,W}$ describes the increase in bond strength typical of water absorptive materials (equal to zero when unknown).

The three different options Eq. (4-5) with τ_{cr} equal to measured bond strength/Eq. (4-5) with τ_{cr} equal to shear strength/Eq. (4-7) are used to compare analytical models and experimental load capacity.

Bond strength is extrapolated by carrying out bond characterisation tests under conditions that exclude any unfavourable condition. Masonry specimens comply with the requirements of EN 846-2 (2000) and characterisation tests are carried out according to the procedures already described in §4.3.2. Due to the use of recycled materials, it was not possible to use exactly the same typology of bricks as for pull-out tests; nevertheless, a masonry with similar mechanical properties was used (Table 4-8).

Anchors for bond characterisation are identical to those used for the pull-outs, except that they are 230 mm long and are installed in 60 mm, instead of 80 mm, diameter diamond-drilled holes passing through the wall.

Table 4-8: Comparison mechanical properties (CoV) of masonry specimens used for pull-out tests and bond strength characterisation tests

	PULL-OUTS	**BOND STRENGTH TEST**	
	Recycled bricks (220x110x70 mm), 20 vertical holes	**Clay bricks (230x110x60 mm), 24 vertical holes**	
Compressive strength	27.3 (19%)	30.1 (10%)	[MPa]
	NHL 5 lime mortar	**NHL 5 lime mortar**	
Mix proportions	1:2	1:2	b.v.
Flexural strength	0.3 (29%)	0.8 (4%)	[MPa]
Compressive strength	1.0 (13%)	2.1 (15%)	[MPa]
	Masonry panels (1.4x0.35x 1.5 m), English bond	**Masonry panels (1.2x0.23x 1.4 m), Flemish bond**	
Compressive strength	6.7 (1%)	6.4 (6%)	[MPa]
Young modulus	3600 (3%)	2230 (10%)	[MPa]

The five bond characterisation tests, which are carried out implementing an instrumentation similar to that described in §4.3.3, lead to an average value of pull out

load equal to 36 kN (CoV 11%); bond shear strength, τ_{cr}=0.83 MPa is calculated by reversing equation (4-4).

As far as shear strength goes, values are determined by looking at tests performed on similar typologies of masonry, with same type of mortar and workmanship as in the current project, by Zhou et al. (2008). The bond strength measured by wrench test correlates to a value of characteristic initial shear strength $f_{vk,0}$ equal to 0.24 MPa. Thus, characteristic shear strength is equal to (EN 1996-1-1: 2005):

4-9) $$f_{vk} = f_{vk,0} + 0.4\sigma_d$$

where σ_d is the compressive applied stress perpendicular to bed joints; in the specific case σ_d is calculated taking into account both the weight of the courses of bricks lying on top of the anchors and the applied vertical compression. It is worth highlighting that due to the density of masonry and geometry of wall panels, the difference in the height at which anchors are installed does not particularly affect the shear strength, whereas the increase of one order of magnitude in vertical load has a high impact.

The values of pull-out load capacity calculated on the basis of shear and bond strength are summarised in Table 4-9. Additional terms of equations (4-5) and (4-6) are, in the specific case, the coefficient for light weight concrete, λ_a= 1, and the coefficients $\Psi_{ed,Na}$= $\Psi_{cp,Na}$=1. The ratio $A_{Na}/A_{Na,0}$ is calculated on the basis of c_{Na}, i.e. the projected distance from the centre of an anchor shaft on one side of the anchor required to develop the full bond strength of a single anchor (ACI 318):

4-10) $$c_{Na} = 10 d_a \sqrt{\tau_{cr}/1100}\,[in] = 10 d_a \sqrt{\tau_{cr}/7.58}\,[MSI]$$

For both the hypothesis of $\tau_{cr}=f_{vk}$ and $\tau_{cr}=f_b$, c_{Na} is such that $N_a=N_{ba}$ (4-5 and 4-6).

Pull-out load capacity is also calculated on the basis of Eq.s (4-7) and (4-8), where the ratios of areas $A_B/A_{g,d}$= 0.82 is estimated by observing the grouted sockets after the test completion and dismantling of the masonry panels.

Table 4-9: Standard anchors – Comparison of experimental and theoretical values of pull-out load

	Exp.	**Theoretical**						
ID	**Pull-out load (B/E)**	**σ_d**	**f_{vk} Eq (4-9)**	**N_a Eq. (4-5) Hp: $\tau_{cr}=f_{vk}$**	**f_b Eq. (4-4)**	**N_a Eq. (4-5) Hp: $\tau_{cr}=f_b$**	**τ_u Eq. (4-8)**	**N Eq. (4-7)**
	[kN]	[MPa]	[MPa]	[kN]	[MPa]	[kN]	[MPa]	[kN]
a	60 / 76	0.707	0.52	46.1	0.83	73.0	2.5	36.1
b	64 / 72	0.713						
c	54 / 71	0.713						
d	58 / -	0.077	0.27	23.8				
e	38 / -	0.091	0.28	24.3				
f	52 / -	0.091						

A summary of the values of pull-out load capacity calculated via theoretical models against experimentally measured values is presented in Table 4-9.

For ease of comparison, the ratios between the values of the theoretical and experimental pull-out loads at point B are calculated and presented in Fig. 4-14, which allow visualising the bias of each of the three implemented models.

The use of Eq. (4-5), in combination with the experimentally determined bond strength, f_b, overestimates the pull-out capacity; in fact, calculated values tend find a better match with the load values at point E (see Table 4-9), which, as discussed above, represent the further increase in load capacity as consequence of mechanical locking. This hints to the fact that, at least for this specific typology of anchors, it might be difficult to identify a characteristic value of bond strength, independent from mechanical locking, unless extensive testing on a wide range of substrata and varying boundary conditions is carried out.

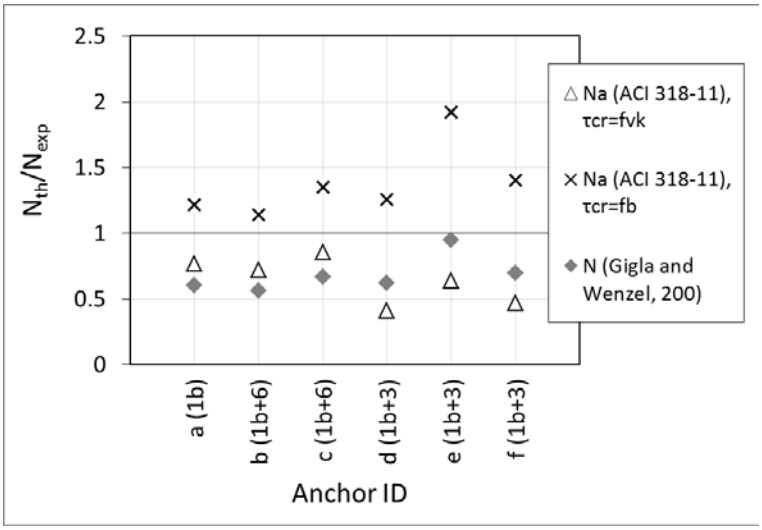

Fig. 4-14: Standard anchors – Ratios of theoretical and experimental pull-out loads

The model proposed by Gigla and Wenzel (2000) and Eq. (4-5) in combination with the shear strength, f_{vk}, provide a better match and tend to err in favour of safety. The latter model, in particular, underestimates of an average 30% actual pull-out values, yet provides a conservative estimate of ultimate capacity.

It should be noted that anchors undergoing a higher vertical compression, namely anchors a, b and c, (Table 4-9) have averagely higher capacity, thus motivating the use of an analytical relationship that involves friction and perpendicular load, such as that of Eq. (4-9).

To complete the comparison between experimental and theoretical values, load capacity is also calculated by inputting the initial shear strength, $f_{vk,0}$, in Eq. (4-5) and comparing the result with the experimental values of point A of the idealised curves. As it can be seen in Table 4-10, a fairly good match is achieved.

This is likely due to the fact that the slight drop in stiffness of the load-displacement curves at point A represents a first micro-cracking at the interface between grout and parent material, which doesn't involve the whole embedment length, but only the outer portion of the anchor. Here the influence of the confinement of the surrounding material is lower, as expressed by $f_{vk,0}$, which neglects the positive contribution of any vertical load

Table 4-10: Standard anchors – Comparison of theoretical and experimental loads at first stiffness loss

	Experimental	**Theoretical**
Anchor No	**Load at point A**	**F - Eq. (4-5), hp: $\tau_{cr}=f_{vk,0}$**
	[kN]	[kN]
a	16	21
b	18	
c	22	
d	10	
e	10	
f	18	
Av. (CoV)	15.67 (31%)	

Such observation is in line with the elastic bond-stress model proposed by Cock (1993), which assumes higher stresses in proximity of the outer surface of the parent material, and also by the observations reported by Malvar (1991), which indicate that bond strength is proportional to the level of lateral confinement, this being lower at the front end of the anchorage.

Overall, anchors achieve levels of maximum loads that are in line with, or even higher than calculated values, meaning that two of the adopted analytical models are able to foresee the load capacity, even if in a conservative manner. The analytical model suggested by ACI 318-11 seems instead to systematically overestimate the load capacity of this typology of anchors. Anchors undergoing lower perpendicular pressure present more of a ductile behaviour, due to the fact that lower frictional forces arises on the failure surface, thus allowing for relative movements between the substratum and the grouted anchor. This is a desirable characteristic in case of strengthening of buildings located in seismic prone areas, even more so considering that the lower level of vertical pressure applied during tests is in fact an average working level in masonry construction and therefore a frequent case scenario.

However, scattering of results is high, meaning that ductility will be hardly predictable, which is a major issue in terms of design. Furthermore, ductility of standard anchors implies a certain level of damage in the substratum, whereas one of the objectives of the strengthening of heritage structures should be the limitation of cracking that might affect precious finishes.

In line with the objective of damage limitation, the most evident result of tests on anchors coupled with the dissipative anchor devices is the effective prevention or reduction of failures in the parent material (Table 4-11 and Table 4-12).

In the case of hysteretic anchors (Fig. 4-15), load-displacement curves show an initial linear behaviour, corresponding to the elastic deformation of the steel element and to small movements, if any, at the interfaces between the various parts of the anchor assembly. The curves then present a non-linear portion, which is determined by the plastic deformation of the hysteretic devices in combination with further movements at the interfaces of the anchor elements. The maximum load capacity is identified by looking at the point where the curves lose stiffness and become jagged. This is due to the fact that the tests are carried out under load control regime, and once the bar starts yielding elongations occur with pressure release at the jack.

As visible from Fig. 4-15, the four curves present a uniform behaviour, with a variation of ultimate load of 10%, a substantial improvement on the 47% scatter in the performance of strength-only anchors. Nevertheless, it is observed during tests that the yielding of the device is accompanied by failure of the bond between the grout and the parent material, which limits the overall capacity of the system.

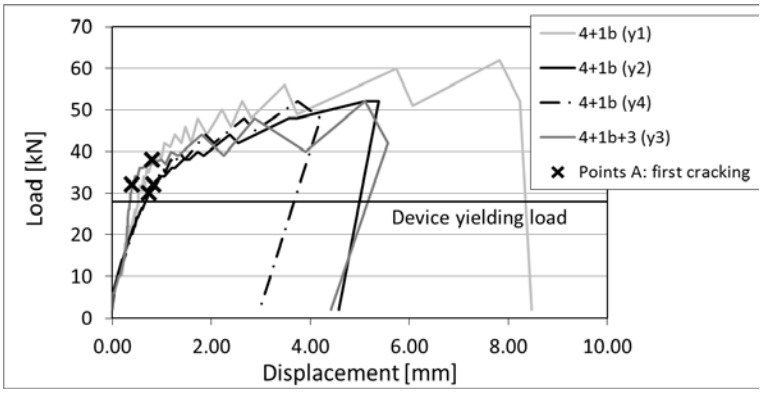

Fig. 4-15: Hysteretic anchors – Load-displacement curves

Table 4-11: Hysteretic anchors – Summary of failure modes of pull-out tests

Sample No	**Failure type**	
y1	4 + 1b	Yielding + bond failure grouted element/ parent material
y2	4 + 1b	Yielding + bond failure grouted element/ parent material
y3	4 + 1b + 3	Yielding + bond failure grouted element/ parent material and mixed mode
y4	4 + 1b	Yielding + bond failure grouted element/ parent material

In the case of frictional anchors, curves (Fig. 4-16) show linear behaviour up to the point when the stick-and-slip device is activated. For lower values of the perpendicular pressures on the device, $F_{\perp}$, and hence for lower values of slip load, $F_{//}$, the second portion of the load-displacement curves is horizontal, as expected for a frictional

mechanism; relative sliding between the frictional plates is achieved. For higher $F_{\perp}$ though, stiffness is developed as consequence of mechanical locking between the frictional plates; the jaggedness of load-displacement curves is mainly related to this stick-and-slip behaviour rather than to the failure of the anchor assembly, even though minor damage at the interface grout/parent material is recorded in certain cases, as higher loads are transmitted to the substratum.

Following the same procedure as per standard anchors, the load capacity measured experimentally, as well as the load values of yielding of the hysteretic devices and of activation of the friction mechanism of the stick-and-slip devices, are compared to the theoretical values calculated on the basis of the material properties and of the main mode of failure, namely grout/masonry bond failure (Table 4-13and Table 4-14). By doing so, one can verify whether a match between theoretical and recorded values exists and which mechanism (bond failure/activation of devices) controls the overall performance of anchors.

In light of the observations drawn in the previous paragraphs, only values calculated by Eq. (4-5) in combination with f_{vk} and by Eq. (4-7) are considered, as these provide a better representation of the standard anchor behaviour.

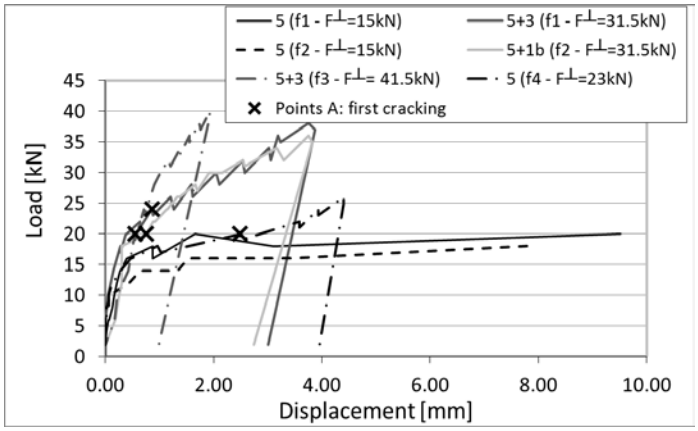

Fig. 4-16: Frictional anchors – Load-displacement curves

Table 4-12: Frictional anchors – Summary of failure modes of pull-out tests

Sample No	**Failure type**	
f1 ($F_{\perp}$=15 kN))	5	Sliding
f1 ($F_{\perp}$=31.5 kN)	5 + 3	Sliding + mixed mode
f2 ($F_{\perp}$=15 kN))	5	Sliding
f2 ($F_{\perp}$=31.5 kN)	5 + 1b	Sliding + bond failure grouted element/ parent material
f3 ($F_{\perp}$=41.5 kN)	5 + 3	Sliding + mixed mode
f4 ($F_{\perp}$=23 kN)	5	Sliding

For hysteretic anchors (Table 4-13), the first drop in stiffness, corresponding to the point A of the idealised load-displacement curves (Fig. 4-17), indicates the transition

from elastic to non-linear behaviour. Such transition is mainly motivated by the yielding of the hysteretic device, although some small movements also occur in the other elements of the assembly (Fig. 4-17); indeed, loads measured at point A are both higher than the yielding of the device and the theoretical threshold based on the value of initial shear strength, which indicates first cracking, as previously discussed.

Table 4-13: Hysteretic anchors – Comparison of experimental and theoretical load capacity [kN]

Anchor No	**Experimental**			**Theoretical**			
	A	**B**	**C**	**Device yielding ($F_y=f_y \cdot A$)**	**F - Eq. (4-5), Hp: $\tau_{cr}=f_{vk,0}$**	**Na - Eq. (4-5) Hp: $\tau_{cr}=f_{vk}$**	**N - Eq. (4-7)**
y1	38	46	52	27.9	21	46.5	36.1
y2	30	38	52			24.0	
y3	32	38	42				
y4	32	38	48				
Av.	33	40	49				
CoV [%]	10	10	10				

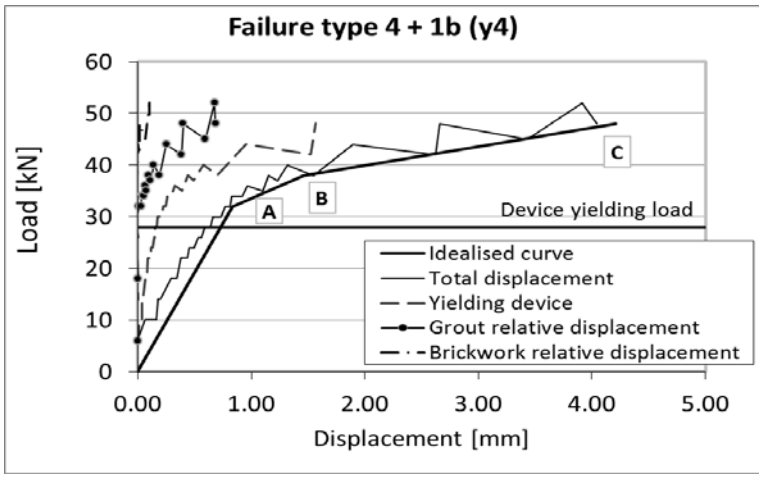

a)

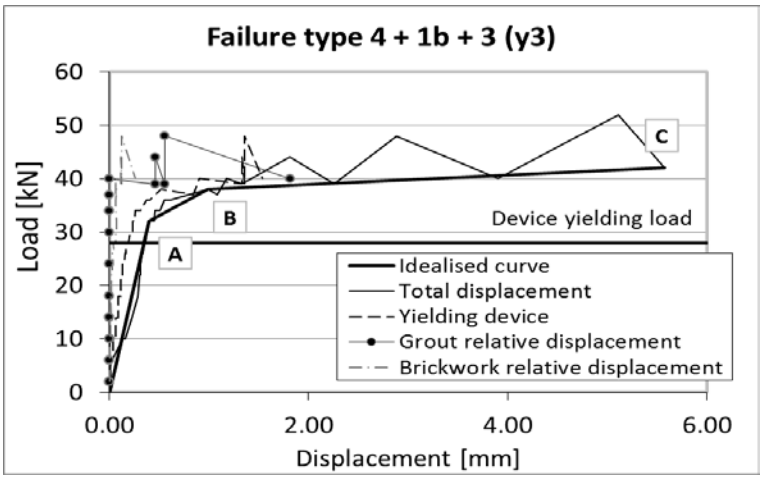

b)

Fig. 4-17: Hysteretic anchoring devices - Comparison between idealised load-displacement curve of the whole assembly with the curves showing relative displacements of the various components

It is interesting to observe in reality plastic deformation of the hysteretic device occurs for values of load higher than the yielding load as calculated on the basis of the yielding strength of the dissipative element (Fig. 4-17b). However, it should also be kept in mind that yielding strength as stated by the producer is a minimum value; therefore a yielding load higher than expected is possible.

In Fig. 4-17a, it is also visible that relative movements in the testing equipment have affected the readings of the total displacement; in case of further testing, it is recommended that total displacement are taken directly on the anchor bar rather than in series with the pulling apparatus.

Maximum load capacity is attained in B; after this point constant load determines continuous movement. It is worth highlighting that load-displacement curves are not perfectly horizontal between point B and C, thus meaning that the anchor still has a residual capacity partly due to mechanical locking, which prevents complete failure of the bond, partly due to the plastic stiffness of the hysteretic device. Values of load attained at point B are in line with theoretical values, meaning that the behaviour of the anchor assembly is nevertheless strongly influenced by the relative displacements at the interface between grouted element and parent material, as visible in Fig. 4-17.

The presence of the hysteretic device has the advantage of providing the assembly with high ductility: although some damage to the substratum is detected, a large part of the total displacement is due to the plastic deformation of the dissipative element (Fig. 4-17). Furthermore the hysteretic devices homogenise the performance of the anchors, as it can be seen by the small variation of values of performance parameters (Table 4-13). Regression analysis is performed to find the equation that describes the behaviour of the anchors. The resulting curve, a logarithmic function, which shows a good match, is reported in Fig. 4-18.

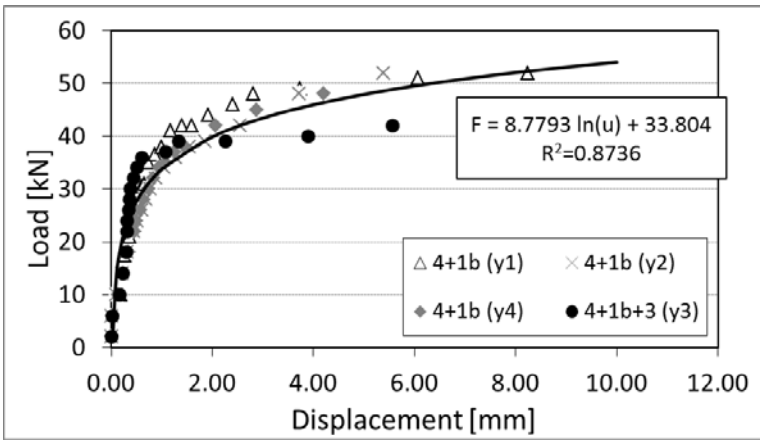

Fig. 4-18: Hysteretic anchors – Regression curve approximating the experimental load-displacement curves. In equation, F is the pulling force and u is the overall anchor displacement

In the case of frictional anchors (Fig. 4-19), theoretical values of the activation of the sliding mechanism are lower than the calculated pull-out capacity (Table 4-14). This

well pictures experimental evidence: the transition from elastic behaviour to fully frictional behaviour occurs before damage is recorded in the substratum; indeed no variation of stiffness is detected before the activation of the stick-and-slip device.

Hence, an additional threshold point is added: F represents the actual slip load, $F_{//}$, for which the frictional mechanism is initiated. For lower values of $F_{//}$ point F also coincides with B, as load beyond it is almost constant up to the point of maximum displacement, C. Conversely, in case of higher values of slip-load, the curve between F and C is jagged and presents a further increase in stiffness.

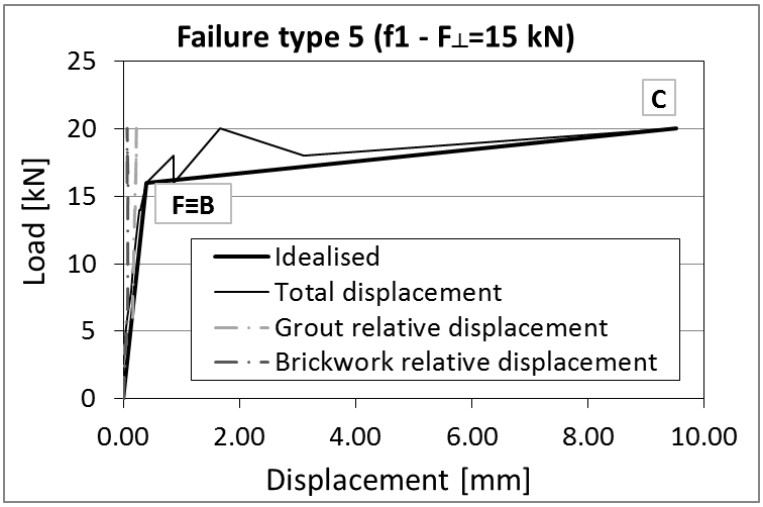

Fig. 4-19: Frictional anchors - Comparison between idealised load-displacement curve of the whole assembly with the curves showing relative displacements of the various components

Such phenomenon depends on mechanical locking occurring among the various pieces of the device assembly as consequence of the higher perpendicular pressure applied to attain a higher slip-load; this creates a “stick-and-slip” behaviour, well visible in Fig. 4-19. A summary of the expected and measured activation points of the sliding mechanism is given in; recorded values are as average slightly higher than those

calculated on the assumption of Φ=0.15, namely plates in pristine conditions, according to results discussed in §4.2. In fact, Φ is equal to 0.36 (CoV 9%).

Table 4-14: Frictional anchors – Comparison of experimental and theoretical load capacities [kN]

Anchor No	Experimental			Theoretical				
	F (Sliding)	**A**	**C**	**$F_{\perp}$**	**Slip load: $F_{//}=2\Phi F_{\perp}$**	**F - Eq. (4-5), Hp: $\tau_{cr}=f_{vk,0}$**	**N_a - Eq. (4-5) Hp: $\tau_{cr}=f_{vk}$**	**N Eq. (4-7)**
f1	16	-	20	15.0	4.5	21	24.3	36.1
	20	18	37	31.5	9.45			
f2	10	-	18	15.0	4.5		23.8	
	18	20	36	31.5	9.45			
f3	30	20	40	41.5	12.45			
f4	16	20	25	23.0	6.9			

Looking in more detail to the relative displacements within the anchor assembly, it is possible to observe that, while for low levels of perpendicular force no relative displacements are recorded at the outer surface of the brickwork and of the grouted element (Fig. 4-19a), the stiffness developed as consequence of mechanical locking due to higher perpendicular loads create some damage in the parent material (Fig. 4-19b). As said before, cracking is so minimal that it doesn't influence the stiffness of the overall load-displacement curve; still first-cracking forces (point A) are reported in Table 4-14 for sake of completeness. It is worth highlighting, that the load values predicted on the basis of $f_{vk,0}$ well fit values of load at which minor damage is recorded. This means that the anchor in series with the frictional device behaves like a standard anchor up to point F; beyond this point friction controls the behaviour.

In case displacement continues up to the maximum value where the device stops are activated, the assembly goes back to the standard anchor behaviour, meaning that it would have a maximum load capacity that could be calculated on the basis of f_{vk}, as per standard anchors.

By comparing the performance of a strength-only anchor, a hysteretic anchor and a frictional anchor (Fig. 4-20) it is possible to observe that whilst standard anchors are very stiff and fail for small displacements, which are due to damage and relative motion between the substratum and anchor assembly, the frictional anchor provide large displacement with relatively small, if any, damage in the masonry, even in the case of higher perpendicular pressure on the friction plates. Hysteretic anchors have a performance in between standard and frictional: even though the assembly doesn't reach the threshold of 10 mm maximum displacement and damage is recorded in the substratum, the performance is improved in respect to a strength-only anchor, with larger displacements mainly due to the plastic elongation of the device rather than major cracking in the substratum.

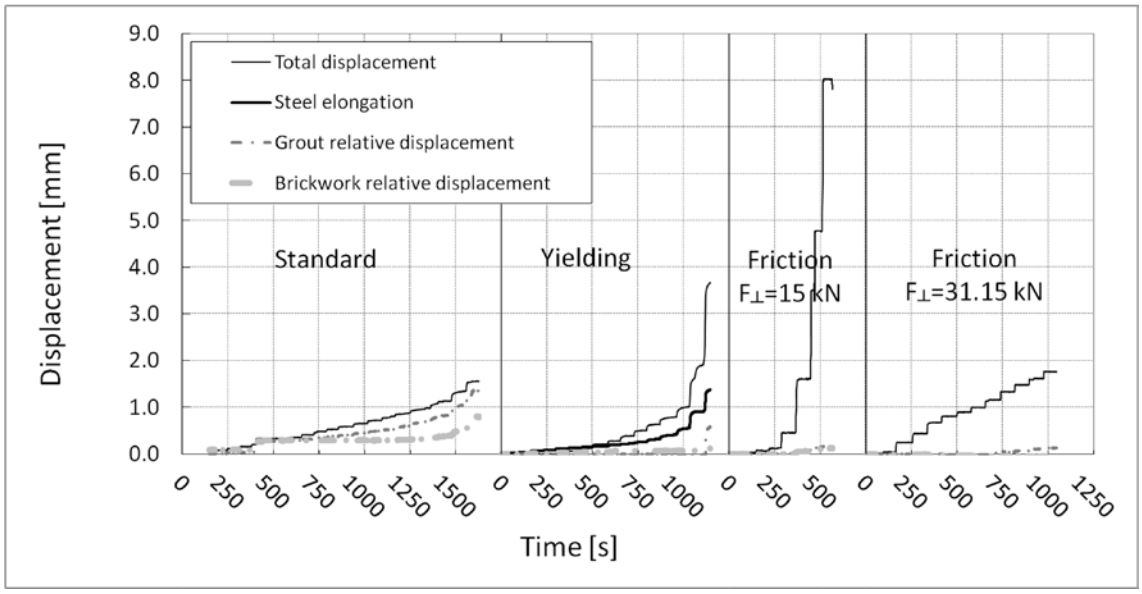

Fig. 4-20: Relative displacements in a standard anchor and in anchors in series with a hysteretic device or a friction device calibrated with two different levels of slip load

4.4 CYCLIC TESTS OF T-SHAPED MASONRY SPECIMENS

4.4.1 Test Set-Up

Pull-out tests focus on the head portion of an anchor undergoing horizontal loading and on its interaction with the wall perpendicular to such action. To this purpose, the test set-up simplistically neglects the phenomena occurring in the other masonry panel belonging to the wall-to-wall connection and in the portion of anchor embedded into it. Although expedient to the task of identifying the parameters that control the anchor performance in its weakest part, the experimental procedure is not exhaustive of the whole plethora of effects that the strengthening system has on the structural connection.

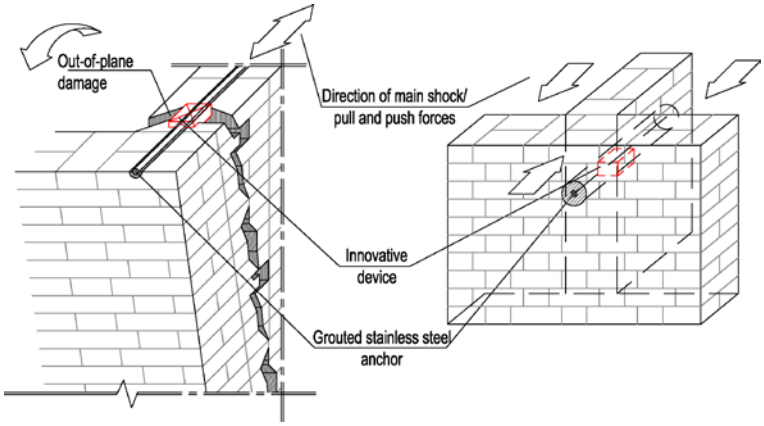

Fig. 4-21: On-site layout and laboratory set-up of cyclic tests

However, the response of the full connection can be observed by modifying the set-up of pull-out tests so as to reproduce a longer part of the anchor and the second wall: samples are T-shaped walls where the “leg” of the T reproduces the wall parallel to the main seismic action, whereas the “head’ of the T represents a section of a panel undergoing out-of-plane damage. The T leg is connected to a strong wall that simulates the rest of the building, whilst the T head undergoes cyclic loading that creates an overturning mechanism and the formation of a crack at the joints between the two walls (Fig. 4-21). Such type of damage is recurring in historic buildings due to the lack of good quality connections, this being recreated in the sample by ensuring a modest overlapping of bricks at the joint.

The horizontal action is applied to the head of the T by anchoring the leg of the T to the strong wall by means of grouted anchors, one at the bottom, running along the T leg only, the other at the top of the wall, running throughout the head and the leg of the T. While the bottom anchor works purely as restraint, the top anchor is the object of testing and its lay-out is representative of standard applications. Indeed ties are generally installed at the top of buildings and the connection to the strong wall simulates the reaction force to pull-out load due to the bond between the parent material and the anchor, which runs along the whole specimen panel (Fig. 4-22).

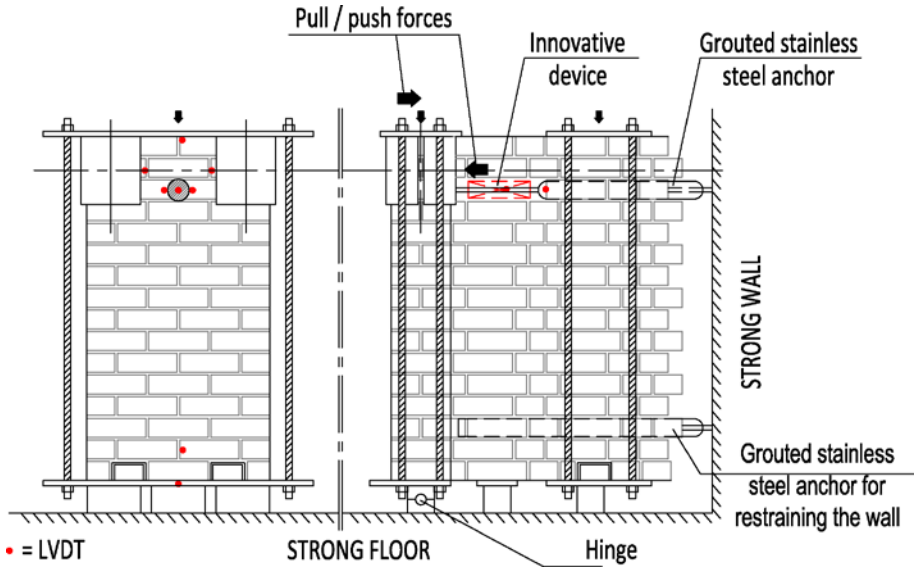

Fig. 4-22: Geometry of T-shaped samples and instrumentation

In those masonry specimens that include a dissipative device (add-on element marked in red in Fig. 4-22), this is inserted in series with the metallic anchor by splitting the fabric sleeve that contains the grout in two: a front part, long as the head of the T is thick, and a rear part, cut to a size that leaves a grout-free recess for the dissipative device. The removal of one brick maintains the device visible for the whole duration of tests and facilitates the placement of instrumentation.

4.4.2 Materials and Samples

A total of 9 walls are built; 3 are strengthened by standard anchors, 2 by hysteretic anchors, and 3 by frictional anchors, whilst one is left unreinforced as means of comparison.

The walls are built in double bond, using recycled hand-cut bricks and natural hydraulic lime mortar. Masonry units are solid fired bricks, sized 220 x 110 x 70 mm. The head of the T is about 700 mm by 220 mm in plan, the leg is about 900 mm by 220 in plan; walls are 1200 mm high.

Characterisation of materials is carried out according to current codes, as outlined in §4.3. Mechanical properties of material at the age of testing are summarised in Table 4-15. For the sake of homogeneity and to allow for the comparison of results, anchors are made of the same profiles used for pull-out tests.

A vertical load representing the dead load of the upper structure is applied throughout the tests by steel plates compressed by tensioned threaded bars, which create a vertical stress field of approximately 0.07 MPa. Steel plates are used to spread the vertical load to the parent material (Fig. 4-22 and Fig. 4-23); this load is controlled by strain gauges placed on the vertical bars that measure deformation resulting from tensioning the rods by locking the hexagonal nuts at their top end.

Table 4-15: Summary of mechanical properties of test material resulting from characterisation tests

Recycled hand-cut solid bricks (220x110x70 mm)		
Compressive strength	12.8 (CoV 14%)	[MPa]
NHL 5 lime mortar		
Mix proportions lime to sand	1:2	b.v.
Flexural strength	0.2 (CoV 19%)	[MPa]
Compressive strength	0.5 (CoV 25%)	[MPa]
T-shaped masonry walls, double bond		
Compressive strength	3.1 (CoV 16%)	[MPa]
Bond strength (by wrench test)	0.5 (CoV 20%)	[MPa]

4.4.3 Testing Procedure

Cyclic load is applied by two hydraulic push jacks and one hydraulic pull jack restrained against the strong wall.

Tests are carried out in displacement control; the control point is at the level of the top anchor, at the midpoint of the front wall. Three cycles of loading and unloading are performed for increasing amplitude of displacement up to 10 mm of displacement or until visible damage occur, according to the same criteria set for pull-out tests.

Displacements are recorded at various levels of the wall, according to the layout shown in Fig. 4-22, so as to observe the displacement profile along the height of the front of each sample and the evolution of damage in the parent material and at the

interface between anchor and masonry. Additionally relative displacements occurring on the T leg are manually recorded every three cycles of load by relying on a reference grid, so as to detect the formation of diagonal cracks in the wall parallel to the direction of application of the cyclic load.

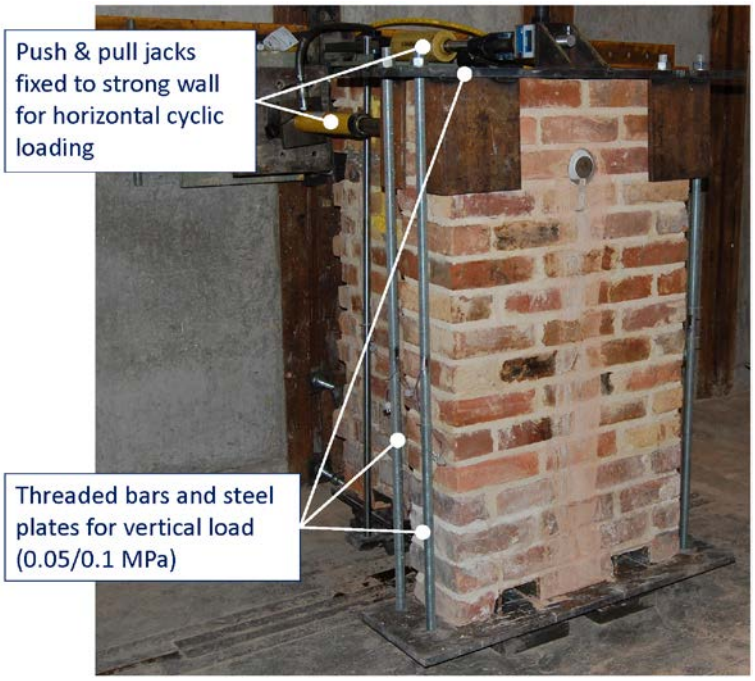

Fig. 4-23: Set-up of T wall

4.4.4 Results

4.4.4.1 Standard Anchors

For the test set-up described above and standard anchors, failure is expected to occur initially by sub diagonal in-plane cracking of the restrained wall parallel to the pull-push action, and eventually by failure of the head of the anchorage according to one of the failure modes described in the previous section (Fig. 4-10).

Due to the use of different recycled materials and differences in the construction quality of samples, which depended on the availability of workmanship and materials at the time of construction, specimens developed lower mechanical properties in respect to pull-out tests. For instance, the use of smooth bricks, rather than bricks with holes, impaired the bond strength. Nevertheless, specimens are representative of low-quality masonry according to Circolare 02/02/2009 n. 617 (2009), which collates the mechanical properties of masonry typologies commonly found across the Italian territory. Indeed values reported in Table 4-15 are comparable to ashlar masonry or roughly-hewn block masonry (f_c=2.0/3.8 MPa, τ_0=0.035/0.074 MPa).

As consequence of the poor mechanical properties of masonry, the bond between the grouted sleeve of the standard anchor in the front walls and the parent material fails at very early stages of tests. This is detected looking at the displacements at the level

of the anchor: values recorded on the brickwork surface are proportional to the applied displacements; conversely, very little motion is detected on the metallic front plate of the anchor (Fig. 4-24). Bond failure is also identified by plotting the displacements at different level of the front wall for each set of three load cycles with the same amplitude (Fig. 4-25).

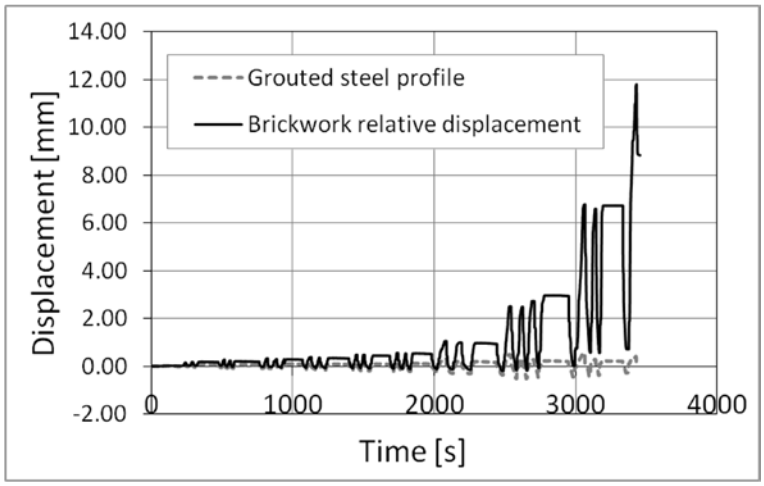

Fig. 4-24: Standard anchor – Displacements recorded on brickwork surface and front end of grouted anchor

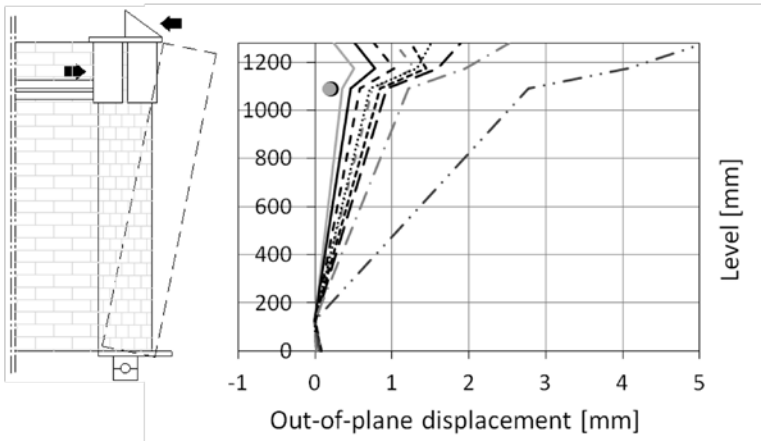

Fig. 4-25: Standard anchor – Displacement profiles along the whole height of the front wall. Differently dashed profiles indicate displacements at different amplitudes of applied displacement cycles; the position of the anchor is marked as a dot

Because of early bond failure, load is not transmitted to the rear wall by the anchor and diagonal in-plane cracking doesn't occur. Instead, a vertical crack opens at the joint between the two parts of the walls following the weak pattern provided during the preparation of specimens by leaving the bricks at the joint with a smaller overlapping. This reflects the fact that, if the anchor is not able to develop a sufficient bond, its effectiveness in reconnecting two walls is reduced, as it could be expected.

The failure of the head of the anchorage in the front wall follows the mode already described for pull-out tests: an initial bond failure at the interface between the grouted sleeve and the parent material is followed by a “wrench” failure (Fig. 4-26a). The formation of cracks in the front wall shows that, even after the failure of the bond, the assembly still transmits a punching action to the head of the T via mechanical locking. The phenomenon of locking can be observed once specimens are dismantled after testing (Fig. 4-27): the grouted sock is indeed shaped according to the voids present in the masonry fabric.

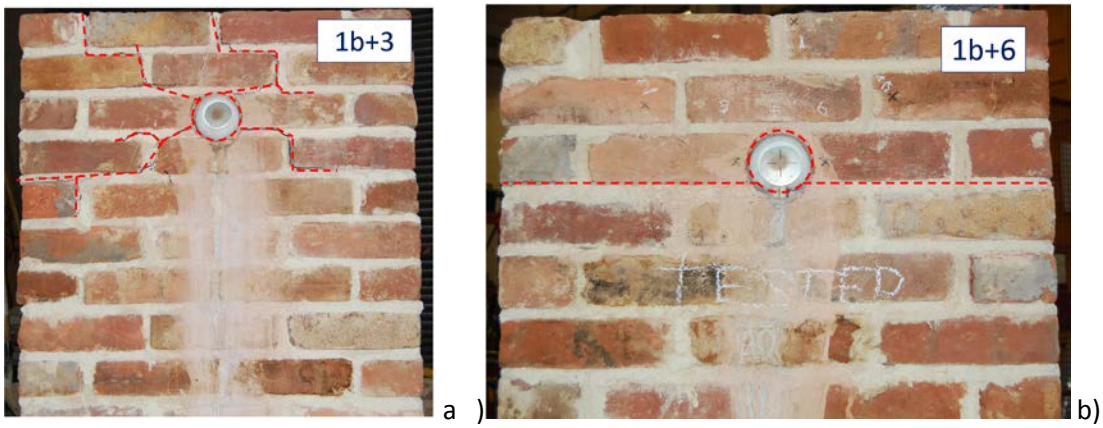

Fig. 4-26: Standard anchor – Bond failure followed by: 1b + 3) wrench failure (Wall No 2T and No 3T) and 1b + 6) sliding shear mechanism caused by the testing apparatus (Wall No 1T)

Fig. 4-27: Irregularities of grouted sleeve causing mechanical locking

Due to the testing set-up and to the weakness of the bond mortar/masonry units, a sliding shear failure occurred in one of the specimens (Failure type No 6, see Fig. 4-26b). In spite of the material weakness and early bond failures, anchors do increase the load capacity of the T joint in respect to an unreinforced sample, as it can be seen from Fig. 4-28.

The improvement in the response of strengthened specimens in respect to the unreinforced one can also be measured by calculating the dissipated energy, i.e. the area included in the loops of the load-displacement curves of the whole system at the wall top level. Indeed the area of hysteresis loops of strengthened specimens is averagely 140% larger than for the unreinforced specimen. Indeed the unloading of

the unreinforced specimen is linear whereas the reinforced specimens lose load capacity as soon as cycles are reversed and before recuperating any displacement.

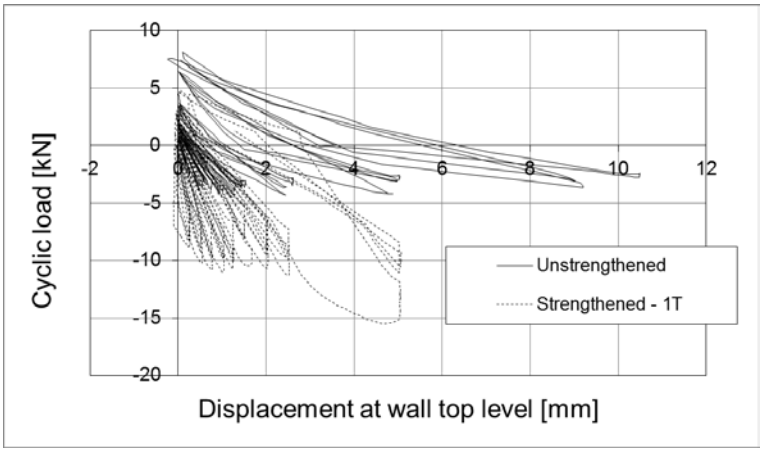

Fig. 4-28: Standard anchors – Load-displacement curves of the unreinforced specimen and of wall No 1T

Similarly to the process followed for pull-out test results, points identifying changes in the stiffness of the load-displacement curves are used to define idealised curves (Fig. 4-29 and Table 4-16). In the graphs, negative values of load correspond to the outward tilting movement of the front wall; positive values are instead recorded when the wall is moved back to the original position. An extra amount of force is needed to push the wall back to the "0 displacement" position due to the presence of debris within the crack and local dislocations of bricks, which prevents the complete closure of the crack.

Table 4-16: Standard anchors – Summary of points identifying the idealised load-displacement curves

Anchor ID	**A**		**B**		**C**		**D**		**E**	
	kN	mm	kN	mm	kN	mm	kN	mm	kN	mm
1T	6.9	0.10	10.9	0.78	11.4	2.52			15.7	5.04
2T	7.1	0.54	17.8	5.06	19.1	10.0	12.6	15.6		
3T	7.6	2.52	21.9	10.0	29.6	20.1				
Av.	7.2	1.05	16.9	5.28	20.0	10.9				
CoV [%]	5	122	33	87	46	81				

Performance points are defined as: A, first damage, B, maximum load, C, maximum displacement and D, ultimate failure. In one case, a further increase of stiffness (point E) occurs after the plateau between point B and C; it is also worth noticing that in all the cases the plateau is not perfectly horizontal, thus indicating a residual capacity in the joint after point B, which can be conservatively considered as peak capacity. Importantly, even for such poor material characteristics of the substratum it is possible to identify a ductile behaviour of the assembly. Ductility is displayed during the first cycle of the suite at constant amplitude; the following two involve lower maximum load and almost linear cycles. The loss of load capacity as consequence of the reversal

of load and of repeated cycles is documented by other authors and is the natural consequence of the wearing of the surfaces along which friction occurs.

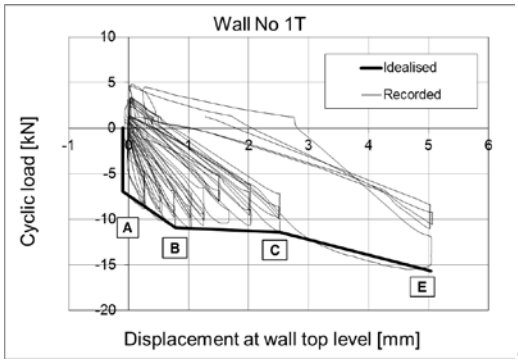

a)

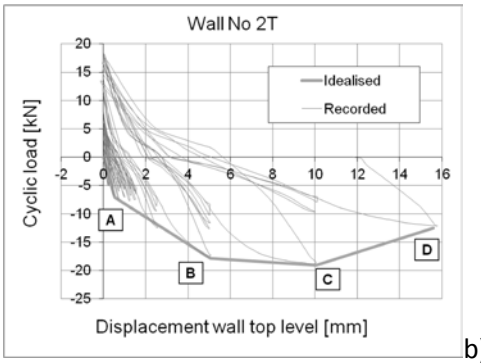

b)

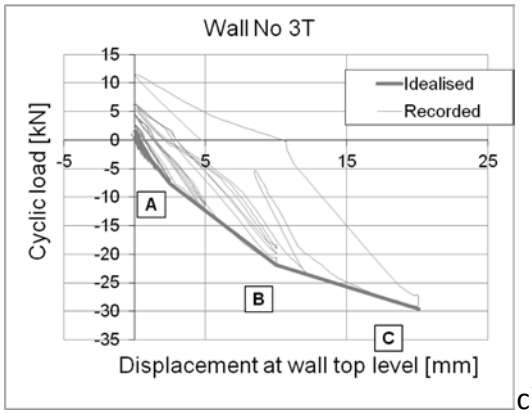

c)

Fig. 4-29: Standard anchors – Recorded and idealised load-displacement curves: a) Wall No 1: 1b + 6 – grout/masonry bond failure of anchor and shear sliding failure of wall, b-c) Wall No 2 and No 3: 1b + 3 –grout/masonry bond failure of anchor and wrench failure of wall

Experimental and theoretical load values of pull-out loads are compared, similarly to monotonic pull-out tests. However, in this case, shear strength is derived directly from the tests rather than using a value borrowed from the literature. The force level that causes the activation of the shear sliding mechanism in the front wall of one of the samples is detected by looking at the displacement profile of Fig. 4-24b and divided by the area in plan of the head of the T. This identifies f_{vk}, namely the shear strength that includes the effect of the vertical load applied on the head of the T. By reversing equation (4-9), the initial shear strength, $f_{vk,0}$, can be calculated. Such value is then used to compute f_{vk} on the basis of σ_d, the vertical load that was continuously recorded during tests.

The way the anchor influences the overall response of the specimen is highly variable, as it can be observed by looking at the load-displacement curves of the grouted anchors in respect to those of the surrounding parent material (Fig. 4-30). Whereas in some cases (Fig. 4-30a) the bond failure occurs so early in the test that the two curves diverge immediately, in others (Fig. 4-30b) a better bond is achieved; when this happens the specimen displays a higher capacity.

For specimens with a good bond between grout and masonry, the performance points of the idealised curve are the same as for curves derived from pull-out tests: A is indeed the point where first damage occurs; nevertheless, the anchor is still able to

contribute to the achievement of the maximum load capacity by maintaining a bond with the masonry (Fig. 4-30b). Accordingly, B is the experimental value of pull-out capacity.

In other cases, like in Fig. 4-30a, the damage occurring at point A is sufficient to provoke an almost independent behaviour between the anchor and the front wall. In these cases, point A is taken into account for the pull-out capacity; the load capacity recorded at point B is instead influenced by the friction occurring at the joint between the two walls, where cracks open, and on the failure surface of the grouted anchor. As the sock moulds into the voids that are present within the wall, its surface can be highly irregular, thus providing a good contribution in terms of resisting force, especially when irregularities are of a size sufficient to create mechanical locking.

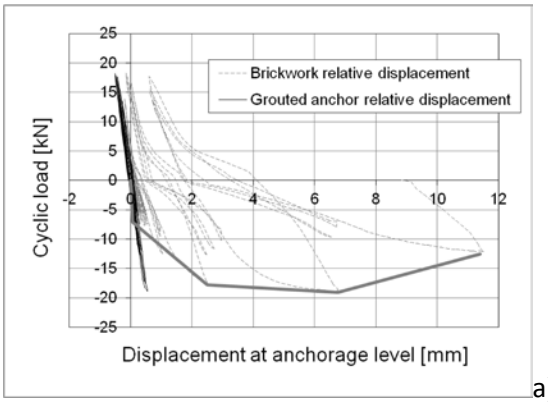

a)

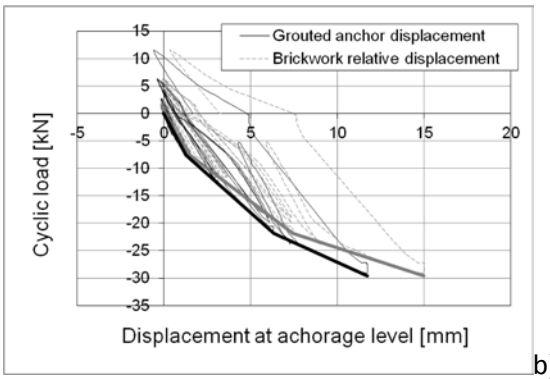

b)

Fig. 4-30: Standard anchors – Recorded and idealised load-displacement curves of grouted anchors and parent material. a) Wall No 2T and b) wall No 3T

Results summarised in Table 4-17 show that in the case of such a weak substratum the model proposed by Gigla and Wenzel (2000) largely overestimates the capacity of the anchors, while the use of shear strength, even though conservative, gives a better approximation of the actual behaviour of anchors.

Table 4-17: Standard anchors – Comparison of experimental and theoretical values of pull-out loads

	Experimental	**Theoretical**					
Anchor No	**Pull-out load (point A or B)**	**σ_d**	**$f_{vk,0}$**	**F - Eq. (4-5), Hp: $\tau_{cr}=f_{vk,0}$**	**f_{vk}**	**N_a - Eq. (4-5) p: $\tau_{cr}=f_{vk}$**	**N Eq. (4-7)**
	[kN]	[MPa]	[MPa]	[kN]	[MPa]	[kN]	[kN]
1T	10.9	0.1	0.04	2.22	0.08	4.44	36.6
2T	7.1						
3T	7.6	0.0			0.06	3.33	

Despite the difference in behaviour that derives from the quality and degree of bond and locking between anchor and parent material, the strengthening system succeeds in improving the performance of the connection. This is a substantial achievement, especially considering the weakness of the unreinforced specimen, which shows that

the technique is effective and offer advantages. Results also suggest that control procedures should be implemented so as to ensure that the drilled hole presents sufficient irregularities to develop an effective bond and performance is less affected by the peculiarity of the local geometry of the hole. This would be particularly important in substrata, like the one of cyclic tests, where shear strength is low and a strong bond unlikely to develop. In substrata like the present, where the shear strength of the parent material is higher and the anchor is naturally able to develop a good bond, this would not be as necessary. Nevertheless, the scattering of the performance and the presence of damage are still considerable pitfalls.

4.4.4.2 Dissipative Anchoring Devices

As for pull-outs, the dissipative devices are partly able to address the issues experienced with the standard anchors. Whilst the yielding threshold of the hysteretic anchors is still too high to avoid final pull out of the head of the anchorage, the frictional devices are able to provide the required level of relative displacement (Fig. 4-31). Indeed, in the light of results obtained with the standard anchors, frictional anchors devices are set to a minimum level of slip-load, so as to avoid the stick-and-slip behaviour observed during pull-out tests, which would have been detrimental to the weak masonry of the T specimens.

The prevalent failure mode at the head of the anchorage is a bond failure between grout and parent material (Fig. 4-31 and Fig. 4-32), followed by a “wrench” failure that spreads to the brickwork surrounding the drill hole.

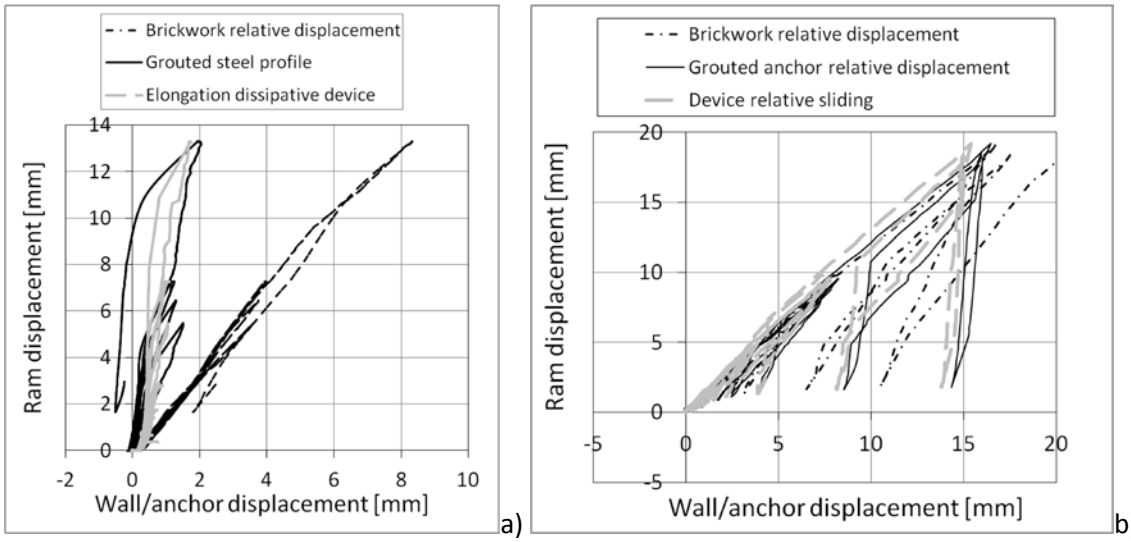

Fig. 4-31: Load deflection curves of T-shaped walls strengthened by a) hysteretic device and b) frictional device

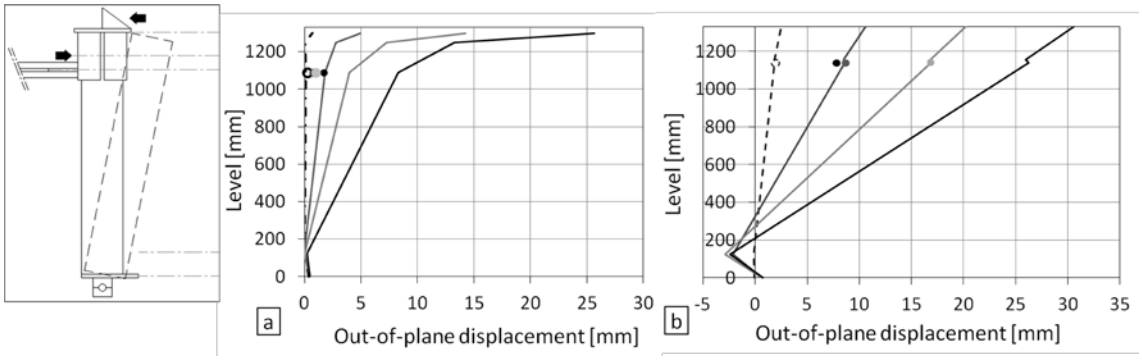

Fig. 4-32 Displacement profiles along the whole height of the front wall in case of strengthening by hysteretic anchoring device (a) and frictional anchoring device (b). Different greys indicate different amplitudes of applied displacement; the position of the anchor at each cycle is marked as a dot of the same grey as the line

The idealised, or backbone, curves (Fig. 4-33a and Fig. 4-33b) help to better understand the behaviour of the strengthening system and to compare the three different typologies of anchors. In the graphs, negative values of load coincide with the outward tilting movement of front wall; positive values are instead recorded when the wall is moved back to the original position. An extra amount of force is needed to push the wall back to the "0 displacement" position due to the presence of debris within the crack and local dislocations of bricks, which prevents the complete closure of the crack.

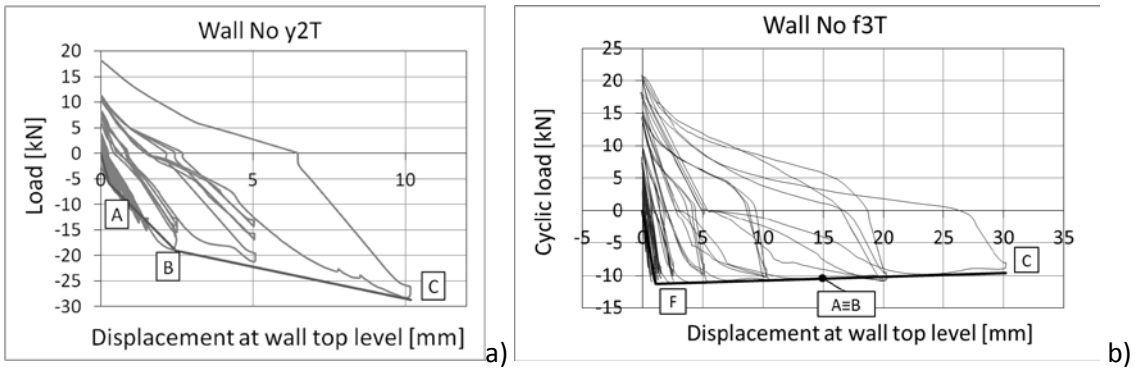

Fig. 4-33: Recorded and idealised load-displacement curves of walls strengthened by a) hysteretic anchoring device and b) frictional anchoring device

For walls strengthened by the hysteretic anchor devices (Fig. 4-33a), performance points are defined as: A, first damage, B, maximum load, and C, maximum displacement. For both tested walls the plateau between point B and C is not perfectly horizontal; this is due the fact that despite a pull-out failure, because of the irregularities of the drilled hole, the front anchor is still able to "grip" to the front wall and hence transmit load to the threaded bar embedded in the grout and through this to the hysteretic device, which maintain the connection with the back wall.

For walls strengthened by the frictional anchoring devices (Fig. 4-33b), identified performance points are: F, activation of sliding in the frictional device and C point of maximum displacement. Even though the load remains fairly constant after activation of the device and no abrupt changes in stiffness are detected, points A and B are also marked on the curve, so as to pinpoint bond failure at the interface grout/parent material. In fact the two points A and B coincide, as pull-out occurs without clear distinction between first damage and full failure.

Looking at the relative displacements occurring at the surface of the brickwork and of the grouted socket, and comparing them with the idealised load curve, the calculated pull-out capacity and device activation load, it is possible to say that:

- For wall strengthened by hysteretic anchor devices, (Table 4-18a and Fig. 4-34): the yielding load of the devices is significantly higher than the shear capacity of the masonry and the bond strength so that the dissipative element remains in the elastic field. The point of first cracking coincides with a failure at the bond between the grouted element and the brickwork. The following increase in load is likely to be due to a locking mechanism that allows the front wall to transmit part of the load to the anchor; this is inferred by the fact that cyclic displacements are still recorded on the dissipative element and the end plate of the anchor (Fig. 4-34). Point A and B can be conservatively calculated by means of f_{vk} and $f_{vk,0}$ as in the previous section.
- For wall strengthened by frictional anchor devices, the observation of relative displacements between the assembly parts confirms that the bond capacity of the anchor in the front wall is higher than expected (Table 4-18b), thanks to mechanical locking between the grouted sock and the drilled cavity. This allows the friction device to be activated and prevent cracking until later stages of tests, as it can be observed in Table 4-18b. The calculated values of slip-load show a good match with those observed, due to the assumption that the ratio between $F_{//}$ and $F_{\perp}$ is Φ=0.33, this being the value calculated from pull-out tests. Φ is indeed equal to 0.31 (CoV 19%).

Table 4-18: Hysteretic (A) and frictional (B) anchors – Comparison of experimental and theoretical load capacities [kN]

	Experimental			**Theoretical**			
A) Anchor ID	**A**	**B**	**C**	**F - Eq. (4-5), Hp: $\tau_{cr}=f_{vk,0}$**	**N_a - Eq. (4-5) Hp: $\tau_{cr}=f_{vk}$**	**Yielding load ($F=f_y \cdot A$)**	
y1T	12.9	26.3	37.7	2.2	6.6	27.9	
y2T	6.0	19.1	28.7		4.4		
B) Anchor ID	**F**	**A≡B**	**C**	**F - Eq. (4-5), Hp: $\tau_{cr}=f_{vk,0}$**	**N_a - Eq. (4-5) Hp: $\tau_{cr}=f_{vk}$**	**$F_{\perp}$ [kN]**	**$F_{//}=2\Phi F_{\perp}$ [kN]**
f1T	7.6	7.5	6.5	2.2	3.3	15	9.9
f2T	9.4	No pull-out	8.5				
f3T	11.2	10	9.6				

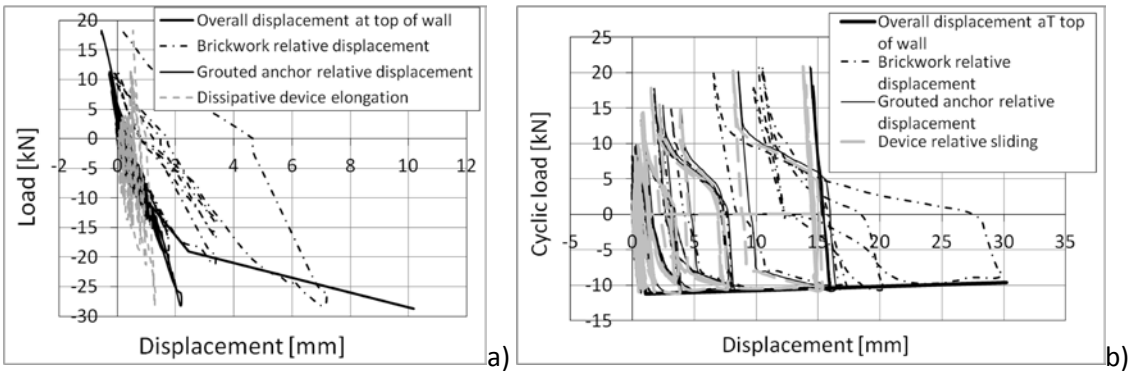

Fig. 4-34: Walls strengthened by: a) hysteretic and b) frictional anchoring devices. Comparison between idealised load-displacement curves and recorded relative displacements of assembly components

To summarise, it can be said that frictional anchors have a good performance thanks to the fact that the slip load at which the sliding mechanism is activated can be set to various levels. Indeed, this allows controlling the behaviour of the devices, which are hence able to deliver the required level of displacement and to control the transmitted load regardless the mechanical properties of the parent material.

Conversely, in a very weak substratum, hysteretic anchors deliver a performance closer to that of standard anchors, as the low shear strength of masonry causes pull-out failure at loads lower than those required to take the hysteretic element into the plastic field. In this sense, the hysteretic device has the limitation that its characteristics (cross sectional area and yielding strength) cannot be freely modified, but are chosen depending on the availability of steel with low strength class and on the basis of safety criteria, i.e. by designing the dissipative element so as to avoid early tensile failure.

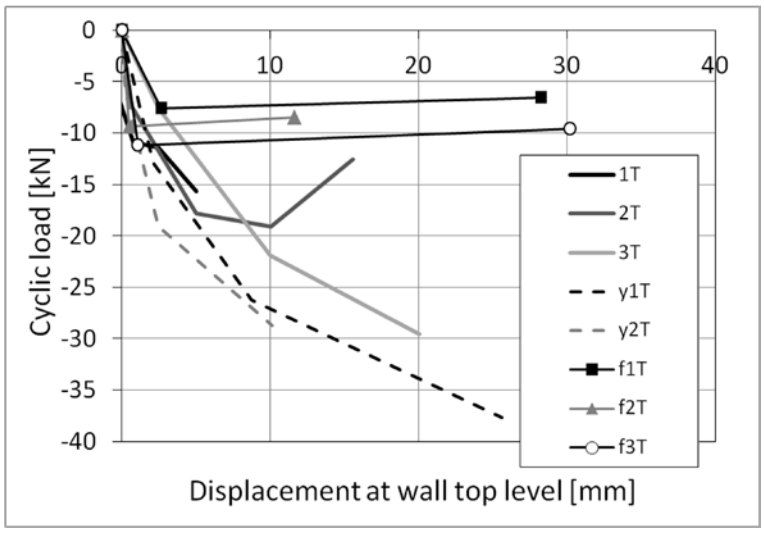

Fig. 4-35: Comparison of load-displacement curves of standard (continuous line), hysteretic (dotted line) and frictional (line with markers) anchors

Yet, even the yielding devices offer an improvement in the performance of the strengthening system in respect to standard grouted anchors: from Fig. 4-35 one can appreciate the more uniform behaviour and higher load capacity in respect to the scattered performance of standard grouted anchors. This means that yielding anchors can be applied whenever strength capacity is more relevant than damage limitation; the method for design the devices on the basis of either a capacity or a performance approach will be discussed in detail in Chapter 7.

4.4.4.3 Failure in the Parent Material

As already mentioned in the previous paragraphs, a "wrench" failure is observed both for standard anchors and anchors in series hysteretic devices. Indeed, the punching effect of the surface irregularities of the grouted socket provokes a series of radial cracks that propagate from the initial failure surface at the interface grout/brickwork to the surrounding parent material. This behaviour is observed in cyclic tests as much as in some of the pull-out tests. The presence of "wrench" cracks indicates that the reaction of sock irregularities bearing in compression against the parent material is sufficient to stop relative motion and trigger a different resisting mechanism.

The crack pattern depends on the geometry of the sample and it is hardly predictable; however, to the purpose of modelling and calculating the failure, it is sufficient to know the overall extent of the failure surface associated to this type of failure, rather than its exact geometry. Therefore, assuming that the failure mechanism is triggered when the strain energy stored in the metallic bar undergoing the axial load equates the fracture energy of the parent material, it is possible to calculate the crack surface area and verify whether theoretical results match the experimental evidence.

The elastic strain energy is calculated considering only the contribution of the strain of the metallic element, as it can be assumed that the strain energy stored in the masonry is negligible and it is released when slippage occurs at the grout masonry interface. As the maximum loads achieved during tests are lower than the yielding threshold of the metallic bars, the linear strain energy density can be written as:

4-11) $$\int_0^{\varepsilon} \sigma_s d\varepsilon = \int_0^{\varepsilon} (E_s \varepsilon_s) d\varepsilon = \frac{1}{2} E_s {\varepsilon_s}^2$$

where all the parameters in equation (4-11) refer to the steel bar.

For uniaxial loading, the linear strain energy per unit length becomes:

4-12) $$U_s = \int_A \frac{1}{2} E_s \varepsilon_{s,xx}^2 dA = \int_A \frac{1}{2} E_s \left(\frac{du}{dx}\right)^2 dA = \frac{1}{2} E_s A_s \left(\frac{du}{dx}\right)^2 = \frac{1}{2} \frac{N^2}{E_s A_s}$$

where the Young modulus and cross sectional area are again those of the threaded metallic bar. N is the axial load acting on the anchor at the moment of the punching failure, which is assumed to be completely resisted by the bearing mechanism of the

grout irregularities, as the bond capacity has already been overcome and frictional forces are negligible as slippage is prevented by mechanical locking. The values of U_s, calculated for each anchor where wrench failure is detected, are reported in Table 4-19.

The fracture energy per unit area of parent material surface is derived by the experimental results by van der Pluijm (1997). This author calculates the fracture energy for a number of masonry specimens tested in tension perpendicularly to bed joints; brick stacks, which are made of materials comparable to those used in the present research, fail at the interface mortar/masonry units, this being the weakest element. Indeed, the values of tensile strength, f_t, by van der Pluijm can be assimilated to the value of bond strength, $f_{b,w}$, determined by wrench test in the material characterisations of §4.3.2 and 4.4.2.

Accordingly, a linear regression of the values of fracture energy reported by van der Pluijm is created (Fig. 4-36). Values of fracture energy densities for the masonry typologies used for pull-out and cyclic tests are identified as the coordinate of the regression points with abscissa equal to the bond strength from wrench tests. Both the values of $f_{b,w}$ and of the fracture energy, U_m, are reported in Table 4-19.

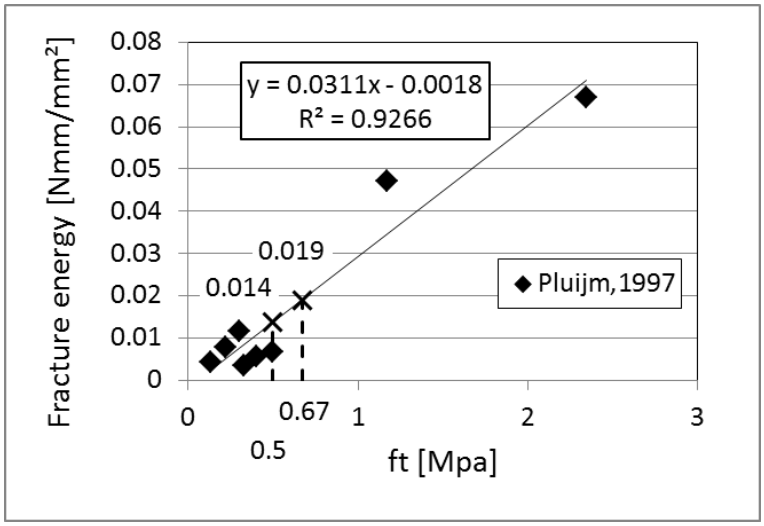

Fig. 4-36: Linear regression of the ratio tensile strength and fracture energy calculated on the basis of the experimental results by van der Pluijm (1997)

At this point the fracture surface, A_f, is identified as the ratio between the product of the linear strain energy of the steel bar times the wall thickness, t, and the strain energy per unit surface of the parent material, namely as:

4-13) $$A_f = U_s \cdot t / U_m$$

In the assumption that cracks forming the fracture surface extend all the way through the wall (Fig. 4-37), it is possible to calculate the length of cracks on the front surface of the wall, L_f, by dividing the result of Eq. (4-13) by the wall thickness, t.

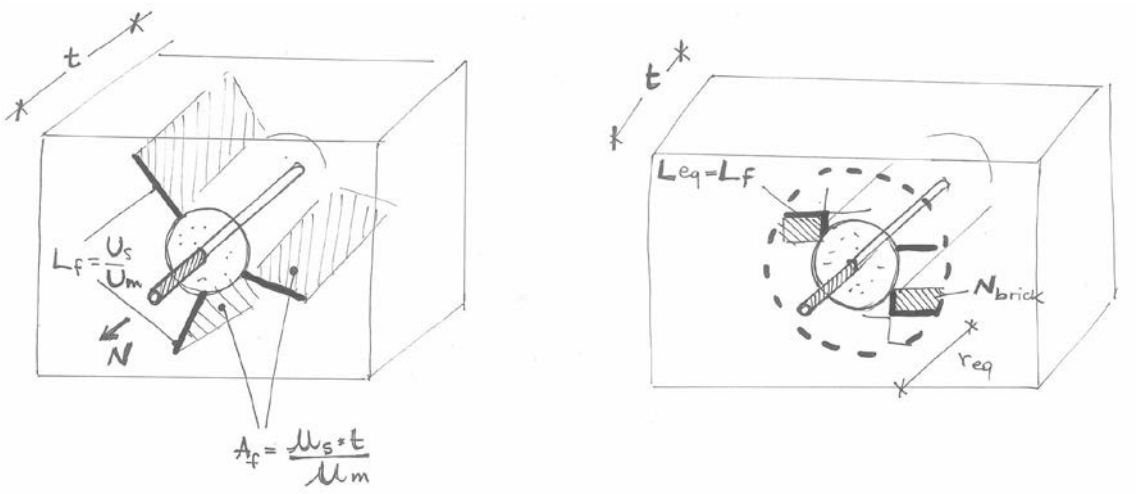

Fig. 4-37: Fracture surface for "wrench" failure

Table 4-19: Failure surface generated by “wrench” failure of the anchor assembly

	Anchor ID	**U_s Eq. (4-12)**	**$f_{b,w}$**	**U_m**	**A_f Eq. (4-13)**	**L_f**	**N_{bricks}**	**r_f**
		[Nmm/mm]	**[MPa]**	**[Nmm/mm^2]**	**[m^2]**	**[m]**	**[-]**	**[m]**
Pull-out tests	d	54.60	0.67	0.02	1.00	2.9	10	0.43
	e	29.36			0.54	1.5	5	0.32
	f	45.88			0.84	2.4	8	0.39
	y3	26.75			0.49	1.4	5	0.30
	f1 ($F_\perp$= 31.5 kN)	20.76			0.38	1.1	4	0.27
	f3 ($F_\perp$= 41.5 kN)	19.65			0.36	1.0	4	0.26
						Av.		0.33
						CoV [%]		20.1
Cyclic tests	2T	20.96	0.5	0.01	0.34	1.5	5	0.33
	3T	13.25			0.21	1.0	3	0.27
	y1T	33.92			0.54	2.5	9	0.41
	y2T	32.93			0.53	2.4	8	0.41
	f1T	12.48			0.20	0.9	3	0.26
	f2T	31.14			0.50	2.3	8	0.4
	f3T	15.68			0.25	1.1	4	0.29
						Av.		0.34
						CoV [%]		20.3

In order to quantify the extent of damage provoked by a wrench failure, an equivalent radius identifying the damaged area is calculated under the hypothesis that cracks

spread within a circular area and along the mortar joints, which are normally the weakest element.

Accordingly the fracture length, L_f, on the front surface is divided by the sum, a + b, where “a” and “b” are the length of two sides of a brick.

4-14) $$N_{bricks} = {L_f}/{a+b}$$

The equivalent radius is then calculated by dividing the number of bricks involved in the failure, N_{brick}, by the average number of bricks per masonry square metre. This is done to the purpose of taking into account the layout of masonry blocks.

Interestingly, the value of the equivalent radius remains fairly constant across the set of specimens (Table 4-19), this showing that the strain and fracture energy might be used to describe the wrench failure type observed for the tested typology of anchors. Therefore, the analytical model will feed into the design procedure of Chapter 7.

4.5 FINAL REMARKS

Chapter 4 deals with the experimental assessment of two innovative dissipative devices designed for the seismic protection of heritage buildings. As described in Chapter 3, the devices are developed drawing on the concepts of performance design and energy dissipation, concepts that, although promoted by current design codes, are seldom applied in practice to the strengthening of heritage buildings. Devices partly rely on the technology of grouted metallic anchors, which are a widespread and well-known technology for the structural upgrade, and partly on additional dissipative elements, which present strong similarities with the damping element used for new-built and infrastructures.

As discussed in Chapter 2, current prescription regarding the experimental procedures for the assessment of structural connection, both in the unreinforced and strengthened configuration, do not cover in detail the issues typical of heritage buildings. Furthermore, codes don’t clearly state how experimental results could and should feed in a standardised design procedure; in fact, specific references to the design methodology to be followed are completely missing.

Therefore the aim of the experimental work reported here is twofold: to assess the performance of the dissipative devices and to outline an experimental procedure that, through reference to existing standards and to the technical literature, can be used as guidance for the development of a comprehensive and robust procedure for the assessment and design of connection strengthening system.

In light of the fact that the final performance of the strengthened connection is a combination of the performance of the dissipative devices, of their interaction with the substratum and of the response of the structural elements to which they are applied, the experimental procedure is split into different phases. The sequence followed during the testing campaigns is the logical reflection of the increasing level of

complexity that one faces when looking first at the behaviour of the dissipative device in an isolated configuration and then proceeds to couple it to an anchor embedded in a historic-like substratum and undergoing a number of loading inputs. Accordingly, the testing programme is articulated in:

- Tests on the devices in the isolated configuration;
- Monotonic static pull-out tests of standard anchors embedded in masonry specimens, with and without dissipative devices;
- Pseudo-static cyclic tests of masonry subassemblies reproducing wall-to-wall connections strengthened either by standard of dissipative anchors.

Tests on the isolated devices largely draw on the prescription for dissipative devices contained in EN 15129:2009, although the methodology is adapted to the needs and scopes of the research project.

The experimental campaign shows that hysteretic devices feature a displacement-dependent behaviour with an initial elastic phase, a post-linear branch and eventually buckling. The dissipative element presents robust and repeatable hysteresis cycles, even after buckling; at the same time, connections to the rest of the anchor remain elastic, thus ensuring ease of replacement in the aftermaths of a seismic event, as required by BS EN 15129:2009.

Frictional devices display a robust and repeatable performance, independent of amplitude and frequency of imposed sinusoidal cycles as well as of temperature. A variation in Φ, the coefficient that expresses the ratio between slip load and applied perpendicular pressure, is recorded throughout the experimental campaign. Such variation can be expressed via a logarithmic function of the number of cycles test specimens have undergone. However, it is worth to highlight that the variation of Φ is also influenced by a number of factors such as mechanical locking and the presence within the assembly of metallic dust produced by the progressive wearing of the frictional surfaces.

Ideally the performance of the devices should be as consistent as possible, as a variation in Φ, although predictable, might create difficulties when dimensioning the device. This issue could be overcome by: installing devices that have undergone a number of cycles in controlled conditions, so that the value of Φ is already on the stable plateau, or coating the frictional surface to the purpose of homogenising the performance of friction plates. The impact of the variation in Φ will be further discussed in the light of results from other tests and the computational validation to the purpose of determining whether further improvement to the design of the frictional device are needed, or the problem can be overcome otherwise.

Pull-out tests aim to identify a set of parameter that, together with those already identified in respect to the isolated devices, can define the performance of the system device-anchor-substratum. Furthermore, pull-tests allow a first comparison between standard and dissipative anchors, thus justifying the development and use of the devices in light of the benefits they have in respect to their strength-only counterpart.

Indeed, tests successfully prove that the devices can address some of the drawbacks that are identified for standard anchors: large scattering of the performance and presence of damage in the substratum, despite a satisfactory level of load capacity. Devices homogenise the response of anchors, considerably reducing, or eliminating damage to the parent material. In particular, the frictional device allows controlling the activation load to the point that almost no relative displacement is detected in the other elements of the anchor assembly.

Parameters measured during tests are correlated with simple analytical models so as to seek a correlation and establish how the load capacity of each assembly component can be calculated in function of the failure mode associated to it. This is done in preparation of the development of a design procedure based on the concept of hierarchy of failures, which will be the focus of Chapter 7.

The same procedure is applied to cyclic tests, which conclude the experimental assessment by supplementing the information obtained by pull-outs through the simulation of a more complex scenario - full structural connection rather than only one wall panel - and a different loading input - cyclic action instead of monotonic pull.

The fact that masonry panels feature a different material, with lower mechanical properties in respect to pull-out tests, allow observing the performance of the three typologies of anchors in a limit case scenario. In particularly poor quality substrata the advantage of using the dissipative devices is considerable and might make the difference between only achieving the safety of occupants at the ultimate limit state and upgrade the structure to the point of ensure reparability.

Experimental results feed partly in the design of an instrumented anchor for on-site validation (Chapter 5) and partly in the calibration of a set of computational models, whereby further scenario will be simulated (Chapter 6).

5 ON-SITE VALIDATION

5.1 INTRODUCTION

Upon completion of the testing campaigns described in Chapter 4, one instrumented prototype of the dissipative anchoring devices was implemented in a case study with the aim of further validating and complementing experimental results. The pilot installation entails that the prototype is exposed to naturally occurring pseudo-static and dynamic phenomena, and that its performance is influenced by the surrounding materials as well as adjacent structural elements. The opportunity of broadening the range of loading and boundary conditions in respect to the experimental campaigns is beneficial to the validation process: instead of relying solely on the set of assumptions that had to be adopted in the laboratory environment, the response of the prototype is monitored under real life conditions, thus providing a full picture of the strength points and pitfalls in the design of the device.

The case study is chosen so as to present a damage pattern relevant to the structural issues that the design of the anchoring devices aims to tackle. A religious building in the historic centre of the city of L'Aquila, Italy, which had been badly affected by an earthquake in 2009, was identified as a suitable case study; the pilot installation was carried out within the framework of the European-funded NIKER project. An instrumented prototype of the hysteretic device was placed in a location as sensitive as possible to seismic tremors or settlements with the goal of maximising the amount and relevance of collected data.

The choice of appropriate instruments for the monitoring of the prototype and of the surrounding parent material was carried out in cooperation with Eatec Ltd., an engineering company specialising in SHM, who provided technical support throughout the design, calibration and installation of the instrumentation system. Details and technical specifications of sensors, and of the rational for choosing them are reported in detail in §5.2, while the calibration of the system is described in §5.3.

Beside the instruments of the anchor prototype, on-site validation relies on the cross-correlation with the data collected by the University of Padua, who also participated in the NIKER project and had an independent monitoring system placed on the same building. Data recorded by this independent system is used as reference as much as benchmark to proof the reliability of the instrumented prototype. Further information regarding the mechanical properties of the masonry and the existing state of damage of the structure are sourced from previous investigation campaigns performed by the scientific partners involved in the case study, as described in §5.4.1.

Results discussed in §5.5 shows how the device performed successfully, although many interesting points for improvement emerged. These are also discussed in light of the future developments in terms of application to further case studies and structural monitoring that will be discussed in Chapter 8.

5.2 TECHNICAL SPECIFICATIONS

A prototype of a yielding dissipative device was instrumented and installed on-site with the following objectives:

- Recording the deformations and accelerations experienced by the anchor; stress field, elongation, relative displacements are calculated from the measured values. These parameters indicate the level of performance achieved by the anchor, thus contributing to the process of refinement and validation of the dissipative anchoring devices;
- Recording the evolution of existing damage to a portion/subassembly of a structure – e.g. opening of a crack between two walls – and correlating it with other phenomena, such as micro-tremors and with the response of the dissipative device.

One main point in the design and implementation of the instrumented anchor was to try to keep a low complexity level: as the dissipative device is still being fine-tuned and on-site applications present a high margin of uncertainty, it was deemed important to avoid overcomplicating the analysis of results.

Accordingly, the yielding, instead of the frictional, dissipative device is chosen for on-site installation. While the frictional device, as seen during the laboratory campaigns, requires a heterogeneous set of sensors to measure the relative displacements of the mechanical parts, the perpendicular pressure determining the frictional force, and the strains on various locations, the yielding device can be monitored simply by a set of strain gauges recording deformations. This of course considerably simplifies the monitoring and acquisition system, providing the opportunity of focusing on other aspects, such, for instance, actions in the plane perpendicular to the axis of the device, which were not simulated during the experimental assessment but could possibly affect a real-life application.

The considerable improvements of technology, both in terms of typology and quality of sensors and of capacity of data acquisition systems, which has been attained in recent years has allowed the development of low-impact monitoring techniques in response to the stringent requirements in terms of location and esthetical impact of sensors for heritage structures. It is worth mentioning among the others: optical fibres (Lima et al., 2008), wireless networks (Anastasi et al., 2009), acoustic emission (Carpinteri and Lacidogna, 2006) and radar techniques (Tarchi et al.; 2000).

In spite of the promising results of these techniques, many challenges regarding the optimisation of the number of instruments and the handling, storing and processing of acquired data remain. Large numbers of sensors provide more accurate information, but at the same time entail higher costs of installation and the management of a bulky amount of data (Anastasi et al., 2009; Carpinteri and Lacidogna, 2006; De Stefano and Clemente, 2006). For some innovative systems, such as wireless networks, loss of data and complexity are further considerable drawbacks, which normally do not affect more traditional monitoring systems (Rice and al., 2011).

In light of the fact that the dissipative anchor device is installed as part of a pilot project, and only in one single location, in the framework of emergency stabilisation works, it is not deemed critical to work on minimising the appearance and wiring of sensors, but rather to obtain reliable information. Therefore, in order to measure the deformations of the dissipative device, it is decided to use more traditional monitoring devices, i.e. conventional electrical resistance strain gauges (ERSG) rather than fibre Bragg grating (FBG), allowing for direct correlation of on-site results with the output of the experimental campaigns described in Chapter 4.

ERSGs are a reliable and commonly applied technique and satisfy a number of requirements, such as size, compatibility with previous results, straightforward installation, and interpretation of results. Furthermore, typical drawbacks connected to the interference with electromagnetic fields from other devices are not expected to be critical in the specific case study.

In addition to strain gauges, a triaxial accelerometer and a temperature/humidity gauge are installed as part of the instrumented anchor (Fig. 5-1), so as to record the occurrence of cyclic and dynamic phenomena, i.e. thermal expansions and tremors, that might induce a response in the instrumented anchor.

The system is devised so as to read with accuracy low-to-medium dynamic phenomena, which should bring the device into the plastic range, thus providing as much information as possible regarding the device response in the most critical stage, namely when its ductile behaviour becomes prevalent

Another important criterion for the development of the on-site application is how data collection is carried out, namely on a continuous basis, or only for events with intensity exceeding a set threshold. On the one hand, the use of a trigger offers the advantage of considerably reducing the amount of collected data, ignoring disturbances or minor entity phenomena and allowing a swifter data analysis. On the other hand, one needs to possess a sufficient insight into the phenomena that will be recorded so as to be able to decide a priori which will be of interest and set up a trigger. The expected intensity of tremors can be derived by studying the regional seismicity and historic catalogues, the structural response can be determined through experimental and computational analysis, but the response of the anchor itself is yet to be fully determined at this stage of the development. In fact, the aim of the on-site validation is to determine whether and how the anchoring device reacts to a range of load/deformation inputs; excluding some events by pre-filtering the acquired data through trigger might interfere with this task. For instance, the assumption that minor intensity events will not affect the anchor might prove incorrect, for reasons that will have to be determined and analysed; but if this is the case, how can the problem be pinpointed, if data has not been recorded in the first place? In the framework of prototype validation, it is hence deemed safer to carry out continuous monitoring and skim data a posteriori.

Lastly, the monitoring system has to be remotely accessible: this is an indispensable requirement in light of the geographical distance between the location of the monitored structure, Italy, and the location where data is handled and analysed. Moreover, it cannot be fully excluded that seismic events might prevent access to the computer where data is stored, in the short or long term. Remote access allows data transfer as well as trouble shooting, at least for basic errors, thus addressing the issue of the geographical distance. Additionally, through remote access, acquired data can be regularly removed from the data acquisition system and stored on a secure server, thus avoiding running out of memory space and preventing accidental loss of data.

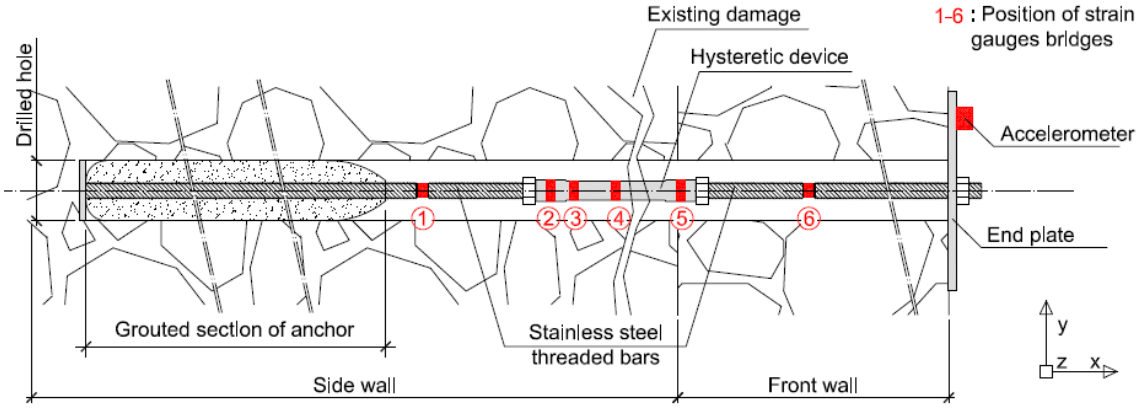

Fig. 5-1: Set-up of instrumented anchor at the connection of two orthogonal stone walls with existing corner crack

Drawings on the above observations, the instrumented anchor is made of the following components:

- **One stainless steel anchor made of three sections** (Fig. 5-1): the first and last sections are made of standard threaded profiles, while the mid-section is the yielding dissipative device. The last section of the assembly is grouted with the Cintec's method ©, so as to provide anchorage within the parent material, the central section is positioned in correspondence of a crack, so as to facilitate the activation of the device as consequence of relative movements, and the front section is dry-installed, with a bolted end-plate to ensure connection and ease of installation and removal of cabling. Various strain gauges are bonded along the anchor, with cables for the connection to the acquisition system laid inside the drilled hole.
- **A set of electrical resistance strain gauges** deployed to form 15 full bridges, positioned at different locations along the anchor, so as to be able to read the deformations on the dissipative element, on the connections with the anchor rods, and on the threaded rods. Monitoring locations are marked with numbers from 1 to 6 (Fig. 5-1). Bridges (Fig. 5-2) include 5 axial, 6 flexural and 2 shear reading strain gauges sets; bending and shear bridges are placed so as to be able to record strains in two perpendicular directions,

identified in the drawings and graphs with the two axes Y and Z, while X corresponds with the longitudinal axis of the device.

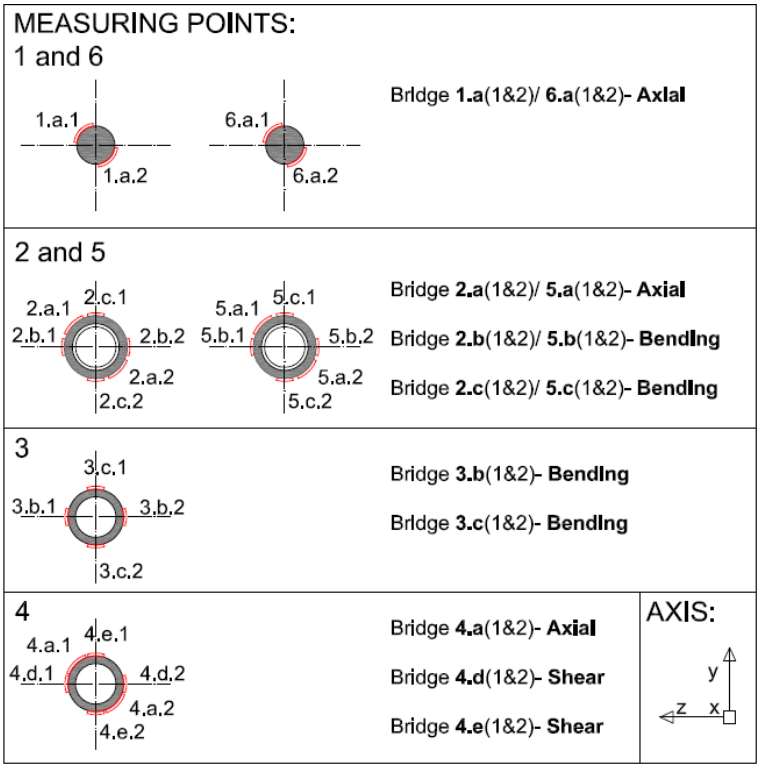

- Fig. 5-2: Types of strain gauges placed at each measuring point

The bridges are designed and positioned to read relative movements between two structural elements; in particular referring to Fig. 5-1, these can be summarised as:

- Out-of-plane motion of front wall, causing tension and possibly bending (rotation round axis Z) in the anchor, recorded by the axial and vertical bending bridges;
- Out-of-plane motion of side wall, causing shear (Z direction) and bending (rotation around Y axis) in the anchor, detected by shear and bending bridges;
- Vertical relative displacements between the two walls, captured by the vertical shear and bending bridges in the other direction in respect to the previous point, i.e. rotation around the Z axis and shear in the Y direction;
- In-plane horizontal movements of the front wall

Strain gauges are bonded by an epoxy-based adhesive and coated by a two-part polysulfide liquid polymer compound to protect them from scratching during installation. Strain gauges are selected from Vishay catalogue (2014):

- Axial gauges: J2A-06-S114L-350, 90° tee rosette gauges;

  - Bending gauges: J2A-06-S035M-350, dual element gauges for bending bridges;
  - Shear gauges: J2A-06-S036R-350, dual element shear pattern gauges.

  Selected gauges are temperature self-compensating for stainless steel and have been chosen because of their size, durability and reading range. The dimension of the gauges is indeed very important, as they must fit on the anchor pieces, but at the same time they must be able to average the readings on a sufficiently wide area, so as to record average strains rather than localised phenomena. Selected gauges are reliable up to 106/107 cycles and therefore adequate to monitor phenomena such as tremors. The reading range is ± 1500/1700 με, which is sufficient to read the deformation expected for micro-tremors and minor seismic events. Although seismic events able to bring the gauges beyond their capacity could have occurred, it was necessary to find a compromise in terms of number of cycles and reading range. Considering that monitoring has a planned duration of about a year, a robust behaviour to fatigue was preferred to a wider reading range.

- **Strain gauge amplifiers**.
- **A tri-axial accelerometer** (Crossbow CXL04LP3). The sensitivity of the accelerometer is 500 ± 25 mV/g; if the data acquisition input range is set to its lowest at ±1.25 V, then the theoretical resolution of acceleration measurement is 76 μg. In practice, such refinement is hard to achieve, but the actual sensitivity is sufficient to detect micro-tremors.
- **A temperature sensor** (Crouzet 89 750 152) fitted near the anchor. The sensor measures temperatures in the range -10/+40°C, with a precision of -0.2/+1.9°C.
- **Embedded computer running Microsoft Windows XP (FES**). This gives a platform for the control of data acquisition, processing and storage of data and for supporting remote communications.
- **Data acquisition card** (DAQe-2206 PCI express card).
- **Enclosure and assembly**. All of the hardware is securely contained in one enclosure.
- **Bespoken software.** A continuously running program causes the data acquisition card to sample all channels at a rate of 100 samples per second per channel. At the end of a specified period, in this case 1 hour, the acquired data is written to a binary block on the hard disk using a name that includes the date and time at which the block started. Summary statistics, namely maximum, minimum, average and root mean square (RMS) of each channel are output to an ASCII file suitable for viewing with Excel. The parallel use of summary and high-speed data is both functional to swiftly identify data of interest and to maximise the amount of information that the system can provide. Indeed, summaries have such a size that they can be transmitted daily to a list of recipients, thanks to an internet connection via

dongle. This facilitates the task of remote monitoring, as it informs the choice of the high-speed data blocks to download: the comparison of maximum, minimum and average on an hour basis allows pinpointing blocks where variations larger than usual have occurred, thus highlighting dynamic events, for instance microtremors. At the same time, average values recorded in the summaries provide a clear indication of pseudo-static trends, such as temperature variations or settlements.

As continuously running, the monitoring system must be connected to the electrical main. However, it is expected that due to the precarious situation of the building and possible seismic events at the time of monitoring, the electrical supply might experience disruptions. Therefore a UPS is connected in series with the system to provide electrical energy in emergency cases and avoid the loss of critical data.

After assembling and before installation, the instrumented anchor underwent a set of tests in the laboratory to check its functioning and calibrate the system, as described in the following.

5.3 CALIBRATION

Laboratory calibration of the monitoring anchor is performed with the purpose of determining the sensitivity factors, i.e. the coefficients correlating the voltage read by the acquisition system to the output values (microstrains, accelerations, etc.) that are to be stored in the data files of the system. While the sensitivities of the accelerometer and of the temperature cell are provided by the producer, strain gauges require going through a calibration process, which consists of:

- Fitting the anchor (Fig. 5-1) on two triangular metallic sections bolted to the strong floor (Fig. 5-3a);
- Imposing an increasing load to the monitoring anchor; load is either an axial load or a shear/bending load. Axial load is obtained by fixing the anchor at one end and tensioning the other extremity by applying a torque to a nut screwed at the extremity of the threaded rod and pushing against the steel triangle. Bending is obtained by hanging weights to the anchor (Fig. 5-3c). Load is applied, released and applied again with increasing values. An independent recording system – e.g. load cell in series with the threaded bars – is used to monitor the load (Fig. 5-3b);
- Reading the voltage as recorded by the data acquisition system;
- Reading actual strains through an independent strain-reader calibrated for a full bridge configuration, i.e. the type of configuration used for all the strain gauges in the assembly;
- Calculating the sensitivity (V/μstrain) as average ratio between recorded voltage and strains. Strains can be double-checked by using the theory of Navier for ideal beams, as boundary conditions, geometry and load are known;

- Inputting the sensitivity coefficients in the configuration file of the data logger. At this point data stored by the system are saved as accelerations, temperatures and strains rather than simple voltage.

The calibration of the monitoring system is repeated varying a number of parameters, e.g. the position of weights so as to modify the lever arms generating bending or type of load.

a)

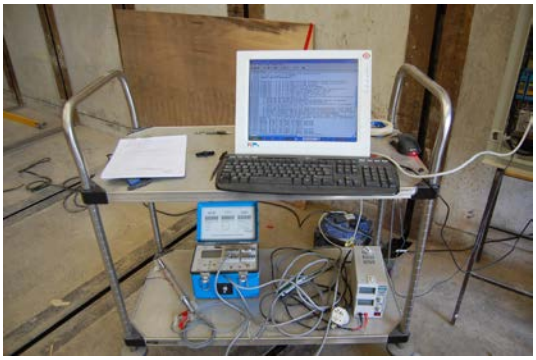

b)

c)

Fig. 5-3: a) Monitoring anchor ready for calibration; b) the data acquisition system and the independent measuring systems used; c) calibration by loading

An example of the results of the calibration process is shown in Fig. 5-4: the graphs shown the correlation between measured voltage and strains as the prototype anchor is tested under bending load (set-up shown in Fig. 5-4e).

The prototype is placed so that the load acts in simple bending, i.e. only one set of bending bridges is affected by deformations, while the other should not record any strain. Indeed, comparing Fig. 5-4a and b, it is possible to see the difference in recorded strains. The correlation coefficients for the three bending bridges in the vertical direction correspond to the inclination of the lines represented in Fig. 5-4a.

Fig. 5-4b shows that minor strains are recorded by the three bending bridges perpendicular to those in Fig. 5-4a; this is acceptable as recorded strains are one order of magnitude smaller than in the other direction and, hence, negligible. It can be expected that minor deformations might occur in the assembly during loading and that

small imprecisions in the positioning of the gauges as well as in the geometry might provoke strain values other than zero.

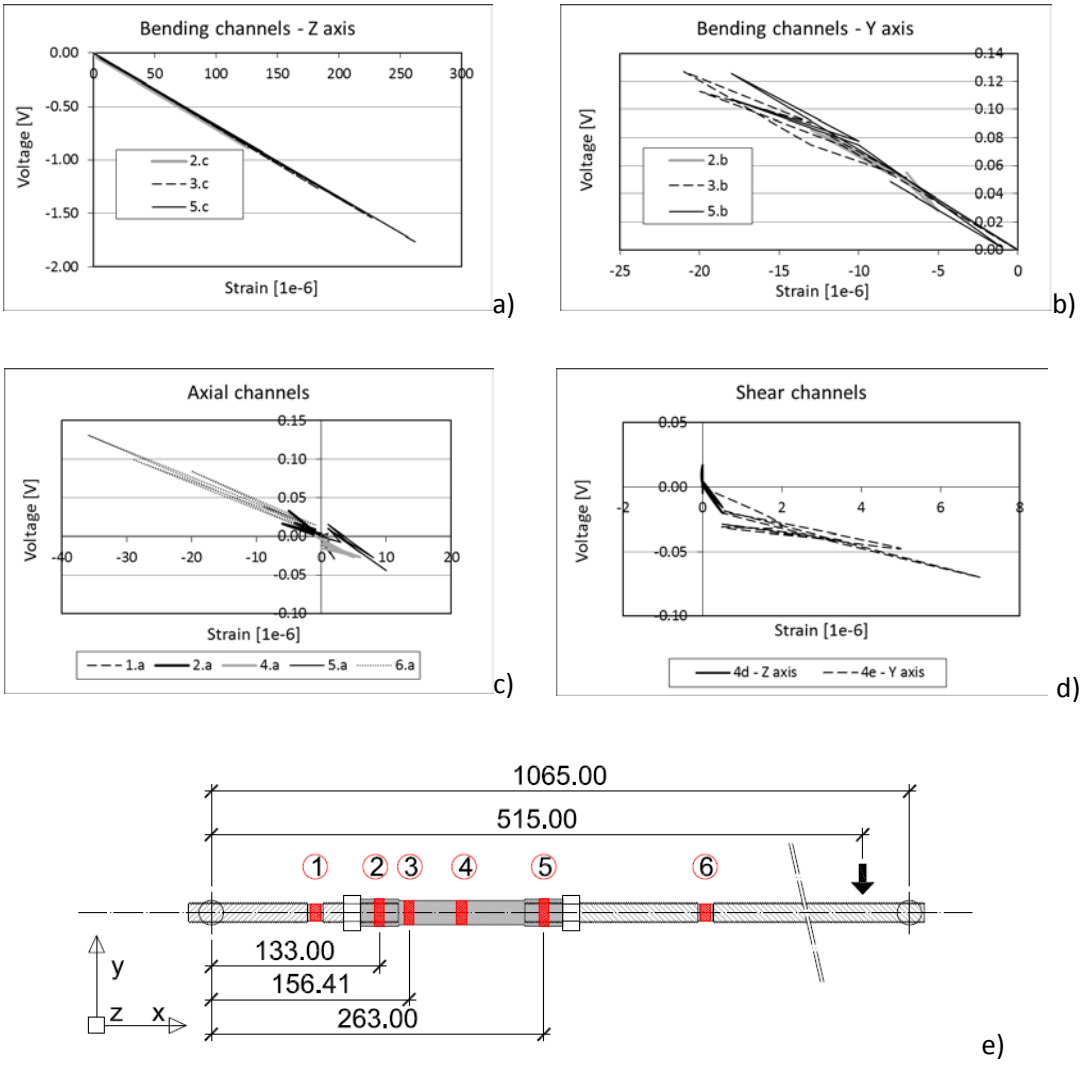

Fig. 5-4: Correlation strain-voltage for bending (a-b), axial (c) and shear bridges (d), as recorded during bending loading of the anchor prototype (e)

A similar situation occurs also for the shear bridges (Fig. 5-4d): strains are recorded in the relevant direction, while only minor deformations are detected in the orthogonal direction.

Axial deformations (Fig. 5-4c) are minimal, although it is worth keeping in mind that one bridge, 6a, seems to be more affected than the others, as if the full bridge configuration were not fully capable of compensating the tensile/compressive actions at the opposite surfaces of the anchor as effect of the bending load or some eccentricity were present. Such effect occurs also in the other direction and will be taken into account and further investigated while analysing on-site results in §5.5.

The correct functioning and calibration of the instrumented hysteretic device is further checked by placing it into a pulling apparatus and applying small amplitude-sinusoidal inputs (Fig. 5-5). In this case the instrumented threaded rods must be removed as their length, which is designed for an on-site application, doesn't fit into the testing machine. This means that only the strain gauge bridges in the measuring points 2/5 are active and that shorter threaded bars are used to fix the prototype to the machine jaws.

Reading of axial strains is satisfactory, as they present the distribution expected for the different sections of the hysteretic device (Fig. 5-5a).

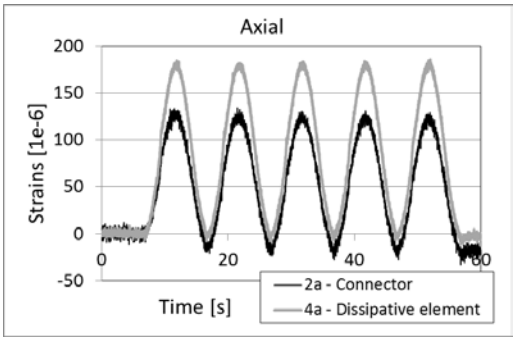

a)

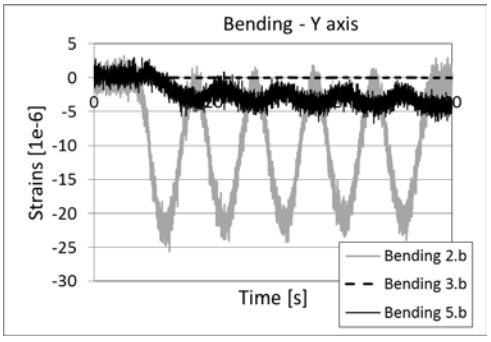

b)

Fig. 5-5: Dynamic calibration

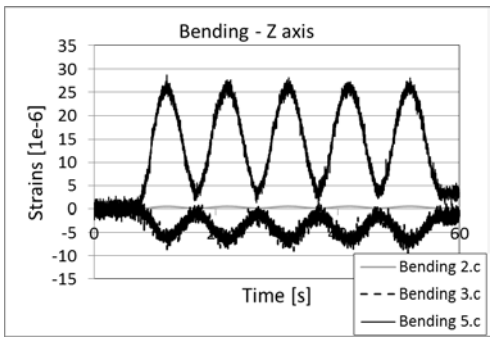

c)

Dynamic tests highlight further phenomena: strain readings present a certain level of noise that can be quantified in the order of about 5 μstrain (Fig. 5-5). Although this value is negligible for the levels of deformations imposed on the instrumented device during testing, the impact on the reading of small phenomena like microtremors will have to be assessed on site. Furthermore, although tests were performed only applying an axial load, values of strains recorded by the bending bridges are different from zero (Fig. 5-5b and c); recorded strains are one order of magnitude smaller than the axial strains and likely depend on geometrical imperfections of the device, such as slight eccentricity due to the fact that device is not a single piece, but is made of different parts screwed together.

Sensitivity factors resulting from the calibration process are shown in Table 5-1. In the table the name of bridges points to the location on the anchor (numbers from 1 to 6, as shown in Fig. 5-1) and to the typology of gauge (as shown in Fig. 5-2): axial (a),

bending around the Y axis (b) and around the Z axis (c) and shear along the Z axis (d) and the Y axis (e).

Table 5-1: Sensitivity coefficients

Correlation mV/μstrains													
-6.8	-6.9	-6.8	-6.8	-6.7	-6.7	-3.4	-3.4	-3.4	-3.4	-3.4	-7.3	-6.3	
2.b	2.c	3.b	3.c	5.b	5.c	1.a	2.a	4.a	5.a	6.a	4.d	4.e	Bridge No
Bending						Axial					Shear		Bridge type

5.4 ON-SITE IMPLEMENTATION

5.4.1 The Case Study: S. Giuseppe dei Minimi Oratory, L'Aquila, Italy

After undergoing laboratory testing, in June 2011, a trial prototype of an instrumented yielding device was installed in a real structure to proceed to the final validation and refinement by comparison with an independent monitoring system. The pilot installation was carried out within the framework of the NIKER project and in collaboration with the University of Padua (UPD), which was carrying out an extensive monitoring programme in the city of L'Aquila, Italy, jointly with the Politecnico of Milan (Binda et al., 2011; Casarin et al., 2011; Modena et al. 2010a; Modena et al. 2010b). Monitoring lasted more than one year, until November 2012.

The chosen building is the Oratory of S. Giuseppe dei Minimi (Antinori, 1777; Antonini, 1993), a baroque chapel adjacent to the church of S. Biagio d'Amiternum, with which it shares a wall. The first construction of the oratory dates back to 1646, when a part of St. Biagio church was given to the brotherhood of the Suffragio to build a new, smaller church. The chapel opened in 1649, but few years later, in 1703, an earthquake partly destroyed it, so that the oratory had to be restored. In the 1930s, the oratory was restored, the baroque decorations removed from the façade and, most likely, the existing r.c. beam built under the roof structure.

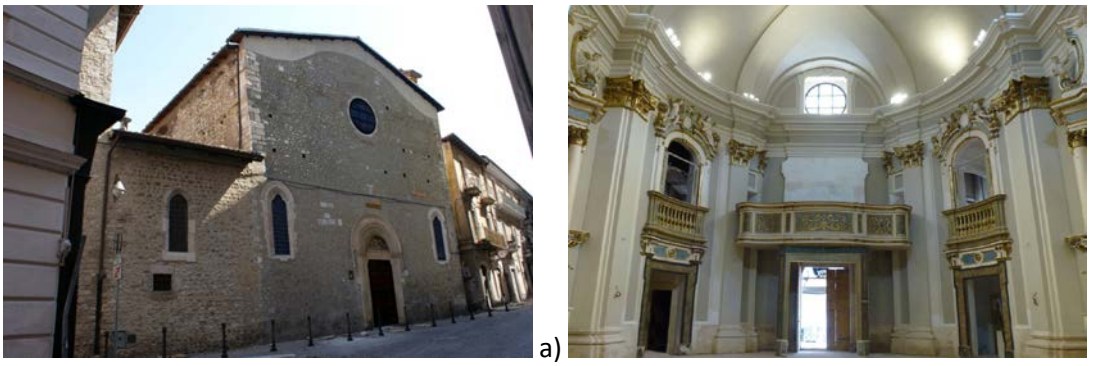
a) b)

Fig. 5-6: S. Giuseppe dei Minimi: a) facade (from Ict-architettura.it), b) inner view (from Newsabruzzo.it)

The Oratory (Fig. 5-6) is made of one single, oval-shaped room, covered by a vault, which on the basis of available historical information is likely to be a false ceiling. The

typology of the structure of the roof could not be determined with certainty at the time of the post-earthquake survey. Due to the presence of a flat ceiling before the restoration works at the end of the 90's, it seems reasonable to assume that the roof is made of wooden trusses. The walls are built with lime mortar and irregular, small stones, typical of the masonry used in L'Aquila in the sixteenth and eighteenth centuries. Corner quoins are made of large squared dressed stone blocks.


a)


b)


c)

Fig. 5-7: a) The oratory of S. Giuseppe dei Minimi in L'Aquila, Italy. The crack between the front wall and side walls as seen from the outside (b) and inside (c)

Fig. 5-8: Damage to the belfry (D9.1, NIKER project)

The oratory reported serious damage as result of the seismic event of the April 2009, (magnitude 6.3 on the Richter scale according to USGS data base); the main damage (Sorrentino et al., 2010) consisted in the overturning mechanism of the façade (Fig. 5-7), probably facilitated by the presence of the belfry structure in the S-W corner; the belfry front column pushed on the façade and accentuated the out-of-plane (Fig. 5-8). Shear damage in the façade and in the back wall of the apse was also detected.

The oratory was chosen as case study for the trial installation and on-site calibration of the monitoring anchor system for the following reasons:

- The clear damage pattern indicating the out-of-plane movement of the front wall and its detachment from the rest of the building as consequence of L'Aquila 2009 earthquake (Fig. 5-7). Even though the instrumentation of the anchor device is designed to read different types of relative movements between structural elements, simple out-of-plane damage is the best possible case for this first application. Indeed, it allows for full correlation of on-site readings with previous experimental results on the dissipative anchoring devices, which have always been designed and tested for this type of application. Furthermore, at the time of installation the façade was strapped back to the rest of the building to avoid collapse, but it was still lining forward while waiting for the repair strategy to be decided and implemented. The presence of an open crack clearly identifies the area most vulnerable to soil movements and seismic events, thus increasing the relevance and magnitude of the data collected by the monitoring anchor.
- Extensive analysis of the building had already been carried out by the University of Padua. Characterisation included non-destructive and partially destructive on-site tests as well as Finite Element modelling. Results of testing campaigns will be referenced as required when discussing the output of the instrumented anchor in §5.5. Furthermore the University of Padua had a general monitoring system recording displacement and acceleration at various critical points of the oratory and of the adjacent church (Fig. 5-10). This allows for the correlation of data coming from the two systems and calibration of the anchor.
- The seismicity of the area, characterised, by small/medium magnitude frequent events, which increases the likelihood of the occurrence of microtremors and further movements between the structural elements connected by the monitoring anchor system. Indeed, L'Aquila is located in a high-seismicity zone, characterized by a Peak Ground Acceleration (PGA) of 0.261g for a 475-year return period (DM 14-01-2008). By searching the database of the EMSC (European Mediterranean Seismic Centre, http://www.emsc-csem.org/, last accessed on the 29th December 2014), it is possible to observe that the area surrounding L'Aquila was affected by 142 seismic events only in the two months following the 2009 earthquake.

The positioning of the monitoring anchors system was influenced by various considerations regarding on-site constraints and the optimisation of the number and quality of collected results. The final decision was to install the anchor at the connection between façade and side wall at the south corner of the building (Fig. 5-9). This corner is “free” whereas the opposite side wall is common to the oratory and the adjacent church, so that, even if damage patterns are similar, movements might be influenced by the degree of continuity of the facades of the two buildings, which could not be thoroughly and explicitly determined during this work.

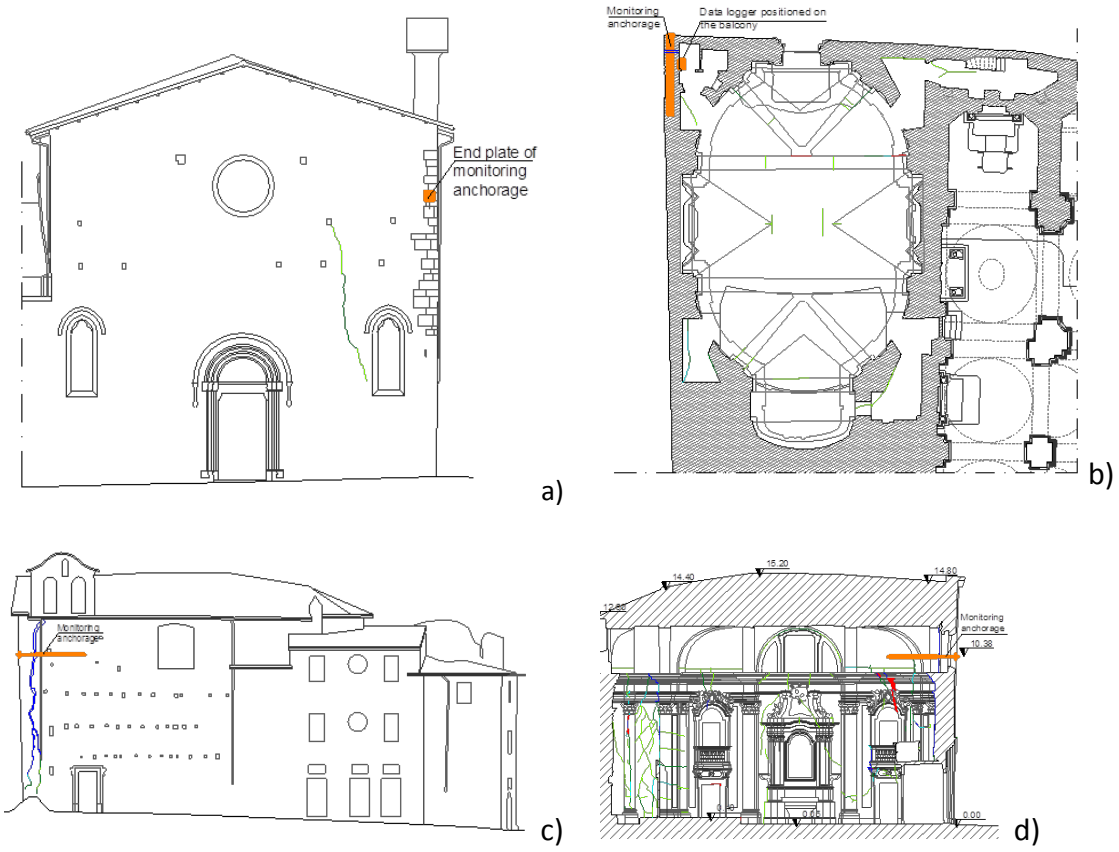

Fig. 5-9: The oratory of S. Giuseppe dei Minimi, L'Aquila, Italy: damage pattern and position of the monitoring anchor system: a) front wall, b) plan, c) South side wall and d) section. Original drawings: courtesy of University of Padua

The monitoring anchor is placed at the top of the wall, where amplification of ground motions is higher, and in parallel with the acceleration and displacement sensors of the University of Padua (CH 3 and 4, and PZ1 respectively in Fig. 5-10).

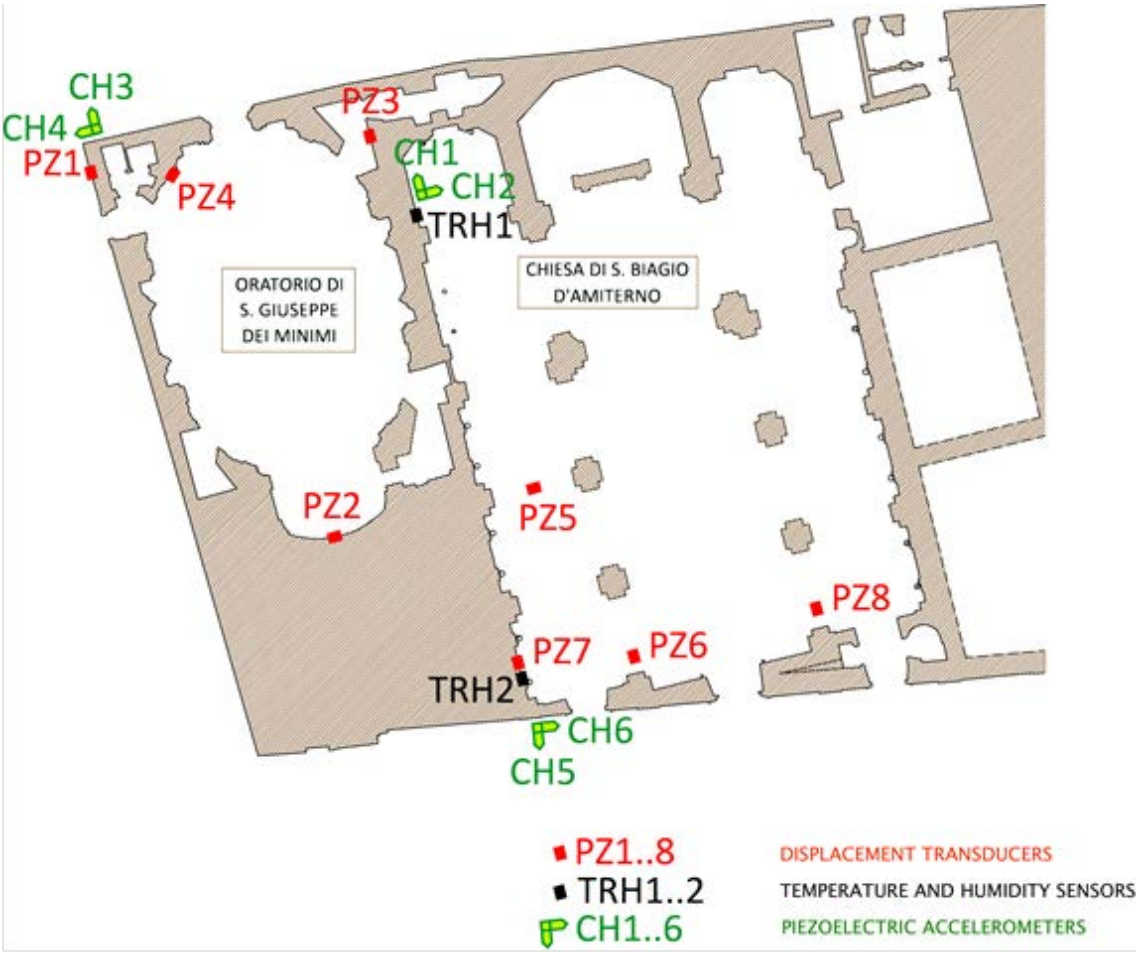

Fig. 5-10: Positioning of sensors of UPD monitoring system. From D9.1 report (www.niker.eu)

5.4.2 Installation

Once the building and installation point were chosen, the calibrated prototype of the instrumented anchor was installed.

The anchor parts and drilling equipment were shipped to Italy and brought to site.

Due to the anchor level off the ground and the lack of scaffolding, a scissor platform was used to reach the top of the façade and proceed to installation, which involves the following steps, as illustrated in Fig. 5-11:

a) *Coring*. The anchor position was carefully set out using a chalk and a string, which was used as reference to ensure that the drilling rig was aligned to the side wall and level. The drilling rig was fixed to the façade by means of one small metallic bolt, so as to make sure that the alignment of the core was maintained throughout drilling, in spite of any vibration of the equipment. Drilling was carried out by diamond rotary drilling rather than percussive drilling, so as to avoid creating damage in the fragile substratum. In the case of historic substrata the use of water for drilling would normally be advised against, especially when

surfaces are decorated by frescoes or paintings, as it can lead to percolation and staining; however, depending on the masonry, the use of water might be necessary to avoid damaging the drilling bits and to cut precisely through hard stones. In the specific case, water was used only as long as drilling into the quoin, which is made of larger stone blocks, whereas the rest of the hole was dry drilled, as the irregular substratum offered less resistance to the penetration of the drilling bit.

b) *Cleaning*. All cores, dust and debris were removed from the bore hole and stains immediately cleaned from the wall surface. The finished hole in the stone block quoin as visible from ground level is shown in figure.

c) *Assembling*. The anchor was unpacked. Small tears in the sock that occurred during transport were repaired using a hot melt glue stick. The part of the anchor with the sock was soaked in clear water to soften the fabric and facilitate grout injection. After few minutes the anchor was removed from the water bucket, shortly left to drain and then joint to the instrumented dissipative device. All parts were delicately screwed together, except the front plate, which was installed only once the anchor is in place in the drilled cavity. Care was taken to ensure that all strain gauges bridges were correctly aligned; this task was facilitated by a set of labels that had been placed on the anchor before the whole surface was coated by the protective polymer compound.

d-e) *Installation*. The anchor and the cables for the connection with the data logger were carefully slid in the bore hole from the front, carefully pushing the anchor in by lifting it over any fissures or voids, without forcing and twisting.

f) *Alignment*. The dissipative device was positioned in correspondence of the crack and cables were pulled into the bore hole, into the main wall crack and finally into the building.

g) *Injection*. Grout was thoroughly mixed with water according to the mixing ratio indicated by the producer. Once ready, the grout was poured into a pressure pot, which was connected to a compressor and to the plastic injection tube that ran along the anchor inside the fabric sleeve. The plastic tube was accessible from the side crack, so that grout could be injected from this position, bonding the portion of anchor lying within the side wall. The pressure was maintained until all the grout milk has been expelled.

h) *Cable connection*. The cables were wired to the data acquisition system and UPS.

i) *Anchor locking*. The front plate was positioned and locked, and the three-axial accelerometer was fixed to the plate surface.

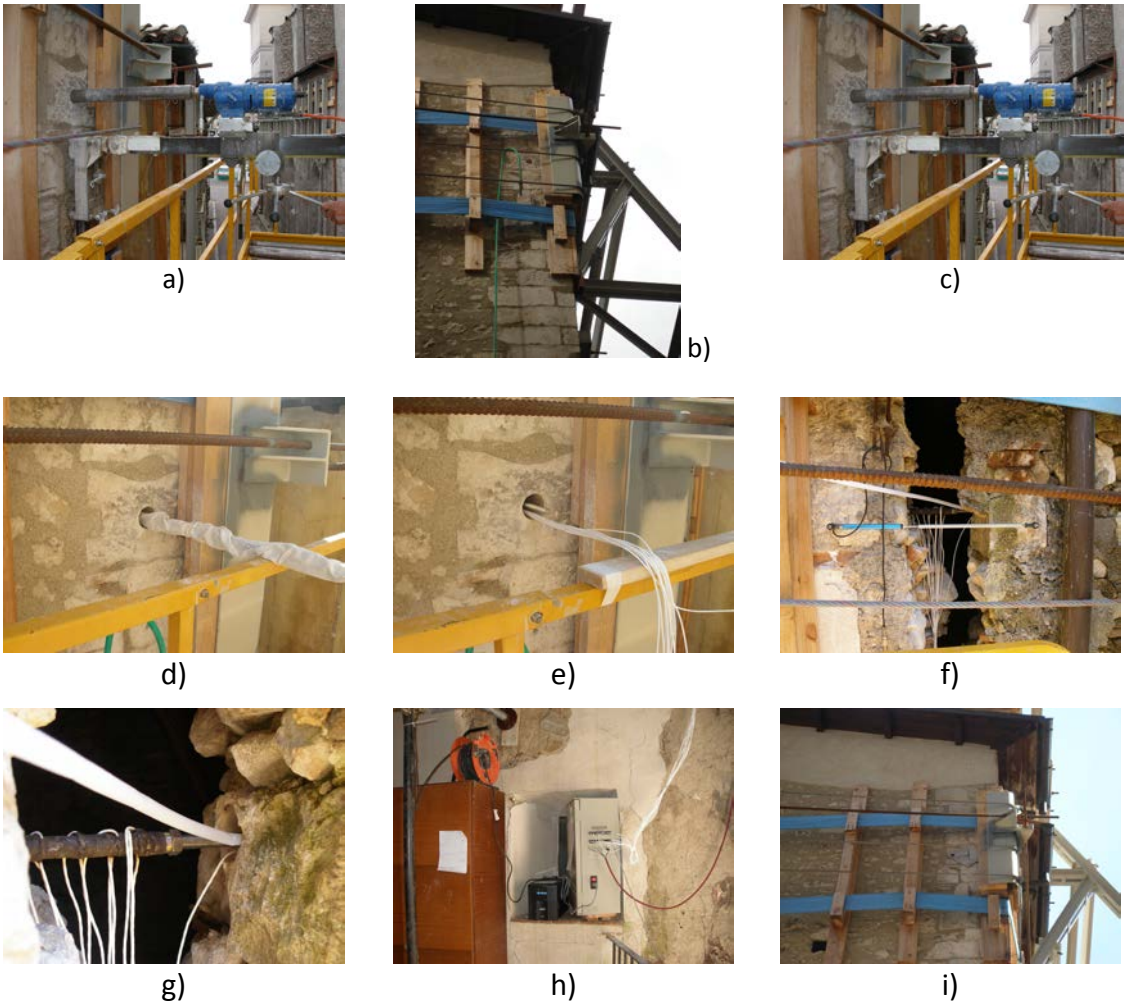

Fig. 5-11: Installation process of monitoring anchor system in the oratory of S. Giuseppe dei Minimi in L'Aquila

5.5 ON-SITE RESULTS

The analysis of on-site data collected during the monitoring period show that the instrumented anchor system is able to read a variety of phenomena.

Firstly, the sensors recorded the increase in strain deriving from the axial load that was imposed when locking the nut of the anchor front plate (Fig. 5-11i). When the nut is tightened, it generates a friction force between the plate and the surface of the front wall, thus ensuring that the plate self-weight is transmitted to the wall surface without bearing on the anchor rod; otherwise this would cause an undesirable bending action on the dry portion of the anchor. Furthermore, a small pretension in the anchor ensures a better contact between front plate and wall, this being critical to the effective transmission of horizontal actions to the anchoring system when the wall moves outward. In case the wall moves inward, this being possible due to the dimension of the main crack and the type of strapping, which prevents tilting, but not

the closing up of the crack, the anchor will lose its contact with the wall and little, if any, load will be transmitted. If a fully grouted connection had been chosen, the anchor would have worked in both out-of-plane directions; however, the choice of the plate system has considerable advantages in terms of installation of the instrumentation system and, later on, of removal, and therefore was preferred. Furthermore, the plate system prevents buckling and hence damage to the strain gauges.

Torque was imposed manually, as it can be seen by looking at Fig. 5-12, where loading steps are clearly visible. The difference in strain values between the various parts of the anchoring system reflects the difference in cross sectional areas, which characterises the hysteretic anchor device, as explained in Chapter 3.

It is worth highlighting that, although the anchor rod has approximately the same values of strain as the dissipative element for the small force applied, this doesn't mean that it would yield at the same level of acting force. The metallic bar is indeed of a higher strength class than the hysteretic device, so as to remain in the elastic field and prevent large deformations in the portion of anchor that work through stiffness rather than ductility.

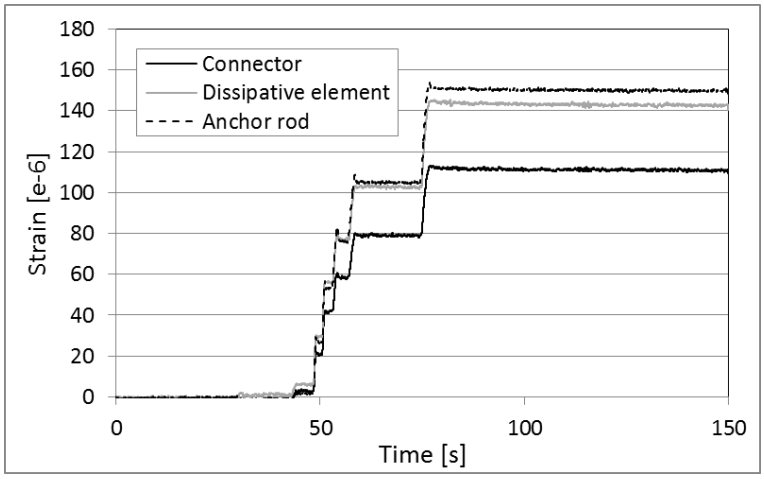

Fig. 5-12: Recorded increase in axial strains deriving from the locking of the end plate.

The level of imposed axial load is calculated through the strains, thus checking that the value of the force is in line with what expected and that the strains of different elements are proportional to the cross-section areas. The well-known Saint-Venant equation for axial load is used:

$$N = A \cdot E \cdot \varepsilon \tag{5-1}$$

With A, cross sectional area of metallic elements, E, Young's modulus of steel (210 GPa) and ε, strain as read by the monitoring system. For the dissipative element, equation 5-1 yields to a value of force equal to 4.2 kN, this being considered an acceptable value for manually-imposed prestress on the basis of the author's

laboratory experience. Reversing the equation, one can use the calculated value of load to predict the strains expected in the connector elements; the calculated value is equal to 127 μstrains, this being in line with the recorded 112 μstrains (Fig. 5-12). Indeed the ratio of approximately 4/5 of the strain in the connection element to the strain in the dissipative element is inversely proportional to the ratio of the cross sectional areas.

The influence of daily temperature variations on the deformation field of the anchor is also recorded by the monitoring system (Fig. 5-13a); again the ratio of strain values between the different parts of the assembly is respected. Considering that stainless steel has a coefficient of linear thermal expansion equal to $17.3 \cdot 10^{-6}$, a gradient of temperature of about 1°C is detected between night and day, this being an acceptable value considering that the anchor lies within a thick wall of masonry that reduces the effects of thermal ranges.

The relationship between temperature gradients and variations of the corner crack width, and hence elongation of the instrumented anchor, is shown in Fig. 5-13b: the plot represents the ratio between temperatures as recorded by the temperature gauge and the elongation of the anchor, which is calculated by summing up the strains times the length of each portion of the anchorage. The ratio is approximately linear, thus showing that deformation in the anchor is largely due to the thermal cycles in the masonry walls. A similar trend has also been recorded by UPD's sensors (Fig. 5-13c), thus showing good agreement in the results of the two independent monitoring systems.

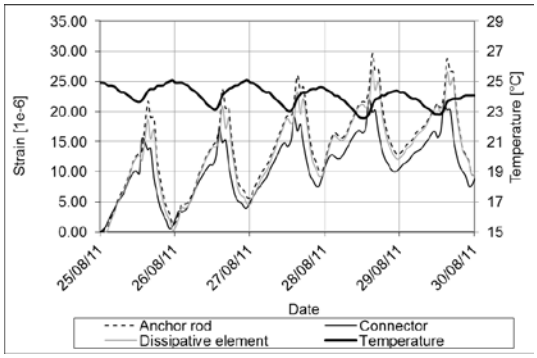

a

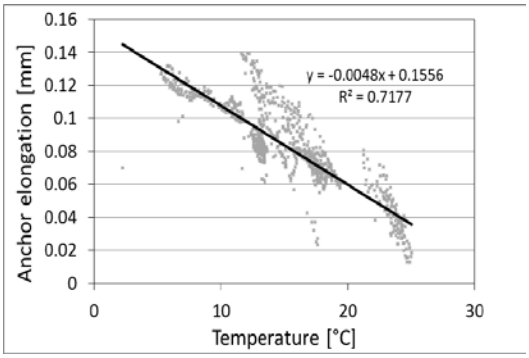

b

Fig. 5-13: Effects of temperature variations on the crack width: daily cycles (a) and ratio of relative displacements and temperature as recorded by instrumented anchor over 3 months (b) and by UPD's monitoring system (c) (D9.5, NIKER project)

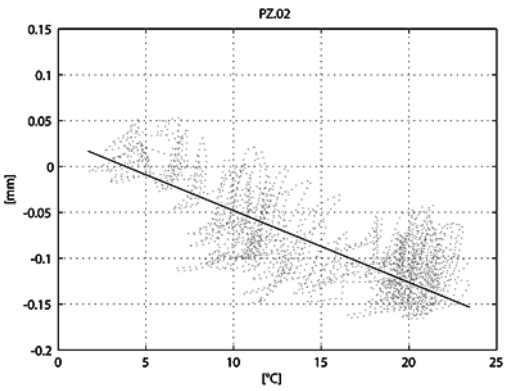

The monitoring system is also able to capture dynamic phenomena. Due to the local seismicity, to the continuity of monitoring over a long time period, and to the fact that restoration works were being carried out in the adjacent church, creating a regular source of ambient vibrations, the instrumentation recorded a considerable amount of data.

The abundance of recorded data is patent by looking at the plot of the summary data for a single axial strain gauge bridge (Fig. 5-14): the graph shows the hourly average, maximum and minimum values from the summary files, plotted over a period of ten days. The numerous peaks of the curve of the maximum values indicate strain variations higher than the standard range caused by temperature gradients and, therefore, pinpoint fast-rate phenomena. As it becomes apparent by analysing the hourly blocks, these peaks are largely due to minor vibrations, rather than proper dynamic events able to cause deformation larger than “negligible” in the anchor. This means that, due to the amount and type of recorded data, an analysis of all the blocks identified by looking at the summary files would not only be highly demanding in terms of time and resources, but might also be little beneficial to the identification of a circumscribed, meaningful set of data blocks.

Therefore, the initial strategy of using the summary files to identify data blocks containing dynamic events had to be complemented, so as to reduce the time and amount of data to be analysed. It is decided to cross correlate information coming from UPD’s monitoring systems and from independent databases, so as to identify a priori a number of time windows, and hence corresponding data blocks, when major events have occurred. Data blocks with date and time that fall in the identified time windows are analysed to check whether the anchor was also able to record the events and how it was affected by them.

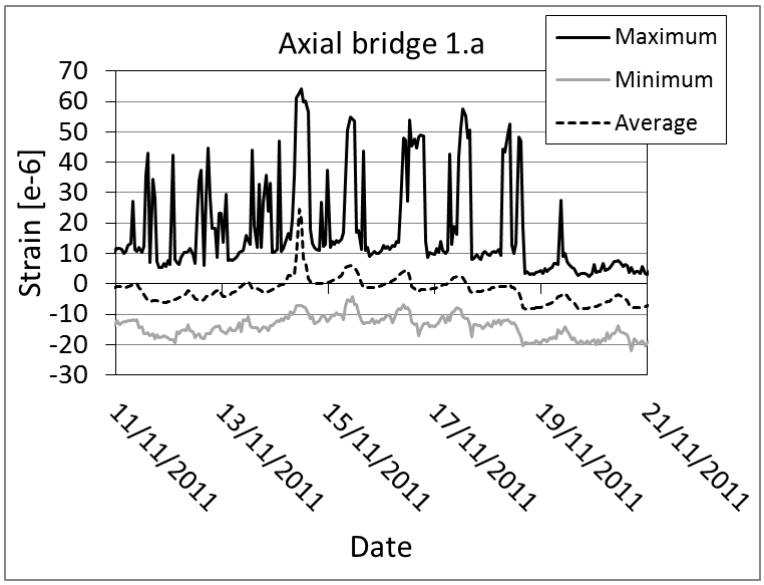

Fig. 5-14: Summary of strains recorded by the system –Example

As first attempt, all data blocks recorded by UPD's monitoring system could be considered, as the system is triggered and, as such, it only records phenomena with accelerations higher than a set threshold. However, the amount of data blocks collected by UPD is also conspicuous, as the system was affected by minor vibration, almost to the same extent as the instrumented anchor. Furthermore, UPD's system was removed due to a number of technical reasons at the end of January 2012, namely several months before the instrumented anchor. It is therefore necessary to source information for the months when only the instrumented anchor was in place.

Seismic databases such as the US Geological Service (USGS) and the Italian Seismological Instrumental and parametric Database (ISIDe) can be searched by selecting a time window and location. This allows the identification of all recorded seismic events with magnitude higher, for instance, than 2 on the Richter scale that occurred in an area with a radius of 100 km around L'Aquila at the time of monitoring. By doing so, a relatively small number of data blocks are identified and can be analysed in order to establish whether the seismic phenomena recorded by international and national seismic networks have also been detected by the instrumented anchor and by UPD's monitoring system.

It is worth highlighting that UPD's LVDT records in the period between April 2011 and January 2012 show a variation in the crack width in the order of half millimetre. Fig. 5-15 shows for instance the trend of the month of August 2011: the anchor elongation, calculated as the sum of the axial elongation experienced by each part of the anchor and measured by strain gauges, is in good agreement with the movements detected by the transducer. Both monitoring systems show the temperature cycles and how the variation in crack width is minimal.

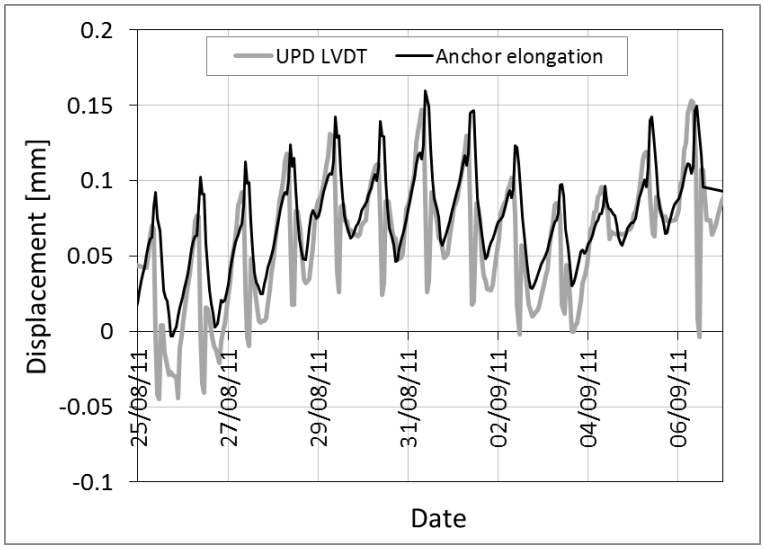

Fig. 5-15: Displacement trend as measured by the two monitoring systems

This means that the local intensity of seismic events was low, and consequently the instrumented anchor has undergone only small, linear deformations, as it will be

possible to see in the following. Indeed, even major events, such as the Emilia earthquake, 2012, had a modest impact on the city of L'Aquila (Fig. 5-16 – L'Aquila lays 200 km away from the earthquake epicentre).

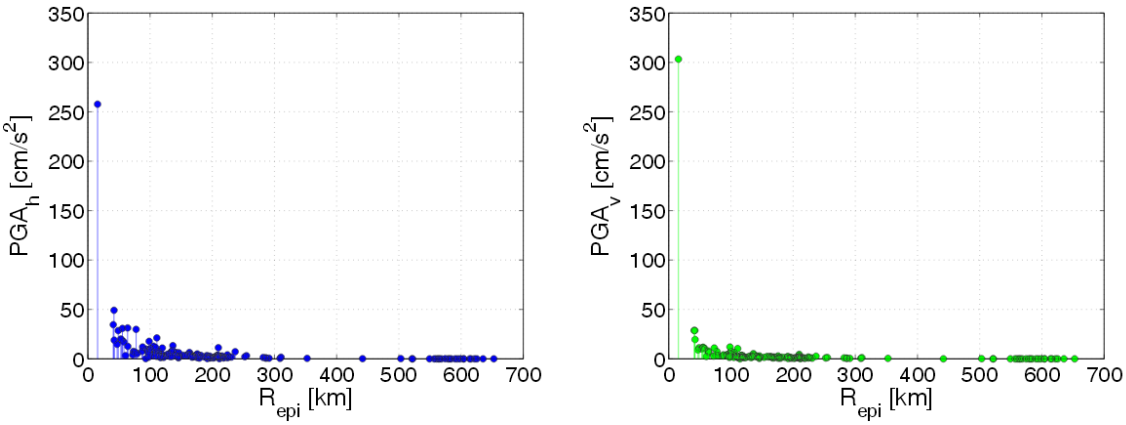

Fig. 5-16: Acceleration attenuation curves of the 2012 Emilia earthquake: geometrical mean of horizontal components (PGA_h) and vertical component (PGA_v) (Chioccarelli et al., 2012)

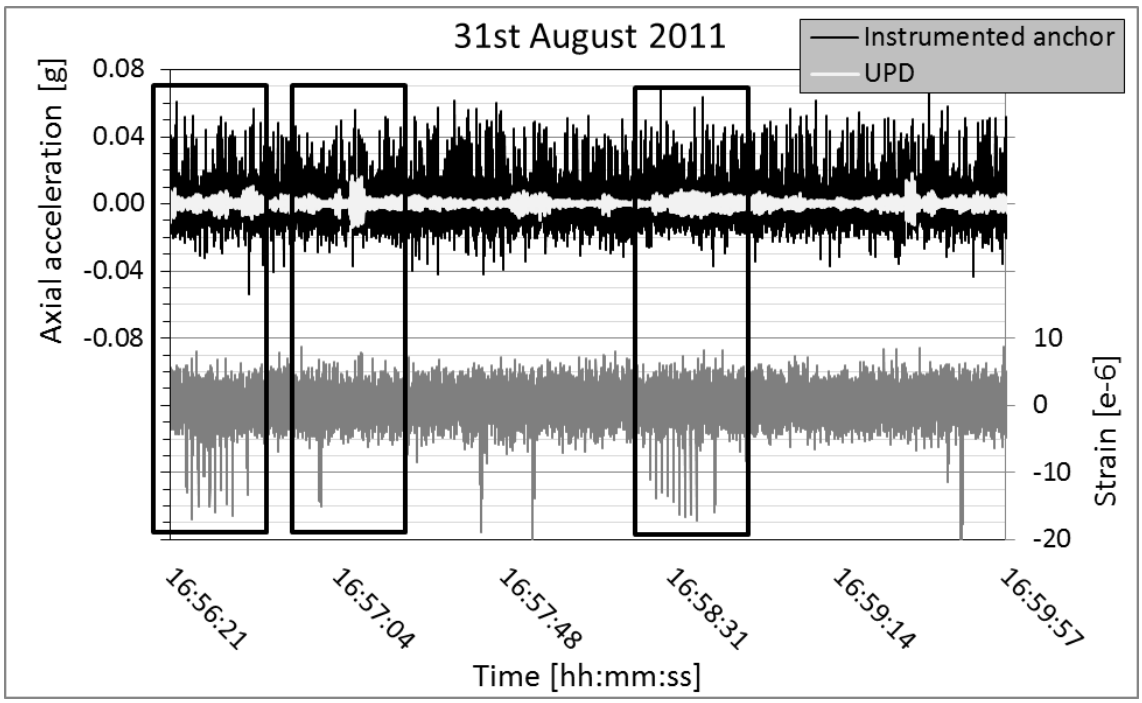

Fig. 5-17: Correlation among accelerations recorded by the instrumented anchor device and UPD's monitoring system (top) and comparison with the strain recorded by the anchor (bottom)

During the initial process of selection of data block and cross correlation of the different database, a pitfall of the instrumented anchor is identified. The noise recorded by the acceleration channels is such that small tremors are hardly readable, as it can be seen by comparison with the accelerations recorded by UPD (Fig. 5-17).

Russo (2013), who worked on another case study in L'Aquila, implemented accelerometers with a sensitivity of 1000 mV/g and observes that sensitivities in this range, although not particularly high, allow reading with clarity signals induced by human activities, which have an acceleration of a higher order of magnitude than ambient vibrations and therefore could interfere with the recording of more sensitive devices (e.g. 10 V/g). However, in the case of S. Giuseppe, human activity, such as the repair works in the adjacent buildings, seem to have a small impact, whereas ambient vibrations are mostly present. Indeed, UPD's accelerometers, which have a sensitivity of 10 V/g, are able to capture small ambient vibrations. Conversely, the accelerometer of the instrumented anchor, which had been chosen to record small to medium intensity seismic phenomena, is mostly insufficiently sensitive to perceive ambient vibration and, unfortunately, the larger scale events for which it was designed didn't occur during the monitoring period. It is also observed (Fig. 5-17) that the level of noise affecting the device is higher than what stated by the producer (10 mg rms); this could also indicate a problem of electrical interference, which affects the device preventing a clear reading of recorded accelerations.

Strain gauges can better capture small vibrations experienced by the anchor (Fig. 5-17). In spite of the level of noise, which has a higher impact for the strain amplitudes recorded on site than for those recorded during calibration, strain bridges display a response in line with UPD's acceleration records. Therefore, the process of search and identification of dynamic phenomena recorded by the instrumented anchor relies both on strain and acceleration records.

Data blocks identified by cross-correlating different seismic databases do show peaks on the strain channels and, in some cases, on the acceleration channels. However, the amplitudes of these peaks are of the same order of magnitude as those of other data blocks, so that the data sample presented in the following can be representative of the average response of the system, rather than being specific to a certain typology of phenomena, namely seismic phenomena against men-generated or ambient vibrations.

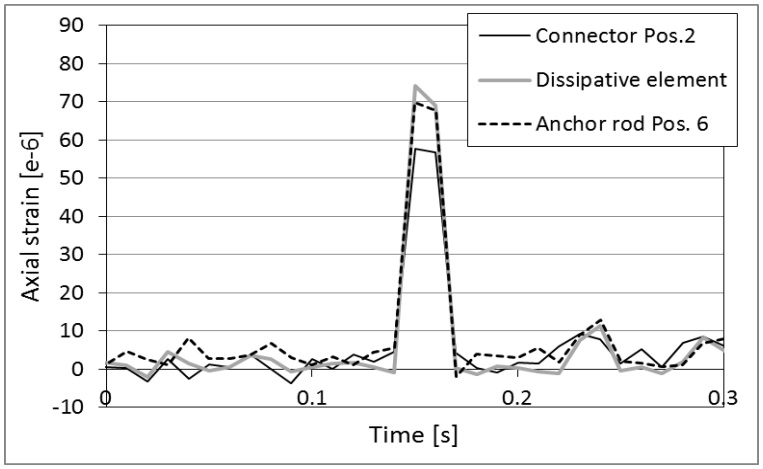

Fig. 5-18: Axial strains - 04/11/11, h 01:10 local time

As already mentioned, strain values are always in the elastic range, in line with the overall trend recorded by UPD's LVDT. In general the recorded values of axial strains reflect the expected distribution, with the anchor rods and the dissipative element experiencing the same level of strain and hence, in the elastic field, stress. The connector has lower strain (Fig. 5-18).

Such distribution of strain is not always recorded by all channels in a consistent way (Fig. 5-19), with some of the channels showing a level of strain different from what expected, for instance lower (channels 1a and 5a in Fig. 5-19a) or negative (channels 1a and 6a in Fig. 5-19b).

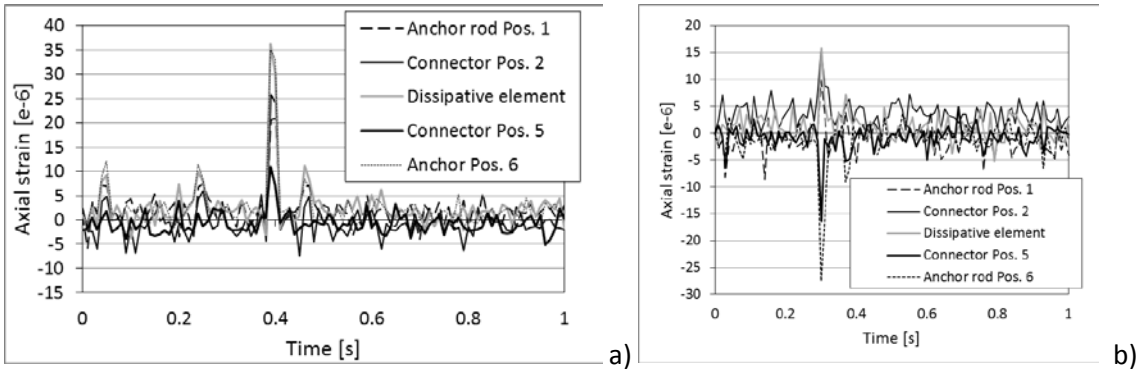

Fig. 5-19: Axial strains – a) 04/11/11, h 02:25 local time, b) 19/05/12, h 16:55 local time

Due to the lay-out of the instrumented anchor, it seems unlikely that the axial load might have been different in the various portion of the anchorage, so the reason for this discrepancy is not clear. This was not detected during calibration and the fact that it is not always the same channels to be affected by it suggests that the problem doesn't lay in an incorrect calibration. Furthermore, the deformations recorded by the various channels (axial, bending and shear) indicate a consistent behaviour of the system in response to a specific input signal (Fig. 5-20).UPD's LVDT only stores low-rate data, so that it was not possible to double check the recorded values of strains. This also underlines that the instrumentation system lack a sufficient level of redundancy so as to be able to study complex phenomena.

In spite these inconsistencies, it has been possible to identify a number of blocks that show an exact match between accelerations and strains recorded by the instrumented anchor.

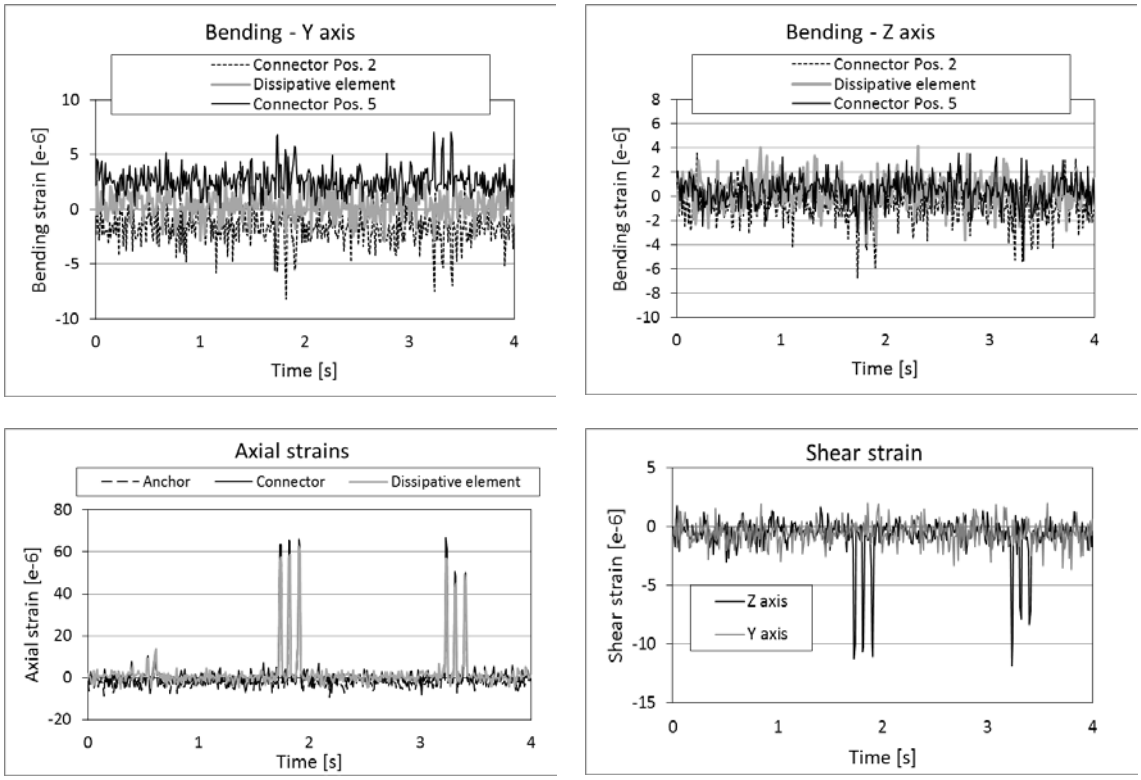

Fig. 5-20: 23/05/12, h 16:00 local time. Record of two three-peak events as recorded by strain bridges

For instance Fig. 5-21a shows a clear correlation between recorded acceleration and strains. By calculating the relative displacements as double integral of the recorded accelerations and as sum of the elongations experienced by each part of the anchor, it is possible to see that the two curves are in good agreement (Fig. 5-21b).

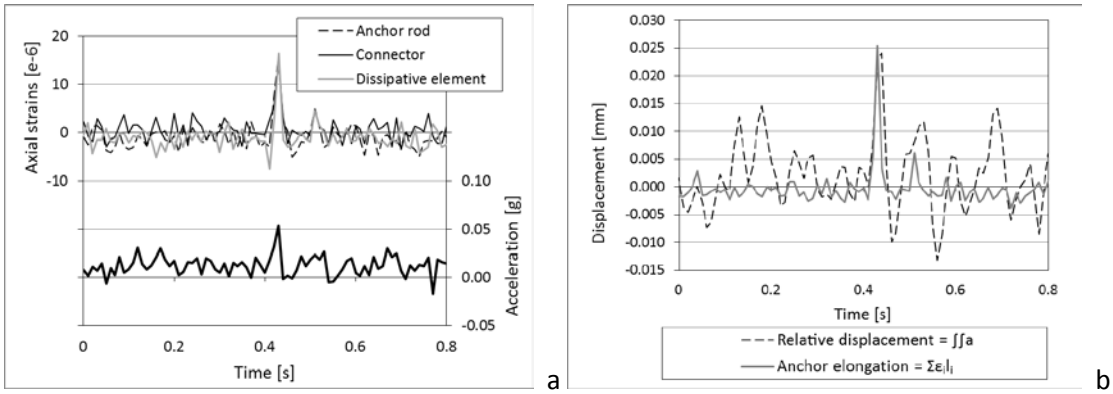

Fig. 5-21: 19/05/12, h 15:45 local time - a) Axial strains and accelerations; b) Relative displacements at corner crack

The data block of Fig. 5-21 is used to calculate the area of wall acting on the anchor. It is assumed that the acceleration recorded by the instrument causes a certain portion of masonry to move and pull the anchor by means of the front plate. As shear and

bending strains are negligible, the force acts on the anchor as pure tension, so that it is possible to write:

5-2) $$m = \frac{AE\varepsilon}{a} = \frac{133.09mm^2 \cdot 210GPa \cdot 16.4 \cdot 10^{-6}}{0.05g} = 916.7kg$$

where A is the cross sectional area of the dissipative element, the strain, ε, and the acceleration, a, are read from Fig. 5-21 and the standard value for the Young modulus of stainless steel, E, is considered.

The tributary area is calculated assuming that the volume of masonry pulling on the anchor by means of the front plate is a truncated pyramid, with one base equal to the area of the front plate (0.3 x 0.3 m^2), height equal to the distance between the façade and the crack, i.e. 1 m and 45° inclined edges (Fig. 5-22).

As the anchor is located near the corner, one side of the major basis of the pyramid can be considered to be approximately equal to the thickness of the side wall. By applying the standard formula for the calculation of the volume of a truncated pyramid, a tributary area with a long side of 1.10-1.70 m is found. Such tributary area is in line with what could be expected for this type of anchorage.

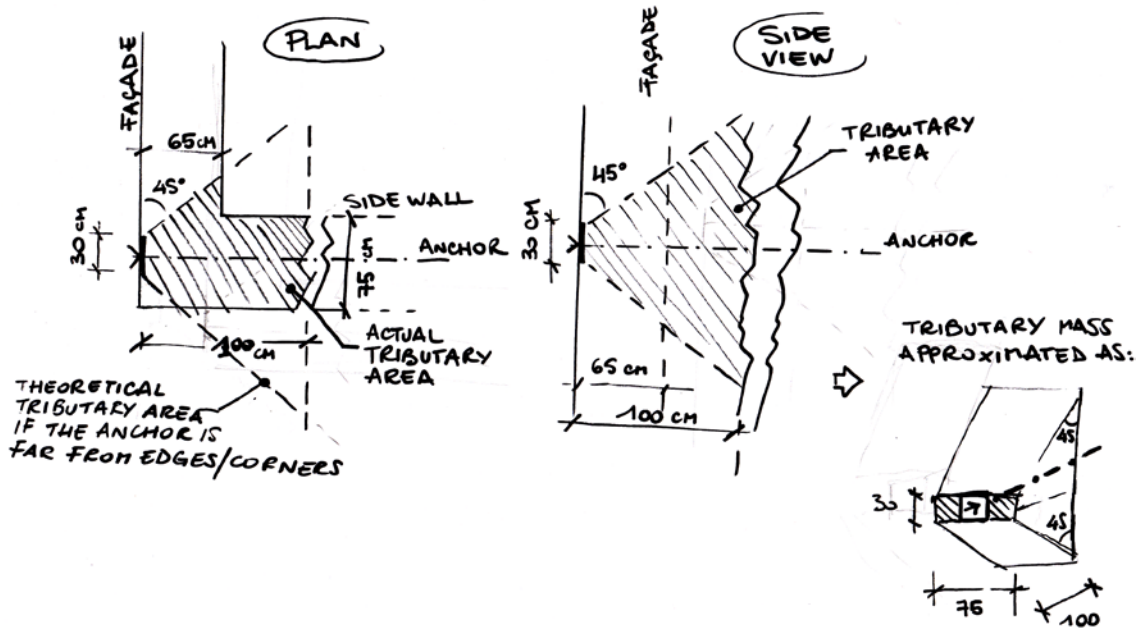

Fig. 5-22: Tributary mass of masonry acting on the instrumented anchorage

A similar calculation can be repeated when the anchor undergoes bending; Fig. 5-23 shows, for instance, the records corresponding to the 1.3 Richter scale earthquake that occurred 25 km from L'Aquila on the 8th June 2012 at 9.59 am, local time (from ISIDe database).

Considering that the lateral force is applied to the anchor in correspondence of the end plate, to which the movement of the wall is transmitted by way of friction, the strain recorded by each bridge is equal to:

5-3) $$\varepsilon = \frac{m \cdot a \cdot l_i}{EI_i} y_i$$

where l_i is the distance between the bridge "i" and the end plate, where a wall portion with mass m, undergoes an acceleration, a. E is the Young modulus of steel and I_i and y_i are the geometrical properties of the section at the location of the bridge "i".

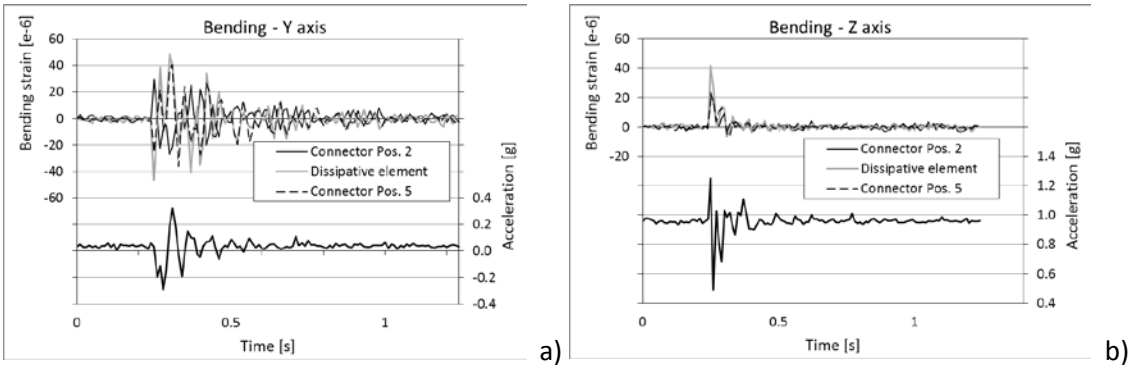

a) b)

Fig. 5-23: Bending strains in two perpendicular directions – 08/06/12, h 10:35 local time

Equation 5-3 can be reversed to make explicit the relationship between recorded accelerations and deformations:

5-4) $$\frac{a}{\varepsilon} = \frac{EI_i}{y_i} \frac{1}{m \cdot l_i}$$

where the ratio a/ε is the coefficient in the equations of the linear trends in Fig. 5-24. The figure shows a number of events similar to that of Fig. 5-23; the plot has been cleared from the noise so that only the peaks of the "real" dynamic events are represented. Both accelerations and strains are plotted as absolute values, so as to find a linear correlation.

The linear regressions obtained by working on the points of the graph strain-acceleration of Fig. 5-24 are consistent with the geometrical properties of the instrumented anchor. It is indeed:

5-5) $$\frac{a}{\varepsilon_2} = \frac{EI_2}{m \cdot l_2 \cdot y_2} = \frac{E \cdot 1.45 I_3}{m \cdot 1.05 l_3 \cdot 1.12 y_3} = 1.23 \frac{a}{\varepsilon_3} \rightarrow 0.0041 / 0.0034 = 1.21$$

5-6) $$\frac{a}{\varepsilon_2} = \frac{EI_2}{m \cdot l_2 \cdot y_2} = \frac{EI_5}{m \cdot 1.2 l_5 \cdot y_5} = 0.83 \frac{a}{\varepsilon_5} \rightarrow 0.0041/0.005 = 0.82$$

As all parameters in equation 5-4 are known from the geometry of the prototype parts, it is possible to calculate the mass, m, acting on the anchor. Results for bridges 2, 3 and 5 are respectively 4.31, 4.21 and 4.28 kg, thus showing a good agreement.

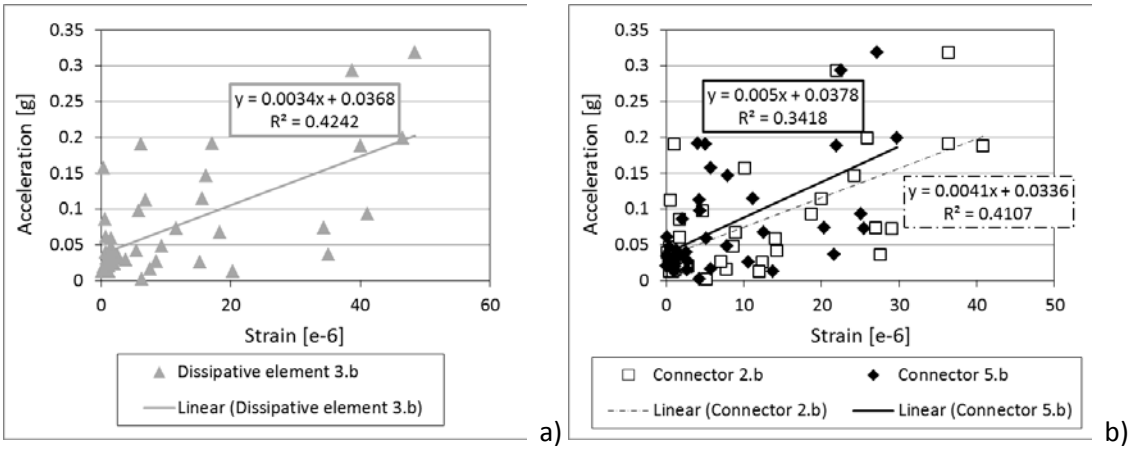

Fig. 5-24: Correlation between recorded strain around the Y axis and acceleration in Z direction in the dissipative element (a) and in the connectors (b)

Even though the variation in acceleration that provokes bending deformation of the anchor is larger than the examples with axial accelerations, mass is much smaller; indeed, it corresponds to a masonry volume area of 30 x 30 cm, i.e. the contact area of the front plate, with thickness of 3 cm. In fact, such a small volume is probably due to the fact that the load transfer mechanism in this direction is far less efficient than when load is transmitted in the axial direction, i.e. through bearing rather than friction, as for loading in the wall plane. This means that the force acting on the anchor is actually less than the inertial force of the tributary masonry volume. As the anchor is affected by vibrations in all the three directions, the contact between the plate and the masonry will also varies during a dynamic event. Accordingly, the friction force at the plate surface changes and only a small percentage of the load generated by the lateral acceleration is transmitted to the anchor.

5.6 FINAL REMARKS

Chapter 5 draws on the results of the experimental campaigns detailed in Chapter 4 and deals with the development of an instrumented prototype of the hysteretic device and its implementation in a case study to the purpose of studying the response of the dissipative device in a real life environment.

On-site assessment aims both to complete the validation of the dissipative devices by broadening the range of boundary conditions and loading scenarios, and to assess the feasibility of possible further application, namely as off-shelf monitoring system and, eventually, early warning system.

The installation is carried out in the framework of the NIKER project, in cooperation with the University of Padua, who ran an extensive monitoring programme in the city of L'Aquila, Italy, in the aftermaths of the 2009 earthquake. The selected case study is a baroque chapel, S. Giuseppe dei Minimi, which presented clear out-of-plane damage of the façade with large, pseudo-vertical cracks at the corner connection with the side walls. Such damage pattern, as already discussed, is typical of historic buildings and is exactly the typology of damage mechanism that the dissipative devices are designed to tackle. Furthermore, the fact that the building had not been repaired but had already been temporary propped allowed a safe installation and, at the same time, gave the opportunity of placing the prototype in correspondence of an open crack, i.e. in a position sensitive to further vibrations, which could be captured by the instrumentation of the anchor prototype.

Instruments are selected so as to be able to read low-to-medium intensity seismic events. This choice is motivate by the fact that, being central Italy a seismic-prone area, such intensity phenomena can be expected to occur with regular frequency and have the potential to bring the hysteretic device in the plastic field; indeed, it is the post-elastic response of the anchoring device that is most interesting to the purpose of on-site validation. On the other hand this choice entails that the selected instrumentation is less sensitive to smaller scale phenomena, such as ambient vibrations.

Beside the choice of the vibration intensity to be measured, and hence of the sensitivity of the instruments, the monitoring system, including the data acquisition and conditioning system too, is designed to respond to a number requirements, dictated by the nature and location of the pilot installation. Robust and reliable performance, comparability with laboratory records and results, continuous monitoring and remote accessibility are the criteria that guide the selection of the system components.

After undergoing laboratory calibration, a prototype equipped with a set of strain gauges, an accelerometer and a temperature/humidity gauge was installed in June 2011 and remained in place for over a year. During this time, the expected small-to-medium intensity earthquakes did not occur, so that the system could not be exploited to its full potential. Nevertheless, the pilot installation has an interesting outcome both in terms of device performance and as far as instrumentation is concerned.

From a preliminary data analysis, it is clear that the anchor responds to a number of phenomena. Besides pseudo-static events, such as the locking of the front plate and thermal gradients, the monitoring system is also able to record dynamic phenomena. Due to the conspicuous amount and low intensity of these events, the selection of a number of data blocks of interest is carried out by cross correlating the information coming from the instrumented anchor, from the monitoring system of the University of Padua and from international and national seismic networks. By doing so, the analysis is restricted to data blocks recorded at the time when seismic events occurred in L'Aquila and neighbouring areas. The response of the anchoring device shows that

these events had little, if any, local impact, yet minor tremors were perceived and recorded.

The hysteretic device behaves as it can be expected for small scale inputs: the pieces remain in the linear field, with higher deformations being experienced by the dissipative element and the anchor rods, according to what designed and already assessed experimentally. Indeed, these two parts have the same cross sectional area and, hence, experience the same level of deformation in the elastic field.

As linear relationships between deformation and stress can be applied, records are used to identify the tributary volume of masonry that acts on the anchor; recorded acceleration and deformations are correlated through Navier's equations. Such result is useful to inform the preliminary design of anchors and, in particular, their layout and spacing, and will therefore feed in the development of the design procedure described in Chapter 7.

As far as the instrumentation goes, collected data shows that the system needs to be further developed as it lacks the sufficient level of redundancy that would have allowed analysing different phenomena with higher accuracy. One problem that might have affected the instruments is electrical disturbance, as data appears sometimes inconsistent. In particular, the accelerometer was often unable to capture tremors; this might be ascribed to the insufficient sensitivity of the instrument; nevertheless it seems also likely that electrical disturbance could be a cause for this, as records feature high level of noise, higher than what expected from the technical specifications. The lack of redundancy, such as for instance the lack of a LVDT with continuous logging, means that dubious phenomena can only be speculated upon but not studied in detail to determine the nature of the interference.

It is therefore recommended that the instrumentation used in the pilot installation is complemented by a LVDT and a second accelerometer with higher sensitivity, to be run on a continuous basis, whereas the lower sensitivity accelerometer could be set with a trigger. It is also suggested that the system is synchronised with any other parallel monitoring system, so as to ensure that no time lag occurs.

If these further measures fail, glass fibres can be used an alternative to ERSG to obviate to the problem of electrical interference. This option was initially discarded, as strain gauges had already been successfully used during the experimental campaigns; full compatibility with previous results and simplicity of application were preferred. Furthermore, on-site validation was carried out in the framework of the emergency conservation of the buildings, at a time when the reduction of aesthetical impact, and hence wiring, was not necessary.

In spite of the need for technical improvements, the instrumented anchor has the potential for further developments. It seems reasonable to assume that, as the hysteretic device behaves consistently in the linear field, it will also do so in the non-linear and could therefore act both as strengthening and monitoring element,

provided that the embedded instrumentation is sufficiently refined to record the desired information.

In case of further trial applications, it is recommended that the anchor is fully grouted, also at the front end. Even though this might complicate the installation activities, it would ensure a full transmission of load at the head of the anchor in case of compressive axial load or for lateral loads, i.e. loads that induce shear and bending in the anchor. It is disputable whether the anchor would have a positive influence for in-plane loads of the façade, namely whether the full grouting of the front end would be beneficial in terms of strengthening in this direction. Nonetheless, grouting would allow the full exploitation of all the strain gauge bridges and would be expedient to the task of monitoring and hence on-site validation.

The lack of events that allow studying the post-elastic response of the anchor device embedded in a structure is made up for in the next chapter, where computational models will be used to explore further scenarios.

6 COMPUTATIONAL VALIDATION

6.1 INTRODUCTION

The validation process followed in Chapters 4 and 5 aims to identify a number of meaningful parameters that can be used to describe the performance of the anchoring devices in function of a number of loading and boundary conditions. The quantification of these parameters in order to identify the device performance ranges is also a main goal of the previous two chapters.

Besides informing the fine-tuning of the anchoring devices, qualitative and quantitative data collected so far feeds into the development of the set of Finite Element models that will be described and commented in this chapter.

The computational validation has a number of objectives:

- Incorporating the analytical models that have been so far devised to systemise the results of the previous chapters and validating their use;
- Simulating further scenarios that, due to laboratory constraints or on-site events, have not been explored yet;
- Observing in detail stress and strain fields in the dissipative devices and in the surrounding materials and yet establishing a number of simplifications that can be introduced in the numerical models, that do not impair their accuracy and that allow optimising computational time and resources, with the goal of…
- Eventually developing the FE model of a whole structure, which will compensate for the lack of large scale testing, but will also be used to exemplify the design procedure described in Chapter 7.

Modelling proceeds in a similar fashion as experimental campaigns: initially the devices are considered only as isolated elements; once robust, reliable results have been obtained, the computational validation can move forward to higher levels of complexity, until a whole structure can be investigated by FEA.

6.2 FINITE ELEMENT MODELS OF THE DISSIPATIVE DEVICES IN ISOLATED CONFIGURATION

6.2.1 Model Description and Assumptions

6.2.1.1 Geometry and Mesh

FE models of the hysteretic device include the dissipative element with two lengths of bar at each end. The bars simulate the anchor rod to which the hysteretic device would be attached in a real case study, and through which the device is actually connected to the pulling apparatus during tests in the isolated set-up (§4.2).

For the dissipative element, the geometry is derived from the drawings of the prototypes described in Chapter 3 and machined for the tests detailed in Chapter 4.

However, for computational purposes, the threads of the sample parts are not modelled; the contact between the threaded bars and the dissipative element is simulated instead via a full bond. Such assumption is motivated by fact that, before each testing session, specimens were slightly pre-tensioned and lock-nuts used to fix pieces in place, so as to avoid any relative movement within the specimen.

Experimental results support the hypothesis of full bond: none of the load-displacement graphs reported in §4.2 feature zero-stiffness branches, which would indicate relative movements, and hence slack, within the device assembly.

Also the radiuses used during the machining of the dissipative element in order to avoid any undesirable stress concentration are simplified to straight elements in the FE model. Nevertheless, ratios between the diameters and cross sectional areas of the parts of the dissipative element and the bars have been faithfully recreated as these are crucial to the behaviour of hysteretic anchors. Indeed, the main objective of the computational analyses on the hysteretic device is the correct reproduction of the stress field, which determines whether or not plastic deformations are located in the desired position, namely at the midpoint of the dissipative element.

The prototypes of the hysteretic device are meshed as solid three-dimensional models made of brick elements (Fig. 6-1); the number of elements is changed during the computational analysis to achieve the best fit with experimental results, as it will be discussed further in §6.2.2.1.

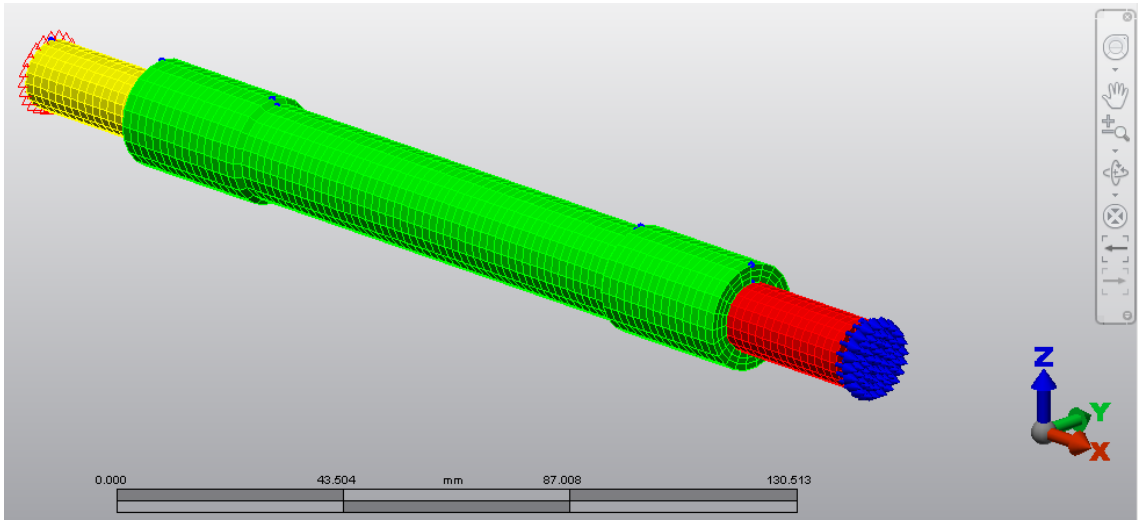

Fig. 6-1: Hysteretic anchor - Mesh

The geometry of the model of the frictional device has been substantially modified in respect to that of the prototypes shown in Chapter 3. Indeed, the assembly of the tested prototypes is fairly complex, with pieces being shaped to avoid undesired stress concentrations, ensure good alignment and most of all allow a good control over the frictional mechanism. However, the precise reproduction of such geometry would lead

to either severely distorted elements or an extremely large number of elements and hence to a high computational burden.

It is therefore decided to sacrifice detailing in favour of a more efficient computational time and to focus on those parts of the model that have an influence on the frictional mechanism, like the slot where the sliding element rests (Fig. 6-2). Experimental results did not evidence any negative phenomenon connected to the presence of high stress concentrations, so that the assumption seems sufficiently justified.

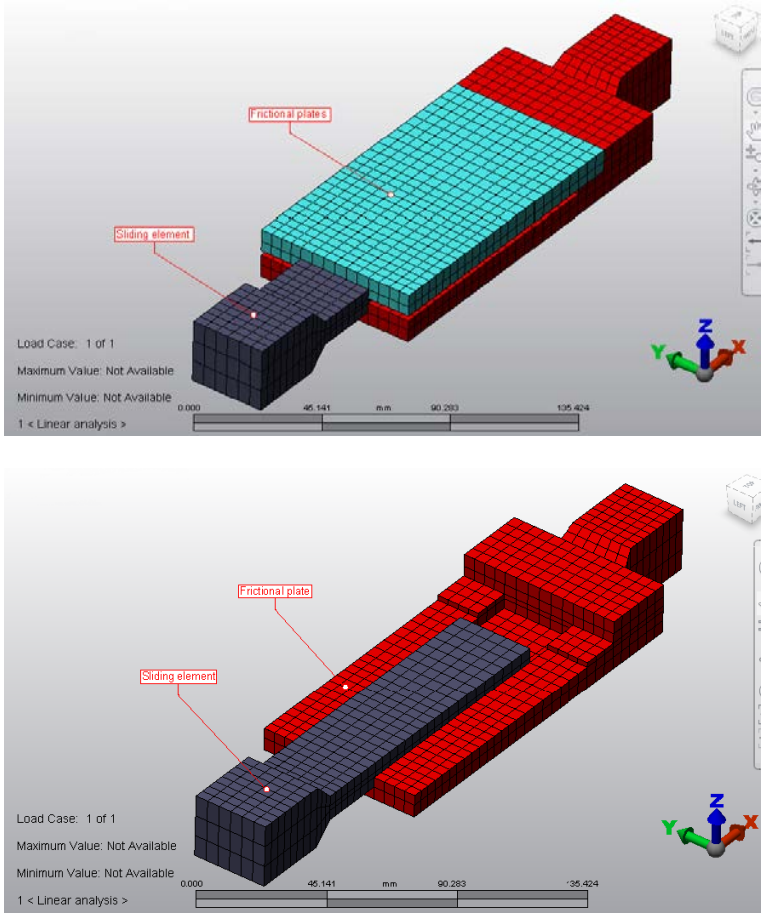

Fig. 6-2: Frictional anchor – Sketch of the device parts as modelled by FEs

In the case of the frictional device, bonded contact is defined for the two elements making up the frictional plates, which are assembled together by pins (red and blue part of Fig. 6-3), whereas surface contact is defined between the sliding element and the inner walls of the slot in the frictional plates (grey element with the inside wall of red and blue elements). The perpendicular pressure that generates friction, $F_{\perp}$, is applied along the direction of axis Z (Fig. 6-3) while a friction coefficient is assigned to contact pairs lying in the plan XY. It is instead assumed that no friction exists on the contact pairs lying in the plans XZ and YZ. The correctness of such hypothesis is verified “a posteriori” by comparison between experimental and computational results. Friction is applied by the model according to a Coulomb law.

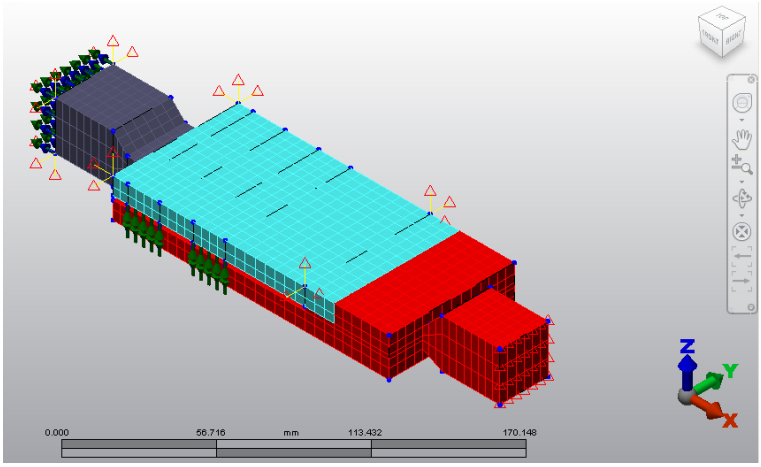

Fig. 6-3: Frictional device – Mesh

6.2.1.2 Material Properties, Boundary Conditions and Load Histories

As previously mentioned, two strength classes of the same stainless steel are used for the machining of hysteretic prototypes: class 50 is used for the dissipative element, class 70 for the threaded anchors. The lower plastic threshold of stainless steel class 50 ensures early yielding and hence larger deformations. Conversely, M16 threaded bars are meant to remain functional throughout seismic events and therefore are made of stainless steel class 70 and have higher yielding capacity. Mechanical parameters of steel are summarised in Table 6-1.

Table 6-1: Mechanical properties of FE stainless steel elements

Stainless steel S304, strength class:	**50**	**70**	
Mass density	80	80	[kN/m^3]
Young's modulus	193	193	[GPa]
Poisson coefficient	0.28	0.28	[-]
Yielding strength	210	450	[MPa]
Ultimate tensile strength	500	700	[MPa]

The non-linear behaviour of steel is modelled through (Fig. 6-4):

1. A von Mises stress-strain curve derived by the application of the Ramberg-Osgood model, as modified by Rasmussen and included by the Eurocode 3 (EN 1993-1-1:2005) for modelling of structural steel;
2. The stress-strain curve derived by experimental tests.

The first model is supposed to appropriately describe the smooth transition between elastic and non-linear fields near the yielding point and has the advantage of being the standard model prescribed by the code for the modelling of steel. However, it generates a curve that is still too similar to an elastic-perfectly plastic material, with a fairly sharp change in stiffness in correspondence of the yielding point Conversely, tested specimens show a highly non-linear behaviour with a larger portion of the graph experiencing the transition between linear and fully plastic fields (Fig. 6-4), typical of

stainless steel. Therefore, it is decided to create a second stress-strain curve model as average of experimental result, which smoothly reaches the plastic field within the threshold of the 0.2% deformation. This is not only more representative of the actual behaviour of specimens during the experimental campaign, but it is also in line with 0.2% proof stress provided by the producers. Proof stress is indeed used instead of yielding stress, when the transition between elastic and plastic is not sharp and is hard to identify. This curve, although more representative of what recorded in the laboratories has the disadvantage of being created on the basis of a set of data, so is neither standard nor repeatable.

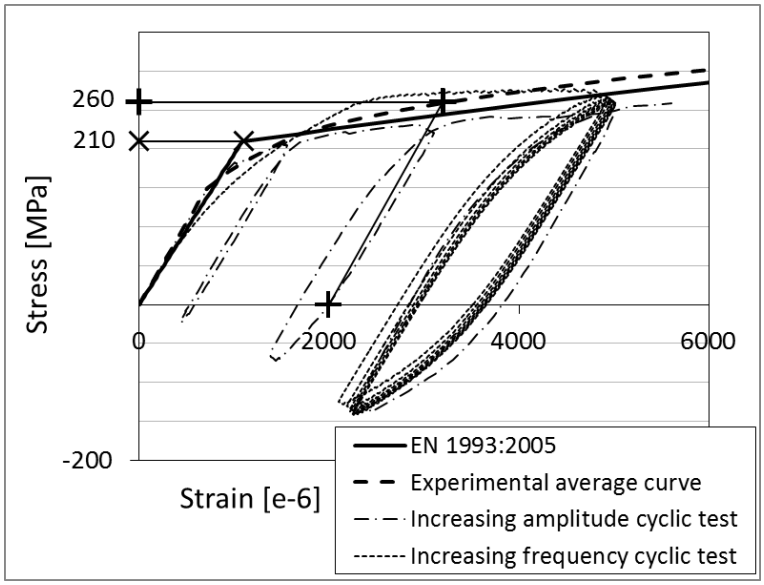

Fig. 6-4: Constitutive laws of FE metallic elements in comparison with test output

It should be noted that strength at yielding for the first typology of material model ("EN 1933:2005" in Fig. 6-4) is considered to be equal to the minimum value stated by the producer; in the second model ("Experimental average curve" in Fig. 6-4) the proof stress is higher than this minimum, as it is calculated as an average of the tested specimens, some of which yielded for a load slightly higher than expected. Aside from specimens that underwent more than one test run, for which the first cycle is affected by the hardening depending on the testing history, this occurred also with some of the pristine samples. The phenomenon is intrinsic to the fact that the stated 0.2% proof stress is a guaranteed minimum, not a characteristic value, so that exceedance of the stated threshold is possible.

The purpose of using two models is to verify which is the most suitable, what impact they have on computational results and if accuracy or standardisation should be favoured. Similarly, both kinetic and isotropic hardening is used during modelling.

Autodesk Algor Simulation software defines hardening according to the classic theory: a material presents isotropic hardening when its yielding surface expands without changing its shape, as stress increases. Such model implies that if tensile and

compressive branches of the stress-strain diagram are initially symmetrical with respect to the origin, then they will maintain this symmetry throughout loading and unloading cycles. This is surely the case for the von Mises curve; indeed, Autodesk Algor Simulation only requires defining the positive branch of the stress-strain curve and derives by default the negative branch. Therefore, according to the model, yielding after a load reversal starts only when an absolute stress value equal to the previous absolute maximum is attained.

Isotropic hardening doesn't account for the Bauschinger effect, namely that a material sample might then have a lower yielding strength after a load reversal than if it were only loaded monotonically. This effect is reproduced by kinematic hardening, which causes the yielding surface to shift, without any variation in form or shape as result of stress variation. As such, kinematic hardening is generally preferred to model cyclic loading, as also suggested by Autodesk Algor Simulation users' manual.

In spite of this and even though kinematic hardening seems to be prevalent in the experimental stress-strain curves (Fig. 6-5), isotropic hardening is still used during modelling. As it will be shown in the following, kinematic hardening is not fully satisfactory in reproducing experimental results and therefore isotropic hardening is used to explore an alternative model and have a term of comparison.

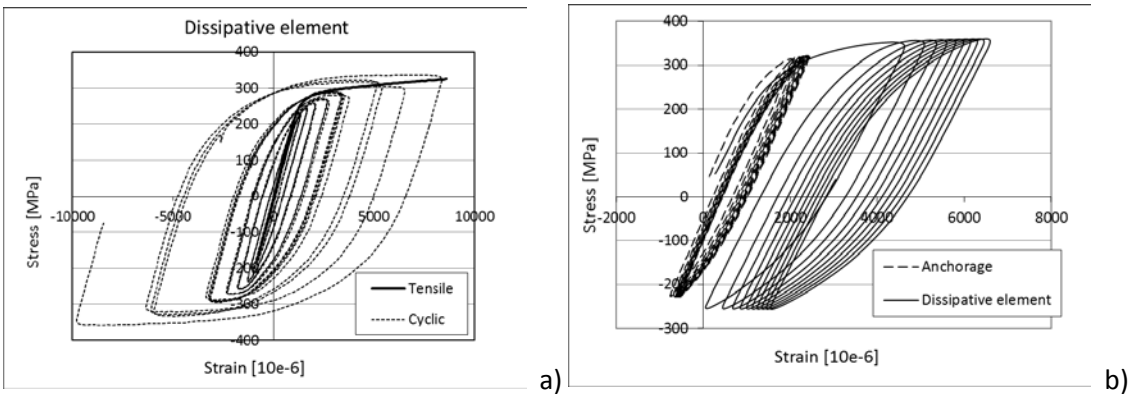

Fig. 6-5: Kinematic hardening as visible in the experimental curves: a) pseudo static cycles with increasing amplitude, b) dynamic cycles with constant amplitude

In the case of the friction devices, the stainless steel of the prototype parts are defined as elastic, as the main focus is on contact problems rather than on the stress field. Such hypothesis eases the computational process and is justified by the fact that frictional sliding should occur well before yielding of any of the part, even localised, as it will be verified a posteriori. Adopted properties are those reported in Table 6-5, excluding yielding stress, which is not part of the input.

The models of both devices are fully constrained to one end and loaded at the other end (Fig. 6-1 and Fig. 6-3), thus simulating the testing set-up, where specimens are gripped into the jaws of the testing equipment: whereas one jaw is fixed, the other moves according to the input signal.

It's worth noticing that in the model of the friction device other constraints have been added to ensure stability. Indeed, whereas one of the friction plates is fully constrained (red part of Fig. 6-3), and the other (blue part in Fig. 6-3) is bonded to it, from an numerical point of view the sliding element remains free despite being in contact with these two parts. Therefore, a set of springs is added to the model (yellow lines in Fig. 6-3) to restrain the degrees of freedom that do not participate in the sliding; springs are connected to the sliding element at one end, while the other end is fully constrained, thus ensuring numerical stability.

Displacement and load time-histories experienced by samples during the testing campaigns and recorded by the testing apparatus are used as input for the FE models, thus ensuring correspondence between experimental and computational signals (short summary in Table 6-2, full details in Table 4-1). This means that, in the case of a dynamic input, when the testing apparatus struggles to cope with high frequency cycles and achieve the required input displacements, both experimental and numerical curves have a maximum amplitude lower than what stated in the testing/modelling programme, e.g. about 2 mm instead of stated 2.5 mm.

Table 6-2: Set-up and loading programme of dissipative devices as simulated by FEA

		Hysteretic model	Friction model
Pseudo-static cyclic	Type of input signal	Sinusoidal	Sinusoidal
	Frequency [Hz]	0.01	0.01
	Amplitude [mm]	Increasing	Increasing
	Number of cycles	One per amplitude	One per amplitude
Cyclic dynamic	Type of input signal	Sinusoidal	Sinusoidal
	Frequency [Hz]	0.1, 0.5, 1	0.1, 0.5, 1
	Amplitude [mm]	0/+1.25	-5/+5
	Number of cycles	10 per frequency	10 per frequency
Time-history	Type of input signal	FE output (as per §4.2.1)	FE output (as per §4.2.1)
	Frequency content	Various	Various
	Amplitude [mm]	FE signal is scaled to maximum amplitude of 1.25, 2.5 and 5 mm	FE signal is scaled to maximum amplitude of 1.25, 2.5, 5 and 10 mm

Analyses are carried out firstly as linear analyses, with all materials simulated as isotropic elastic materials, so as to perform a first check on the distribution of stresses and mechanical behaviour for loads within the linear field. Once computational results are in line with experimental results, non-linear analyses are performed.

6.2.2 Results

6.2.2.1 The Hysteretic Device

As already stated, a number of parameters are varied throughout the computational calibration of the hysteretic device, so as to identify which model better reproduces the behaviour of devices undergoing a variety of input signal. Parameters varied in the analyses are summarised in Table 6-3.

The first three models of Table 6-3 are those with the higher level of simplification, as they have the lowest number of elements and the material model is taken from the code, i.e. the constitutive law is calculated via standard parameters and therefore no additional testing would be needed if one wanted to vary the model materials.

Table 6-3: Hysteretic device - Summary of parametric calibration of FEMs

Model	Input type	Material	Hardening	Mesh element number
Y-D/EN/K	Displacement	EN 1993:2005	Kinematic	1320
Y-L/EN/K	Load	EN 1993:2005	Kinematic	1320
Y-D/EN/I	Displacement	EN 1993:2005	Isotropic	1320
Y-D/Exp/K+	Displacement	Experimental	Kinematic	1500
Y-D/Exp/I++	Displacement	Experimental	Isotropic	1800
Y-D/Exp/K+++	Displacement	Experimental	Kinematic	8646

By looking at the results of model Y-D/EN/K (first row in Table 6-3), it is possible to observe that experimental and numerical load-displacement curves (Fig. 6-6) are in good agreement although, as expected from the constitutive laws, the computational model is not able to follow the exact shape of the hysteretic cycles.

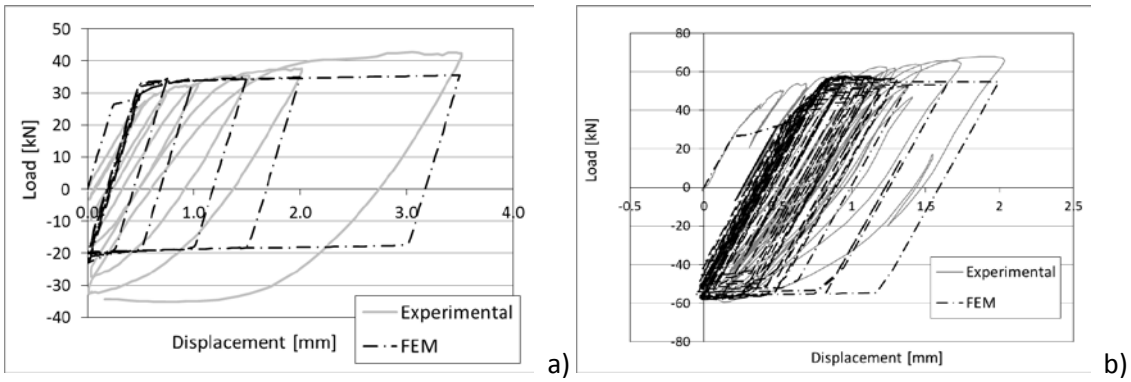

Fig. 6-6: Hysteretic device – Model Y-D/EN/K – Input: a) increasing amplitude cycles; b) AQV signal scaled for a max. amplitude of 2.5 mm

The major drawback of the Y-D/EN/K models is that they are not able to represent the smoothed shape of the cycles and the further increase in stiffness that characterise the post-yielding behaviour. In the case of pseudo-static cycles (Fig. 6-6a), the FEM tends to underestimate the dissipated energy, as the flat plastic branch of the graph in combination with the kinematic hardening model cannot reproduce the full cycles. In

the case of the dynamic signal (Fig. 6-6) the shape of computational cycles is again not fully fitting and, in this case, overestimates the cycles.

Similar conclusions are drawn by looking at the stress-strain curves (Fig. 6-7): computational models are imprecise in representing the energy dissipated by each hysteretic cycle, as they cannot fully reproduce the smooth variation in stiffness experienced by the specimens during the transition between linear and plastic field. Nevertheless, the distribution of strains in the various parts of the FE device is in agreement with what expected on the basis of the concept design and of the experimental evidence.

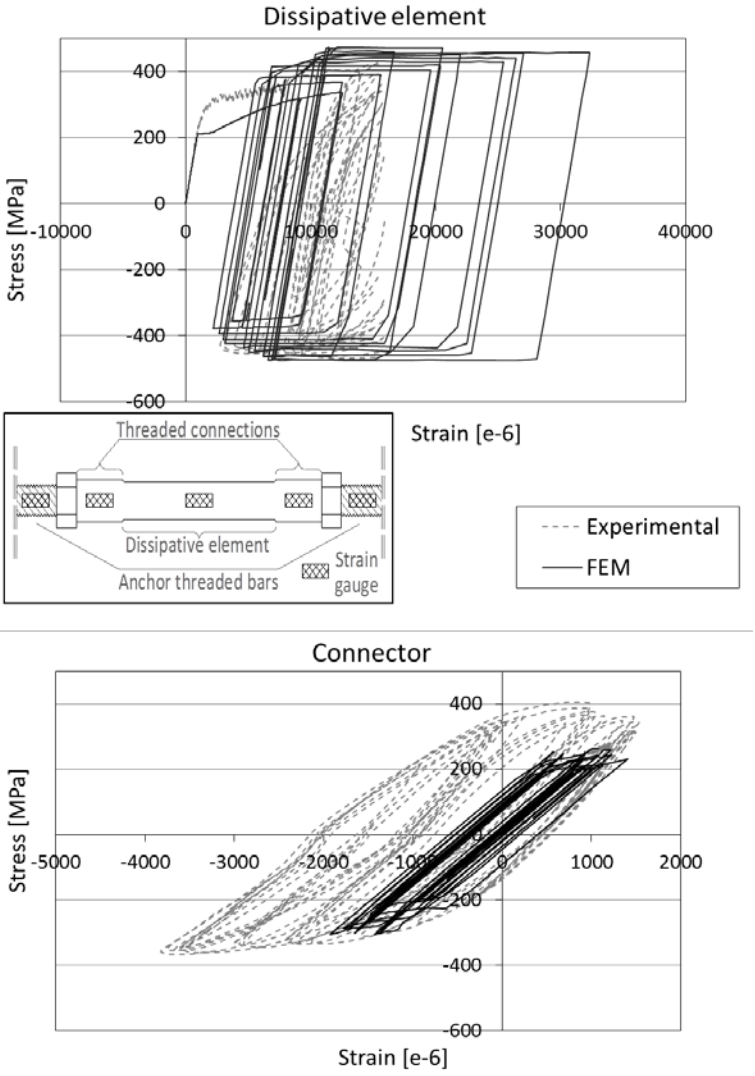

Fig. 6-7: Hysteretic device – Model Y-D/EN/K – Input: AQV signal scaled for max. amplitude of 5 mm

The difference in shape between experimental and computational curves only affects cyclic loading, while monotonic curves are in better agreement, in spite of a slightly higher stiffness of the computational curve in the elastic field (Fig. 6-8, left). Such

higher stiffness is likely to be due to the different lengths of threaded bars that were gripped in the testing apparatus at the time of testing, as the chosen Young modulus is instead in line with the experimental results (Fig. 6-8, right).

Isotropic hardening (Fig. 6-8), as could be expected, does not solve the issue; it actually worsens the discrepancy between computational and experimental results by generating increasingly larger cycles. Similarly, running models in load rather than displacement control negatively affects the precision of results, as the low stiffness of the force-displacement curve in the plastic range means that the resulting displacements cannot reflect precisely the actual experimental records (Fig. 6-9).

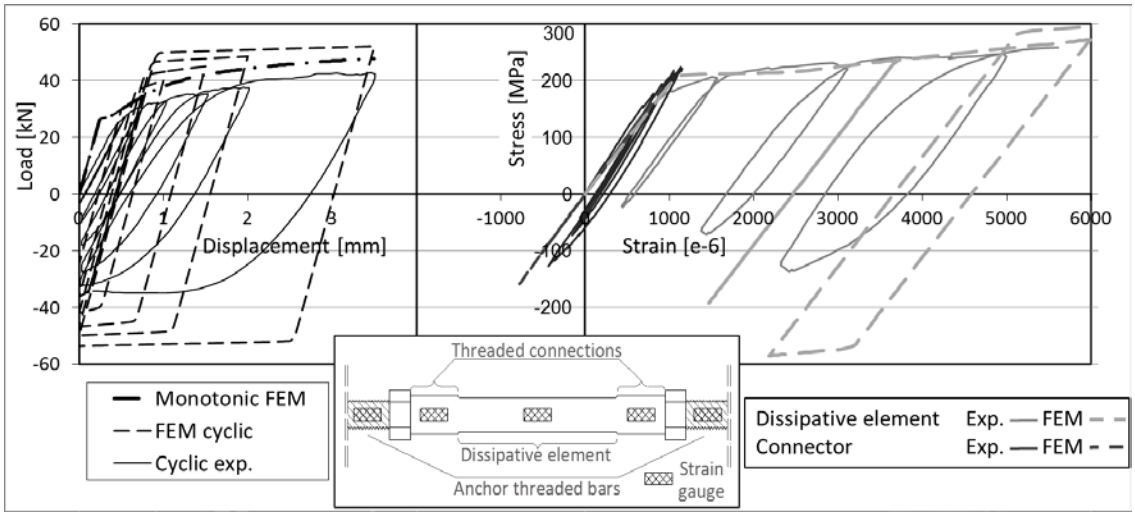

Fig. 6-8: Hysteric device – Model Y-D/EN/I – Input: Monotonic and cyclic increasing-amplitude

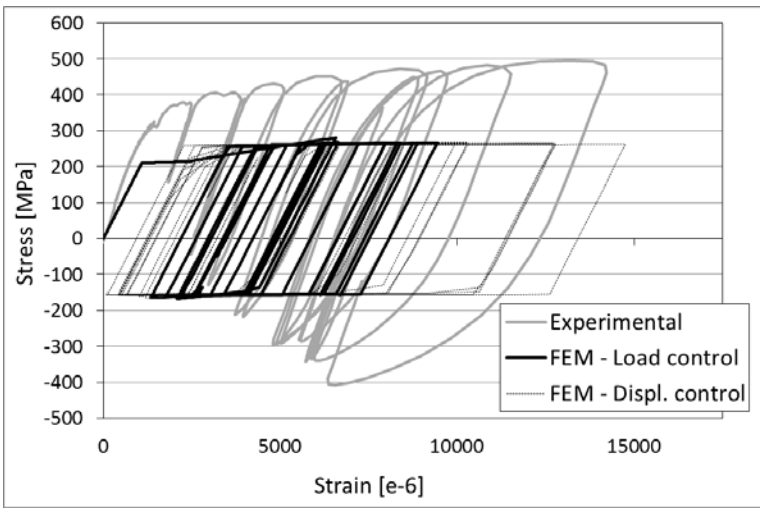

Fig. 6-9: Hysteretic device – Models Y D and L/EN/K – Input: AQV signal scaled for max. of 2.5 mm

The effect of the various modelling parameters is further investigated by repeating the analyses, but using the constitutive law derived experimentally and refining the mesh,

in the attempt of achieving a more realistic distribution of yielded areas over the FE dissipative element. A summary of this parametric study is given in Fig. 6-10.

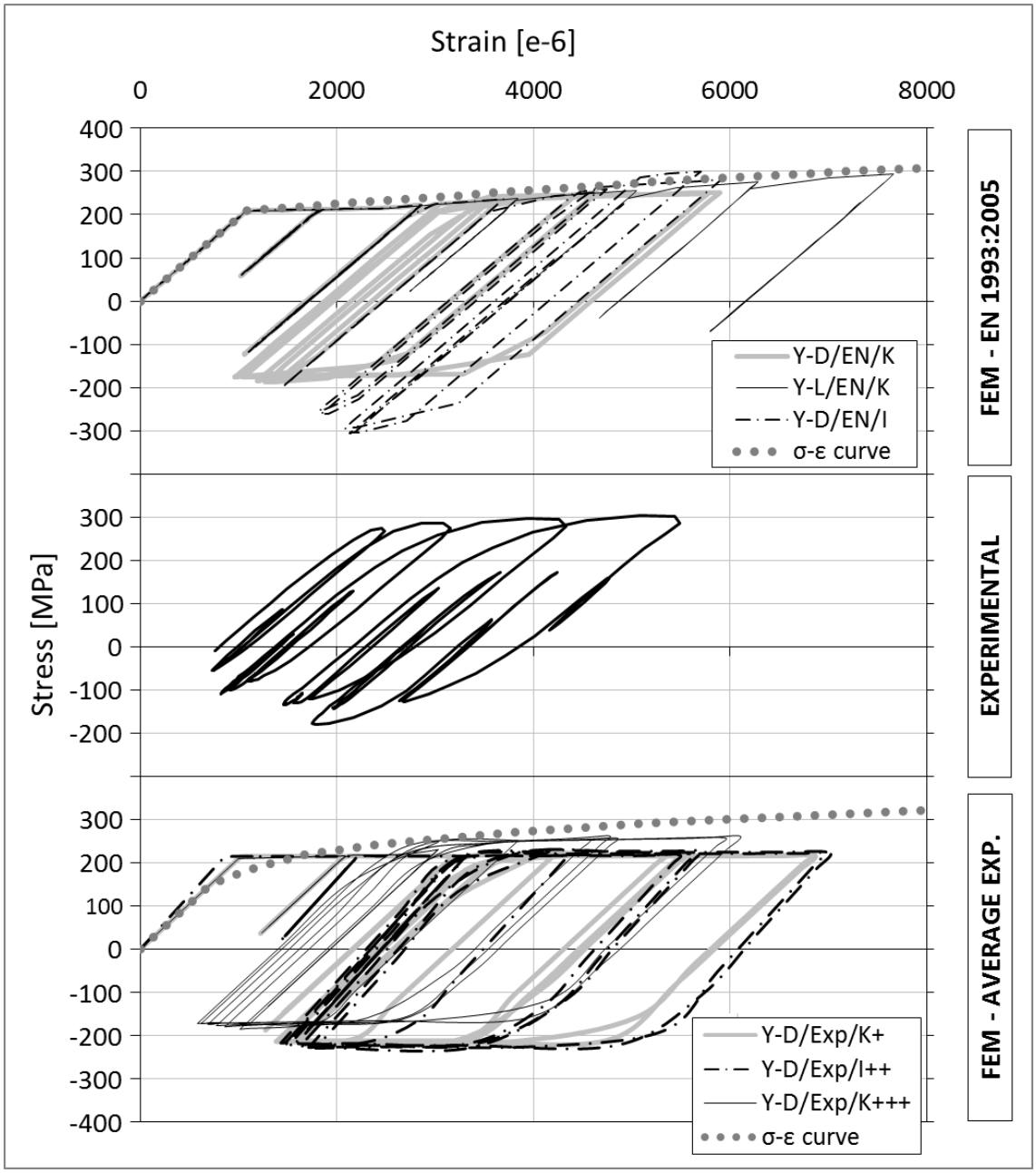

Fig. 6-10: Hysteretic device - FE parametric study – Input: AQV signal scaled for max. of 1.25 mm

In spite of a certain improvement in the shape of the cycles, it is possible to say that the effect of changing the constitutive stress-strain relationship and refining the mesh is less substantial than what expected. The major drawback, which seems to be connected to the software itself rather than to the modelling parameters, is that the increasing stiffness of the plastic branch in the σ-ε constitutive law is not reproduced under cyclic loading.

In fact, the inclination of the σ-ε law is better reproduced by using the simple Ramberg-Osgood model (EN 1993:2005, top of Fig. 6-10). When using the average experimental stress-strain correlation (bottom of Fig. 6-10), only a considerable increase in mesh elements, i.e. model Y-D/Exp/K+++, can reduce the discrepancy between monotonic and cyclic σ-ε.

It should also be noted that the yielding point might differ from computational and experimental results: indeed, as already discussed in §6.2.1.2, the threshold value defined in the numerical models is either derived from a producers' defined minimum (EN 1993:2005 model) or from the experimental average over the tested samples. This means that the recorded values of yielding force (Fig. 6-10) vary from test to test and hence from the defined thresholds.

This complicates the use of FE models for the prediction of the behaviour of the dissipative devices. As the yielding load of the device is crucial to determine and fine tune their performance, values higher than expected are not beneficial, as it would be the case for other steel structural element, where a slightly larger strength than the guaranteed minimum is not seen as a drawback. Nonetheless, devices cannot be underdimensioned as this might result into premature yielding, i.e. damaging of the devices for minor seismic actions.

From the parametric study, it is possible to conclude that:

- Load input signals are not suitable to reproduce the behaviour of prototypes via FEMs. Indeed, the stiffness of the plastic branch of the load-displacement curve is such that even a small variation in the load input can result in a large error in the assessment of displacements, and hence of deformations experienced by the device (Fig. 6-10 top). The use of displacement as input ensures a higher accuracy of computational results;
- An isotropic hardening model largely overestimates the energy dissipated by the device, especially in the unloading branch and loading in compression (Fig. 6-10 top and bottom);
- Overall, neither simulations with the EC recommended constitutive law nor the experimental constitutive law are fully able to reproduce the smooth transition between linear and plastic field (Fig. 6-10). The mesh refinement has a positive effect on the negative portion of the curves (Fig. 6-10), yet the benefits in terms of result accuracy in respect to the computational burden are scarcely satisfactory, as far as stress-strain curves resulting from a number of loading input go;
- The main advantage of the mesh refinement is a considerable improvement in the precision of the stress and strain field. As visible in Fig. 6-11, both the Y-D/EN/K and Y-D/Exp/K+++ are able to reproduce the concentration of strains and higher stresses in the central portion of the dissipative element, but the latter model has a higher accuracy. From the two bottom graphs of Fig. 6-11, it is possible to see that while the central portion of the dissipative element is uniformly yielded, with higher deformations right in the middle,

the stress in the anchor rods is still in the linear field. The connection elements are partially near yielding, but experience deformation far lower than the central part of the device. This is in good agreement with the experimental results and achieves the performance envisioned during the design and calibration of the devices. Fig. 6-11;

- The use of standard or average yielding strength values might create discrepancies in respect to the actual performance of single devices, which will yield for loads higher than expected.

In conclusion, the FE software is able to reproduce the behaviour of the devices, as assessed experimentally. The FEMs can overcome the limits of testing apparatus, thus allowing the simulation of further scenarios. However, the system whereby constitutive laws are input in the FE software doesn't allow a full control on the shape of cycles, so that computational results tend to overestimate the performance of prototypes in terms of energy dissipation. Similarly, the exact yielding point might be complicated to define with precision. This means that computational results can be used, but purposely chosen safety coefficient should be applied in case numerical results were used for the validation of the devices in real case studies.

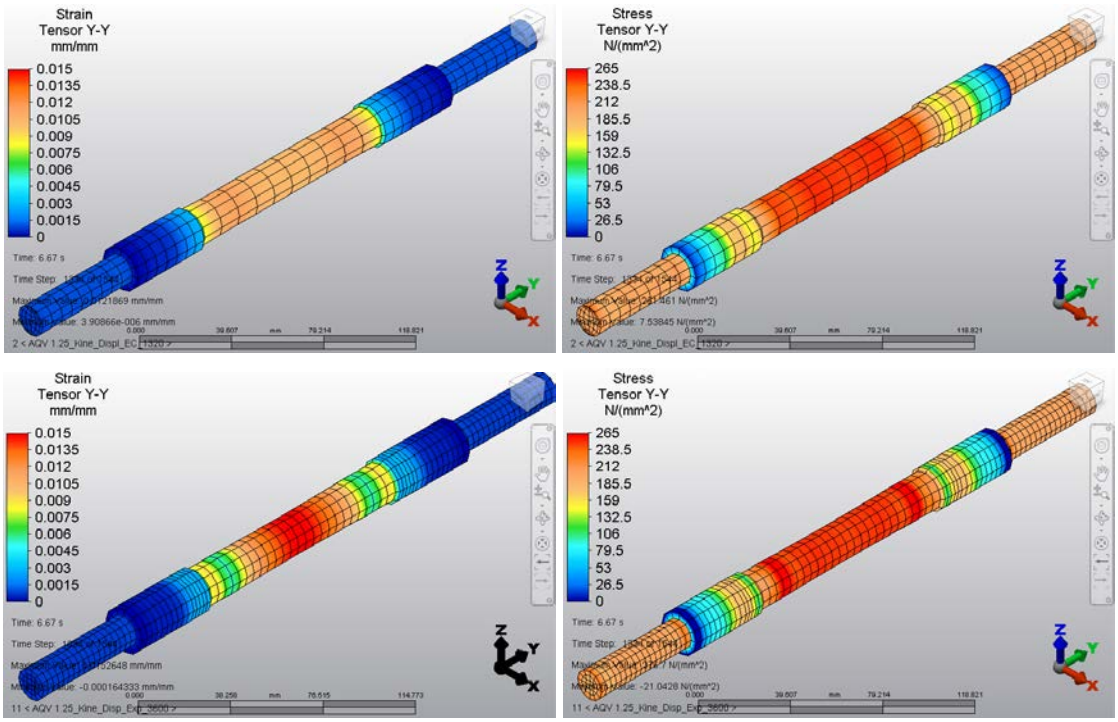

Fig. 6-11: Stress and strain field. Model Y-D/EN/K (top) and Y-D/Exp/K+++ (bottom)

6.2.2.2 The Frictional Device

The critical point of the computational modelling of the frictional devices is the appropriate definition of the parameters controlling the contact among surfaces. Indeed, experimental results collected and described in §4.2 show that the ratio, Φ,

between slip load and perpendicular pressure recorded during tests vary as a function of the number of cycles and wear and tear of the frictional surfaces.

In particular, up to 50 cycles, Φ tends to increase from the initial value of 0.15 to then progressively settle on the value of 0.55. The observed variation can be ascribed to a number of factors: firstly, the repeated rubbing of the frictional plates, which provokes wearing of the surfaces and enhances the material roughness, thus increasing friction. Secondly, the number of cycles also affects the perpendicular pressure, which is observed to increase from the initial nominal value imposed. This could be due to the effect of repeated cycles on the locking of tension bolts and to the presence of debris between the friction plates: metal dust created by the wearing of the friction surfaces might remain within the assembly, thus creating additional pressure. The trend changes after 50 cycles when the coefficient drops as consequence of further wear and tear of the frictional surfaces, which, after the initial roughening, become smoother as cycling continues.

The variation of the coefficient Φ can be described by a regression curve, which identifies a maximum, 0.55, and minimum value, 0.15. These limit values can be considered as the lower and upper bounds that identify the performance range of the device according to EN 15129:2009; as such, they can be used in FEA for identifying the possible scenarios determined by the conditions of the frictional plates.

The graphs in Fig. 6-12 show the experimental curves recorded during pseudo-static increasing-amplitude cyclic tests (only positive displacements) and the bilinear curves obtained by running the linear models by applying the same vertical pressure as per tests and varying the coefficient of friction. The use of the average coefficient of friction recorded during the loading session (0.26 for vertical pressure $F_{\perp}$=12.5 kN, 0.4 for vertical pressure $F_{\perp}$=17.5 kN) leads to a very good match. However, the use of the limit values identifies a range that well describes all the possible scenarios regardless of the peculiarities of each specimen.

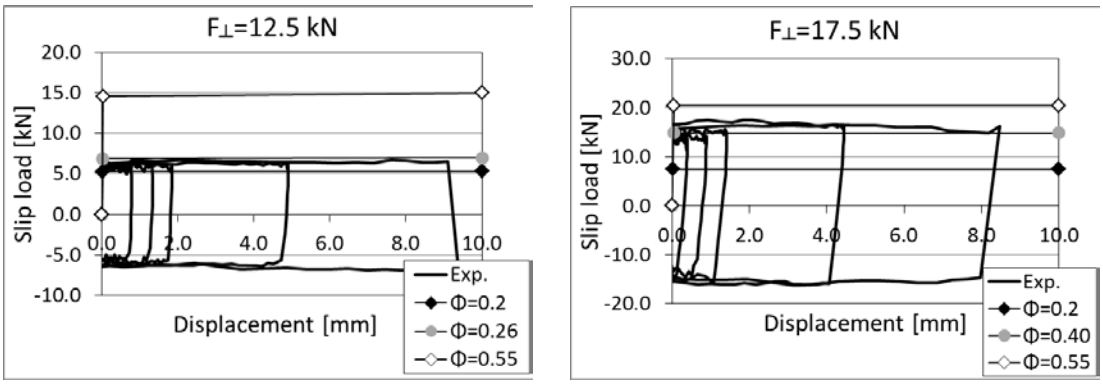

Fig. 6-12: Frictional device – Comparison between experimental and computational results

It is worth mentioning that Fig. 6-12 only shows the positive branch of both computational and experimental load-displacement curves, as the FEMs generate perfectly symmetric curves, as it could be expected by a numerical model, which

cannot be affected by geometrical imperfections or errors in the testing apparatus. Indeed, it should also be considered that any asymmetry recorded during testing is to be ascribed to imprecisions in the displacements imposed by the testing machine, as already commented in §4.2.3.

FEMs successfully reproduce the behaviour of specimens observed during the testing campaigns.

Indeed, it is possible to observe that the distribution of vertical stresses generated by the application of pressure well represents the fact that friction is not homogeneous over the surface of the frictional plates. The higher concentration of stresses (Fig. 6-13) due to the position of pressure bolts and geometry of the sample matches the most worn parts of the specimen, thus proving the correlation between the two phenomena.

Furthermore, as explained in §6.2.1.1, the geometry of the model has undergone a process of simplification in respect to the real prototypes in favour of more efficient computational time. Such simplification is carried out under the hypothesis that the geometry and mechanics of the friction device are such that high concentration of stresses do not occur in parts such as connections. This hypothesis is verified by looking at the distribution of stresses in the direction of the longitudinal axis of the device (Fig. 6-14). Even in the case of the highest value of coefficient of friction (0.55) and highest perpendicular pressure, stresses are well within the elastic range of stainless steel.

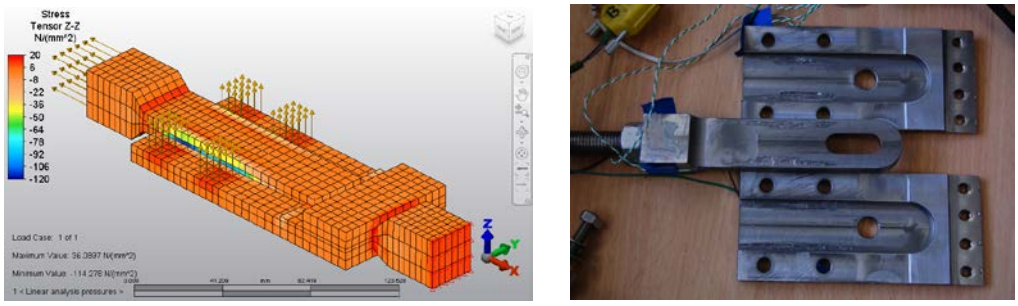

Fig. 6-13: Comparison between the distribution of the vertical stress component in the FEM and the superficial wearing of the frictional plates at the end of a testing session

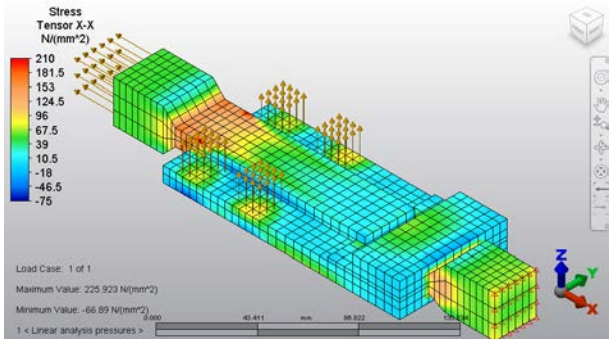

Fig. 6-14: Frictional device – Distribution of the stress component in the direction of the device main axis

6.3 FE MODELS OF ANCHOR ASSEMBLY

6.3.1 Introduction and Objectives

The purpose of simulating single parts of the anchor assembly is to optimise the accuracy and computational time of small-size numerical models while reproducing experimental and on-site results. By working on the single parts of the anchor assembly, one can better understand what laws rule their response; these laws can be then implemented in larger, more complex models, where mesh and geometry need to be simplified to avoid an excessive computational burden.

Accordingly, once a good compromise between accuracy and expediency has been found for single parts, a model of a whole structure strengthened by the anchoring devices can be created and run, so as to complete the validation process and complement the output of Chapters 4 and 5. Indeed, as it has been discussed previously, due to laboratory constraints and resources as well to the lack of major seismic events during the monitoring period of the instrumented prototype, it was not possible to exhaust the whole range of loading scenarios and boundary conditions that might affect the devices and their response.

A model including a full structure will not only provide interesting information regarding the behaviour of the devices, but is also crucial for the development of the design procedure described in Chapter 7. As already discussed in the introduction, non-linear modelling of the structure is an essential step in the seismic assessment of historic structures and in the design/optimisation of the upgrade intervention.

While in the previous paragraphs the modelling of the devices as isolated elements has been discussed, this section will focus on their behaviour when embedded in a masonry substratum. In fact, as already observed during the experimental campaigns, the most critical element of the anchor assembly is the interface between the grouted socket and the surrounding masonry. It is the capacity of this element, especially in comparison with the capacity of the dissipative device that is installed in series with the anchor rod, that determines the performance of the whole assembly, and hence of the strengthened connection.

Therefore, only the portion of the strength-only anchor embedded in the masonry is simulated in the following. This allows focussing on the optimisation of the material and element properties apt to reproduce the real-life behaviour of the tested typology of anchors.

In the final paragraphs of the chapter, the results obtained for the isolated devices and for the embedded anchor will be gathered and implemented in a model reproducing the case study structure of Chapter 5, with and without strengthening elements.

6.3.2 Model Description and Assumptions

6.3.2.1 Geometry

The geometry reproduced in the models is derived from that of the samples of the pull-out tests, as described in §4.3. The anchor assembly consists of a 400 mm long threaded M16 bar embedded in an 80 mm diameter grouted socket passing through a 350 mm wall.

Each of these elements, i.e. masonry, grout and steel bar, are simulated by one model part in Autodesk Algor Simulation, using 3D solid elements. The end plate that is normally included in Cintec's anchor assembly doesn't feature in the model, as its function, i.e. preventing pull-out failure of the anchor rod from the grout, can be simulated assuming a full bond between these two parts, which is far more convenient in terms of computational resources than meshing the plate.

Conversely, a "fictitious" part is used to simulate the interface between grout and masonry (green part in Fig. 6-15). This is a common modelling technique, implemented to a different extent and through a variety of element typologies by various authors (Bajer and Barnat, 2012; Giambanco et al., 2001; Lourenço and Rots, 1997). In the specific case, the advantage of using an interface part is that analyses can be run with linear materials, saving computational time and simplifying the calibration process. Yet a good match with experimental results is achieved, as suitable mechanical properties are attributed to the interface part, so as to reproduce the overall behaviour of the anchor, which is controlled by the grout/masonry pull out failure. In brief, the non-linearity of the anchor embedded in a masonry substratum is localised in a fictitious elements, which comes to represent the bond/slip behaviour as recorded during experimental campaigns.

From the software point of view, this methodology is more efficient too: the use of regular solid elements for the interface part offers a much wider spectrum of material properties and yielding criteria than what is available for contact pairs. Indeed, contact in Autodesk Algor Simulation can be only defined through friction. Although a friction-based model is ideally in very good agreement with the experimental results, it created a number of problems in terms of convergence at the time of the calibration of the model and was therefore abandoned in favour of the model including the interface part.

The property of the interface part, i.e. Young modulus and post elastic properties, are calibrated on the basis of the experimental load-displacement curves, as it will be discussed in §6.3.2.3. Another parameter to be chosen is the thickness of the interface part, as this influences the axial stiffness and hence the response to axial loading; such decision is taken by running analyses where the thickness varies and studying its impact on the computational results.

During pull-out tests, a set of anchors are installed in a masonry panel and tested one by one; in the model, only one anchor is considered, as the applied boundary and loading conditions are the same for all the specimens and the FE model should

represent the average behaviour. Because of this, only a portion of the masonry wall is reproduced; its dimensions are such to allow the visualisation of the diagonal pattern of shear/tensile stresses that would indicate cone pull-out failure.

In fact, cone failures were not detected during testing; however, this typology of damage is recurring in on-site observations and therefore cannot be ruled out a priori during modelling. Even if the masonry material is modelled as isotropic elastic, the distribution of strain and stresses can indicate whether such a damage pattern would develop.

6.3.2.2 Mesh

Brick elements are mainly used for the mesh, although some tetrahedral elements are also present due to the geometry and connection among the parts (Fig. 6-15). The number of elements used in each part is summarised in Table 6-4.

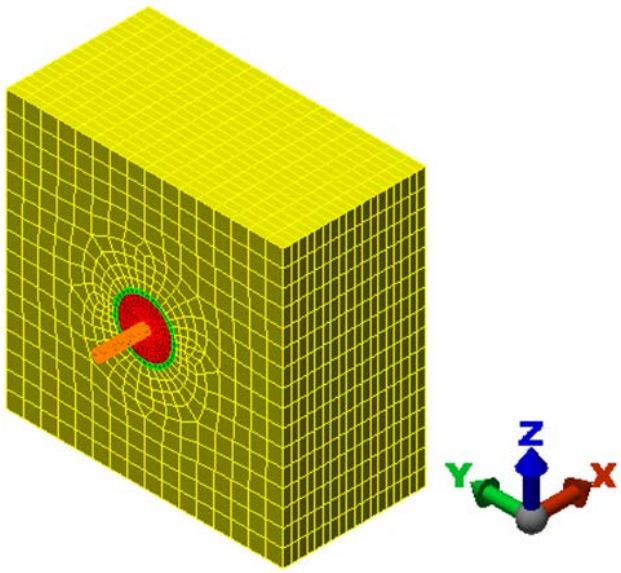

Fig. 6-15 – Mesh of anchor assembly. Masonry (yellow), interface (green), grout (red) and anchor rod (orange) are visible

Table 6-4: Number of elements of each part of the anchor assembly model

Part	No. of elements	Total No. of nodes	Total No. of elements
Masonry Wall	6534	15253	13908
Interface	630		
Grout	3960		
Steel bar	2784		

Contacts between parts are simulated via:

- Bonded contact at the interface between the threaded rod and the grouted element. This assumption is supported by the fact that bond failure between the grout and the metallic element is not detected during tests, thanks to

the adherence provided by the crests of the threads embedded in the grout, but also to the presence of the end plate.

- Bonded contact between the interface part and its neighbouring parts. As the interface part is used to simulate the phenomena occurring at the interface between the grout and masonry as well as the pull-out mechanism, the contact between the parts is left as bonded.

6.3.2.3 Material Properties, Boundary Conditions and Loading

Linear mechanical parameters of materials are reported in Table 6-5.

As already mentioned, the interface part is the only one where the non-linearity of the material is taken into account. As the part is fictitious, it is necessary to find a set of equivalent properties that define the behaviour of this part and lead the assembly to perform in the same way as it was observed during the experimental campaigns.

The Young modulus that appears in Table 6-5 is calculated on the basis of the experimental curves of Fig. 6-16: the experimental load-displacement curve of the grouted element, which the FE interface part aims at simulating, largely corresponds to the total load-displacement curve as, indeed, the bond failure at the interface grout/masonry controls the overall performance of the anchor. Accordingly, the point A of the experimental idealised load-displacement curve, i.e. the point of first cracking, can be taken as threshold for the constitutive law of the interface. In correspondence of such point, namely for a load of 18 kN and a displacement of 0.14 mm, the constitutive law ceases to be linear. These two values correspond respectively to a stress of 15.3 MPa and strain of 400 μstrain. The stress is calculated by dividing the pull-out force by the cross section area of the hollow cylinder of the interface part; this has a thickness of 10 mm in the FEM. The Young modulus, calculated according the well-known linear relationship between stress and strains in the elastic field, is hence equal to 38,197.00 MPa.

Table 6-5: Mechanical linear properties of model materials

Part	Mass density	Young modulus	Poisson's ratio	Shear Modulus of Elasticity
	[kN/m^3]	[MPa]	[-]	[MPa]
Masonry	17.5	3600	0.2	-
Interface	17.5	38197	0.2	-
Grout	24.0	25000	0.15	-
Steel bar	80.0	210000	0.29	86000

Beyond the linear field, a Von Mises yielding criteria is used to define the behaviour of the interface part; the curve strain-stress is defined by approximating and smoothing the experimental curve (Fig. 6-16). This choice might seem unusual, as in Chapter 4 it is discussed how a law based on friction is suitable to describe the pull-out behaviour of anchors; it would hence seem more logical to apply a Drucker-Prager criterion, which is indeed equivalent to the relationship between tangential strength and perpendicular

pressure that is normally applied to masonry and has been implemented in this thesis to study the experimental results.

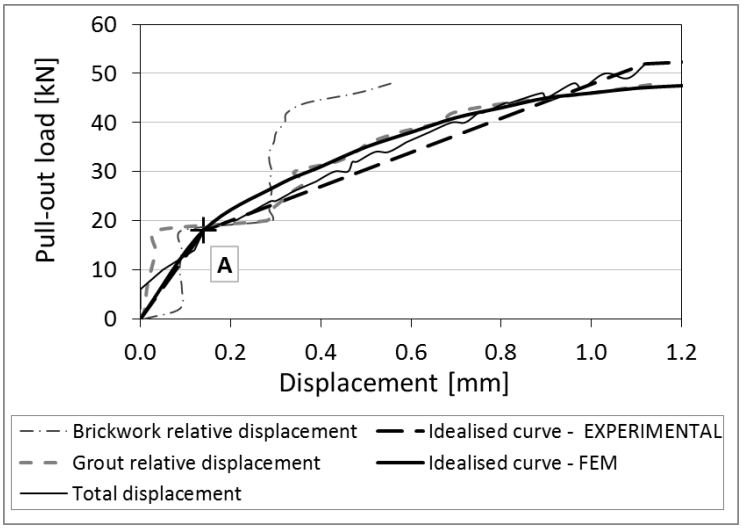

Fig. 6-16: idealised load-displacement curve used for the FEM in comparison with reference experimental curves

However, it should be remembered that the yield surfaces defined by the Von Mises and Drucker-Prager criteria are equivalent once the position of the π-plane is given, namely once the values of the three stress invariants are fixed (Fig. 6-17).

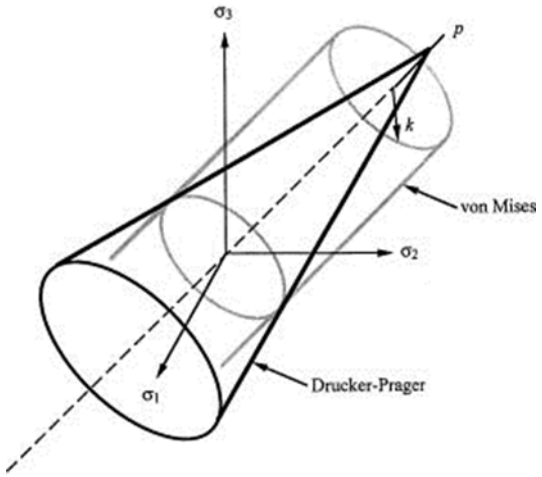

Fig. 6-17: 3D yield surface according to the Von Mises and Drucker-Prager criteria

Two different curves (Fig. 6-18) are used in the models, so as to study the impact of the yield criterion: the first curve is derived from the experimental results, while the second matches more closely an elastic-perfectly plastic behaviour.

The model (Fig. 6-19) is pinned at the bottom, namely all the points of the bottom surface of the masonry part are restrained against translation in the three directions. It must also be decided whether to constrain the model in the other directions, i.e. in the

X direction at the top and back surface and in the Y direction on the side surfaces, so as to simulate the containment effect of the wall panel, which is missing from the numerical model, but surely had an influence on the experimental results.

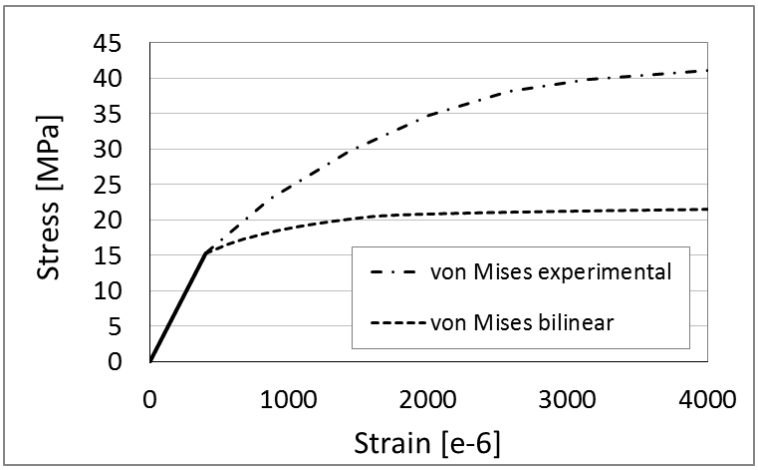

Fig. 6-18: Stress-strain Von Mises curves used in the modelling of the interface part

Three options are considered and rapidly checked by a linear analysis, so as to establish which better simulates the laboratory behaviour:

a) Translational constraint at the top surface in the X direction (Fig. 6-19a);
b) Translational constraint at the top and back surface in the X direction (Fig. 6-19b);
c) Translational constraint at the top and back surface in the X direction and on the side surfaces in the Y direction (Fig. 6-19c).

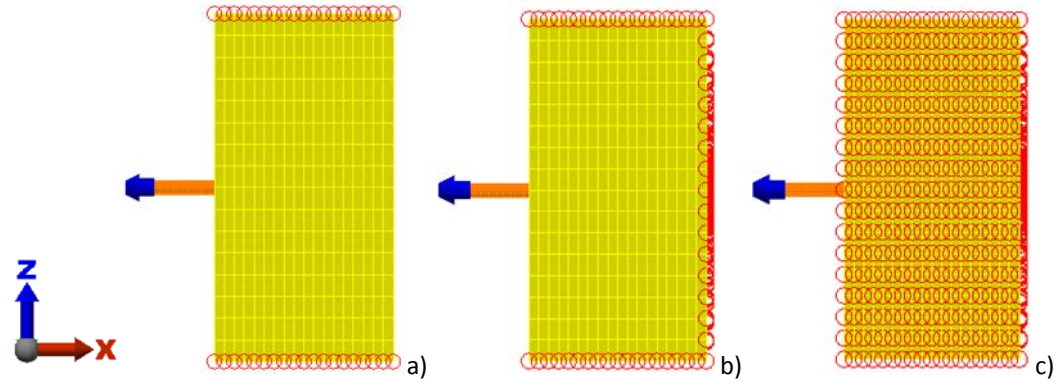

Fig. 6-19: Boundary conditions: a) bottom constraints in X, Y and Z, and top constraint in X; b) like model (a) plus back constraints in X; c) like model (b) plus side constraints in Y

Linear analyses (Fig. 6-20) show that a good match with the experimental results is obtained both by constraining the back surface only and the back as well as side surfaces of the model. Conversely, the boundary conditions type a, namely the less restrained model, is not adequate as it doesn't sufficiently account for the confining

effect of the masonry surrounding the simulated block. Therefore, the boundary conditions type “b” are used for the non-linear analysis.

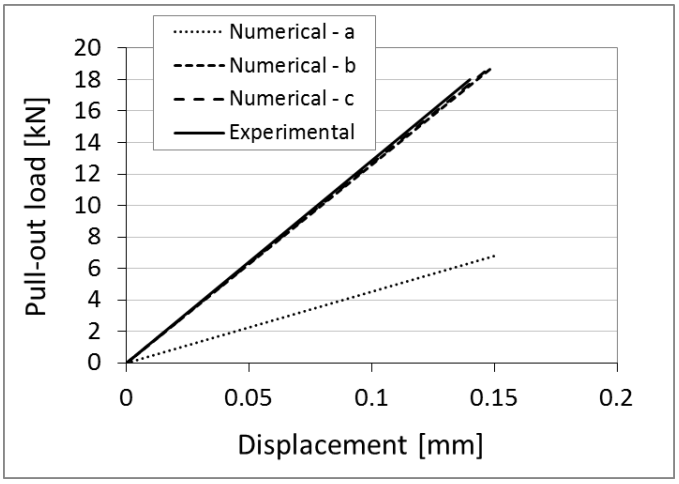

Fig. 6-20: Linear calibration of boundary conditions

Increasing displacements are imposed to the free end of the anchor rod, so as to simulate the pulling action of the testing rig on the anchor assembly (Fig. 6-21). The choice of running models in displacement control is in line with the experimental tests, where displacement is used as damage indicator, as well as with the design philosophy of the dissipative devices, which aim to control displacements among structural parts and to be dimensioned according to a performance approach. The choice makes also sense from the point of view of material properties: as the interface part, where non-linearities are concentrated, is characterised by a von Mises yielding criterion, the use of displacements allows to better control the extent to which the analysis progresses.

The model is run by imposing displacements to the bar, as well as by simulating the vertical pressure that was applied to the laboratory samples throughout testing (Fig. 6-21).

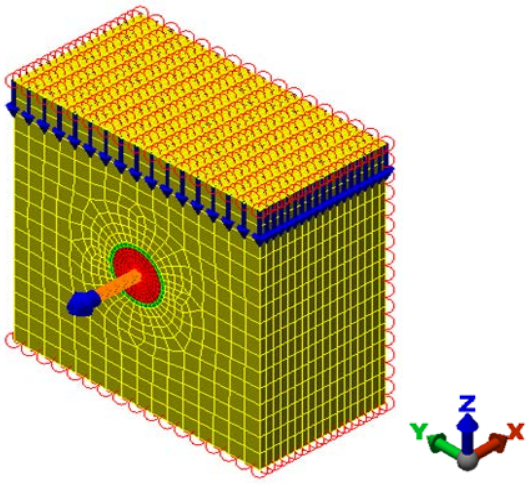

Fig. 6-21: Imposed displacement on the anchor bar and vertical load on the masonry part

6.3.3 Results

The displacement field attained in the various parts of the model can be visualised in first instance through an analysis run with isotropic linear materials only (Fig. 6-22). A maximum displacement of 2 mm is set as target, since this is sufficient to bring the interface part beyond the linear field when the material non-linearity is accounted for and, yet, it is functional in terms of expediency.

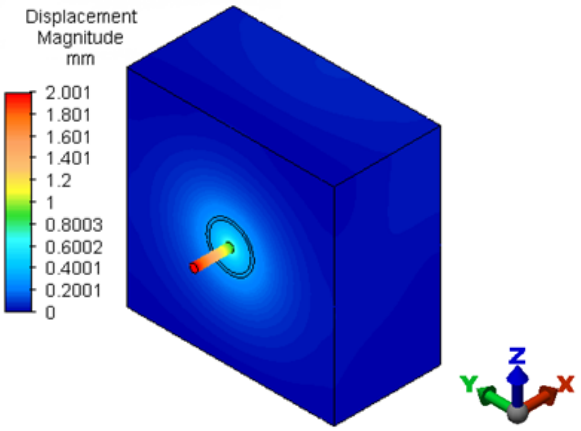

Fig. 6-22: Displacement in the anchor assembly

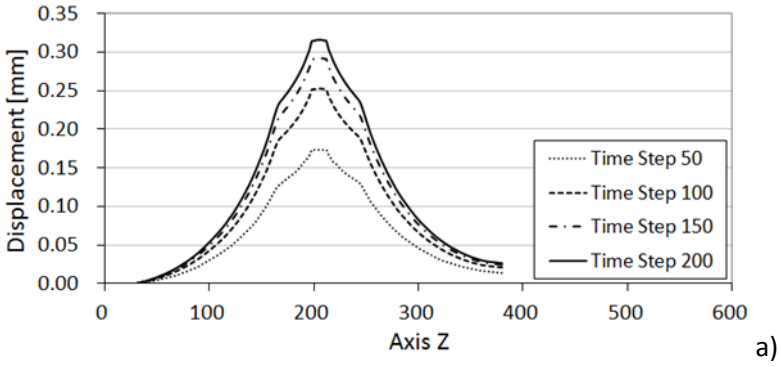

a)

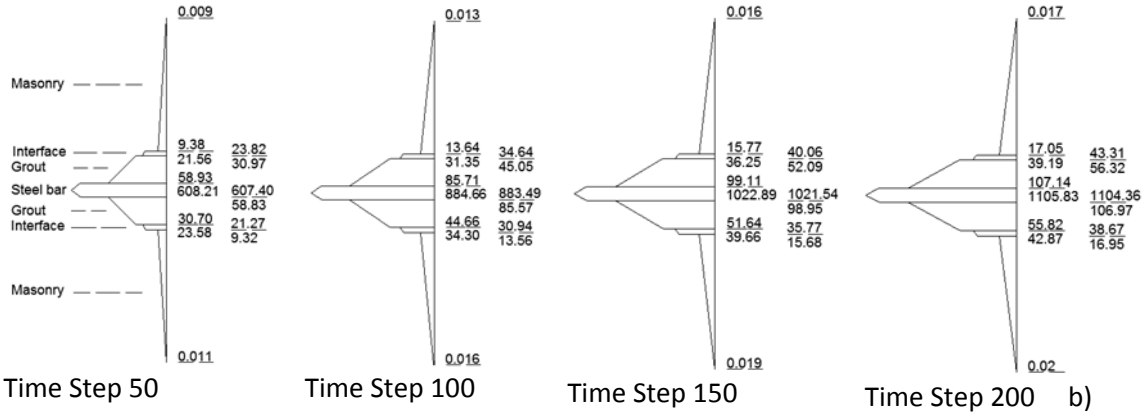

Time Step 50 Time Step 100 Time Step 150 Time Step 200 b)

Fig. 6-23: a) Displacement profile in the plane XZ – anchor rod not visualised; b) stress levels

By cutting the model along the mid XZ plane and plotting the results along the Z axis, it is possible to visualise the distribution of displacements (Fig. 6-23a) and stress (Fig. 6-23b) among the parts at different time points of the analysis.Being the analyses linear, the relationship between the displacements experienced by the parts as consequence of the imposed displacement and the stress field is also linear and only depends on the axial stiffness of the different parts.

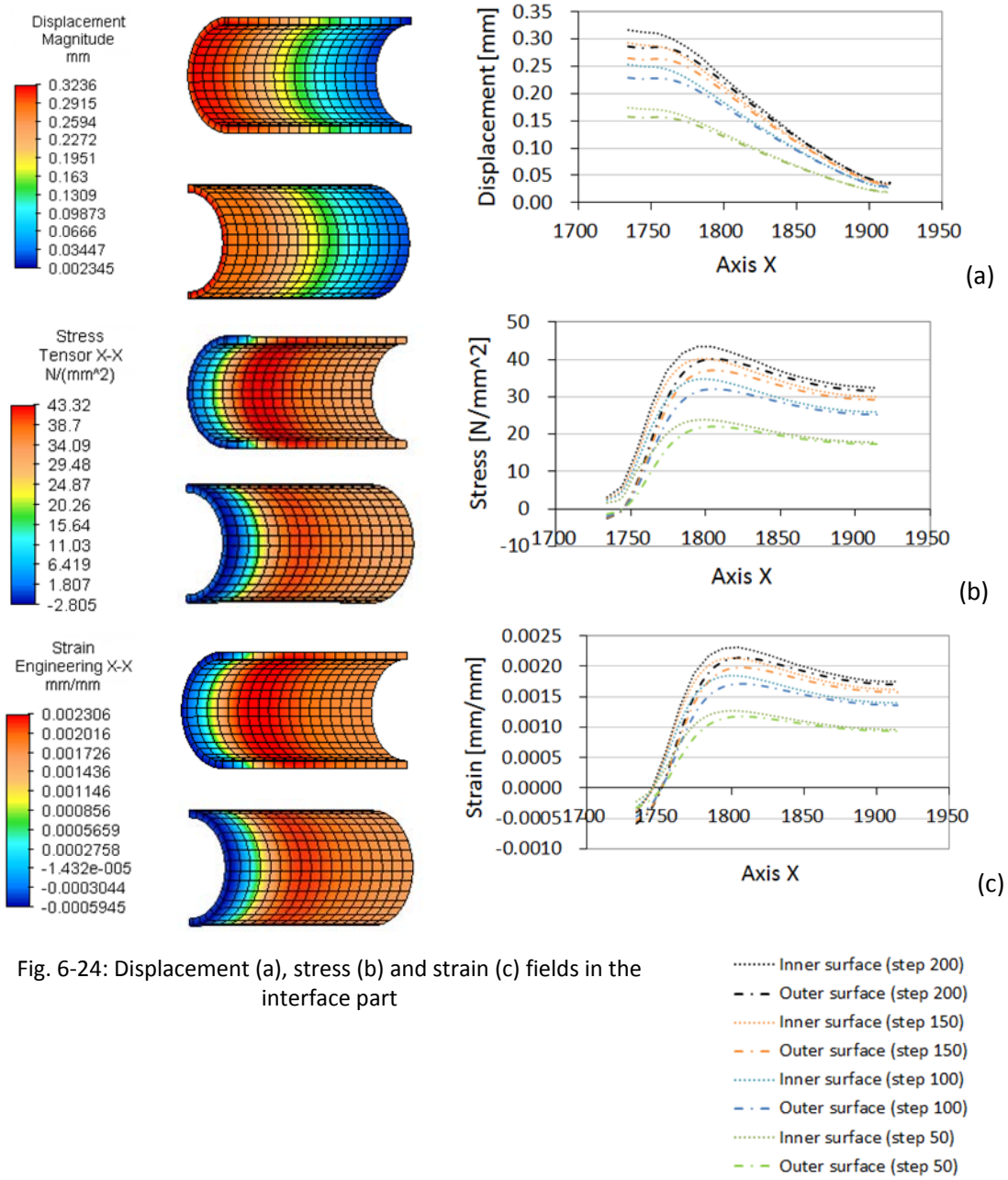

Fig. 6-24: Displacement (a), stress (b) and strain (c) fields in the interface part

Nevertheless, it is interesting to notice that, even neglecting the material non-linearity, the choice of the elastic parameters of the interface part allows reproducing the fact that deformations mainly occur at this location, meaning that the bond failure

mechanism is correctly reproduced. Indeed, looking at Fig. 6-23a, one can notice that while the variation in displacements in the area of the anchor rod and grout between 50 and 200 steps is around 0.05 mm, the variation in the area of the interface and masonry is about 0.12 mm.

As it can be seen in Fig. 6-24a, b and c respectively, the displacement, stress and strain fields of the interface part are such that:

- Values at the inner surface of the interface part are always slightly higher than at the outer surface. Indeed, the inner surface is where the anchor rod, to which the input displacements are imposed, and the interface part are connected and nodes experience equal displacement, accordingly to the assumption of full bond between model parts. Displacements, as well resulting load and stresses are then transmitted in a radial fashion over increasingly larger surfaces, thus resulting in a reduction of stress and strains between inner and outer surface;
- Larger displacements are experienced at the front of the interface part, whereas the rear portion is little involved in the pull-out;
- Both the strain and stress distributions show that the peak values are reached not at the very front of the part, yet a few centimetres back, thus implying that the front portion of the anchorage experiences little deformation and hence low stresses.

Once the non-linearity of the interface part is integrated in the model, further observations regarding the behaviour of the anchor can be made.

The stress, strain and displacement fields (Fig. 6-25) are substantially similar to those of the linear analysis. The only difference is that the peak stress at the moment of the transition between linear and non-linear moves from their initial position and shifts to the very back of the part, where this is constrained.

By running non-linear analyses, it is possible to assess which material model is more suitable in order to correctly reproduce the experimental behaviour. The use of an experimentally-approximated σ-ε relationship yields better results (Fig. 6-26), as it could be expected, also on the basis of the results of the FEMs of the isolated prototypes. The pseudo-bilinear von Mises leads to a flat plateau in the plastic field, which differs considerably from the experimental and von Mises experimental curves, which have instead a more marked non-linear behaviour.

As the assessment of energy dissipation, and hence of load-displacement cycles, is crucial in the design phase, as it will be discussed in detail in Chapter 7, it is important that the post-linear curve is reproduced as faithfully as possible. Therefore, the use of the experimentally-calibrated curve as input is preferable.

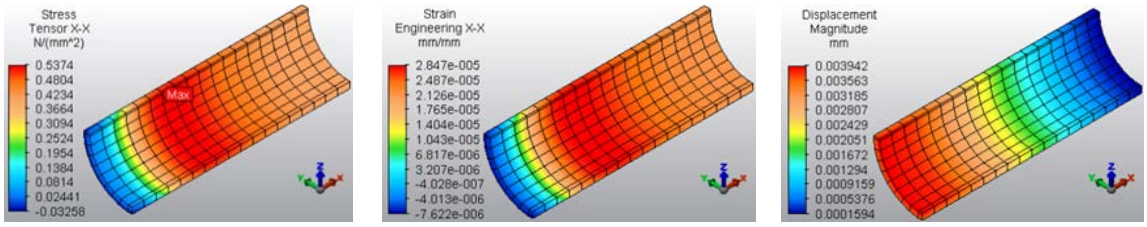

Time: 0.05s; Time Step: 1 of 200

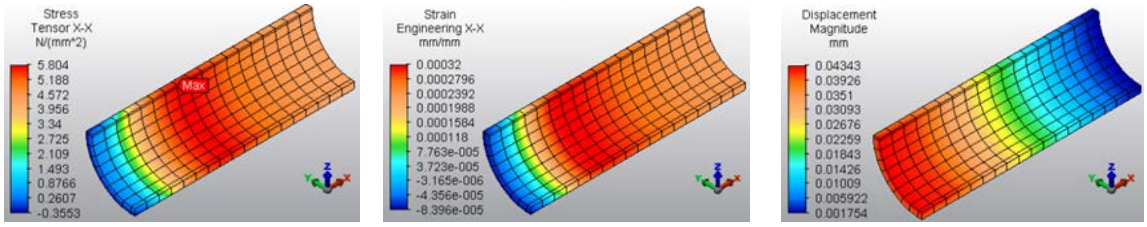

Time: 0.55s; Time Step: 11 of 200

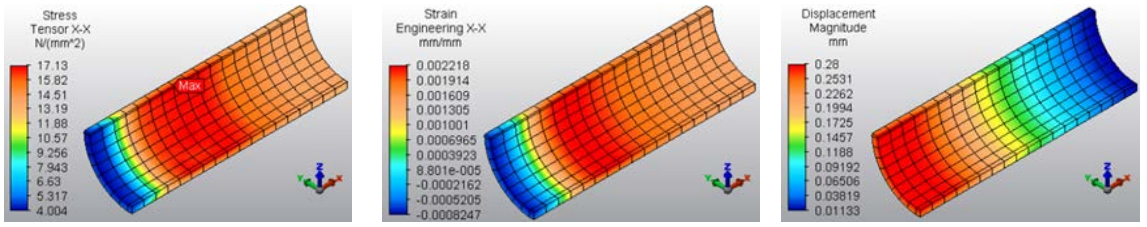

Time: 6s; Time Step: 120 of 200

Fig. 6-25: Stress, strain and displacement fields at various time steps

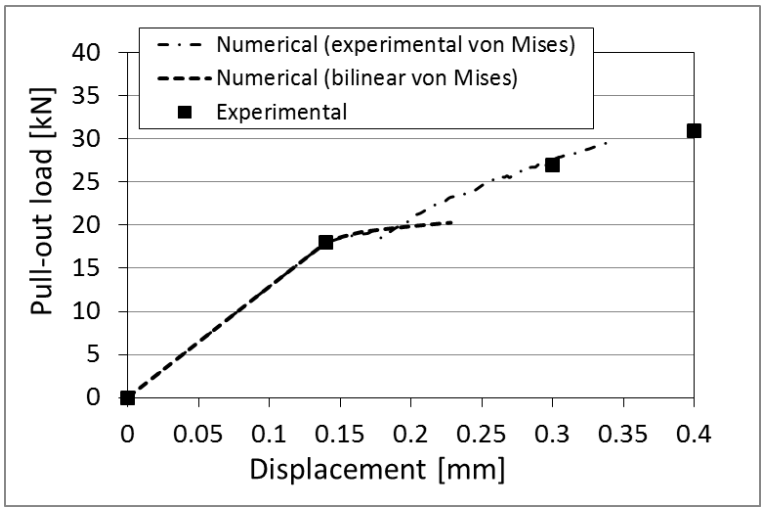

Fig. 6-26: Comparison between two material constitutive laws

Finally, the influence of the thickness of the interface part is investigated (Fig. 6-27). As expected, an increase in thickness, and hence cross section area of the part, results in an increase in stiffness, as the constitutive σ-ε law has not been modified. This means

of course that FEMs could be calibrated for matching pairs of constitutive laws and thicknesses of the parts, so as to obtain equivalent results regardless of how the geometry of the interface part is defined. However, as the used elements are bricks with longitudinal and radial dimensions in the order of 20 mm it is deemed best to use the option with the thickness of 10 mm so as to avoid an excessive distortion of the elements.

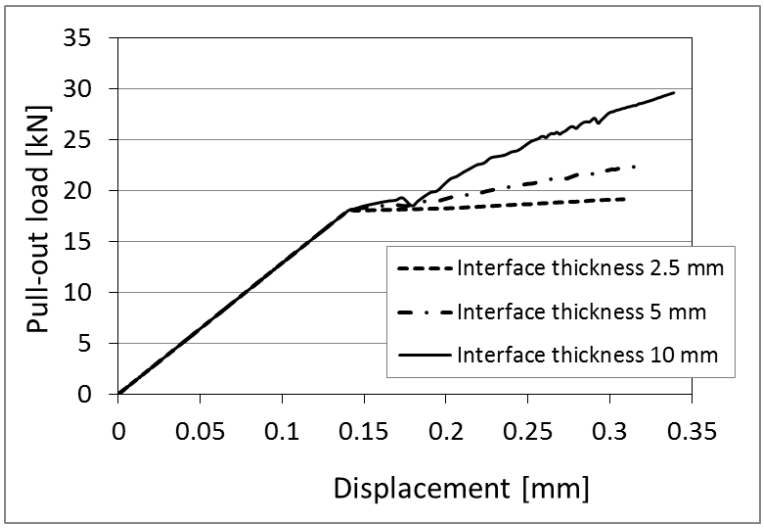

Fig. 6-27: Comparison of models with different thickness of interface part

Furthermore, the slightly higher thickness allows redistribution along the length of the anchorage to take place over several steps of the analysis, thus better representing the global behaviour.

In conclusion, the Finite Element model described in the paragraphs above succeeds in replicating the bond failure between the parent material and the grouted element of the standard anchor, this being the failure mode that controls the performance of the whole assembly. A number of parameters have been analysed so as to determine which give the best results in terms of computational expediency and accuracy in respect to the behaviour of the laboratory samples. These parameters, together with those identified for the FE models of the dissipative devices, feed in the model of a structure that is used to study the effect of standard and dissipative anchors ties on a larger scale.

6.4 FE MODELS OF STRUCTURE, UNREINFORCED/STRENGTHENED BY STANDARD/DISSIPATIVE ANCHORS

6.4.1 Model Description and Assumptions

6.4.1.1 Geometry and Mesh

The prototype building chosen for the computational validation of the dissipative anchoring devices is S. Giuseppe dei Minimi, L'Aquila. The building provides indeed a

suitable case study: it falls into the category of heritage masonry buildings affected by overturning damage of the façade, which are the object of this thesis; furthermore, it has been already analysed from different points of view in the framework of the NIKER project, so that material data and geometrical surveys are available. Finally data has already been collected through the instrumented device during on-site validation, so that it is possible to draw an interesting parallel with previous results.

As the simulation of the whole structure, as well as neighbouring buildings, would be burdensome, it is decided to only consider a portion of the building. This is in line with the macroelement approach (Doglioni et al., 1994) that is normally adopted when dealing with the seismic assessment of historic religious buildings. Such approach considers that different structural elements and subassemblies respond independently to a seismic action and that they develop damage according to a number of standard modes; such assumption in this specific case is justified in light of the damage caused to the structure by the L'Aquila 2009 earthquake. Indeed, the façade tilted forward, with a clear pseudo-vertical crack opening at the interface between the square stone blocks of the quoins and the rubble masonry of the side walls. The failure is typical of façade walls and causes them to behave independently from the rest of the building, so that the interaction with surrounding structures is not as influential as if one had to assess the global seismic response of a building with strong connections.

The modelling of the substructure façade/side walls is functional to the validation of the anchoring devices, which are designed with the purpose of addressing out-of-plane modes of failure; at the same time, a partial model allows the comparison with the data collected by the instrumented device implemented in the church, which recorded small-intensity phenomena, localised in correspondence of the pseudo-vertical crack.

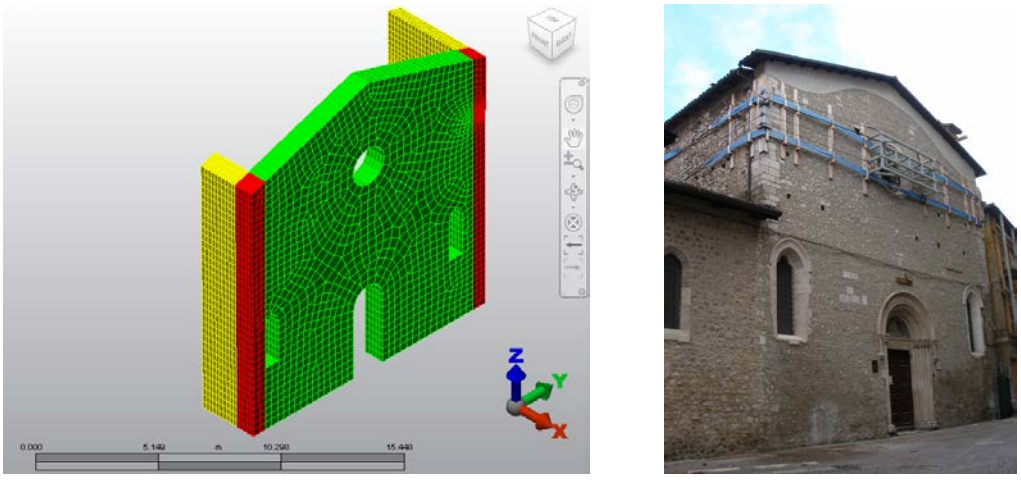

Fig. 6-28: Façade of S. Giuseppe dei Minimi in L'Aquila, FE model (a) and reference building (b)

The geometry of the building is used as reference for creating the FEM (Fig. 6-28). Only the façade, including the rubble-stone wall and the stone quoins, and part of the side walls are recreated by using 3D solid elements (see Table 6-6 for a summary of the

elements). Openings in the side walls are omitted from the model in light of their reduced dimensions.

Other constructive elements, such as the roof and the belfry are considered only in terms of stiffness, mass and constraints, so as to be able to reproduce the behaviour of the building and yet maintain the computational burden to the minimum while keeping the main focus of the numerical simulations on out-of-plane response of the façade.

As Autodesk Algor Simulation does not allow applying different accelerations at the same time, it is not possible to simulate mass as lumped masses and have gravity acceleration and dynamic loading to act upon them in different directions at the same time. Hence, the horizontal components of mass are simulated by means of lumped masses, which participate in the dynamic response when a horizontal acceleration is applied to the model, whereas the vertical components are rendered by means of load, which is calculated so as to be equal to the dead weight of structural elements and remain constant throughout dynamic loading.

Table 6-6: Number of elements and nodes of the FE model

Part	**No. of elements**	**Total No. of nodes**	**Total No. of elements**
Façade	5935	16290	12800
Quoins	1565		
Side walls	53000		

The belfry (Fig. 6-29a) plays an important role in the dynamic response of the building, as its front column facilitated the formation of the crack between façade and side walls (Fig. 6-29b). Therefore, its presence is modelled by means of lumped masses and vertical loads (Fig. 6-29c), which bears at the locations of the three piers of the belfry; the stiffness contribution is neglected, as non-influential.

The roof structure is simulated as a load/mass bearing on the side walls. The exact typology of the roof is unknown, due to the difficulty of accessing the roof for inspection after the earthquake and the lack of pre-existing documentation in these regards. The roof is likely made of timber trusses; vaults are most probably decorative and the presence of a filling between them and the roof also likely. As the façade is slightly higher than the side walls, it is assumed that the roof does not bear on it, but only on the side walls. Drawing on these hypotheses and considering the overall geometry of the roof, as taken from the survey drawings, a linear load of 51.2 kN/m is applied along the side walls to simulate the roof self-weight.

The influence of the roof is also modelled by means of horizontal truss elements; even though the numerical analyses do not aim to reproduce in detail the response of the roof, its presence has an influence on the side walls, as it connects them and prevents a completely independent behaviour of the two parts.

When simulating the unreinforced structure in the framework of the calibration process, all parts are considered bonded: if the maximum stress components follow the same pattern as the damage in the real building, the model is able to reproduce the behaviour of the structure and is suitable to numerically validate the anchoring devices.


a)


b)

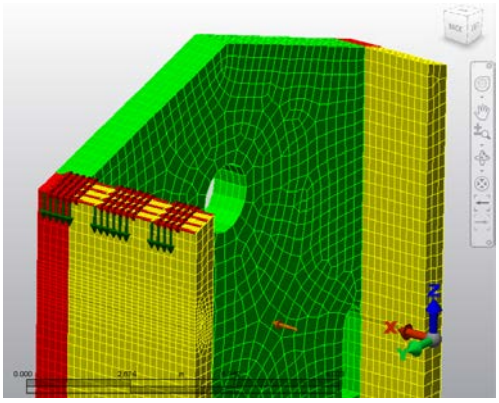
c)

Fig. 6-29: Belfry: a) as simulated in the FEM by loads and lumped masses, b) on site. c) Detail of the position of the front column in respect to the main crack

Once the calibration is completed, the quoins and side walls are disconnected along a surface in line with the extension of the crack as surveyed on site. A frictionless contact is set at the location of the disconnection, so that parts are able to move relatively to each other, without any penetration. This depicts the situation of the building after damage and represents the starting point for the implementation of the anchoring devices. The whole refinement procedure of the FEM is detailed in §6.4.2, where stress field and contact conditions are shown with further detailing.

Initially, only one anchor is included in the FEM. The location of the anchor is the same as per on-site validation, namely on the same side of the building as the belfry, at approximately three quarters of the building height. Later on, a second anchor is inserted in the left quoin, so as to analyse a symmetrical setup. The model

strengthened by standard anchors provides a term of comparison between a strength-only system against and the anchors in series with the dissipative devices.

The mechanical and geometrical properties of both anchors are the same as those of the prototypes tested in the laboratories.

The anchor parts, including the dissipative devices, are modelled by a set of truss and beam elements. Truss elements can only resist tensile loads, which well simulates the fact that anchors are mainly implemented to work in tension and influence the response of wall panels perpendicular to their axis. Conversely, beam elements can also experience stress and strains in bending and shear. However, the main difference between the two typologies of elements is how the software computes cyclic behaviour on the basis of the user-defined material stress-strain curve. Beam elements can be defined by an isotropic hardening, von Mises criterion, whereas truss elements, even when defined by the same σ-ε curve as beam elements, are not able to follow the pattern linear/non-linear under load reversal. Therefore, the stress-strain graph of truss elements does not describe a full cycle; it only follows the input curve back and forth. This is not a problem for elements defined as linear, but for the devices it is a main drawback, as the dissipation of energy, i.e. the shape of cycles, is crucial. On the other hand, truss elements facilitate convergence; therefore, a combined use of truss and beam element has been chosen – see §6.4.1.2 for further details in combination with material properties.

Anchor elements are bonded to the side walls and to the façade; only one element is left free, so as to simulate the portion of anchor located in correspondence of the crack, which is not grouted within the surrounding masonry material (Fig. 6-30).

6.4.1.2 Material Properties, Boundary Conditions and Load Histories

The mechanical properties of the materials of walls are taken from Circolare 02/02/2009 N. 617 (2009), choosing from materials that match those surveyed on site by means of endoscopy, thermal, radar and ultrasound survey as well as flat jack test.

Table 6-7: Mechanical properties of masonry materials used in the model of S. Giuseppe

Part	ρ	f_c	τ_0	E	Poisson's ratio	c	ϕ
	[kN/m^3]	[MPa]	[MPa]	[MPa]	[-]	[MPa]	[rad]
Façade	20	2.0	0.035	1020	0.2	0.2	0.17
Quoins	22	6.0	0.09	2400	0.2	0.6	0.15
Side walls	20	2.0	0.035	1020	0.2	0.2	0.17

UPD's results show that the masonry of the walls can undergo a pressure of 1.5/1.6 MPa without considerable drops in stiffness; hence, the compressive strength, f_c, is chosen to be higher than these values. The Young modulus, E, measured on site varies between 1700 MPa and 2720. Hence, the masonry type defined as "roughly hewn ashlar" (Circolare 02/02/2009 N. 617, 2009), which well approximates the irregular stone masonry fabric of the walls of the Oratory, is used as reference. Quoins are

simulated instead drawing on the values of mechanical properties of the class “squared stone blocks”.

Masonry materials are modelled as isotropic in the linear analyses and by means of a Drucker-Prager yielding criterion in the non-linear analyses, using the values of cohesion and friction angle summarised in Table 6-7.

The properties of the anchorage system depend on which part and mode of failure is included in the model (Fig. 6-30):

1. Standard, grouted anchor: this is the portion of the standard anchor embedded in the side wall and it is simply modelled as a truss element with the linear properties typical of stainless steel AISI 304;
2. Head of the standard, grouted anchor: this part, which lays in the quoin, is particularly vulnerable to pull-out, as proved by the experimental campaigns. Hence, the stress-strain curve of this part is adapted from the material curve of the model of the anchor assembly of §6.3. As such, the overall behaviour of the anchor head is summarised by a set of equivalent properties; the cross sectional area of the truss element is defined so that the load capacity is equivalent to the pull-out capacity of a grouted anchor with the same length as the quoin depth and a diameter of the drilling hole equal to that adopted in the laboratories and on site. Due to the use of equivalent properties, it is not possible to use a beam element, because its stiffness is not accepted by the software. On the other hand, the energy dissipated through pull-out is negligible, so that the use of a truss element, which does not define a full stress-strain cycle, is deemed a suitable approximation;
3. Hysteretic device: whereas a standard anchor is defined only according to the criteria described at points 1 and 2, when a dissipative anchoring device is included in the model, the free, unbonded element of the part “anchor” is defined by a beam element characterised by stress-strain curve that reflects the response of the device. In this case the stress-strain curve of the hysteretic element is used. Connectors are not considered as they have a behaviour similar to the anchor rod in terms of deformation;
4. Frictional device: as for the hysteretic device, the frictional device is simulated by a beam element. An equivalent stress-strain curve is used together with a purposely chosen cross sectional area so as to generate a load-displacement behaviour equivalent to that of the device prototypes tested in the laboratories.

The model is pinned at the bottom, but adequate constraints are provided to simulate the presence of the surrounding structures, such as the walls of the adjacent church as well as the remaining portion of the side walls of the oratory itself. This is done by constraining the translational degree of freedom of the nodes corresponding to the surfaces or sections, where the FE model misses further portion of the structure.

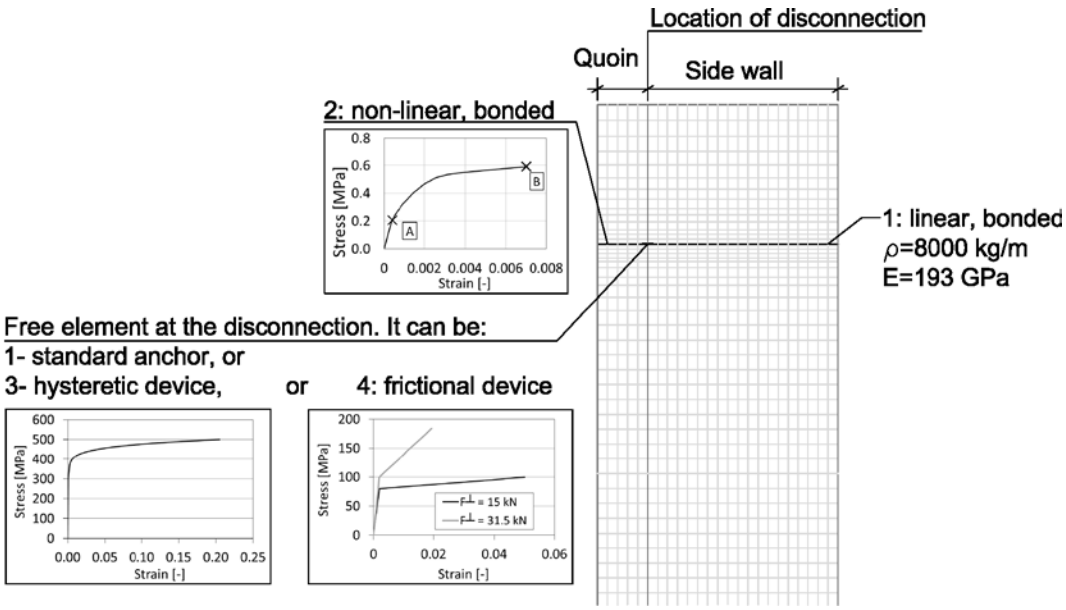

Fig. 6-30: Parts of the FE anchorage

For instance, the side walls of the oratory are constrained at the ends in the X direction, thus simulating the remaining part of the wall.

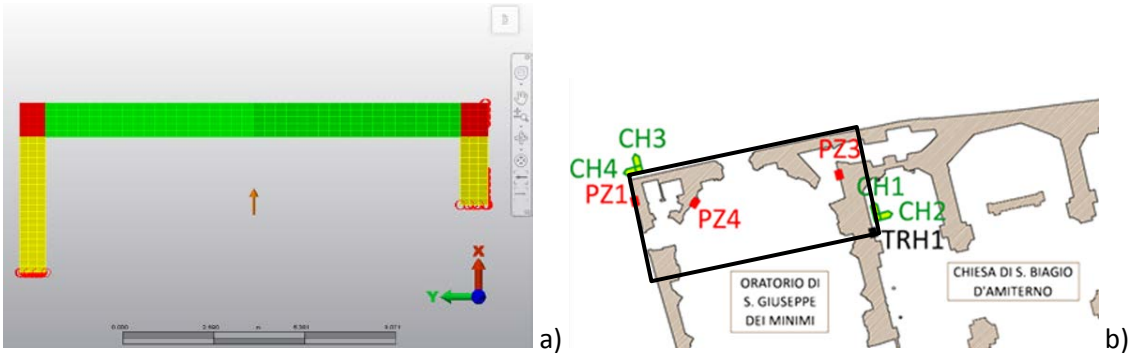

Fig. 6-31: Constraints on the FE model (a) introduced to simulate the presence of adjoining structures (b)

Part of one side wall is also constrained in the Y direction, so as to simulate the presence of the neighbouring building, as shown in Fig. 6-31.

Besides the loads applied to the mesh so as to simulate building parts, other loads are applied to the model depending on the typology of analysis being performed:

- Linear analysis:
  - Self-weight: in this case only gravity acceleration is applied to the model, so as to analyse the stress field in case of static loading;
  - Modal analysis: no load is applied. All elements are modelled either by mesh or by lumped masses so as to include their effect into the analysis.
- Non-linear analysis:

- Dynamic analysis: the self-weight of masonry walls is simulated by distributed loads, whereas the dynamic signal is input as horizontal acceleration. Dead loads slowly increase during the analysis until reaching the nominal value (Fig. 6-32a), and are then left constant during horizontal loading. (Fig. 6-32b). The chosen accelerogram is L'Aquila 2009 main shock, as recorded at the station of L'Aquila - Valle Aterno - Centro Valle, station code AQV (ITACA http://itaca.mi.ingv.it/ItacaNet/CadmoDriver).

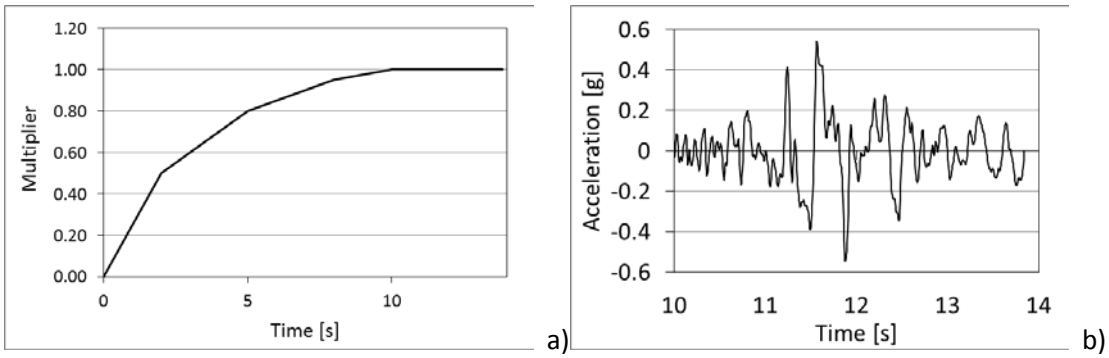

Fig. 6-32: a) Load multiplier for dead loads, b) input signal for horizontal acceleration

6.4.2 Results

6.4.2.1 Calibration – Linear and Non-Linear Analysis of the Undamaged Structure

The first analyses, as already mentioned previously, are run in the linear field, without any disconnection, with the objective of verifying the initial set of assumptions and calibrate the model.

Under gravity load (Fig. 6-33), as expected, the highest stresses are recorded at the foot of the building, especially at the bottom of the quoins; these elements have indeed a higher Young modulus and, therefore, experience higher stresses than the other masonry parts. This is particularly evident in the corner where vertical loads are higher, namely on the side where the belfry bears.

On average, the vertical component of the stress tensor at the base of the FEM is equal to 0.35 MPa, against the values measured by UPD, which are respectively equal to 0.24, 0.44 and 0.78 MPa, depending on the location at which the single flat jack test was performed (Casarin et al., 2010). As masonry is modelled as a homogeneous continuum, the variations in the stress field that characterise the on-site measurements are not reproduced; nonetheless, average values are in agreement.

It is worth pointing out that a stress value of 4.51 MPa was recorded by UPD at the corner below the belfry; however, such peak value depends on the deformation and out-of-verticality of the façade at the time of on-site tests. As the preliminary FEM does not account for these characteristics, it cannot reproduce the variations in the

stress field that derive from them. Nevertheless, it reflects the overall distribution of stress.

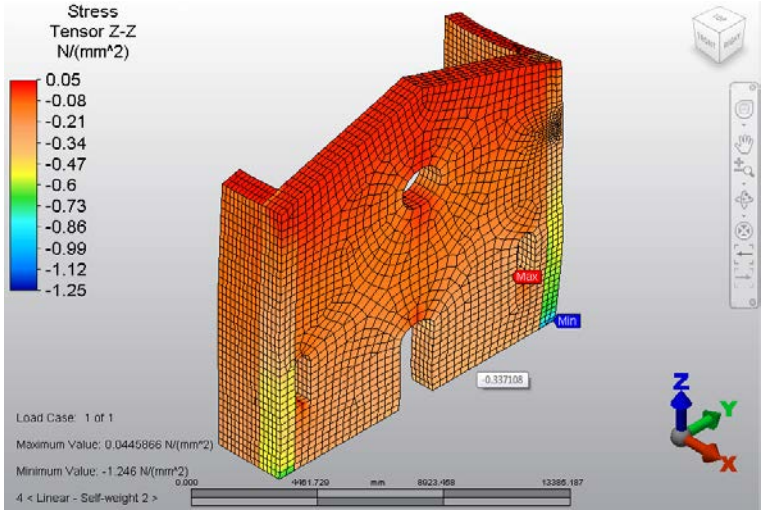

Fig. 6-33: Unreinforced, undamaged FEM, linear FEA – Vertical component of stress under gravity load

The comparison between the results of the modal analysis and of the dynamic characterisation performed by UPD (Casarin et al., 2010) is shown in Table 6-8.

Table 6-8: Comparison of mode shapes as identified by FE modal analysis and by dynamic identification (Casarin et al., 2010)

FE modal analysis					Dynamic identification	
Mode No	Frequency	Modal effective mass			Frequency	Modal shape
		X	Y	Z		
	[Hz]	[%]	[%]	[%]	[Hz]	
1	-	-	-	-	3.32	Bending of side walls
2	3.24	31.44	0.73	0.00	3.56	Global longitudinal mode
3	4.67	0.11	43.38	0.10	4.15	Bending of side walls
4	5.66	5.80	0.83	0.03	4.55	Out-of-plane bending of façade
5	7.32	2.01	0.71	0.00	5.12	Out-of-plane bending of façade
6	8.18	0.00	15.60	1.39	9.55	Out-of-plane bending of façade

The first mode detected by dynamic characterisation cannot be reproduced by the numerical model, because it only involves the side walls, which are not fully included in the FEM. Such pitfall is unavoidable considering the initial assumptions of the FEM, but on the other hand it has little impact on the computational results, as the pure flexural response of the side walls doesn't influence the out-of-plane response of the façade, and hence of the anchoring devices.

Natural modes present a good agreement in terms of frequencies and modal shapes (Table 6-8 and Fig. 6-34). It should also be considered that the dynamic characterisation was carried out in the aftermaths of the earthquake, when the

deterioration of stiffness and the change of geometry as consequences of damage had already affected the dynamic response of the structure, whilst the linear model is “undamaged”; some differences might be ascribed to this.

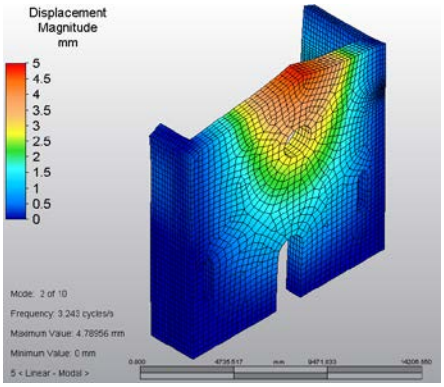

3.243 Hz

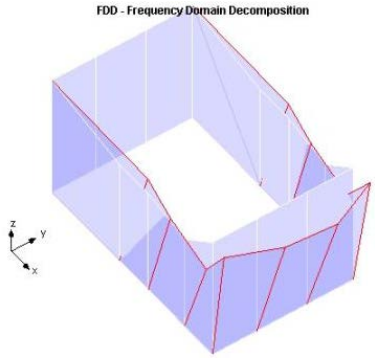

3.56 Hz

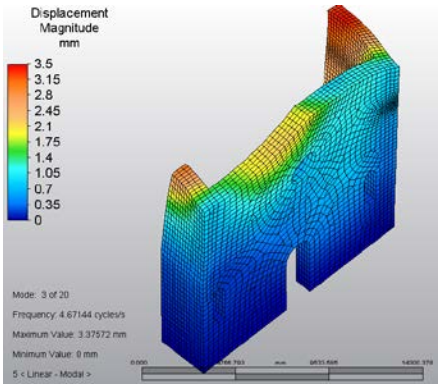

4.67 Hz

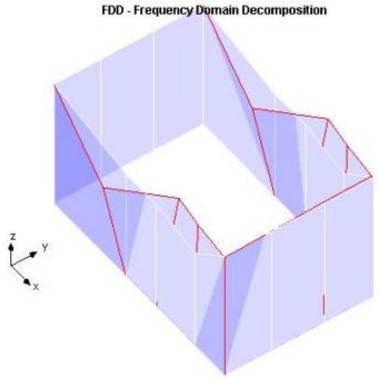

4.15 Hz

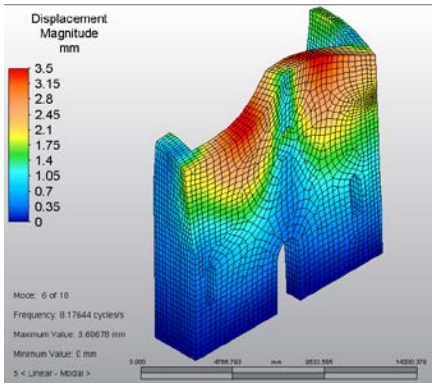

8.18 Hz

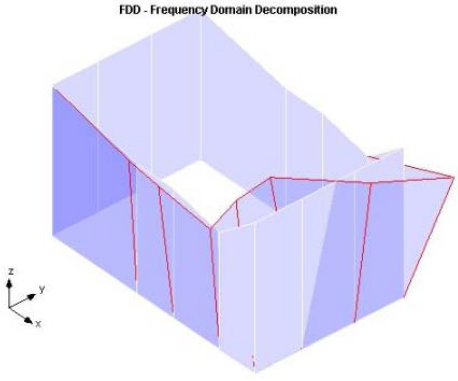

4.55 Hz

Fig. 6-34: Natural frequencies and modal shapes of the FEM (left) in comparison with results of the dynamic characterisation by UPD (right) (Casarin et al., 2010)

Nevertheless the model is able to capture the fact that the out-of-plane bending of the façade is the main mode in the X direction. As next step, a non-linear analysis is carried out only with gravity load, so as to check that the distribution of loads and masses used to simulate at the same time dead weight and the effect of horizontal accelerations on the structural mass is correct.

This is indeed the case, as shown by the stress field of the vertical tensor component depicted in Fig. 6-35a, which presents the same distribution as the linear analysis shown in Fig. 6-33.

The maximum principal stress (Fig. 6-35b) shows that tensile stresses are concentrated in the areas of the openings and in correspondence of the joint with the wall of the adjacent structure. However, the maximum value is still lower than the material tensile strength.

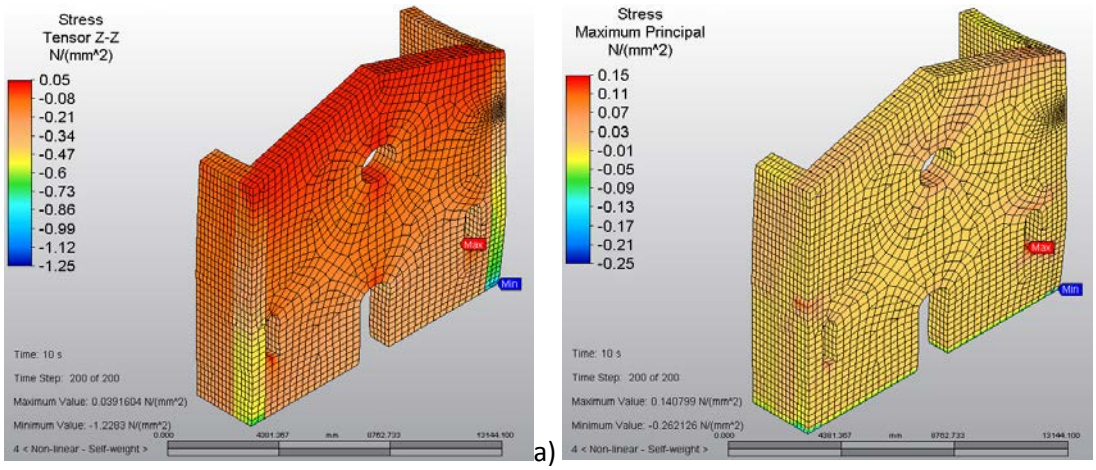

Fig. 6-35: Unreinforced, undamaged FEM, non-linear FEA - Stress tensor (a) and maximum principal stress (b) under gravity load

As linear and non-linear results for gravity load show a good agreement with each other and with on-site data, a horizontal acceleration is applied to the model.

The analysis stops converging at 11.6 seconds, i.e. approximately one second and half after the beginning of the seismic load (Fig. 6-36b), in correspondence of a major acceleration peak. At this point, the very top of the façade and the corner where the belfry bears are experiencing the largest displacements (Fig. 6-36a).

The plot of the maximum component of the principal stresses shows that pure tensile stresses concentrate in the corner area, at the material discontinuity between the façade, quoins and side walls (Fig. 6-37), which is exactly the position where the major crack opened during the L'Aquila earthquake. Hence, the FE model is able to reproduce the failure mechanism detected on site and can be used to compare the influence of different types of anchoring devices on the dynamic response.

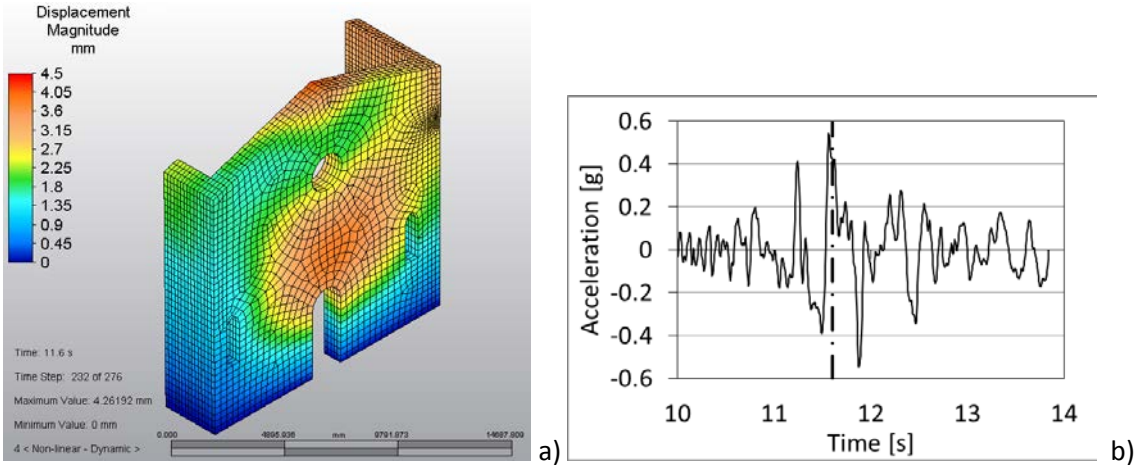

Fig. 6-36: Unreinforced, undamaged FEM, non-linear FEA - Displacement at failure

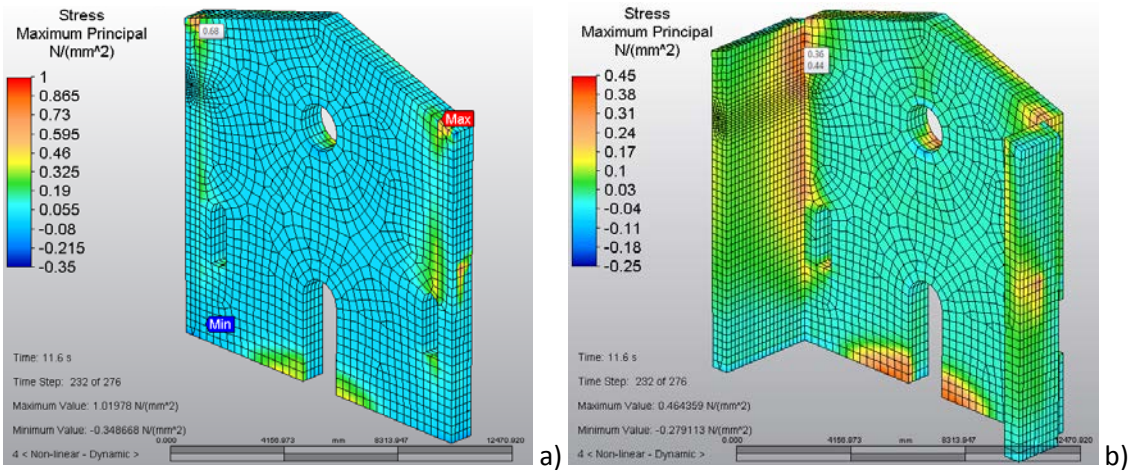

Fig. 6-37: Unreinforced, undamaged FEM, non-linear FEA - Maximum principal stress: a) in the quoins and b) in the side walls and façade

6.4.2.2 The Damaged Structure – Comparison between Unreinforced and Strengthened Set-Ups

After calibration, the FE model is modified to account for the damage of the prototype building: quoins and side walls are disconnected and a frictionless surface contact defined, so as to allow relative movements between the parts without allowing for penetration between the solids. This means that any frictional effect at the crack interface is being ignored, but on the other hand, the main crack in S. Giuseppe had such a width, that it seems reasonable to assume that the interlocking of the two damaged parts has little influence. Applying a frictionless contact allows simulating the complete disconnection also resulting from the residual tilting of the façade.

The same dynamic input as for the undamaged model is applied, causing the damaged, unreinforced structure to fail at approximately the same point in time, namely shortly after the highest peak of the acceleration input. However, failure occurs due to the tensile stresses at the bottom of the disconnected part (Fig. 6-38), rather than at the

corner connections. Indeed, the lack of the lateral constraints provided by a strong connection entails that a horizontal arch mechanism cannot form; hence, the façade behaves like a cantilever undergoing bending.

It is fairly straightforward to imagine that, if the damaged prototype building had undergone another seismic event, for instance a major aftershock, before having been propped, the façade would have collapsed by completely detaching from the side walls and moving outward, until complete loss of equilibrium. The response depicted by the FEA is representative of such hypothetic scenario.

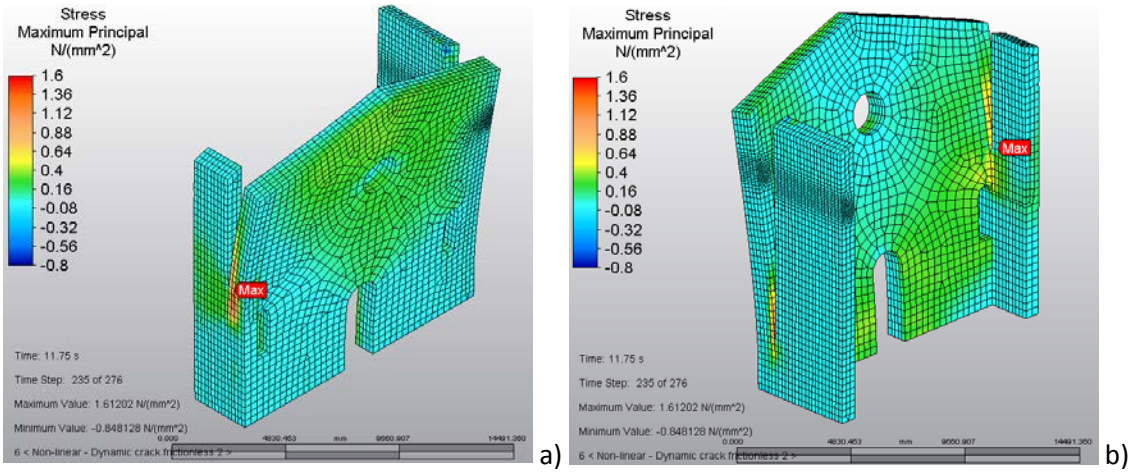

Fig. 6-38: Unreinforced, damaged, FEM, non-linear FEA - Maximum principal stress, front (a) and back (b) views

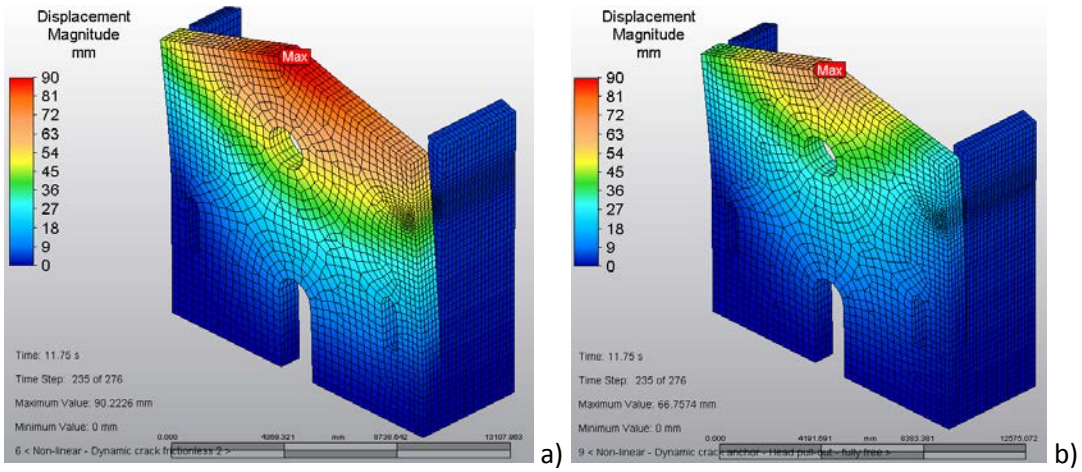

Fig. 6-39: Damaged FEM, non-linear FEA - Displacement magnitude before failure: a) unreinforced structure, b) structure reinforced by standard anchor

The presence of a standard grouted anchor modifies the displacement field experienced by the façade. In the damaged, unreinforced model (Fig. 6-39a), the joint lack of adjacent buildings providing constraint and the presence of the belfry on the right hand corner result in a larger extension of the crack and, hence, in larger flexural deformability and larger displacements. As the anchor partially restores constraint

against out-of-plane actions on this one side, the asymmetry in displacement field is also decreased, so that the movements on the two sides become comparable (Fig. 6-39b and Fig. 6-40).

Displacements become lower as consequence of strengthening not only at the point where the anchor is located, but also at the very top of the façade, which is the point that undergoes the largest displacements in both models (see the comparison between Fig. 6-39a and b, and Fig. 6-40).

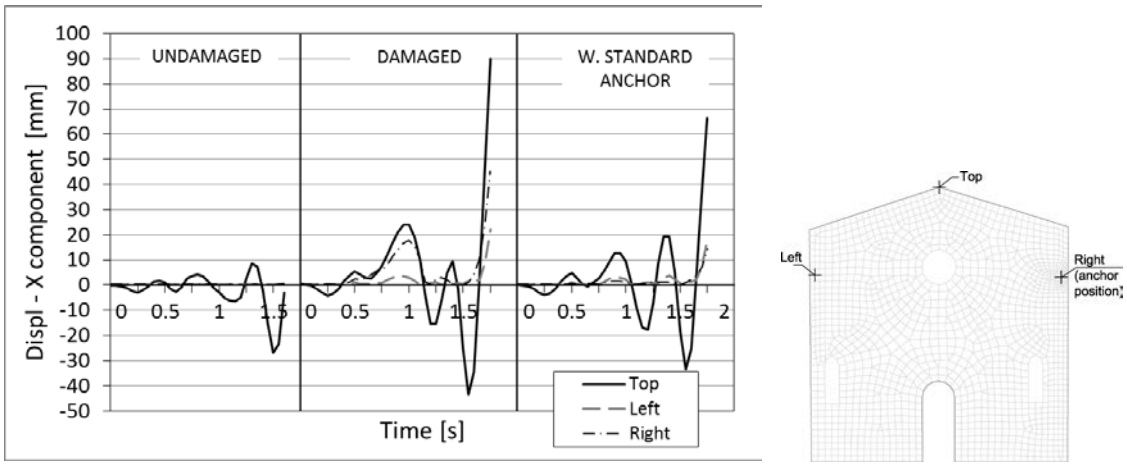

Fig. 6-40: Comparison of displacement component X for different structural set-ups. Only the dynamic part of loading is shown in the graph

The distribution of maximum principal stresses at failure shows that in the strengthened set-up the left quoins still presents a concentration at the bottom of the disconnected part, this being the natural consequence of the fact that on this side the corner connection has not been restored by means of an anchor. The cantilever behaviour still prevails (Fig. 6-41b), although the values of tensile stress in this position are not as high as in the case of the unstrengthened model.

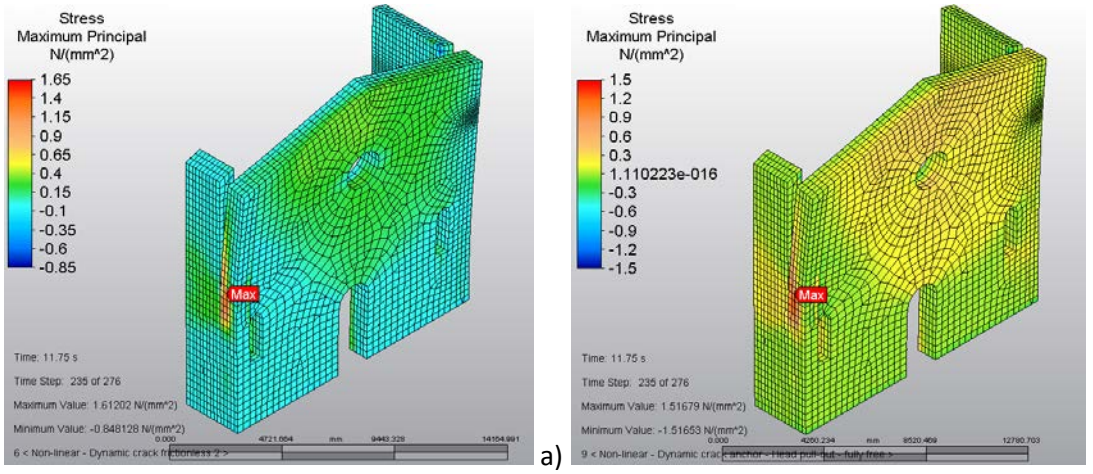

a) b)

Fig. 6-41: Damaged FEM, non-linear FEA – Maximum principal stress in the a) unreinforced set up and b) structure strengthened by standard anchor

The presence of the anchor considerably changes the stress field on the side where it is located: the tensile stresses at the bottom of the disconnected quoin are moderate (Fig. 6-42a), whereas high stresses are concentrated at the location of the anchor.

To observe in detail the stress field in the material surrounding the anchorage the FE solids are sectioned along the vertical (Fig. 6-42a) and horizontal (Fig. 6-42b) planes where the longitudinal axis of the anchor lies. This allows observing the typical cone-shaped distribution of the tensile stresses that characterise the pull out failure of strength-only anchors.

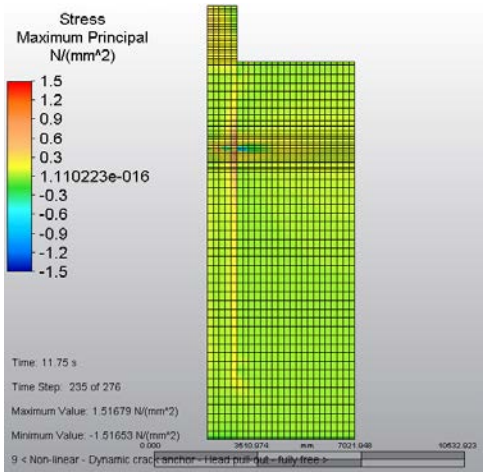

a)

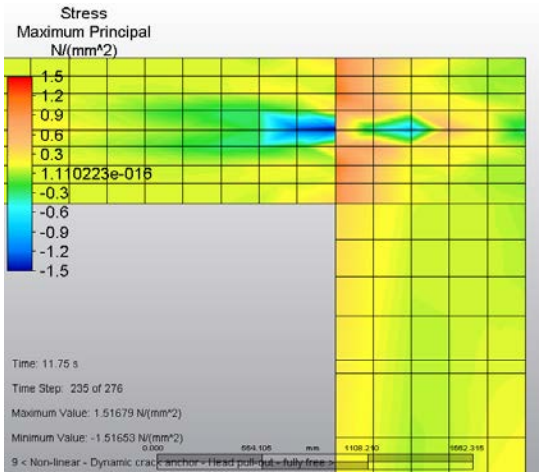

b)

Fig. 6-42: FEM strengthened by standard anchor – Maximum principal stress at the anchor head: a) vertical section of the side wall at the anchor position, b) horizontal section at the anchor level

Furthermore, from Fig. 6-42b it becomes clear that one portion of the anchorage has already failed; indeed, the stresses in the material surrounding the failed section are negative.

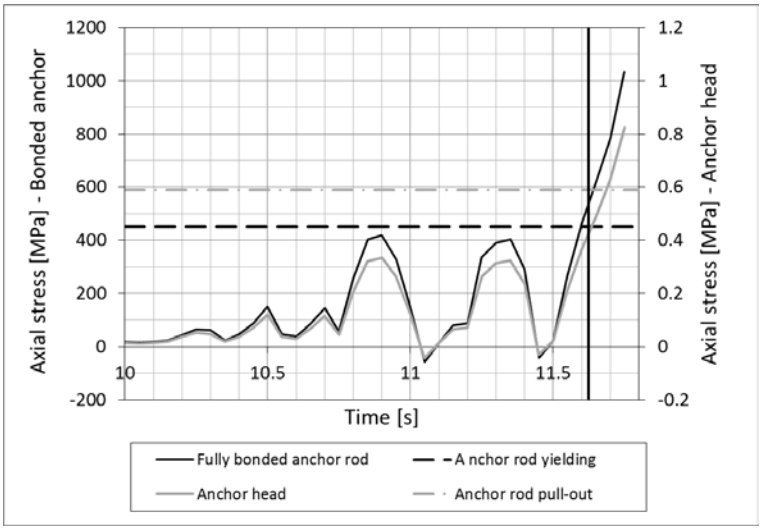

Fig. 6-43: Damaged, strengthened FEM - Maximum axial stress values in the head of the anchor and in the anchor lying in the side wall at the crack interface

Fig. 6-43 shows the evolution of the maximum values of axial stress in the portion of anchor lying in the side wall, namely the anchor fully bonded and only defined by the linear properties of the steel rod, and in the anchor head, which is instead defined by a stress-strain law that represent the pull-out capacity. The two values are obtained by plotting the results of the points adjacent to the disconnection with two different scales to allow the comparison with the pull-out strength, 0.59 MPa (corresponding to point B of the idealised curves, as defined in §4.3), and the yielding strength of steel, 450 MPa.

The anchor rod yields shortly before the acceleration peak of the input signal at 11.6 s, followed closely by the head of the anchor, which starts pulling out of the quoin (Fig. 6-43).

Yielding and pull-out failure do not extend to the whole anchor, but affect instead the length adjacent to the disconnection, i.e. the vertical crack between quoin and side wall (Fig. 6-44). The drop in pressure along the anchor length, as shown in Fig. 6-44, is indeed connected to the change in material definition from the head at the front, where the 2D elements are defined through the equivalent pull-out stress-strain curve and the anchor embedded in the side wall, defined by a linear σ-ε law.

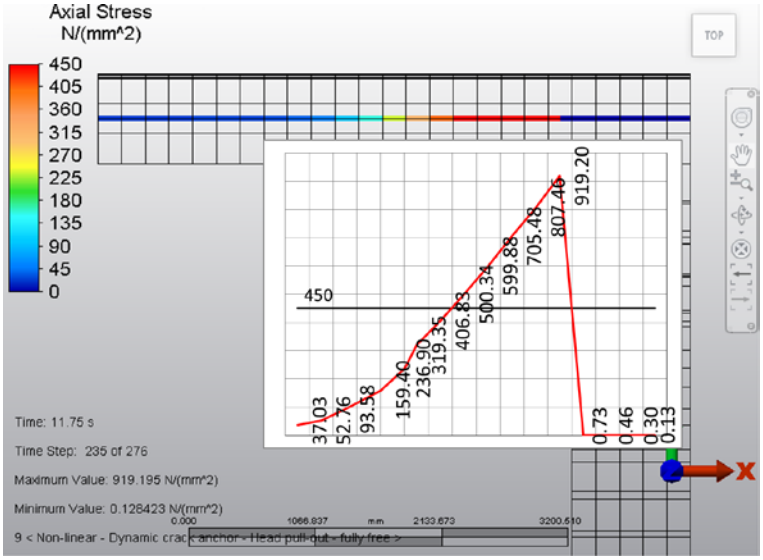

Fig. 6-44: Damaged, strengthened FEM - Distribution of axial stress along the anchor

This analysis shows that a standard anchor is able to control displacements, as long as it does not pull out; as this eventually occurs at peak acceleration, no considerable increase in capacity is achieved for the used seismic input, and the analysis stops at roughly the same point in time as the unreinforced FEM. A further analysis is set up in the attempt of allowing, if possible, a larger portion of the anchor head to fail by pull-out so as to test the ultimate capacity of the anchor and its influence on the overall structure, before the software stops converging. Indeed, the fact that the wall opposite to that where the anchor lies is not constrained provokes high tensile stresses

at the bottom of the façade; these are a likely cause of the numerical problem that prevents the software from converging.

Another anchor element, defined exactly like the one on the side of the belfry, is inserted in the left hand side of the façade, so as achieve symmetric strengthening. By doing so, the right hand side of the façade, because of the mass of the belfry, is expected to experience higher accelerations, and the anchor on this side to undergo the worst loading conditions. The other anchor should instead prevent the formation of a cantilever mechanism, thus reducing the tensile stresses at the bottom of the disconnection on the left side of the façade.

Indeed, façade displacements become symmetrical on the two sides (Fig. 6-45a) and the maximum tensile strength is recorded in the area of the head of the anchor (Fig. 6-45b). Displacement and anchor tensile stress histories do not show substantial differences from those shown in Fig. 6-40 and in Fig. 6-43; therefore, graphs are not plotted to avoid repetitions.

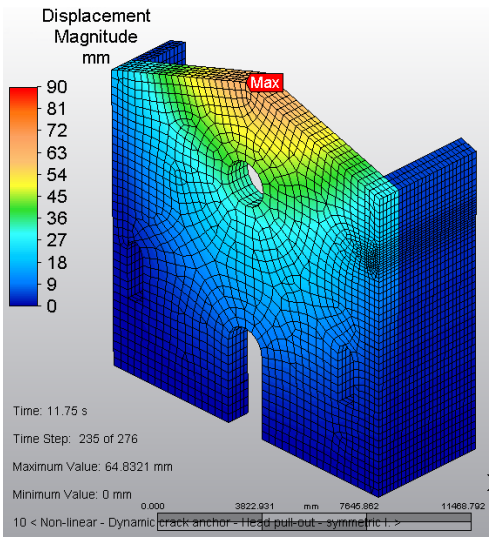

a)

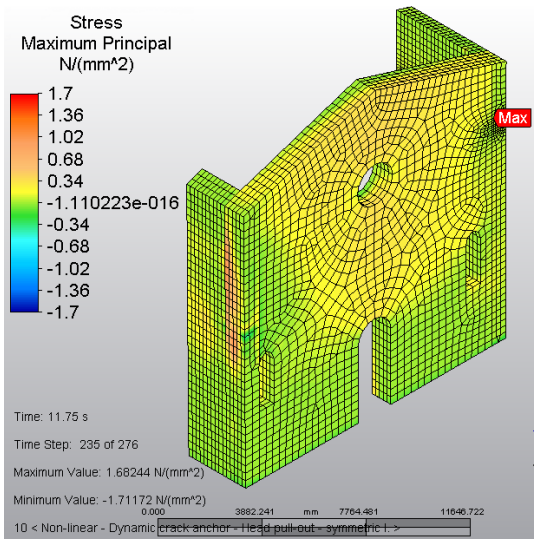

b)

Fig. 6-45: Damaged FEM strengthened by two standard anchors: a) displacement magnitude, b) stress maximum principal

However, the stress fields on the anchor itself (Fig. 6-46a and b) and in the material surrounding it (Fig. 6-46c) show that the fact of reducing the deformations experienced by the left side of the façade allows reaching the ultimate capacity of the anchoring system, in this case represented by a combination of pull-out failure of the head and tensile failure in the material surrounding it.

The influence of the dissipative anchoring devices on the computational results depends on the type of device implemented in the model, even though the FEMs all stop converging about after 1.75 s from the beginning of the dynamic input, regardless of which type of anchor or device is used for the strengthening.

As the dissipative devices are implemented only on the side of the belfry, i.e. the right side of the façade, while a simple standard anchor is left on the other side, the displacement fields consequently become asymmetric due to the difference in stiffness between the standard anchor and the anchor in series with a dissipative device (Fig. 6-47).

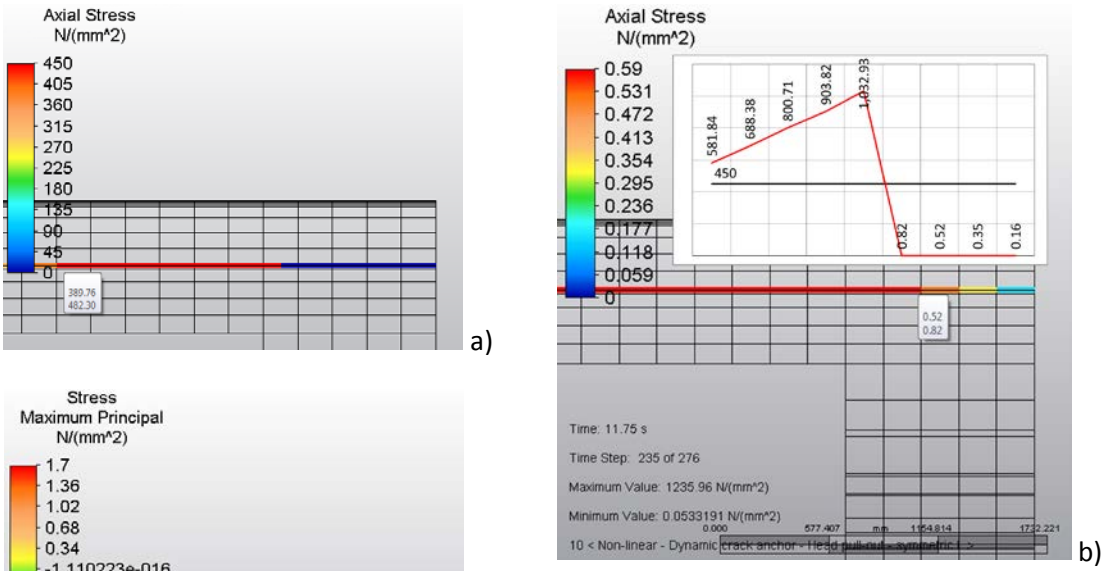

Fig. 6-46: Damaged FEM strengthened by two standard anchors – Anchor head: a) axial stress (scale maximum equal to steel yielding strength); b) axial stress (scale maximum equal to pull-out maximum strength); c) maximum principal stress

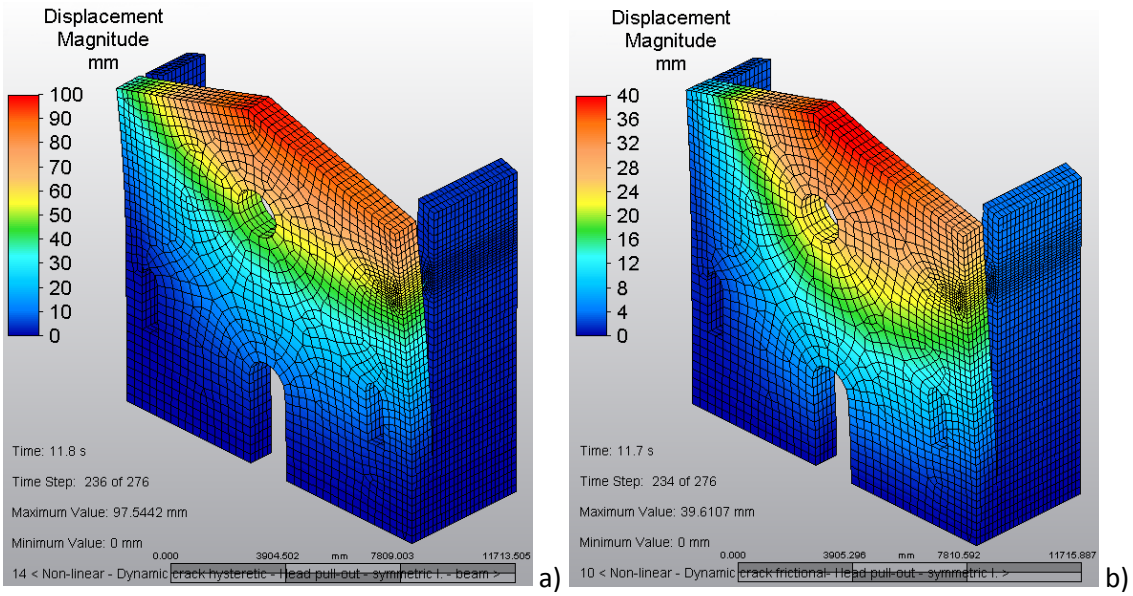

Fig. 6-47: Displacement magnitude at failure, FEM strengthened by one standard anchor (left side of the façade) and one: a) hysteretic device; b) frictional device (right hand side of the façade)

The frictional device is the most effective in limiting the displacement experienced by the structure (Fig. 6-48). The standard anchor also controls the displacements, but mainly at the position where it is inserted, not at the top of the gable, while the frictional device has a positive effect at both levels; the hysteretic device is the least effective in limiting the displacements.

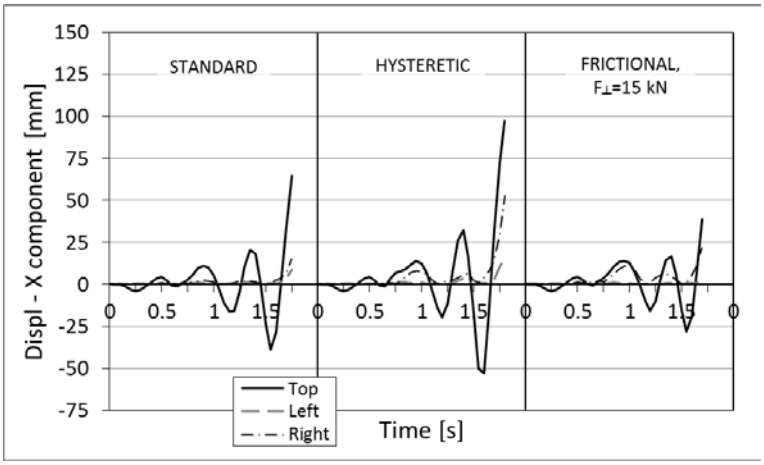

Fig. 6-48: X component of displacement of the FEMs strengthened by the three different typologies of anchors

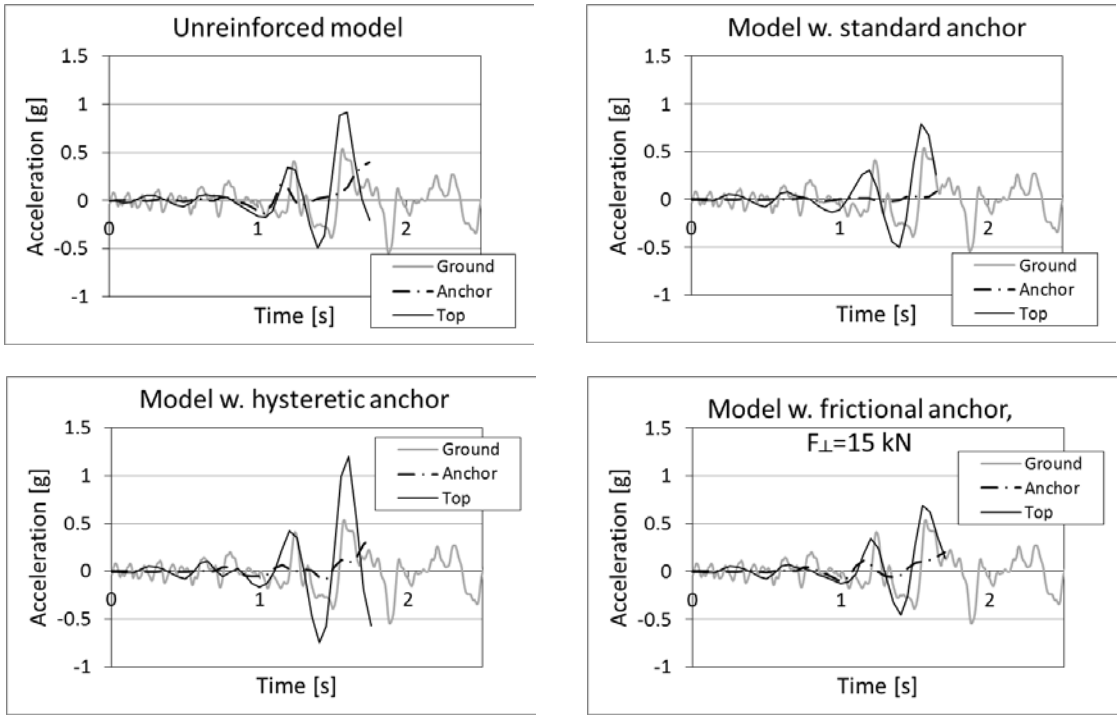

Fig. 6-49: Acceleration history at different levels and for different types of strengthening

Similarly, acceleration histories (Fig. 6-49) show that the hysteretic device cannot reduce the amplification experienced by the façade of the building, whereas both the

standard anchor and even more so the frictional device reduce the amplification of the gable at maximum peak acceleration from 1.7 of the unreinforced model to 1.5 and 1.3 respectively.

Looking more in detail at the mode of failure and stress concentration, it is possible to say that the FEM strengthened by one hysteretic device stops converging due to a high concentration of tensile stresses on the side of the building strengthened by the standard anchor (Fig. 6-50a).

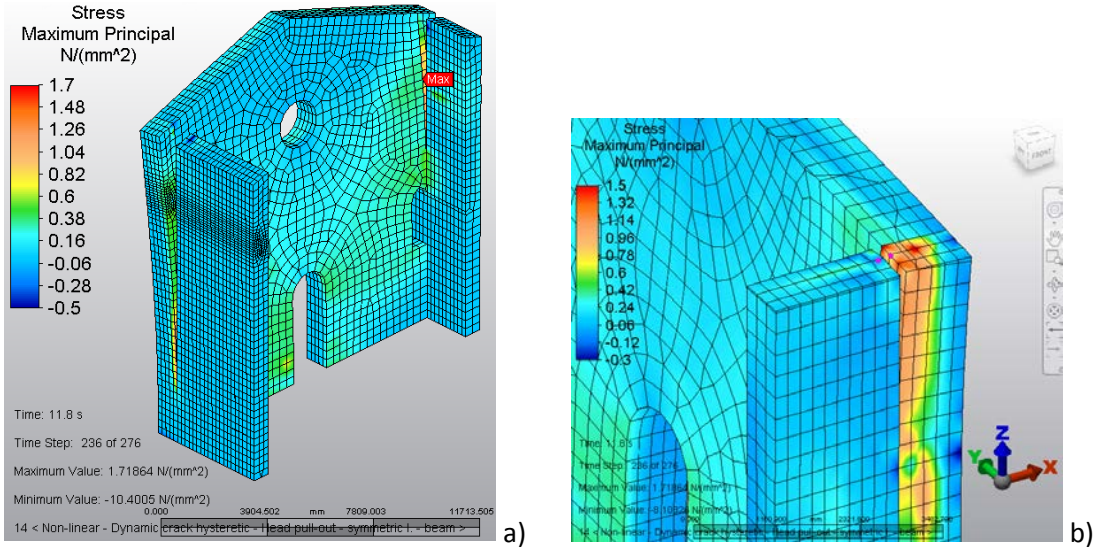

Fig. 6-50: Maximum principal stress field in the FEM strengthened by one hysteretic device and one standard anchor: a) overall view; b) section at the location of the standard anchor

Tensile stresses in the material surrounding the head of the standard anchor are considerable, and sufficient to cause widespread cracking around the grouted element (Fig. 6-50b). Furthermore, the truss elements belonging to anchor parts adjacent to the crack feature stresses higher than the pull-out capacity and yielding strength, which respectively represent the maximum acceptable values for the anchor head in the quoin and the anchor embedded in the side wall. The failure of the standard anchor by means of pull-out and yielding confirms what already observed in the case of the FEM strengthened only by standard anchors.

On the side of the hysteretic device, tensile stresses are instead within an acceptable range (Fig. 6-51a). However, when one plots the stress-strain curve of the hysteretic device, it is possible to observe that the dissipative element is already beyond its ultimate capacity, which is marked as a dot on the material model input curve (in grey in Fig. 6-51b). The software does not stop the analysis as soon as it reaches the last defined stress-strain point probably due to the choice of using an isotropic hardening law for the material. This causes the device to experience deformations higher than what defined by the user and anyway beyond what can be expected, also on the basis of the evidence from the experimental campaigns described in Chapter 4. In spite of this incongruity, the material model still gives, shape wise, a good agreement between

input and output curve; it's also worth mentioning that isotropic hardening is the only option offered by the FE software in terms of hardening law.

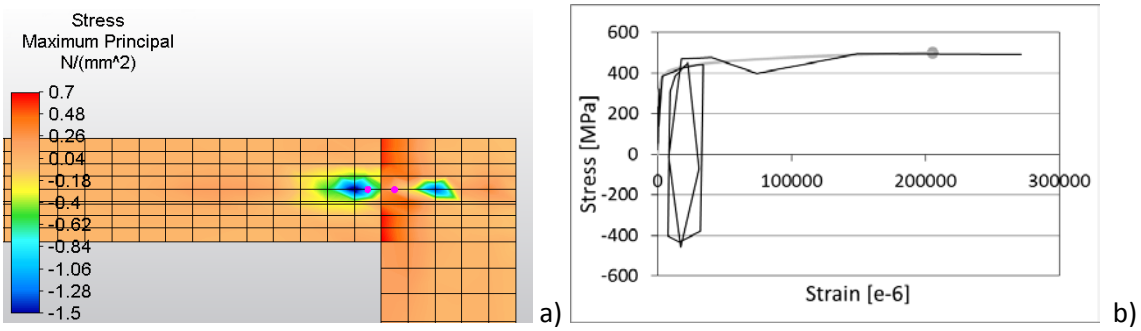

Fig. 6-51: FEM strengthened by hysteretic device: a) maximum principal stress field in the masonry surrounding the hysteretic device; b) stress-strain curve of the dissipative element

Ultimately, the structure fails not only for the high tensile stressed on the side of the standard anchor, but also because the hysteretic device reaches the ultimate tensile capacity. This would be of course an issue in a real case study; the problem of how many devices should be installed into a structure, and how these can be designed to avoid the attainment of the ultimate capacity and eventual detachment of the façade wall will be therefore discussed in the following chapter.

Most importantly, the computational validation shows that the hysteretic device is able to avoid pull-out at the interface grouted element/masonry and damage to the masonry and anchor system. Indeed, the stresses in the parent material as much as in the head of the anchor and in the anchor embedded into the side wall are within the defined limits; this is a main point to prove the viability of the concept of the anchoring device. The main issue that will have to be tackle in Chapter 7 is the fact that the hysteretic device seems less able to control displacements and accelerations, this being instead an important requirement for the anchoring devices.

The frictional device, in spite of a far better performance in terms of displacements and acceleration, delivers a performance similar to that of the hysteretic device in terms of mode of failure and stress fields.

High concentrations of tensile stresses are located in correspondence of the material discontinuity between corner quoin and façade on the side strengthened by the standard anchor (Fig. 6-52) although in this case the values of stress are lower than in the previously discussed model.

Damage to the parent material surrounding the anchorage, to the grouted element and to the anchor rod embedded in the side walls is prevented thanks to the presence of the frictional device. Indeed, maximum principal stresses in the parent material (Fig. 6-53a) are lower than the maximum tensile strengths; neither the truss elements of the head of the anchorage nor of the anchor in the side wall have reached the stress thresholds of bond pull-out and yielding.

The presence of negative stresses indicates the point at the interface between the dissipative device, which is free, and the anchor rod, which is fully bonded to the parent material. As already observed for the FEM of the pull out, the front portion of parent material where the anchor is embedded experiences negative stresses as the anchor is pulled outward.

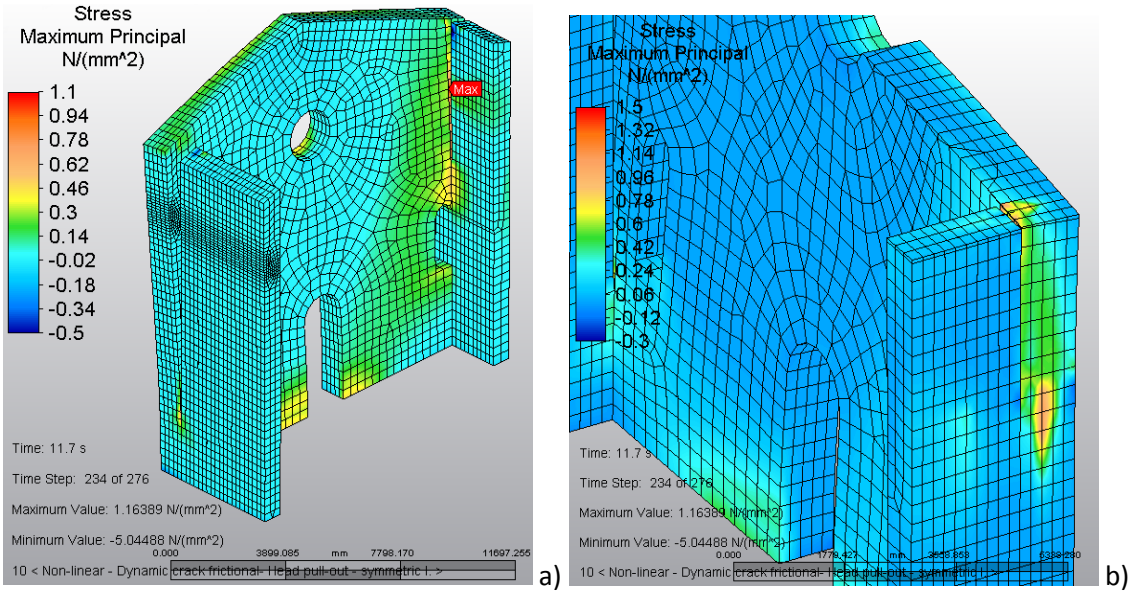

Fig. 6-52: Maximum principal stress field in the FEM strengthened by one frictional device ($F_{\perp}$=15 kN) and one standard anchor: a) overall view; b) section at the location of the standard anchor

As for the hysteretic device, the software does not stop the analysis upon attainment of the last point of the stress-strain curve used as material model input (Fig. 6-53b); this means that, beyond the point at which the analysis stops converging, the structure would substantially have the same behaviour as the unreinforced model, i.e. the anchor connections, with or without device, would fail and the façade would eventually overturn.

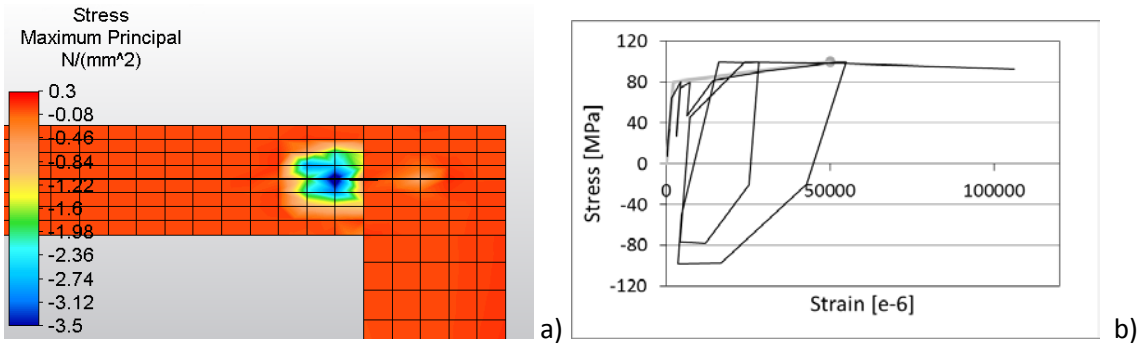

Fig. 6-53: FEM strengthened by frictional device ($F_{\perp}$=15 kN): a) maximum principal stress field in the masonry surrounding the frictional device; b) stress-strain curve of the dissipative element

It is worth considering that, in the case of the frictional device, the limitation imposed by the software in the definition of the material model under cyclic loading has further implications as in the case of the hysteretic device. Not only isotropic hardening entails that the device undergoes deformation larger than those allowed in reality for the prototype, but cycles are also missing the further increase in stiffness that occurs when the sliding plates hits the device mechanical stop.

Indeed, after reaching the end of the run, the frictional device behaves like a strength-only element controlled by the stress-strain capacity of the anchor rod, of the connections and of the pins that secure the mechanical assembly. This has been shown by impact tests during the experimental campaign, but cannot be modelled in the FE software. This has twofold consequences: firstly, the FEM shown in this chapter assumes that the frictional device has not stops, which could be possible by modifying the prototype, but might not be desirable, if one seeks to limit relative displacements between building parts. Secondly, that the simulation of the frictional device requires the combined use of different elements and numerical expedients to faithfully reproduce its actual behaviour; for instance, the presence of stops could be simulated by adding a further element with such a stiffness that it only influences the behaviour at the crack interface when the device reaches its displacement limit.

The option of introducing further parts in the FE model will be explored in the next chapter, as it has far reaching consequences in the framework of the optimisation of the device layout and design. In this respect it is also worth mentioning that, although only results with a frictional device set for a perpendicular pressure $F_{\perp}$=15 kN have been reported, analyses have also been run for the case $F_{\perp}$=31.5 kN. In fact, differences in results between the two are minimal and therefore the discussion is limited to one case; nonetheless, the option of using different levels of frictional force will be taken into account in the design procedure of the devices.

Another important point that will be discussed in depth in the next chapter regards the desirable level of dissipated energy/ductility to be attained by the chosen dissipative device. As visible by comparing the stress-strain cycles of Fig. 6-51b and Fig. 6-53b, the hysteretic device dissipates more energy, approximately ten times more, than the frictional device and allows larger deformations. This results in the frictional device delivering a better performance in terms of displacement and acceleration reduction; indeed, it creates a “strong” connection and yet it is able to dissipate energy and reduce the load transmission, thus avoiding damage as in the case of the standard anchor. Conversely, the hysteretic device is too flexible, so that its effect on drift limitation is reduced. The fine tuning of the devices to optimise the performance in order to meet all the objectives of a strengthening intervention on a heritage structure is the main goal of the design procedure described herein.

6.5 FINAL REMARKS

After completing the experimental and on-site validation of the dissipative anchoring devices, numerical assessment has been carried out through the FE software Autodesk

Algor Simulation ©. The numerical simulations have the twofold objective of complementing from a quantitative point of view the results described in the previous chapters and to allow the calibration of a stable numerical model that can be used to exemplify the procedure for the design of a strengthening intervention including the dissipative devices, which will be the main topic of the next chapter.

The aim of Chapter 6 is hence the development of a set of Finite Element models suitable to reproduce the samples tested in the laboratories or installed on site, to allow the fine tuning of material properties so as to achieve a behaviour comparable to that of the actual prototypes and to study those parameters that the experimental set-up and on-site measurements were not apt to record such as, for instance, the stress or deformation field in the whole material surrounding the anchorage.

Additionally, the chapter discusses how a reasonable compromise between result accuracy and approximation can be achieved without compromising the computational efficiency, also in light of the increasing level of complexity of the models. Indeed, the computational validation is carried out in a fashion similar to the experimental assessment, starting from the isolated devices, which are then integrated in a model including the grouted element of the anchorage and the surrounding masonry and, eventually, a full structure.

The issue of accuracy and numerical efficiency is relevant since the very first stages of the numerical calibrations: as the FE models of the isolated devices are run exploring a whole range of options in terms of material yielding criteria, constitutive laws and mesh refinement, it becomes apparent how the use of a specific software determines a number of limitations in terms of result accuracy.

For instance, the FEMs of the prototypes reproduce correctly the behaviour of the devices; however, the shape of cycles doesn’t completely follow that of the recorded data. In the case of the frictional device, this depends on the use of an average coefficient of friction, which cannot reproduce the variations due to mechanical locking observed during the experimental campaigns. In the case of the hysteretic devices, the differences between experimental and computational results depend instead on the material model and yielding criteria available in the software.

If on the one hand one could argue that another software could be chosen, it must be also kept in mind that this option is not always viable for the practicing engineer, who might have a limited spectrum of resources at disposal. Therefore, in the framework of this research project, it is deemed more meaningful to discuss how models can be fine-tuned so as to minimise discrepancies in respect to the actual structural behaviour and yet achieve an effective, simplified model, working within the constraints typical of small commercial project.

In the case of the frictional device, for instance, the boundary values of the friction coefficient can be used, as these allow reproducing the two limit cases of the range of possible performance of the device, in line with EN 15129:2009. For the hysteretic anchor devices it is observed instead that, once the most suitable yielding criterion has

been chosen, the mesh refinement brings little improvement in terms of accuracy. Therefore, one can choose to optimise the numerical efficiency by limiting the mesh refinement without considerably losing accuracy. Still, care must be taken when assessing the energy dissipated by the hysteretic devices, as this must be corrected to take into account the numerical imprecisions.

The process of calibrating FE models is expedient to the purpose of identifying what parameter are most influential, how these should be correlated with experimental or on-site results and what fictitious, additional elements might be needed to obtain robust results.

The use of a fictitious model part placed between the grouted socket and the masonry substratum is indeed the modelling technique chosen for reproducing the bond failure observed when a grouted anchor is installed in a weak masonry substratum. The FE models can be run with linear materials and yet one can achieve satisfactory results in terms of correspondence with the experimental results. Indeed, the non-linearities inherent to the bond failure are localised exclusively in the fictitious part, which is defined by an equivalent stress-strain law, calibrated on the basis of the recorded load-displacement curves.

The same concept of an equivalent stress-strain law is also applied to the FEM of the façade of S. Giuseppe dei Minimi. The advantage of this modelling technique is that simple 2D elements, such as truss and beam elements, can be used to define the anchor parts without the need for modelling the whole geometry of the devices. This would be highly burdensome in terms of mesh and calculation time and, at the scale of the whole structure, would not be beneficial in terms of output information.

The comparison of the response of the façade in its damaged, unreinforced setup against a hypothetical strengthened set-up featuring standard anchors, hysteretic devices or frictional devices confirms the results obtained in the previous chapters. Indeed, the devices reduce the stresses transmitted to the masonry substratum and hence prevent cracking and pull-out failure. The frictional device has also positive effects in terms of displacement and acceleration control.

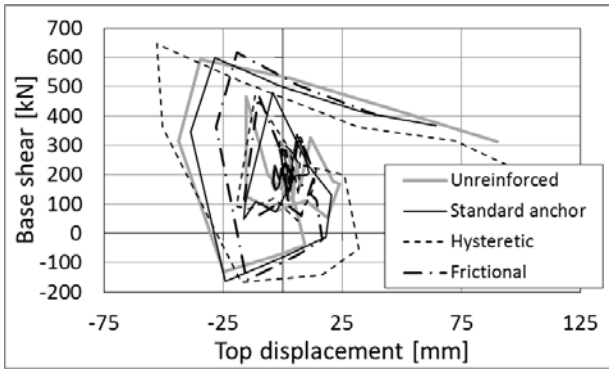

Fig. 6-54: Force-displacement graph comparing the effect of the different types of anchors on the overall behaviour of the structure

As only one/two anchors have been included in the FE models, their impact in terms of capacity improvement is not patent; yet they do influence the overall structural performance (Fig. 6-54).

The goal of the Chapter 7 will be to devise a methodology whereby the overall structural performance can be controlled in such a way that an optimum in respect to a set of requirements can be found and pursued. In practice, this means calibrating the influence of the devices on the overall dynamic performance, so that a number of chosen parameters - acceleration, drift, and the like - fall in line with the code prescribed limits. This is pursued by modifying the number, layout and properties of the anchors and of the dissipative devices according to the principles of a multilevel performance design.

7 DESIGN PROCEDURE

7.1 DEVELOPMENT OF A DESIGN PROCEDURE

As discussed in the introductory chapters, current codes give very little guidance in terms of design procedures for strengthening systems of historic structures in earthquake prone areas. To keep to the European example, both EC8 (EN 1998-3:2005) and the Italian guidelines (DPCM, 2011) regulate the design approach and recommend a number of suitable techniques specific to heritage structures, but they both fail to provide detailed guidance of how these systems should be designed, even though this is the key to a successful intervention.

The Italian code (DPCM; 2011) lists, among the others, a number of strengthening systems for the improvement of connections, such as anchor ties, ring beams and wrapping/confinement through different materials. It also describes the steps needed to assess the initial conditions of the structures, such as the on-site experimental characterisation of the mechanical properties of the construction materials, and gives instructions as far as computational modelling goes. On-site investigations and numerical simulations enable the comparison between the current behaviour of the structure and the enhanced response achievable by strengthening. Thus, the need for a structural upgrade is determined and its extent minimised, still ensuring a sufficient level of safety. Nonetheless, the code remains vague when it comes to the design of the strengthening elements to the purpose of optimising the intervention.

For traditional, strength-based systems, the practicing engineer should possess the sufficient knowledge to carry out a preliminary design and then assess the improvement of the overall structural response according to the code instructions. For instance, if traditional anchor ties are implemented, these can be designed simply assuming that each will undergo a force proportional to the mass of the portion wall it restrains and to the horizontal peak acceleration experienced by this mass. An estimate of the natural period of the structural system can be used to determine the correct spectral ordinate and the distribution of amplification over the height of the structure, either using standard response spectra or spectra derived from microzonation studies (D'Ayala and Ansal, 2012). The cross ties are designed to meet the load demand according to the prescriptions for steel structures. Once the preliminary design is completed, the dynamic response of the strengthened structure is assessed, reiterating the procedure and varying the lay-out of the cross ties until the target performance is achieved.

However, in some cases, especially for energy-based strengthening systems and for a multi-level performance design, the design process might require additional, not-so-obvious steps. Indeed, the preliminary design of a cross tie as outlined above is typical of a load-driven capacity design, where structural elements must display a linear behaviour even for high-intensity excitations, whereas current codes require to check

the performance of the structure, and hence of the strengthening systems, for a number of limit states.

When looking at serviceability and damage limitation, displacement should be the controlling parameter. Hence, the cross ties is designed on the basis of deformation, which must be in line with the allowable relative displacement between the two walls that the tie connects for damage limitation limit state, as well as for the load demand at the ultimate limit state. In case the cross tie is used in series with a dissipative element, like in the case of the dissipative anchoring devices, energy also plays a key role, both in terms of the design of the anchor tie itself and from the point of view of the seismic demand, as function of the structure ductility.

Furthermore, the design of the strengthening system cannot ignore the interaction between the new, additional elements and the existing construction materials; in other words, one needs to ask oneself what impact a cross tie dimensioned to withstand a certain level of pull will have on the masonry underlying the end plate: will the masonry crush? This might not be acceptable not only for the level of damage limitation, but even for lower level of excitation if the façade of the building is decorated. And can be crushing accepted for extreme seismic actions, or is a different design solution possible? A correct balance between damage prevention and achievement of a satisfactory level of safety must be ultimately stricken; this in turn means that a number of design parameters must be incorporated in the decisional process.

Experimental, on-site and computational results discussed in the previous chapters show that the dissipative anchoring devices successfully improve the behaviour of standard metallic anchors by increasing the ductility of the strengthening system, thus limiting, or even fully preventing, damage in the substratum.

As summarised in Table 7-1, the experimental campaigns have shown that:

- For yielding devices, the ductility doesn't particularly increase on average in respect to standard anchors; however, the performance is far more uniform (i.e. lower scattering, expressed as standard deviation), especially for pull-out tests, where the devices where brought beyond yielding. In cyclic tests, the positive effect was limited due to the type of parent material of samples;
- For frictional devices, the increase in ductility is the most evident effect, except for high levels of perpendicular pressure, where the stick and slip behaviour of the friction plates is prevalent and large displacement cannot be allowed without damage occurring to the parent material. Ductility varies considerably, but this is also due to the fact that some devices were not brought to the end of their run, so that scattering depends on the test set-up rather than on the performance of anchors.

The use of damage and maximum achievable displacement as performance indicators throughout the validation process is expedient to the purpose of proving the suitability of the devices for the strengthening of historic connections, but also allow quantifying

the set of parameters that feeds into a performance-based design. How this is done is explained and exemplified in this chapter.

Table 7-1: Ductility of tested anchors (μ: mean, σ: standard deviation)

Type of anchor			**Type of test**	**Point B**		**Point C**	
				μ	**σ**	**μ**	**σ**
Standard	Average (6 samples)		Pull-out	5.57	3.37	9.16	47.9
	Average (6 samples)		Cyclic	7.05	2.78	17.25	8.69
Yielding	Average (4 samples)		Pull-out	2.04	0.33	9.11	3.83
	y1T		Cyclic	4.13		12.07	
	y2T			9.07		37.54	
Frictional		$F_{\perp}$ [kN]	Pull-out				
	f3	41.5				1.91	
	Av. (2 samples)	31.5				18.46	8.42
	f4	23				1.56	
	Av. (2 samples)	15				44.09	47.95
	f1T	15	Cyclic			10.7	
	f2T					23.2	
	f3T					27.5	

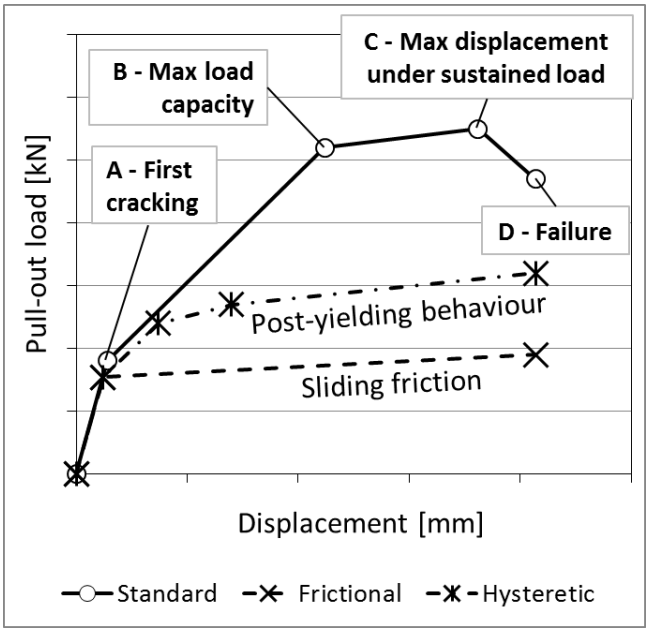

Fig. 7-1: Idealised load-displacement curve of a grouted anchor embedded in masonry substratum and undergoing a pull-out load. The curve is compared with the target performance of the dissipative devices, which are tuned to activated and avoid any damage in the substratum

The design approach draws on the work by Filiatrault and Cherry (1990) and Ciampi et al. (1995): although these authors are mainly concerned with the optimal distribution of dampers within a structure, still the underlying concept is that devices are chosen so as to match an expected level of either ductility (Ciampi et al. 1995), strain energy

(Filiatrault and Cherry 1990), or of any other parameter that can quantify the reduction of structural damage.

Indeed, the energy input into the structure by the earthquake is initially stored as elastic strain energy and then dissipated by damage, unless this can be fully or partially dissipated by sacrificial elements. The anchoring devices are designed by reiterating the dimensioning process until their geometry determines load-displacement cycles sufficient to dissipate seismic energy and prevent damage in the non-ductile portion of the anchorage.

Although the process described in the following refers to a specific strengthening system, the procedure is applicable to other techniques and, as such, it can be used as a guideline to address the general lack of technical prescriptions.

The behaviour of the structure strengthened by standard anchors is determined through linear and non-linear analyses, according to the prescriptions of EN 1998-3:2004. This allows verifying the compliance of the structural response with the requirements for the limit states of Damage Limitation (DL –seismic event with a probability of exceedance of 20% in 50 years), Significant Damage (SD – 10% in 50 years) and Near Collapse (NC – 2% in 50 years); devices are then designed to enhance the performance and optimise the design of the strength-only part of the anchor.

As first attempt, the strength-only part of the anchors is designed for DL, as this is the best compromise between ensuring a margin of safety and minimise the force capacity that this part of the anchoring system needs. The force $F_{D,DL}$, which acts on the building when this reaches the displacement required for DL limit state, is distributed among anchors depending on their number and layout, and on the prevalent modal shapes of the structure. The load capacity of the grouted portions of the anchors is checked according to the results discussed in Chapter 4, as well as to Paganoni and D'Ayala (2014).

The dimensioning procedure is based on the idea that a strengthening system can be divided into sub-components to which one type of failure controlled by a single parameter can be associated. These parameters can be used in the formulae prescribed by design codes or developed during the validation process to calculate the capacities of components and hence determine the hierarchy of failure. The values of the design parameters can be obtained via a number of sources: producers' specifications, recommended or limit values provided by codes, and, if any, bespoke laboratory and/or on-site tests.

Table 7-2 exemplifies the break-down for the calculation of the tensile capacity of the dissipative anchoring devices in series with a grouted metallic anchor. Maximum capacity is reached if one of the components fails or when the dissipative device is activated. Further checks can also be performed in terms of displacement and ductility, as it is discussed in the following paragraphs.

Table 7-2: Design of dissipative anchors: parameters that identify the tensile capacity, value range achieved during experimental validation and range prescribed/recommended by design codes

<table>
<tr><th>Performance parameters</th><th>Achievable range</th><th>Expected range</th></tr>
<tr><td>1a) F_{yield}: yielding capacity of hysteretic dissipative device (kN)</td><td>F_{yield}=33 kN
(for hysteretic device of size suitable to coupling with M16 threaded bar)</td><td>$F_{yield}= f_{y,yield} \cdot A_{yield}$ =27.8 kN
(EN 1993-1-1:2005)
$f_{y,yielding}$: yielding strength of steel of hysteretic element
A_{yield}: net cross sectional area of hysteretic element</td></tr>
<tr><td>1b) $F_{//}$: slip-load of frictional dissipative device (kN)</td><td>Range of recorded values at constant level of F⊥, imposed value of perpendicular pressure
<table><tr><th>F⊥</th><th>$F_{// min}$</th><th>$F_{// Max}$</th></tr><tr><td>12.5</td><td>3.25</td><td>14.5</td></tr><tr><td>15</td><td>5.7</td><td>18.3</td></tr><tr><td>17.5</td><td>6.65</td><td>22.4</td></tr></table></td><td>$F_{//}=\Phi \cdot n \cdot F_{\perp}$
Φ: ratio between F⊥ and $F_{//}$
n=2 number of frictional surfaces
F⊥ applied perpendicular pressure.
<table><tr><th>F⊥</th><th>$F_{//}$ (Φ=0.15)</th><th>$F_{//}$ (Φ=0.55)</th></tr><tr><td>12.5</td><td>3.75</td><td>13.75</td></tr><tr><td>15</td><td>4.5</td><td>16.5</td></tr><tr><td>17.5</td><td>5.25</td><td>19.25</td></tr></table></td></tr>
<tr><td>2) F_{steel}: tensile capacity of metallic bar at yielding (kN)
  </td><td>F_{steel}=71 kN
(for M16 threaded bar - values stated by producer)</td><td>$F_{steel}=f_y \cdot A$ =71 kN
(EN 1993-1-1:2005)
f_y: yielding strength of steel
A: net cross sectional area of metallic profile</td></tr>
<tr><td>3) $f_{b,a/b}$: bond strength anchor/binder (MPa) calculated on cylindrical surface of embedded bar
 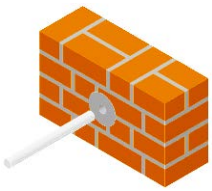 </td><td>$f_{b,a/b}=F_{s/b\ bond}/A_{steel}$=2.07 MPa
(CoV 4% - For pull-out tests of M16 threaded bars from 550 mm long grouted socks)
$F_{s/b\ bond}$: recorded load at failure
$A_{steel}=\pi \cdot l \cdot d_{pitch}$, cylindrical lateral surface
l: embedment length
d_{pitch}: pitch diameter of steel bar</td><td>$f_{b\ a/b}$=
3.4 MPa –BS 5268-2
2 MPa –EN 1996-1-1:2005</td></tr>
<tr><td>4) $f_{b,b/p}$: bond strength binder/parent material (MPa) calculated on cylindrical surface of grouted socket
 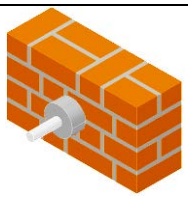 </td><td>$f_{b,b/p}=F_{b/p\ bond}/A_{hole}$
$F_{b/p\ bond}$: recorded load at failure
A_{hole}: inner cylindrical surface of drilled hole of length l
For pull-out tests with vertical load σ_d:</td><td>$f_{b\ b/p}=f_{vk}=f_{vk,0}+0.4\sigma_d$
(EN 1996-1-1:2005)
$f_{vk,0}$ initial shear strength (calculated through experimental results)
σ_d vertical load</td></tr>
</table>

		l (mm)	σ_d (MPa)	$f_{b,b/p}$ (MPa)	σ_d (MPa)	$f_{b,b/p}$ (MPa)
	Brick masonry, f_c=6.7 MPa, f_w=0.7 MPa	350	0.70	0.67 (CoV 8%)	0.7	0.52
			0.07	0.57 (CoV 18%)	0.07	0.27
	Brick masonry f_c=3.1 MPa, f_w=0.33 MPa	220	0.10	0.26 (CoV 34%)	0.10	0.08
			0.05	0.4	0.05	0.06
5) $f_{masonry}$: Shear strength of parent material (MPa) 		This type failure, although expected, did not occur during experimental campaigns			$f_{masonry}=f_{vk}=f_{vk,0}+0.4\sigma_d$ (EN 1996-1-1:2005). In the tested case it would be expected: 0.52 MPa 0.27 MPa The failure surface, A_f, is a truncated cone with smallest base corresponding to the drilled hole, apothem inclined at 45° and height equal to the wall thickness	
6) $f_{masonry}$: Tensile strength of parent material (MPa) 		A "wrench" failure occurs instead of the expected "cone pull-out" failure. Failure surface, A_f, develops along vertical joints. $f_{masonry}=f_w$=0.67 MPa (from wrench test)			No mention about this type of failure has been found in the technical literature or design codes	

The column "Achievable range" of Table 7-2 above collects the values obtained during tests described in Chapter 4 or otherwise performed during the development of the dissipative devices, whilst the column "Expected range" refers to code prescriptions. When these are not available, an analytical model is suggested on the basis of the experience acquired during the development of the research project.

Each sub-component is dimensioned in terms of strength:

7-1)
$$\begin{cases} F_{steel} \geq F_{D,LD} \\ F_{a/b,bond} \vee F_{b.compr} \geq F_{D,LD} \\ F_{b/p,bond} \geq F_{D,LD} \\ F_{masonry} \geq F_{D,LD} \end{cases}$$

The conditions expressed by equation (7-1) can also be written as:

7-2) $$F_B \geq F_{D,LD}$$

where F_B is maximum load capacity of the overall anchor assembly, i.e. the load at point B of the idealised load displacement curves as derived from tests.

For standard anchors without dissipative devices, $F_{D,LD}$ from equations 7-1 and 7-2 should be substituted by $F_{D,SD}$, meaning that anchors are designed for the Severe Damage limit state. As no reduction in seismic excitation as consequence of high ductility can be expected, like in the case of anchors in series with the dissipative devices, the grouted portion of the anchor as well as the steel rod must be able to withstand severe earthquakes.

Current codes also provide for a Near Collapse limit state (2% probability of exceedance in 50 years); the dimensioning of point B of the anchor assembly according to this threshold is advised against, as requirements are stringent and this would either lead to over-dimensioned anchors or result in unfeasible designs. However, some of the tested samples reach a point of maximum displacement, C, and others are even able to develop further stiffness, up to point E, this suggesting that anchors could also be designed for the ultimate limit state. Unfortunately, the anchors' response is scattered, this being the reason for not relying upon any performance point after B for design at Life Safety in the first place. Furthermore, the load increase between point B and C is averagely equal to 3% for pull-out tests and to 16% for cyclic tests, this not being sufficient to withstand a severe earthquake. Conversely, the increase between C and E is roughly equal to the 40% for both pull-out tests and the one case of cyclic test when point E was reached; unfortunately, not all the tested anchors display point E. Therefore, it is suggested that further investigations of specific treatments of the surface between grout and parent material are undertaken to the aim of achieving homogeneous load response of the anchors and be able to fully exploit the load capacity of anchors.

DD CEN/TS 1992:2009 suggests an additional check in terms of strength of the assembly: the yielding load of the steel element needs to be lower of all the other failure loads associated to the concrete substratum by a factor of 0.6. This should ensure the ductility of anchors in seismic prone areas. However, the design deriving from such requirement might be counterproductive: indeed, the bond capacity between the steel bar and the substratum decreases after yielding as a consequence of the Poisson effect, as discussed by Lowes (1999) on the basis of several authors' research work. This is not a problem for the tested type of anchors, as the bearing mechanism of the rear plate, when this is designed to this purpose, is sufficient to prevent the steel from sliding out of the grouted cavity.

Nevertheless, if the equation suggested by DD CEN/TS was applied to masonry anchors, it would lead to extremely small sized steel elements in respect to the rest of the assembly. Whereas in concrete maximum loads for substratum failures have values comparable with steel yielding load, this is not the case for an anchor in a masonry

substratum, where loads associated to failures of the parent material are several orders of magnitude smaller than steel yielding.

Therefore, the formula is instead written as:

7-3) $$0.6 \cdot F_{b,compr} \geq F_{steel}$$

By complying with equation (7-3) one ensures that the bearing mechanism of the rear plate can prevent the sliding of the metallic bar from the grouted socket even in case of yielding of the anchor rod.

Additionally, one needs to ensure that cracking of the anchor assembly is reduced in case of frequent seismic events, so that continuous occupancy can be granted. Therefore, one should check that the design load at the limit state of Damage Limitation (probability of exceedance of 20% in 50 years according to EN 1998-3:2004) is lower than the load of anchors at the point of first cracking, A.

7-4) $$F_A \geq F_{D,DL}$$

For Damage Limitation, anchors should also comply with requirements imposed on interstorey drift. The chosen value of maximum allowable drift, d_r=0.003, for damage limitation is taken from Circolare 02/02/2009 N. 617 (2009) that, on the contrary of EN 1998:2004, specifically refers to ordinary masonry buildings when stating drift limits. This limit is also in line with the expected drift stated in FEMA 356 (2000) for unreinforced masonry buildings at the limit state of Immediate Occupancy. The drift is decreased by the reduction factor ν=0.4, which is taken from EN 1998:2004 and accounts for the fact that devices are designed to be used in heritage structures, which fall in the importance category III of Eurocode 8 (EN 1998:2004).

It is therefore:

7-5) $$d_r = d_{UD} + \Delta_A \leq 0.003 \cdot h / \nu = 0.003 \cdot (3000mm) / 0.4 = 22.5mm$$

where:

d_{UD}: interstorey drift of the building in its undamaged configuration, i.e. before cracking of corner connections occurs. Indeed it is assumed that anchors, designed according to the discussed procedure, are able to prevent any major cracking, thus justifying the assumption of undamaged configuration. However, while calculating d_{UD}, one must account for the higher stiffness of the structure as consequence of anchors in respect to the unreinforced configuration.

Δ_A: the displacement recorded in the anchors at point A, first damage, in the idealised performance curves. Δ_A represents the relative displacement of the panel perpendicular to the seismic action in respect to the other walls as far as permitted by the anchor at the limit state of damage limitation.

h: interstorey height, or vertical distance of installation of anchors. A standard distance of 3 meters has been assumed in the calculations, but anchors might need to be spaced more closely on the height of the wall to prevent substratum failures.

Ideally the sizing of a strengthening element for seismic protection should be mainly driven by requirements expressed in terms of displacement, rather than rely on a capacity design, as done above. However, anchors present a highly scattered performance, as it can be seen by calculating the ductility as the ratio between displacements at point B/C and point A (Table 7-3). Therefore, similarly to the case of load capacity at NC limit state, the variability in performance prevents the full exploitation of the anchors' potential, unless a system to remedy such pitfall was designed and implemented.

Table 7-3 Ductility of standard anchors

	Point B		Point C	
Type of test	Average	Standard deviation	Average	Standard deviation
Pull-out	5.57	3.37	9.16	47.9
Cyclic	7.05	2.78	17.25	8.69

A hierarchical sequence for the overall design procedure is given in the diagram of Fig. 7-2 (shown at the end of this section), which shows the iterative process that should be followed when sizing an anchor for a specific case study and set the priority to constrain the design.

After this first phase of capacity design, the performance of the dissipative elements is defined. Devices are designed to start dissipating energy for the level of seismic action that initiates cracking for overturning mechanism and punch/pull-out damage to the standard anchors (G2). For the yielding device this means reaching the non-linear field before F_{G2} is attained, whereas the frictional devices start dissipating energy as soon as sliding is activated, thanks to the zero stiffness branch of the dissipative device. It is therefore:

7-6) $$F_{yield} < F_{G2} \quad \text{or} \quad F_{//} \leq F_{G2}$$

The design of the dissipative devices is completed by checking that the drift between two anchor levels falls within the limits imposed by codes for the different limit states. This is done by calculating the total displacement at the location of each anchor head, which is a function of the structure displacement plus the relative displacement of the devices.

The relative displacement of the devices is computed assuming that the inertial energy of the portion of masonry restrained by the anchor is dissipated through the device cycles, which is represented by the area underlying the load-displacement curve of the device.

As the shape of cycles is known from the experimental characterisation and after having chosen the activation threshold of devices, displacement is univocally determined.

Inertial energy is chosen for dimensioning devices instead of, for instance, strain energy, as such methodology is deemed more appropriate for masonry. Indeed, according Griffith's theory (1921) one could calculate the strain energy released through the formation of the crack at the corner joint and assume that the dissipative devices should dissipate such amount of energy. However, the energy released by the formation of the crack is fairly reduced in the case of masonry, which has a fragile behaviour under tension; even more so under the hypothesis of an existing crack, such as that of the case study of S. Giuseppe dei Minimi, where the seismic excitation would cause out-of-plane movement without a considerable formation of new cracks.

The use of the inertial energy allows the anchoring devices to dissipate a larger amount of energy, independently from the initial condition of the joint, i.e. undamaged or already damaged.

Devices also need to be designed so that they can offer additional capacity at NC limit state, so as to avoid failure:

7-7) $$\Delta_{NC} < \Delta_{\max}$$

Where Δ_{max} represents:

- For yielding devices, the threshold of the 5% elongation, beyond which devices can still offer extra capacity both in terms of displacement and load capacity;
- For frictional devices, the end of their run. This ensures a safety factory of 10 on devices' load capacity.

After completing the design of the dissipative elements, the tentative design of the strength-only parts of the anchors is validated by checking that the reduction in demand due to the higher ductility and higher damping provided by the dissipative devices is such that the anchor can also withstand levels of seismic forces higher than DL.

The reduction of seismic forces as consequence of dissipative elements is for instance taken into account by FEMA 356 (2000). Indeed, the American code requires that structural elements can withstand a pseudo lateral load, V:

7-8) $$V = C_1 C_2 C_3 C_m S_a W$$

where S_a is the spectral acceleration and W the effective seismic load of the structures.

Whereas the reader can refer to the original document for the explanation of the coefficients in the formula, it is important to know that S_a is reduced in function of the damping of the strengthened structure, which is calculated as:

$$\beta_{eff} = \beta + \frac{\sum_j W_j}{4\pi W_k} \quad \text{7-9)}$$

where β is the damping in the structural system and shall be set equal to 0.05, W_j is the work done by the j^{th} device in one complete cycle corresponding to floor displacements δ_i (the summation extends over all the j devices), and W_k is the maximum strain energy in the structure, determined as:

$$W_k = \frac{1}{2}\sum_i F_i \delta_i \quad \text{7-10)}$$

where F_i is the inertia force at i^{th} floor level and the summation extends over all floor levels.

While new buildings are designed so that their capacity can match an expected level of seismic demand, in the case of historic structures one can increase the dissipated energy until the demand is lower than the capacity of the structure, as determined on the basis of the existing geometry and materials.

Accordingly, the procedure is reiterated until the capacity design of non-dissipative parts is satisfactory as much as the performance design of the dissipative elements.

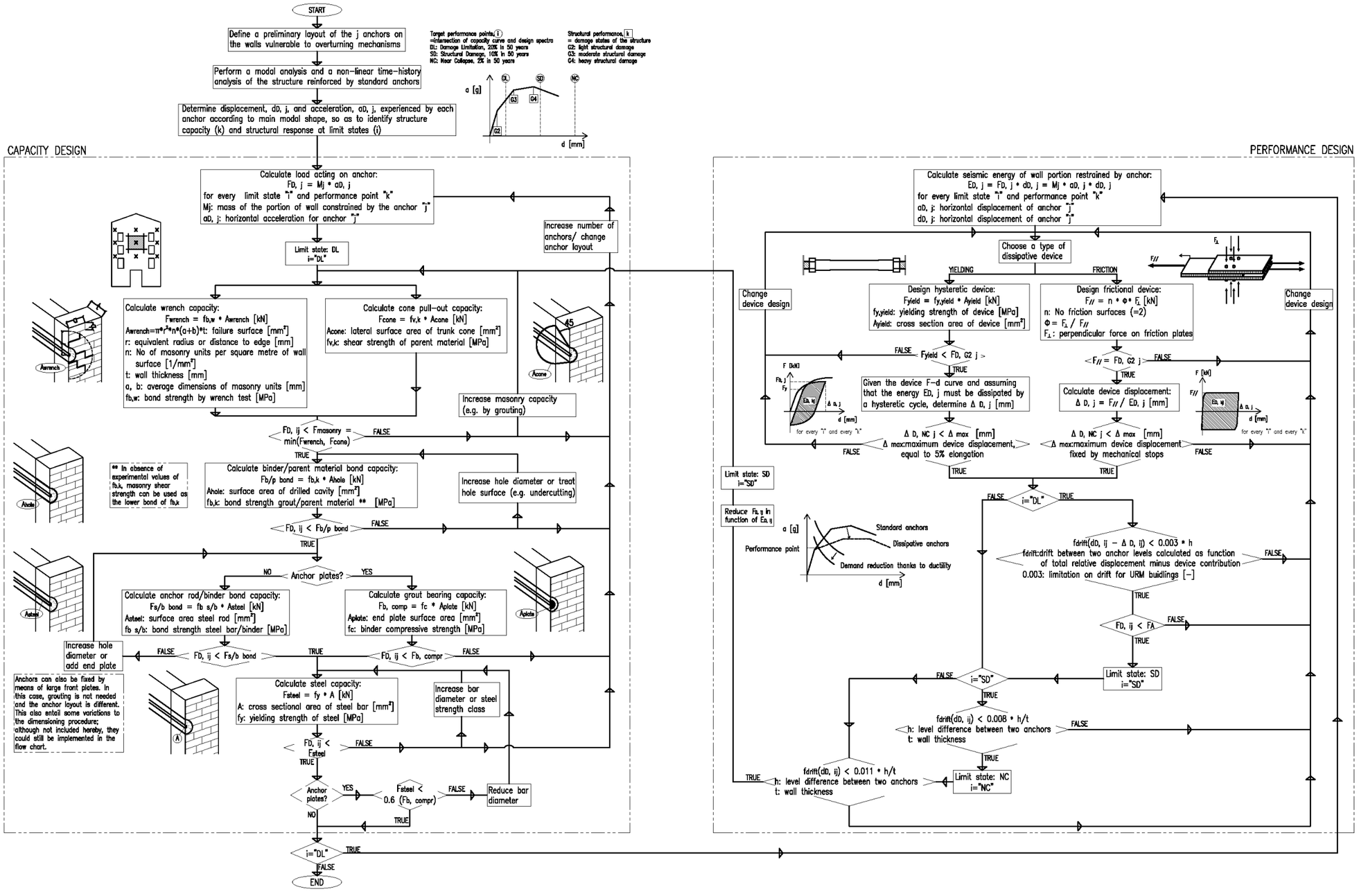

Fig. 7-2: Flowchart of the design for metallic anchors grouted in a historic masonry substratum

7.2 EXAMPLE OF IMPLEMENTATION OF THE DESIGN PROCEDURE

An example of how the procedure is applied is illustrated herein by working on the example of S. Giuseppe dei Minimi, L'Aquila; the goal is to repair the overturning damage of the façade by using either standard or dissipative anchors, and to upgrade the performance of the façade macroelement in line with the design codes referenced above.

The very first step of the procedure consists in the choice of the input to be used for the non-linear modelling of the structure. Both the Eurocode (EN 1998:2005) and the Italian code (DM 14-01-2008) allow for the use of recorded earthquakes, as long as they are scaled so as to approximate the relevant design spectra. Accordingly, the same AQV signal used during the experimental campaign and the computational validation is scaled (Fig. 7-3) to match the elastic design spectra for the prescribed limit states.

The design spectra shown in Fig. 7-3 are built according to the instructions contained in the Italian technical code (DM 14-01-2008), which falls in line with the Eurocode 8, but contains specific guidelines concerning the Italian territory.

The expected building life is assumed to be 100 years and the structure Class II, namely of public utility, so that the reference period for the design seismic input is of 150 years. Soil class is A and topography T2.

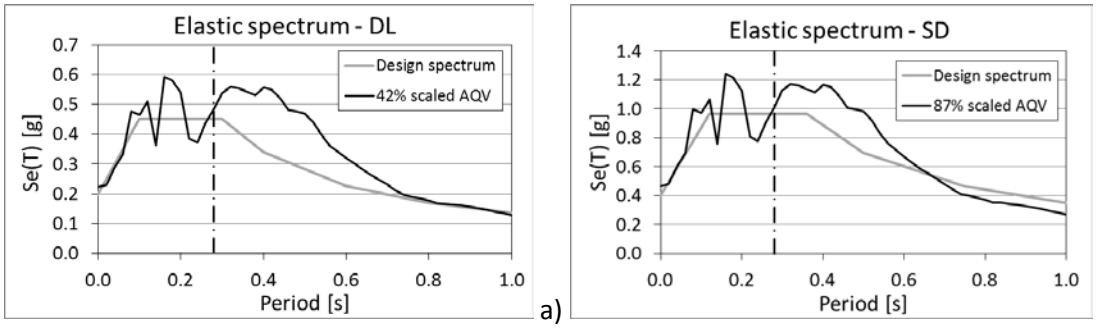

Fig. 7-3: Scaling of the AQV earthquake signal according to the design spectra for (a) Damage Limitation and (b) Severe Damage limit states

In Fig. 7-3, the first natural period of the façade of S. Giuseppe, as recorded by the University of Padua during the on-site dynamic characterisation, is also plotted. This period corresponds to the out-of-plane mode of the already damaged façade, namely the most interesting mode for the design of the anchors, which is therefore taken into account when first defining the anchor layout, as it will be discussed in the following.

The damaged unreinforced FEM of S. Giuseppe undergoes the dynamic signal scaled for Severe Damage limit state, so as to provide an initial term of comparison. The unconstrained façade is able to withstand the earthquake prescribed by codes without collapsing, as indeed maximum principal stresses remain within the allowable range, even at peak acceleration (Fig. 7-4a). Nevertheless, the plot of the ratio between the

displacement at the top of the gable and the base shear in the out-of-plane direction shows that the façade experiences out-of-plane displacements beyond the threshold of the allowable drift prescribed for SD limit state (Fig. 7-4b).

Indeed, the total height of the façade is 14.74 m and its thickness one meter. According to FEMA 356, the drift limit at SD should be equal to the 0.8% of the ratio between interstorey height and wall thickness. As the façade is unrestrained and no horizontal structure is present along its height, the interstorey drift is in fact the drift calculated over the whole façade. The maximum allowable value would therefore be equal to 118 mm, while the FE façade is experiencing a maximum displacement of almost 125 mm (Fig. 7-4b).

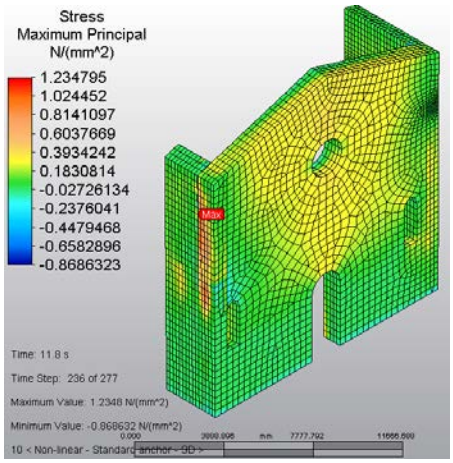

a)

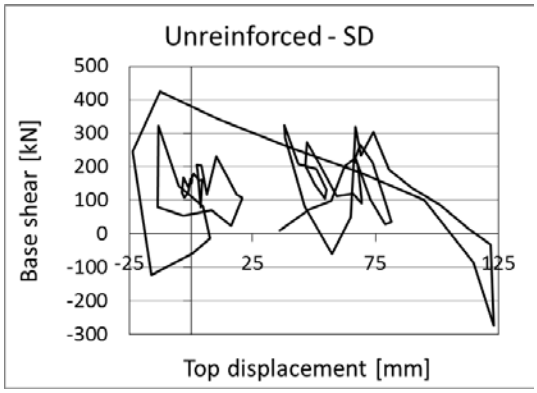

b)

Fig. 7-4: Unreinforced, damage FE of S. Giuseppe, SD limit state – a) Maximum principal stress at peak acceleration; b) load-displacement curve

The difference between maximum allowable and experienced drift is not particularly large; however, as it has already been noted in Chapter 6, should the damaged façade undergo an earthquake with the same intensity as that recorded in L'Aquila in 2009, which had intensity higher than the prescribed SD spectrum, collapse would eventually occur by forward tilting of the façade.

One further element that motivates a strengthening intervention is the considerable out-of-plumb of the front wall; although this is not represented in the computational model, the state of the building after seismic damage is in fact calls for precautionary measures to avoid that the equilibrium of the façade panel is compromised by tremors or long-term phenomena, like ground settlements.

At first, the façade is strengthened by means of standard anchors, placed at regular distance along the disconnected height of the quoins; the goal is to investigate whether this would be an acceptable solution and provide a term of comparison in terms of efficiency and viability with the dissipative anchoring devices.

In the flowchart of Fig. 7-2, the strength-only part of the anchor is firstly designed for Damage Limitation limit state, as the dissipative devices, thanks to their ductility, can

be set up in order to limit the load demand on the anchorage heads; as such, the required load capacity, and hence geometry of the strength-only parts is minimised. However, if only standard anchors are implemented in the strengthening intervention, no reduction in the seismic demand is to be expected and one can proceed immediately to design the strength-only portion of the anchorage for Severe Damage limit state.

An initial layout of the anchors must be defined before proceeding to the design. As discussed in Chapter 5, on-site measurements indicate that each anchor bears a portion of masonry with a shape of a truncated cone with a long side in the range of 1/2 meters, this being then the maximum distance centre to centre at which anchors should be installed. A distance of 1.2 m is taken as reference and the ratio demand/capacity of the various components of the strength-only part of the anchor is checked according to "Capacity Design" part of the design procedure of Fig. 7-2. Checks are carried out on the basis of the force experienced by the most loaded anchor, which is expected to be the one at the top of the quoin as consequence of the deformation shape of the first natural model, i.e. the out-of-plane mode of the façade.

The force experienced by the anchor is estimated by adapting the procedure for the numerical seismic assessment by equivalent static loading (DM 14-01-2008), namely by applying the formulae:

7-11) $$F_i = F_h \, z_i W_i \Big/ \sum_j z_j W_j$$

7-12) $$F_h = S_d(T_1) \cdot W \cdot \frac{\lambda}{g}$$

where F_i is the load to be applied to the mass "i", i.e. to the mass of the portion of façade constrained by the topmost anchor, W_i and W_j are the weights of the masses "i" and "j", z_i and z_j are the levels of the masses "i" and "j" from the floor. $S_d(T_1)$ is the spectral ordinate of the design spectrum, W is the total weight of the building (in this case of the façade), λ is a coefficient, in this case equal to 1, and g is the acceleration of gravity.

Accordingly:

7-13) $$F_{h,SD} = 0.96g \cdot 4022kN \cdot \frac{1}{g} = 3861.22kN$$

where $S_d(T_1)$ is taken equal to the spectral ordinate at Severe Damage limit state, while W, the overall weight of the façade, is derived from the FEM, i.e. in line with the assumptions regarding the densities of the construction materials and the geometry surveyed by the University of Padua and reproduced by the numerical model.

7-14) $$F_{i,SD} = 3861.22kN \cdot \frac{18.48kN \cdot 12m}{26777.60kNm} = 31.98kN$$

where the sum at denominator is calculated by multiplying the weights of the parts of the façade by the levels of their centres of mass. Assuming a distance centre to centre of the anchors of 1.2 m, the topmost anchor is located at 12 m from the ground.

The force $F_{i,SD}$ is multiplied by a factor of safety of 1.5, so that finally the load demand on the anchor is equal to 47.97 kN. This value is checked against the capacity of the anchor components as shown in Table 7-4.

Table 7-4: Capacity design of the strength-only parts of the anchor – Iteration No 1 for Significant Damage

Type of failure	**Anchor properties**	**Capacity**	**>$F_{Di,SD}$=47.97 kN?**
Wrench	f_t=0.6 MPa A_{wrench}=7.7 m^2 (block size 0.5x0.2 m) γ_M=1.5	$F_{wrench,D}=f_t \cdot A_{wrench}/\gamma_M$= **3080 kN**	YES
Cone pull-out	$f_{masonry}=f_{vk}=f_{vk,0}+0.4\sigma_d$= 0.09 MPa+0.4$\sigma_d$= 0.12 MPa A_{cone}=1.69 m^2 γ_M=1.5	$F_{cone,D}=f_{masonry} \cdot A_{cone}/\gamma_M$= **135 kN**	YES
Bond failure	$f_{b\ b/p}=f_{vk}=f_{vk,0}+0.4\sigma_d$= 0.09 MPa+0.4$\sigma_d$= 0.12 MPa A_{hole}=0.25 m^2 (Φ=80 mm, l=1 m) γ_M=1.5	$F_{b/p\ bond,D}=f_{b,b/p} \cdot A_{hole}/\gamma_M$= **20.1 kN**	**NO!**
Grout crushing	f_c=50 MPa A_{plate}=2827 mm^2 (Φ=60mm) γ_M=1.35	$F_{b,compr,D}=f_c \cdot A_{plate}/\gamma_M$= **105 kN**	YES
Rod yielding	f_y=450 MPa A=156.7 mm^2 (M16) γ_M=1.1	$F_{steel,D}=f_y \cdot A/\gamma_M$=**64 kN**	YES
Ductile failure?	$F_{b,compr,D}$=105 kN $F_{steel,D}$=64 kN	$F_{steel,D}/F_{b,compr,D}$=**0.6**	OK

As clearly visible from the table, the chosen layout and dimensions/properties of the standard anchors do not satisfy the check on the bond capacity at the interface grout/parent material. It is therefore necessary to change the layout/properties and reiterate the procedure as long as all checks are satisfied.

For the second iteration, it is chosen to place the anchors with a smaller distance centre to centre. This is done in light of the fact that, as widely discussed in the previous chapters, the bond capacity at the interface grout/masonry presents a large scattering in the experimentally recorded values, so that a conservative approach must

be taken as long as further testing campaign prove that the treatment of the inner surface of the drilling hole is able to ensure higher bond capacity.

In the revised layout, anchors have a distance centre to centre of 0.55 m. The whole procedure, including the calculations of equations 7-13 and 7-14, is repeated. The design load demand is hence 19.72 kN.

Table 7-5: Capacity design of the strength-only parts of the anchor – Iteration No 2 for Significant Damage

Type of failure	**Anchor properties**	**Capacity**	**>$F_{Di,SD}$=19.72 kN?**
Bond failure	$f_{b\ b/p}=f_{vk}=f_{vk,0}+0.4\sigma_d=$ 0.09 MPa+0.4σ_d= 0.12 MPa A_{hole}=0.25 m^2 (Φ=80 mm, l=1 m) γ_M=1.5	$F_{b/p\ bond,D}=f_{b,b/p}\cdot A_{hole}/\gamma_M=$ **20.1 kN**	YES

All checks on the load capacity of the anchor components are now satisfied (Table 7-5). The anchor layout is then implemented in the FE models and undergoes the seismic excitation of the input signal AQV scaled for Severe Damage and Damage Limitation.

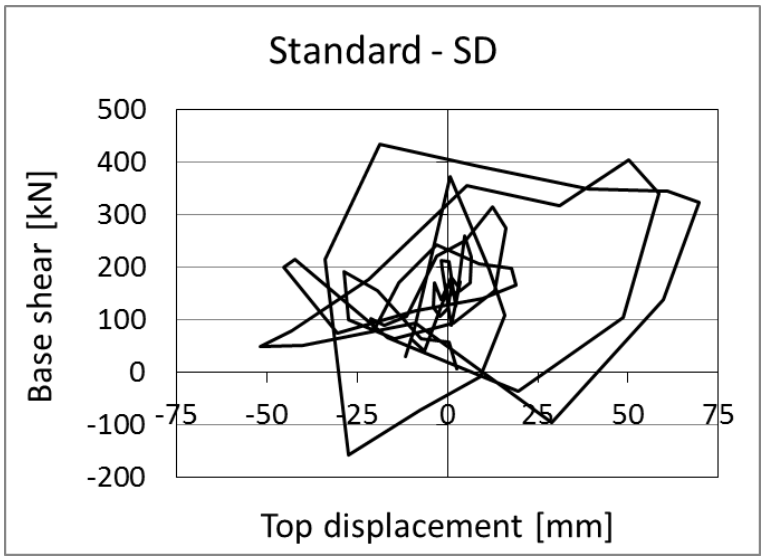

Fig. 7-5: FEM reinforced by standard anchors – Load-displacement curve at SD limit state

A first remarkable, and expected, effect of the anchors on the building response is the considerable reduction in experienced out-of-plane displacements, which is the logical consequence of the lateral constraint of the façade by means of the anchors (Fig. 7-5).

On the other hand, the acceleration experienced by the gable element is higher than in the case of the unreinforced, damaged façade (Fig. 7-6). Indeed, when the façade becomes constrained on the sides up to the top level of the side walls, the gable elements, which is quite flexible, remains vulnerable to the seismic excitation in larger

measure than in the unreinforced situation, where the deformation mode is characterised by almost linearly increasing outward displacements along the whole height of the façade.

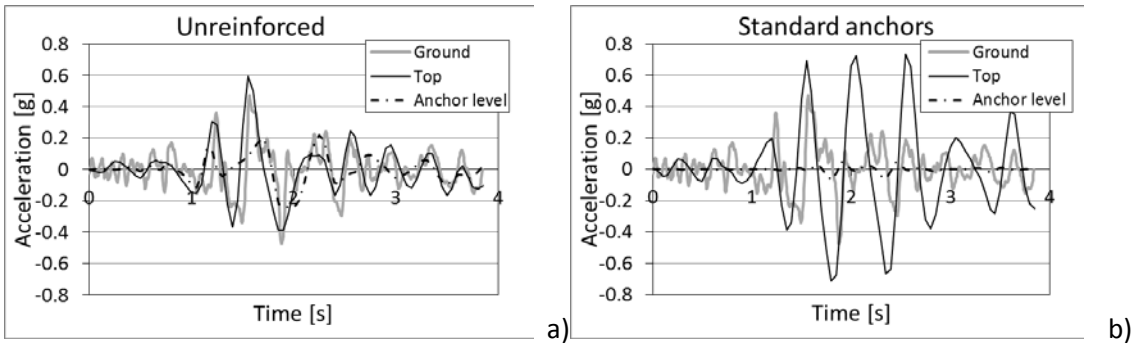

Fig. 7-6: Acceleration time histories at SD limit state for: a) unreinforced FEM, b) FEM reinforced by standard anchors

In terms of feasibility of the strengthening intervention by the use of standard anchor and of compliance with the checks of the design procedure, it is possible to say that the standard anchors provide a sufficient level of constraint so that the drift between the levels of the topmost anchor and the top of the gable at Significant Damage remains in the limits imposed by the codes (Fig. 7-7).

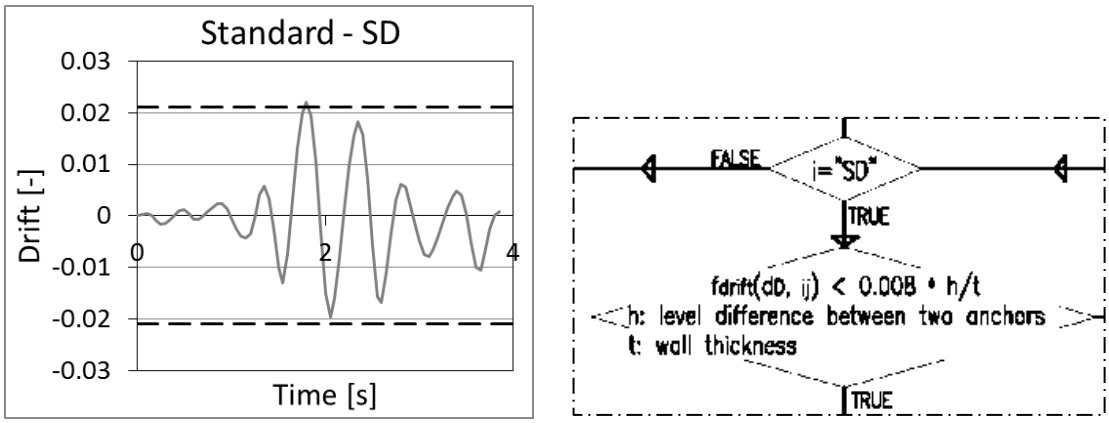

Fig. 7-7: Drift time history for FEM strengthened by standard anchors

The steel rods of the standard anchors remain in the elastic field (Fig. 7-8a), except at one single position where the steel profile experiences stresses slightly higher than yielding. This occurs in compression, but only for one loading cycle, meaning that the risk of buckling is reduced.

It is worth pointing out that at one position the stress at the head of the anchor also goes beyond the threshold that defines the equivalent pull-out capacity at the interface grouted element/masonry (Fig. 7-8b); this means that although standard anchors are able to satisfy the checks of the design procedure at Significant Damage, some damage will still occur at the head of one anchorage and in one steel profile.

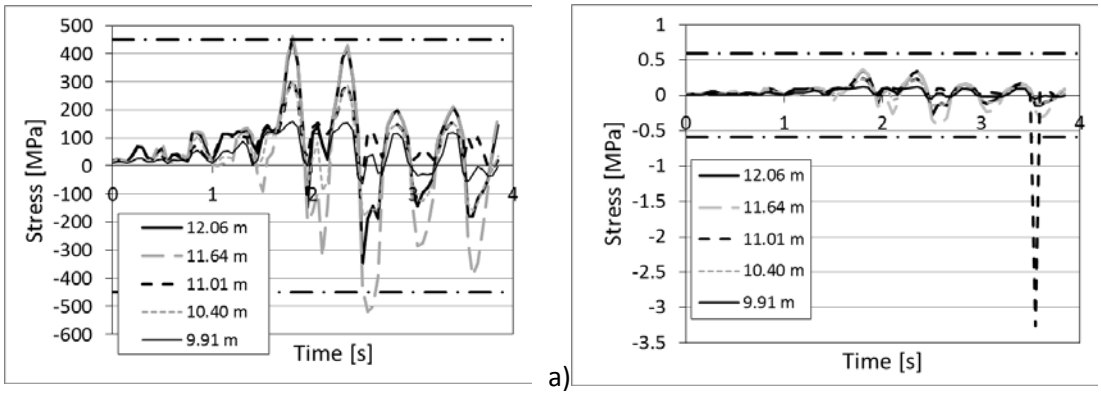

Fig. 7-8: Stress time histories at the levels of the 5 topmost standard anchors: a) steel rod tensile stress; b) equivalent tensile stress in the grouted element embedded in the quoin

This might still be considered acceptable, also because the spacing between anchors has already been notably reduced in respect to the first iteration of the procedure, meaning that placing more closely spaced anchors with the purpose of reducing the load demand might not be a viable option when pursuing a low-impact intervention.

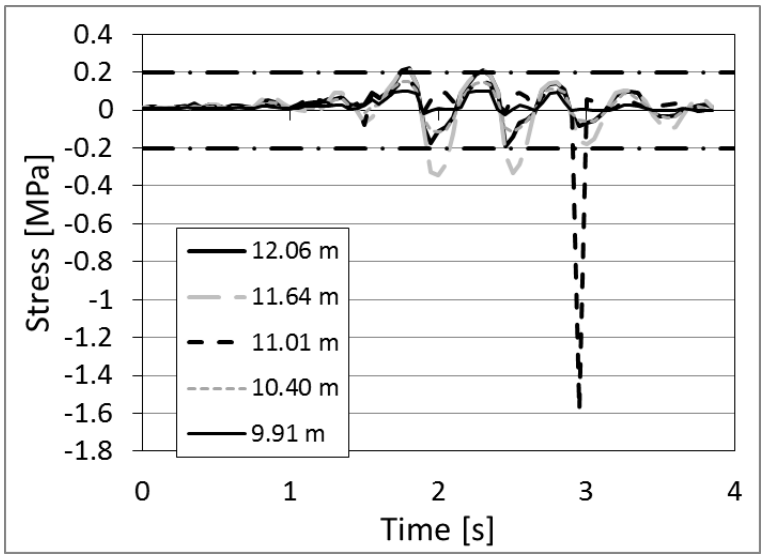

Fig. 7-9: Equivalent tensile stress in the grouted element embedded in the quoin of the 5 topmost standard anchors – Damage Limitation limit state

At the limit state of Damage Limitation (Fig. 7-9), a similar issue arises: the stress experienced by the head of one anchor is higher than the stress at the point A, i.e. point of first cracking of the idealised load-displacement curve of standard anchors undergoing pull-out loading; this means that for this level of dynamic action one of the anchor heads is already beyond the linear field.

Furthermore, when looking at the drift between the top of the gable and the topmost anchor, this is above the limit prescribed by codes: the level difference between the two points is indeed equal to 2.7 m, so that the difference in out-of-plane

displacements between the two points should be lower than 8 mm, which is not the case (Fig. 7-10).

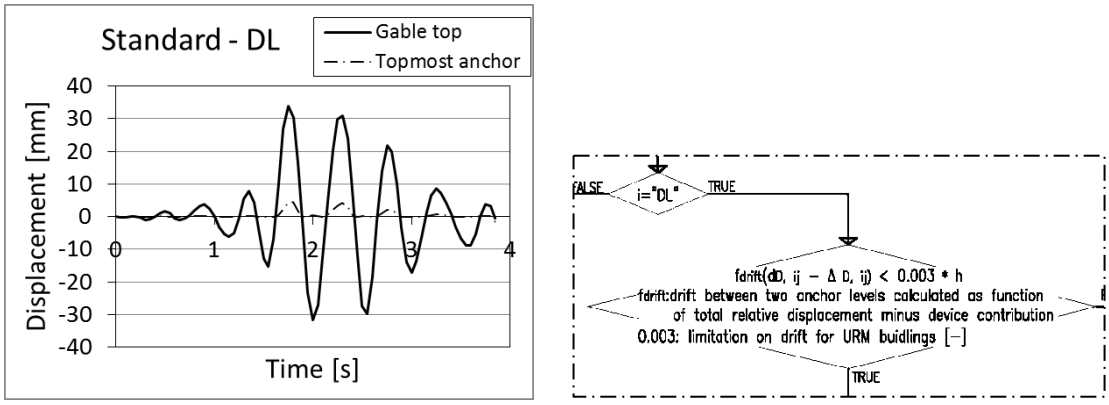

Fig. 7-10: Displacement time histories of the FEM strengthened by standard anchors at Damage Limitation

In summary, the standard anchors might be an option for the strengthening of structures, but as discussed throughout the dissertation they present a number of pitfalls that are not easily remediable, as proved above. One could still consider the strengthened intervention discussed above sufficiently satisfactory, as long as the façade gable is also restrained so as to limit the outward tilting for both low and high intensity horizontal loading. Nevertheless, it is highly desirable to reduce the number of implemented anchors, minimise the damage to the parent material and achieve a better performance in terms of drifts. This is done by implementing the dissipative device.

First of all, the load capacity of the components of the strength-only portion of the anchor can be reduced. Indeed, the parts are dimensioned for the load demand at Damage Limitation.

It is therefore:

7-15) $$F_{h,DL} = S_d(T_1) \cdot W \cdot \frac{1}{g} = 0.45g \cdot 4022kN \frac{1}{g} = 1809.9kN$$

7-16) $$F_{i,DL} = F_{h,SD} \, z_i W_i \Big/ \sum_j z_j W_j = 1809.9kN \cdot \frac{18.48kN \cdot 12m}{26777.60kNm} = 15kN$$

where the distance centre to centre between anchors has been taken equal to 1.2m.

The checks of the anchor components according to the capacity design procedure are shown in Table 7-6. As they are all satisfied, the number of anchors implemented in the model can be reduced to a half of the standard anchors.

Table 7-6: Capacity design of the strength-only parts of the anchor – Iteration No 1 for Damage Limitation

Type of failure	**Anchor properties**	**Capacity**	**>$F_{Di,SD}$=15 kN?**
Wrench	f_t=0.6 MPa A_{wrench}=7.7 m^2 (block size 0.5x0.2 m)	$F_{wrench,D}=f_t \cdot A_{wrench}$= **4620 kN**	YES
Cone pull-out	$f_{masonry}=f_{vk}=f_{vk,0}+0.4\sigma_d$= 0.09 MPa+0.4$\sigma_d$= 0.12 MPa A_{cone}=1.69 m^2	$F_{cone,D}=f_{masonry} \cdot A_{cone}$= **203 kN**	YES
Bond failure	$f_{b\ b/p}=f_{vk}=f_{vk,0}+0.4\sigma_d$= 0.09 MPa+0.4$\sigma_d$= 0.12 MPa A_{hole}=0.25 m^2 (Φ=80 mm, l=1 m)	$F_{b/p\ bond,D}=f_{b,b/p} \cdot A_{hole}$= **30 kN**	YES
Grout crushing	f_c=50 MPa A_{plate}=2827 mm^2 (Φ=60mm)	$F_{b,compr,D}=f_c \cdot A_{plate}/\gamma_M$= **141 kN**	YES
Rod yielding	f_y=450 MPa A=156.7 mm^2 (M16)	$F_{steel,D}=f_y \cdot A/\gamma_M$=**70.5 kN**	YES

After dimensioning the strength-only part of the anchors, the load-displacement cycles, and hence the mechanical properties, of the dissipative devices must be defined.

This is done by looking at the energy that should be dissipated by hysteresis/frictional cycles, which is calculated as the area included in the curve expressing the ratio between the load generated by the mass acting on one anchor under horizontal acceleration and the out-of-plane displacement of the façade at the point where the anchor is installed.

Fig. 7-11 shows, for instance, the energy pertaining to the topmost standard anchor in the layout designed in the previous paragraphs.

The energy demand is fairly small when compared to the energy that the device prototypes can dissipate, about one hundredth, even considering that the anchors in series with the dissipative devices are further apart, so that the tributary mass is larger than in the case of the standard anchor of Fig. 7-11. Therefore, the same properties of the devices tested and modelled so far are maintained in the FE models.

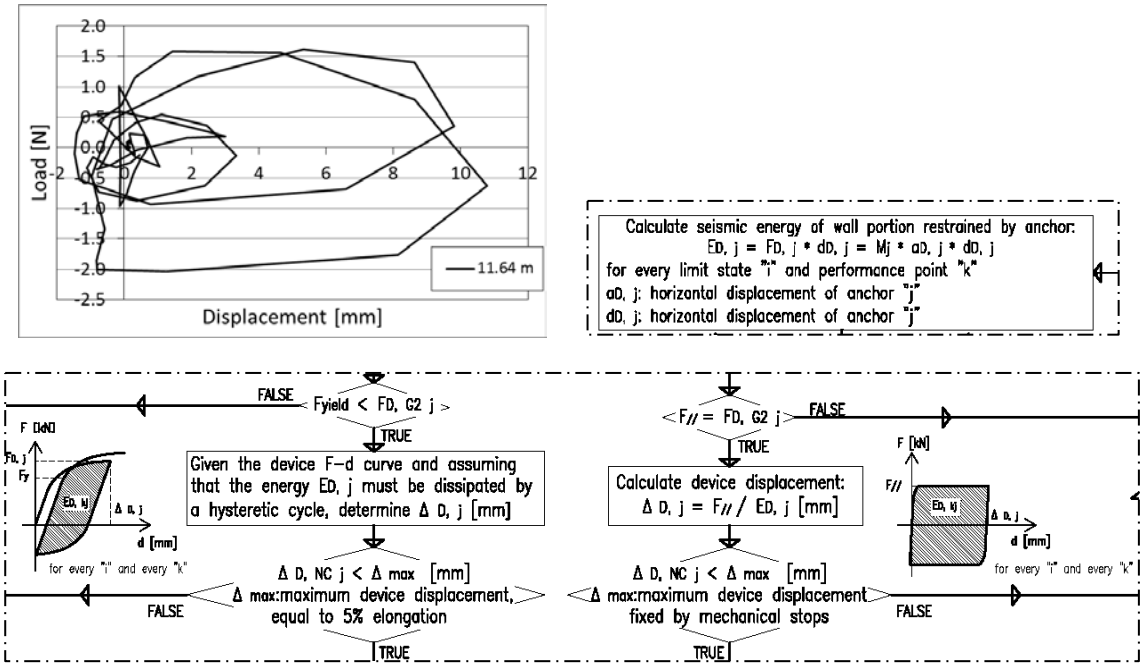

Fig. 7-11: Energy to be dissipated by the anchoring devices

The chosen devices are:

- Hysteretic device with a yielding load of 40 kN;
- Frictional devices with sliding load $F_{//}$=16 kN and maximum allowed displacements of ±20 mm. Stops are modelled by a coupling element, which is activated when its length becomes larger than 20 mm and has the same stiffness as the steel rod (210 GPa.) This represents the sliding blade reaching the end of the run and the frictional anchor behaving again like a standard anchor.

When the FEMs featuring one or the other typology of devices placed at 1.2 m distance undergo the dynamic input for SD limit state, the analyses fail to converge (Fig. 7-12).

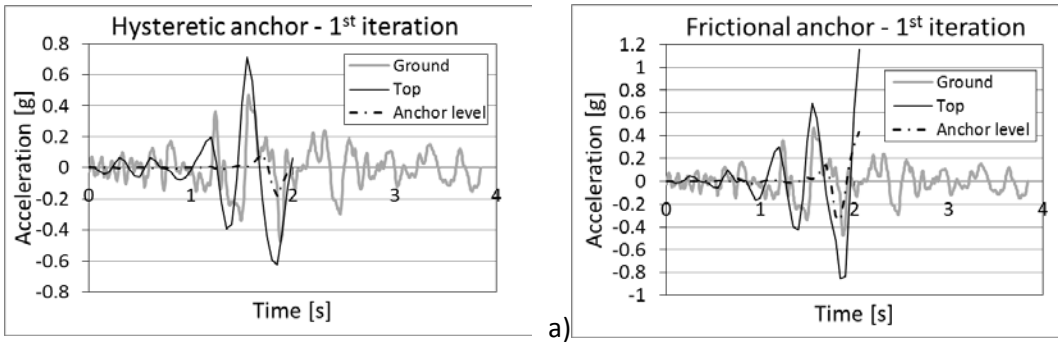

Fig. 7-12: Acceleration time histories at Severe Damage of FEMs strengthened by: a) hysteretic anchor, b) frictional anchor

In the case of the hysteretic devices the problem lays in the hardening of the device, which reaches the maximum allowable stress before experiencing maximum strains (Fig. 7-13).

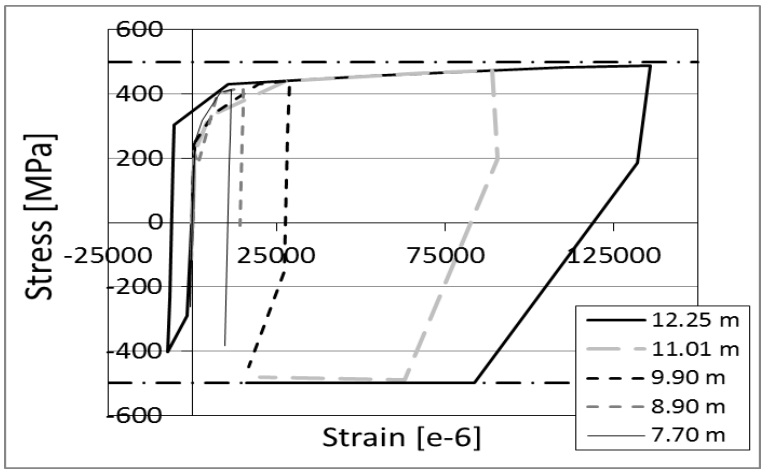

Fig. 7-13: Stress-strain cycles of hysteretic devices at SD - 1st iteration

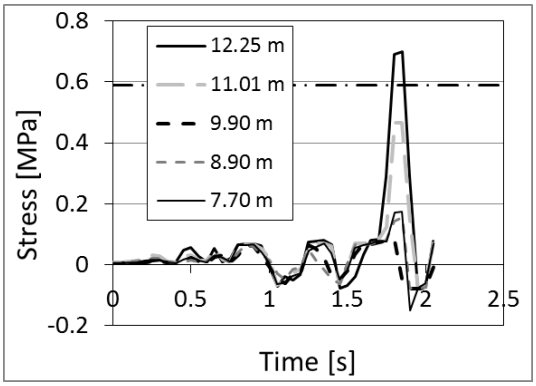

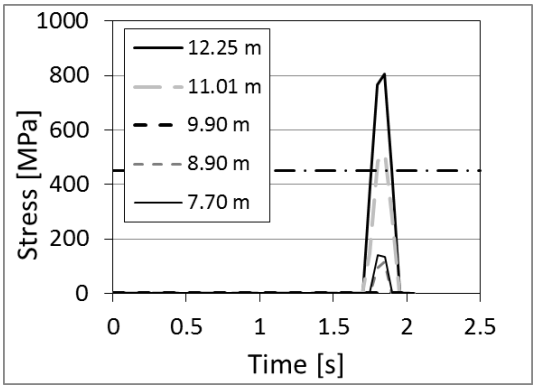

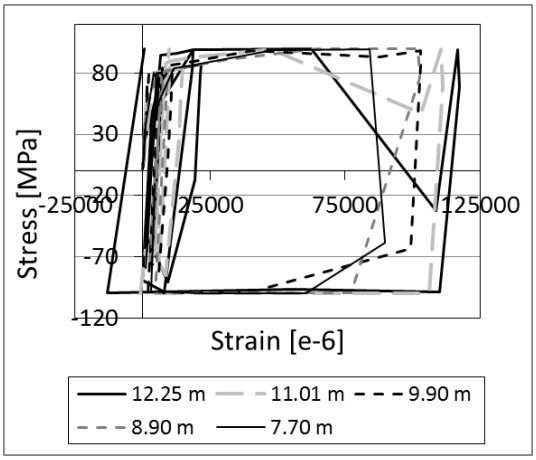

Fig. 7-14: FEM strengthened by frictional devices at SD limit state: a) equivalent tensile stress at the head of the anchorage, b) tensile stress in the stops of the frictional device, c) stress-strain cycles of the frictional devices

In the case of the frictional devices, the problem is that the sliding blade reaches the end of the run. This generates high stresses both in the anchor rod and in the head of

the anchorage, so that yielding of the rod and pull-out damage occur in the two topmost anchors (Fig. 7-14a and b). At the same time the frictional cycles cannot be fully exploited as they are “interrupted” by the blade reaching the end of its run (Fig. 7-14c).

In the case of the hysteretic devices the attempts done to improve the performance by increasing the cross sectional area of the dissipative element, and hence the yielding load of the device, do not bring to the desired results. Indeed, one would want to tune the yielding load so that the devices do not harden, and hence fail, as quickly, but in fact, an increase in the yielding load does not completely solve the problem, especially when one also looks at the performance of the revised devices at DL limit state. The performance for stiffer yielding devices, with a spacing double to that of the standard anchors, lead to increased drift, beyond acceptable limits. The only solution is therefore to use the least stiff devices, as done so far, with the same spacing as the standard anchors (0.55 m c/c).

In the case of the frictional devices, thanks to the adaptability of the friction mechanism, its ductility and larger capacity of dissipating energy, it is possible to find a set-up of the device that works without modifying the spacing of the anchors.

Indeed, for the second iteration the frictional devices are set-up to have a sliding load $F_{//}$=35 kN and no limitation on the run of the sliding blade. It is also assumed that the devices have a perfect frictional behaviour, namely that no increase in stiffness as consequence of higher perpendicular pressure on the frictional plates and of mechanical locking arises.

With the second set-up, analyses converge. The performance of the hysteretic anchors in terms of drift and displacements becomes very similar to that of standard anchors, both at Severe Damage and Damage Limitation (Fig. 7-15a and Fig. 7-16). Conversely, frictional anchors (Fig. 7-15b and Fig. 7-16) are able to considerable limit drifts at both limit states.

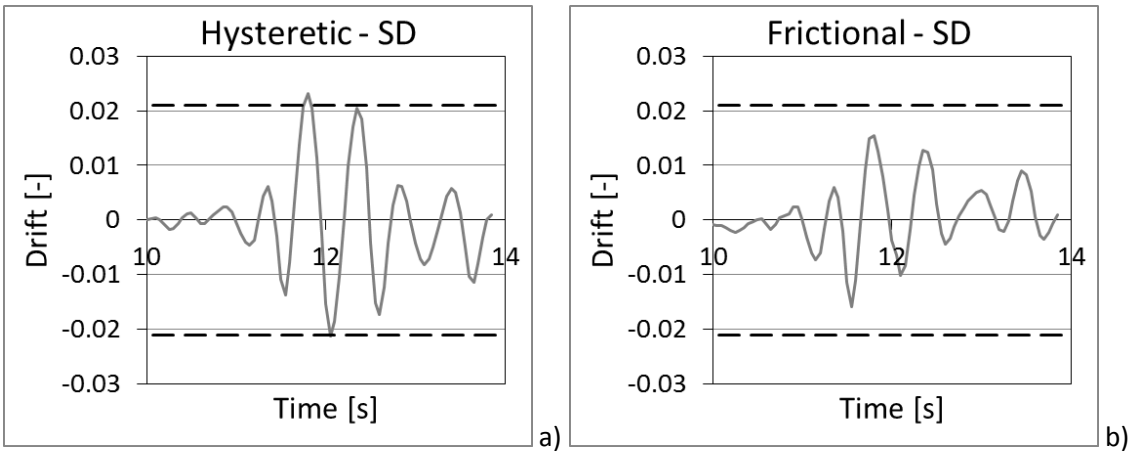

Fig. 7-15: Drift time histories at SD - FEM strengthened by: a) hysteretical devices; b) frictional devices

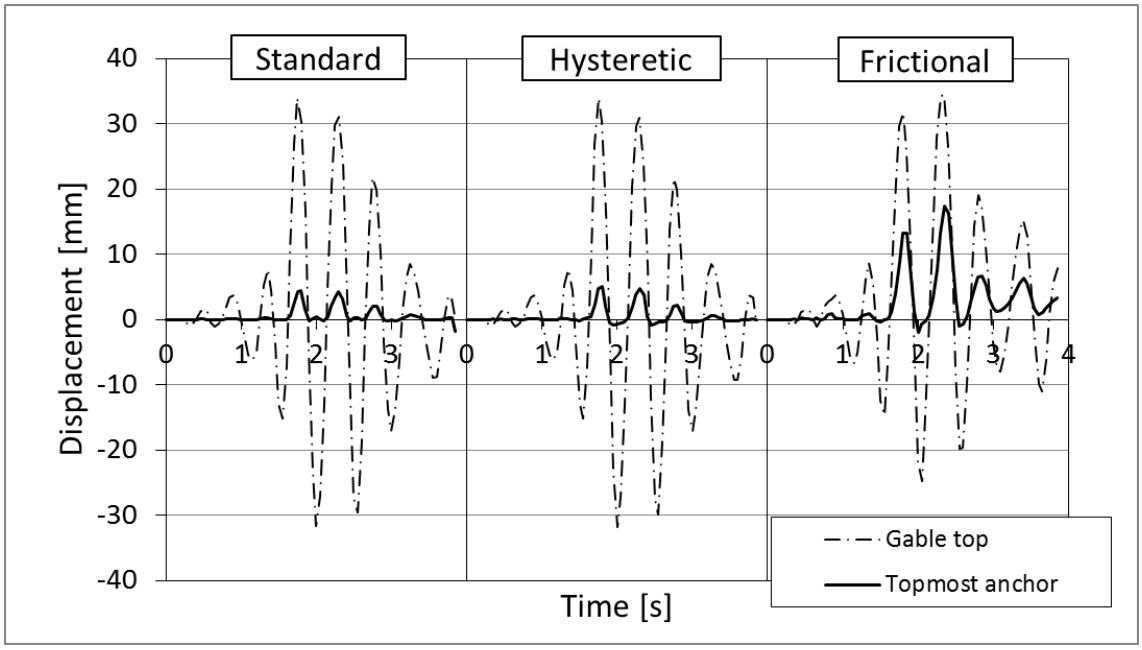

Fig. 7-16: Displacement time histories at LD - Comparison between FEMs strengthened by different anchor typologies

This depends on the different flexibility of the two typologies of devices: hysteretic devices have stiffness comparable with that of a standard anchor, so that the difference in displacements between the top of the gable and the topmost anchor remain considerable. On the other hand, frictional anchors allow larger displacements and hence a better control on drift.

In respect to standard anchors, the hysteretic devices present the benefit of limiting the stress experienced by the head of anchorage, so that pull-out failure is prevented. Indeed, the equivalent tensile stresses at the head of the anchorages always remain below the limit value of 0.59 MPa (Fig. 7-17b) and yielding is located in the dissipative element (Fig. 7-17a), so that once the dynamic excitation is over, the strength-only parts of the anchor are undamaged.

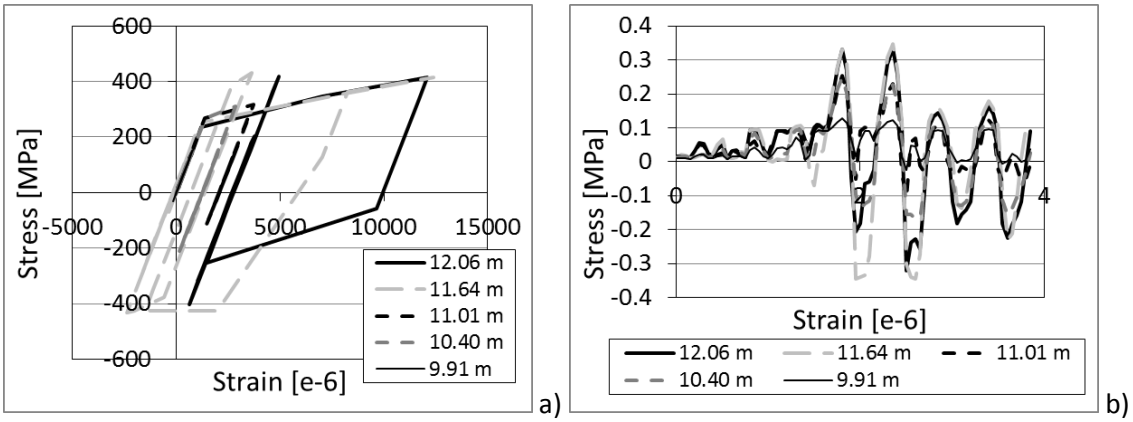

Fig. 7-17: Hysteretic devices at SD: a) stress-strain cycles, b) stress time histories at the anchor head

Such effect is even more patent in the case of the frictional devices: indeed, the stresses experienced by the head of the anchorage grouted in the quoin element are event lower than the threshold set for first cracking, i.e. 0.2 MPa, meaning that the anchor head remain completely undamaged (Fig. 7-18b).

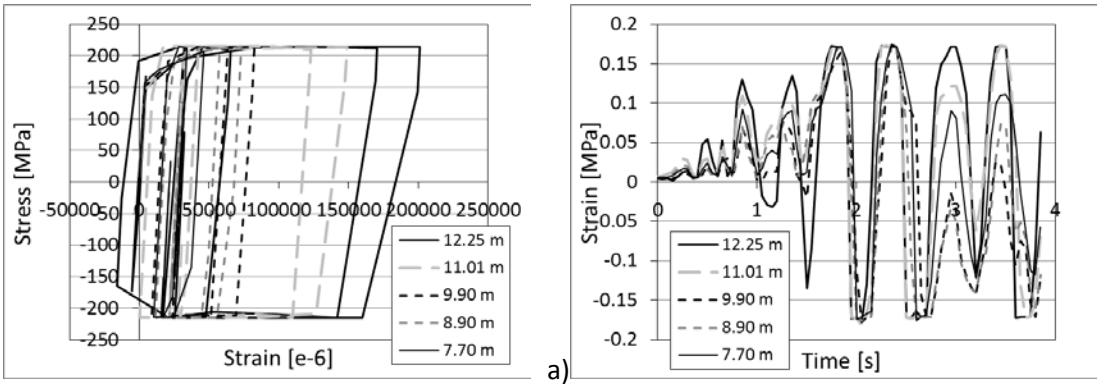

Fig. 7-18: Frictional devices at SD: a) stress-strain cycles, b) stress time histories at the anchor head

Frictional devices have the largest ductility and dissipate far more energy than the hysteretic anchors (Fig. 7-18a). As such, they provide the best performance, as they are able to control the displacement of the façade element (Fig. 7-19) and they considerable reduce the stress transmitted to the parent material. Most importantly, this is achieved with half the number of anchors than in the set-ups involving standard or hysteretical anchors, meaning that the frictional devices are the most suitable in terms of low-impact and compliance with the principles of conservation of heritage assets.

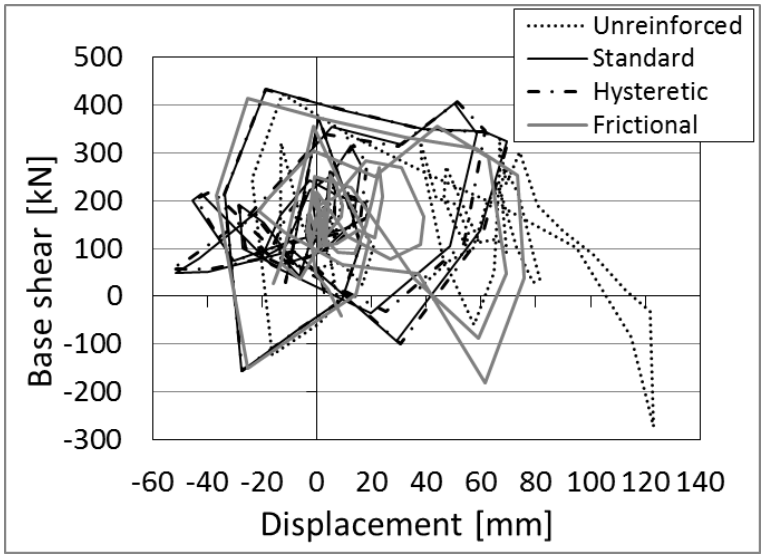

Fig. 7-19: Load-displacement cycles of FEMs strengthened by different devices (SD)

7.3 FINAL REMARKS

To conclusion of the validation process followed in this dissertation, Chapter 7 discusses the development of a design procedure for the dissipative anchoring devices and presents an example of their implementation and optimisation with the purpose of remedying the out-of-plane overturning of the façade of S. Giuseppe dei Minimi, L'Aquila, Italy.

The development of a design procedure is highly crucial for the application of the device concept and of the prototypes to real case studies: the paucity of innovative, ductility-based strengthening techniques applied to heritage structures might indeed be ascribed, among the others, to the lack of ad-hoc prescriptions, which guide the users through the design process of these systems in accordance with both structural codes and conservation good practice.

Techniques such as damping systems and ductile/sacrificial elements would bring considerable advantages to the seismic protection of historic buildings. The reduction in load demand and the possibility of controlling the structural response for different performance levels are two among the considerable benefits one could resort to when dealing with weak materials and fragile finishes. The fact that strength-based techniques are still allowed in principle and widely applied in practice points out to the difficulties of end users in sourcing methodically collated quantitative data that feed in a robust methodology for the design.

In the previous chapters, the focus has been purposely on data collection and interpretation: experimental, on-site and computational results both prove the viability of the concept of the dissipative devices and exemplify how validation of a new strengthening system for connections should be carried out. Although the results presented herein are not extensive, due to the vast number of parameters and materials typical of historic substrata, attention has been paid to record, measure and correlate data meaningful to the device performance.

Accordingly, in this chapter, experimental and on-site data of Chapters 4 and 5 is implemented in simple analytical models that can be used to calculate the load capacity of the various parts of the grouted anchors and of the dissipative devices. This allows setting a capacity hierarchy: in case an anchor, in the basic setup or in series with a dissipative device, undergoes an axial load, one can calculate which assembly parts are able to withstand the load and which not. This means that the failure type can be determined and counteracted; vice versa, one can choose the geometry and properties of the single parts, so as to achieve a "preferred" type of failure for a determined level of loading. Data ranges and formulae are collected in a table, which works as a reference and could be further expanded through future work.

In spite of this first part based on capacity, the design procedure mainly draws on concepts typical of performance-based design: interstorey drifts at various limit states as much as energy dissipation are used as indicators to fine tune the devices and to achieve the desired dynamic response. In this respect, computational assessment plays

a key role: whereas load demand on anchors can be assessed in a simplified way and verified a posteriori, the quantification of parameters such as drift requires more refined calculation systems, i.e. reliable numerical models.

The FE models developed and calibrated in Chapter 6 are used to carry out the reiterative procedure needed to identify a suitable layout of the anchors and of the dissipative devices in the case study of S. Giuseppe dei Minimi. Three different options of strengthening intervention, each featuring a different typology of anchorage, are identified through this process.

The frictional device proves to be the best solution when one wishes to minimise the impact of the strengthening intervention: thanks to its high ductility and larger energy dissipation capacity, this typology of device reduces the stress field in the parent material, thus completely avoiding cracking, and better controls relative displacements and accelerations, bringing the dynamic response well within the code limits. It is worth pointing out that the flexibility of the device in terms of settings, .i.e. perpendicular pressure and hence sliding load, is a great advantage, because it allows greater freedom when tuning the devices and searching for a suitable solution to meet the set performance targets. Indeed, the FEM strengthened by anchors in series with the frictional devices require half the number of anchors in respect to the other strengthening options.

FE models also show that an intervention by means of standard anchors is possible, although minor damage at the head of the anchorage and at the anchor rod cannot be avoided. In this sense, the hysteretic devices can still provide an improvement: although not as effective as the frictional devices, they deliver a performance very similar to that of the standard anchors, but with the non-negligible advantage of preventing damage at the anchor heads.

8 CONCLUSIONS AND RECOMMENDATIONS

8.1 SIGNIFICANCE OF RESEARCH

8.1.1 Background and Goals of the Research

The development of the dissipative anchoring devices was driven by the awareness of the contradictions that afflict the seismic protection of heritage structures: while on the one hand a great effort has been put into understanding the phenomena that control the dynamics of historic buildings – effort that has brought to considerable results – the development of ad-hoc techniques for structural connections and the application of forefront concepts for strengthening interventions hardly follow.

Such technical gap stems from a number of issues, among which the challenge of striking a compromise between innovative techniques and requirements typical of the conservation of heritage assets. Furthermore, in spite of a few recommendations and case studies, codes and technical literature lack specific protocols and rules that guide the development, testing and implementation into historic structures of energy and ductility-based systems.

The research project described in this dissertation strives to concept prove a strengthening system that meets the requirements of both modern seismic engineering (e.g. DM 14-01-2008; DPCM, 2011; EN 1998:2005; FEMA 450) and conservation best practice (i.e. ICOMOS/ISCARSAH, 2005). At the same time, it aims to develop a methodology for the validation of the prototypes and for the collection of results into a procedure that might be generally applicable and might provide guidelines for the design and optimisation of strengthening systems for the structural connections of heritage buildings.

8.1.2 The Concept Design

The design of the dissipative anchoring devices draws on an existing and well-established strengthening technique, i.e. anchor ties, and aims to exploit its advantages and to tackle its pitfalls, which are mainly connected to the high stiffness of metallic elements in respect to historic masonry.

The fact of relying on a technique, the anchor ties, that has been long implemented in historic buildings and can in fact be considered, at least in its most basic form, traditional, has a number of advantages from the point of view of conservation practice. First of all, anchor ties are very little obtrusive, as they have minimum aesthetic impact. The type chosen for this project can be used either as a fully grouted, bonded element or jointly with an end plate, and hence as a dry steel element, so that, depending on the specific requirements and conservation approach, it can be either concealed or set up so as to be clearly recognizable from the original constructive elements and materials. Furthermore, the use of a fabric sleeve system for grouting ensures that anchors are also little intrusive, because the grout is constrained within

the drilled cavity and the surrounding masonry voids, and it cannot overflow. Stainless steel and grout have a good compatibility with masonry materials and remain contained within the fabric sleeve, so that “punctual” interventions, rather than extensive interventions like in the case of masonry grouting and injections, are possible.

Furthermore, standard steel anchors offer the advantages of being economically viable, familiar to the professionals working in the construction industry and conservation field and, above all, they provide a technique to restore faulty and weak connections between masonry walls, thus preventing overturning failures, with a negligible increase in the structural mass.

Indeed, standard anchors respect the authenticity of the original structural system (ICOMOS/ISCARSAH, 2005), as they do not modify the dynamic response; they simply ensure that connections are sufficiently strong so that the in-plane capacity of walls parallel to the main seismic action can be exploited, before those perpendicular to it become severely damaged. The so called box-like behaviour is a “good” dynamic response for masonry structures; nevertheless it involves considerable damage in form of diagonal in-plane cracking of wall panels, which might not be acceptable from both a structural and conservation points of view. Furthermore, beyond a certain level of seismic intensity, the pull-out/punching of the anchors and the consequent, independent response of wall panels out of their plane are still likely.

Dissipative anchor devices are designed as an add-on, so that they do not disrupt the appearance, or function of the anchor ties; instead, they complement them thanks to their capacity of allowing controlled displacements and reducing the load transmitted to the surrounding parent material. Consequently, the ductility of the connection system is increased, while widespread cracking in the parent material and fragile failures, such as pull-outs, are mitigated. This, of course, entails allowing a controlled out-of-plane failure, rather than completely relying on the in-plane stiffness of side walls, but it also means deciding for what level of seismic intensity this occurs and setting up the devices to perform accordingly. The modified dynamic response of a structure strengthened by dissipative devices is still authentic, as the outward tilting of walls is a recurring mode of failure for historic masonry structures, except that in this case the opening of cracks is controlled and taken advantage of.

The exploitation of ductility and hysteretic damping by means of the anchoring devices falls in line with the modern philosophy of seismic engineering, which has long abandoned the pursuit of load capacity in favour of displacement and energy-dissipation. This allows, as per latest design codes, the application of a performance-based design, namely a design whereby the devices must comply with a number of targets, depending on the expected earthquake intensity. Such design methodology is at the core of the design concept of the devices and allows their optimisation in term of number, size and characteristics, according to both the principles of minimal intervention and structural reliability, also recommended by the ICOMOS/ISCARSAH (2005).

8.1.3 The Validation Process: Experimental Results

The validation process of the prototypes consists of three stages: experimental, on-site and computational. Each of these stages aims to contribute qualitative and quantitative results to the assessment of the prototypes and at the same time provide an example of how to proceed to the development of a strengthening system.

The experimental campaigns are devised by referring, where possible, to existing codes, in order to ensure the comparability of results and the respect of the minimum standards set for laboratory work in the current scientific practice. The validation process is broken down into further stages, in line with the principles of PBD. Indeed, each element of the strengthening system is characterised by a resisting mechanism, fulfils a specific function (i.e. the dissipative element provides ductility, the connections ensure that the anchor rod and the device remain connected throughout loading, etc.) and must feed into a hierarchy of capacities, so as that the system is able to respond selectively to the seismic input. Accordingly, the experimental characterisation must be functional to the identification of the relevant parameters and their quantification; splitting the systems is subcomponents and proceeding to testing from the lowest to the highest level of complexity serves well this task.

8.1.3.1 The Isolated Devices

The first step of the experimental assessment focuses on the performance of the device prototypes as isolated elements with the purpose of quantifying their load and displacement capacity.

The experimental campaign shows that hysteretic devices feature a displacement-dependent behaviour with an initial elastic phase, a post-linear branch and eventually buckling. Each of these stages can be defined through load and displacement thresholds, in line with the necessity of defining performance limits compatible with the concept of a multi-level design.

The dissipative element presents robust and repeatable hysteresis cycles, even after buckling, this being crucial for the implementation in buildings undergoing seismic loading. At the same time, connections to the rest of the anchor remain elastic, thus ensuring ease of replacement in the aftermaths of a seismic event, as required by BS EN 15129:2009.

Frictional devices also display a robust and repeatable performance, independent of amplitude and frequency of imposed sinusoidal cycles as well as of temperature. The device parts remain in the elastic field throughout cycling and actually provide an additional margin of security should the friction plates hit the device stops. Indeed, when this occurs, the device behaves like a standard anchor rod, controlled by the stress-strain properties of the chosen steel class.

A variation in Φ, the coefficient that expresses the ratio between slip load and applied perpendicular pressure, is recorded throughout the experimental campaign. Such variation can be expressed via a logarithmic function of the number of cycles test

specimens have undergone; nevertheless, a number of other factors such as mechanical locking and the presence within the assembly of metallic dust produced by the progressive wearing of the frictional surfaces influence this phenomenon. Although the coefficient variation doesn't impair the performance of the device, it constitutes a problem in terms of design, as it should ideally remain constant regardless of the number of input the prototype undergoes. Such issue should be kept into account and be the subject of future studies, as it will be discussed further down.

From the point of view of energy dissipated per cycles with equal amplitude, the frictional device dissipates less than the hysteretic. However, the axial force necessary to obtain energy dissipation is also considerably lower, this being a main advantage as it means that lower stresses are transmitted to the weak parent material. Furthermore, the frictional device has a more favourable ratio between dissipated energy and applied axial load.

8.1.3.2 Pull-Out Tests

The following step in the experimental validation is pull-out tests, which focus on the behaviour of the anchor and dissipative devices when embedded in a masonry material. These tests successfully prove that the devices can address some of the drawbacks of standard anchors, such as the large scattering in the performance and presence of damage in the substratum, in spite of the achievement of a satisfactory level of load capacity. Devices homogenise the response of anchors, considerably reducing, or even eliminating, damage to the parent material. In particular, the frictional device allows controlling the activation load to the point that almost no relative displacement is detected in the other elements of the anchor assembly.

The overall performance of the anchorage system, with or without dissipative devices, is approximated by idealised load-displacement curves, which are defined by a set of points that identify four main stages: appearance of relative movement, achievement of maximum load, achievement of maximum displacement under sustained load and ultimate failure.

Parameters measured during tests, as well as material characterisation, are built into simple analytical models so as to seek a correlation with the load capacities of the elements of anchor assembly in correspondence of the abovementioned points. Models are then assessed in function of their ability of generating a hierarchy of load capacities in agreement with the modes of failure detected in the laboratories. Collected evidence suggests that a shear-based model and an energy-based model are the best fit to represent respectively bond and wrench failures. Hence, these two analytical models feed into the part of the design procedure concerned with the ultimate load capacity of elements at the limit state of structural damage.

8.1.3.3 Cyclic Tests on Masonry Assemblies

The same procedure is applied to cyclic tests, which conclude the experimental assessment by supplementing the information obtained by pull-outs through the

simulation of a more complex scenario - full structural connection rather than only one wall panel - and a different loading input - cyclic action instead of monotonic pull.

The fact that masonry panels feature a different material, with lower mechanical properties in respect to pull-out tests, allows observing the performance of the three typologies of anchors in a limit case scenario. In particularly poor quality substrata the advantage of using the dissipative devices is considerable and might make the difference between only achieving the safety of occupants at the ultimate limit state and upgrade the structure to the point of ensure reparability.

The experimental validation has main outcomes for the overall process: it shows that devices can perform under a set of conditions, meaning that the concept is viable; it allows the quantification of their performance and, most of all, exemplifies how laboratory testing can inform a design procedure. Indeed, results are always collated and analysed in view of their implementation in a multi-level PBD, namely trying to identify performance stages and the parameters controlling them. Although the campaigns presented herein are not exhaustive, the creation of a strong logical link between tests and design ensures that the procedure can be built up with further work, while its core remains generally applicable.

8.1.4 The On-Site Validation of One Instrumented Prototype

In addition to experimental campaigns, one instrumented prototype of the hysteretic device is installed in a case study with the purpose of broadening the range of boundary conditions and loading scenarios to which the sample undergoes. Indeed, on-site assessment allows exploring the viability of the concept of the dissipative devices outside of the controlled laboratory environment.

The case study is chosen on the basis of a number of criteria: the presence of a clear damage pattern due to an overturning mechanism, the high probability of microtremors, and the possibility of cross-correlating the measurements taken by the prototype instrumentation with those coming from an independent, parallel monitoring system. The instruments and the system for data collection and conditioning are chosen keeping in mind the same objective that guides the experimental set-up: measured quantities must be functional to fully define the performance of the anchor.

In spite of the long monitoring period, appreciable seismic events did not occur, so that it was not possible to observe large load-displacement cycles of the prototype. The hysteretic device behaves as it can be expected for small scale inputs: the pieces remain in the linear field, with higher deformations being experienced by the dissipative element, according to what was designed and already assessed experimentally.

Regardless of the initial ambitions for the case study and the fact that a number of environmental, uncontrolled factors prevented the full achievement of the goal set at the time of the prototype installation, the on-site assessment well exemplifies how

results, even minor, can be useful if their analysis is carried out with a final objective in mind. Indeed, as linear relationships between deformation and stress can be applied, records are used to identify the tributary volume of masonry that acts on the anchor. Such result is important to inform the preliminary design of anchors and, in particular, their layout and spacing.

8.1.5 The Numerical Validation

The following step of the validation process is numerical modelling: the development of robust and reliable computational models is crucial to the design and implementation of the devices, as models are the necessary means whereby the calculations and checks required by design codes for seismic strengthening are carried out.

Accordingly, the computational validation focuses on the calibration of Finite Element models on the basis of experimental data with the purpose of identifying a set of suitable modelling techniques that are able to overcome the limits, if any, of the used software and yet deliver reliable results and reduce as much as possible the computational burden. Indeed, it is deemed crucial to provide an example of how the experimental output can be implemented in a numerical model, how the most important parameters are chosen and rendered through Finite Elements and what compromises it is possible to make when both numerical efficiency and result accuracy are pursued.

Numerical validation is carried out through the commercial software Autodesk Algor Simulation © and in the same fashion as the experimental assessment, i.e. gradually increasing the level of complexity of the model and number of the anchor assembly parts involved in it. This allows studying the impact that parameters have on the model, thus choosing simplified laws that can be implemented in more complex models so as to reproduce the behaviour of the prototypes without increasing the computational time.

For instance, the numerical modelling of the isolated devices is used, in the case of the hysteretic devices, to assess which type of input, load or displacement, and which type of hardening, isotropic or kinetic, better fits experimental results. Additionally, the impact of the mesh refinement and of the input stress-strain curve is studied. Numerical results highlight that models are best run under displacement control and by using kinematic hardening. Although the mesh refinement improves the distribution of stress and strains in the thee-dimensional models, the software fails to precisely simulate the smooth transition between the linear and plastic phases, regardless of the used stress-strain relationship. Nevertheless a sufficiently good agreement between numerical and experimental results is achieved, with the only limitation that care must be taken when assessing the dissipated energy, as numerical cycles tend to overestimate this parameter.

For the frictional device, numerical results follow the Coulomb's friction law and therefore do not take into account the mechanical locking that occurs for higher level

of perpendicular pressure on the frictional plates of the prototypes. The progressive variation of the coefficient of friction of the prototypes cannot be reproduced either, as this parameter is defined by a single, constant input value. Nonetheless, the model reproduces satisfactorily the distribution of stress in the device and its cyclic behaviour; it can be therefore employed by using the limit values of the coefficient of friction, so as to identify the whole range of possible load-displacement curves recorded experimentally. Such approach falls in line with the indications of EN 15129:2009, which prescribes to identify the boundary values that define the performance of dissipative devices.

The study of the isolated devices is complemented by the calibration of a Finite Element model of the anchor rod and the grouted element embedded in a portion of masonry substratum. This model reproduces the pull-out tests through 3D brick elements, as far as the strength-only portion of the anchorage is involved, and aims to identify the most suitable modelling technique and set of computational parameters, such as geometry, material properties and yielding criterion, that best fit the response of a standard anchor undergoing pull-out load and failing at the interface between the grouted element and the masonry.

Numerical results show that the definition of a fictitious part located between the grouted socket and the parent material and defined by a von Mises yielding criterion is suitable to this purpose. The material properties of the fictitious part are defined on the basis of experimental results, creating an equivalent stress-strain curve compatible with the chosen failure criterion. The selection of other parameters, such as boundary conditions and thickness of the fictitious part is also discussed.

The positive outcome of the model of the pull-outs means that the modelling technique of fictitious parts and equivalent material curves can be applied to the model of the façade of S. Giuseppe dei Minimi too. The materials and boundary conditions of the model building are calibrated so that the results of the linear analyses fall in line with those of the dynamic identification and the numerical model is able to reproduce the mode of failure surveyed on site. Non-linear analyses are then run to compare the damaged, unreinforced building with the building in a hypothetical setup strengthened by standard, hysteretic or frictional anchors. The use of anchors, both with and without devices, reduces the displacements between the disconnected façade and the side walls. This is indeed the expected result when using this typology of strengthening system: anchors restore the connection between perpendicular walls, thus allowing a better distribution of horizontal forces. However, the devices offer the additional advantage of reducing the stress field in the masonry substratum, meaning that the historic material is less prone to cracking when a ductile element is inserted at the location of the structural connection.

8.1.6 Implementing the Results into the Design Procedure

The results of the numerical validation are in substantial agreement with what already observed in the laboratories and on site. The last remaining issue is how this

information can be used so as to devise a strengthening intervention for a case study. The question is answered in the final chapter, where all the information gathered throughout the validation process feed into the development of a design procedure.

The procedure is illustrated by means of a flow chart and it is conceived as a proposal as well as an example of the methodology to be followed for the application of innovative strengthening systems to heritage structures. The flow chart contains both elements of capacity and performance design and it is structured in cycles that are iterated as long as the layout, dimensions and properties of the anchors and of the devices determines a structural response that comply with the prescribed requirements, both in terms of load and drift.

The procedure not only provides guidelines that address the issue of the technical gap affecting the seismic strengthening of historic structures, but also allows assessing exactly the advantages and pitfalls of standard grouted anchors against anchors in series with the dissipative devices.

By following the procedure, a hypothetical strengthening intervention for the façade of S. Giuseppe is designed: frictional devices, thanks to their ductility, energy dissipation capacity and flexibility in terms of settings, deliver the best performance. Indeed, frictional devices best protect the historic material and allow achieving the desired performance in terms of drift, yet limiting the number of anchors needed for the intervention. Hysteretic devices must be used in a larger number; nevertheless they avoid damage in the substratum. Standard anchors are still an option, but it is clear that their performance is not as efficient: a higher number of anchors must be implemented, so that the strengthening intervention results more disrupting, and yet localised damage is likely.

In conclusion, the achieved results provide a strong argument in favour of the further development of the dissipative devices and of their application to further case studies.

8.2 CHALLENGES, LIMITATIONS AND RECOMMENDATIONS FOR FUTURE WORK

8.2.1 Main Outcomes and Open Challanges

The validation process of the dissipative devices has given a number of promising results; nevertheless, the prototypes are yet to be exhaustively validated. Indeed, because of the extent of the specific research field, it was not feasible to explore all the possible testing and design scenarios with the available financial resources and within the set timeframe.

Then again, this was not the goal set for this research project either: the work carried out and described in the previous chapters aims to provide a set of guidelines for the development and design of strengthening systems for historic connections, as well as a robust basis for refining the concept, increasing the confidence level, and widening the range of possible applications of the dissipative anchoring devices.

Whilst these two objectives have been fulfilled, as discussed above, a number of challenges and open questions remain. Indeed, the results achieved so far prove that the dissipative anchoring devices, as outcome of a pilot project, respond to a set of requirements and are able to deliver the expected level of performance under specific boundary conditions. For much a variety of approaches and techniques have been implemented during the validation process, one cannot assume that the prototypes would perform as efficiently under different conditions, without requiring further tuning. In the same way, the failure modes and relevant analytical models catalogued and developed herein might not include all the possibilities. Further research work is therefore strongly recommended, especially in case the concept was brought to a commercial level.

8.2.1.1 Challenges Connected to Materials and Constructive Techniques

The first challenge regarding the design and implementation of the anchoring devices is the great variety of materials that characterise historic substrata: brick or stonework, regular or rubble, with infill or solid, the possibilities are endless and the impact that this has on the bond capacity and failure modes of the strength-only part of the anchor still needs investigating. The exact knowledge of how and for what load level the standard anchor fails is crucial to calibrate the dissipative devices.

The goal is the creation of a database collating the most recurring typologies of materials and their mechanical properties; drawing on this classification one can carry out experimental campaigns comparable to those described herein with the purpose of studying the influence of the parent material on the anchor response. In fact, databases of masonry typologies, which can be taken as reference, already exist (e.g. Table C8A.2.1 from Circolare 02/02/2009 n. 617, 2009), so it would be more the case of expanding on the catalogued typologies and performing a number of tests sufficient from a statistic point of view. Extensive experimental campaigns would also allow for the further validation of the set of analytical models that have been created during this research project and would complement the existing results with new quantitative data.

As it has been observed in the experimental chapter, the extreme weakness of the masonry might be an obstacle to the application of the devices, which still improve the response of the structural system, yet to a lesser extent. Therefore, it should be also investigated whether the treatment of the masonry, for instance by means of injections, could be used in parallel with the installation of the anchoring devices, so as to allow the intervention in weak, or highly damaged substrata.

Similarly to masonry typologies, connections, for instance C, or L connections instead of a T connection, or floor/wall connections rather than wall/wall connections, and how they are recreated in the laboratory in terms of set-up, constraints, and loading programme can be varied to widen the range of testing scenarios

Another option in terms of testing would be large scale testing, which would positively contribute complementing the validation of the anchoring devices. Rather than looking

at the influence of the devices on a single connection, their impact on the dynamic response of a whole structural system could be analysed. As shaking table tests often feature in the technical literature, results could be compared with those achieved by other strengthening techniques. Attempts in this sense were made during the research project; unfortunately, due to financial and management problems of the testing facilities at the time when shaking table tests were scheduled, this part of the research programme did not provide results sufficient to be included in the dissertation.

Besides the properties of the masonry and of the connection, the characteristics of the standard anchor – the embedment length, the diameter of the drilling hole in respect to the anchor rod, the typology of grout – could be investigated by a parametric study. Their influence on the behaviour of the anchor is of great interest in view of the development of a comprehensive method for the testing and design of anchor ties in general, and dissipative anchoring devices in the specific. Indeed, the writing up of guidelines for anchors embedded in masonry comparable to those for cement substrata (EOTA 2006, DD CEN/TS 1992:2009) would be highly beneficial from both the technical and commercial point of view.

The treatment of the surface of the drilling hole should also be the object of in-depth studies: the influence of the mechanical locking on the pull-put capacity of the anchoring system can be monitored and become a resource for the control of capacity and performance, rather than an incognita that cannot be exactly quantified.

8.2.1.2 Possible Improvements to the Design Concept

In this dissertation it has been proved that the dissipative anchoring devices are able to tackle some of the pitfalls that affect conventional strengthening systems. On the other hand, as already stated, the financial and time limits of the project meant that the target of the research had to be circumscribed to a restricted field. The challenge for any future work regarding the devices will be to enhance their reliability and expand their use by making them more flexible and easier to tune. For instance, the hysteretic devices have been tested and modelled only in one size, as it was difficult to source a circular hollow section of such diameter and wall thickness that it could be machined to join to the threaded profile of the anchor rod without weakening the connection, but at the same time that could be cut in the centre to a depth sufficient to ensure such a proper difference in cross sectional areas. This is, of course, a limit in terms of load and deformation capacity. Indeed, the hysteretic devices did not perform as well as the frictional ones during the cyclic tests on the T-shaped masonry subassemblies.

The use of several devices in series, of prototypes of various sizes that could be joined with larger or smaller anchor rods, or of special connectors to adapt the hysteretic prototype to different threaded bars are all options worth considering in order to improve the performance of the hysteretic devices in function of the mechanical properties of the parent material.

On the other hand, the frictional device could benefit from investigating different typologies of materials to coat the frictional plates. As it has been discussed in the experimental chapter, the use of stainless steel, which is susceptible to wearing, provokes variations in the coefficient of friction. As the coefficient becomes stable only after a certain number of cycles, the devices would need conditioning before being installed in a case study, otherwise it would be difficult to control their performance. The use of synthetic materials might overcome this issue and ensure a stable behaviour, regardless of the number of cycles. Indeed, plastic materials are commonly used in large scale dampers as well as in seismic isolators.

8.2.1.3 Future Improvements and Applications of On-Site Testing and Monitoring

A further challenge for future work regards on-site validation. The pilot project carried out within the framework of this research work was affected by the fact that the building selected as case study did not undergo seismic events of such an entity that they could activate the instrumented device. In spite of some interesting results, the opportunity of observing the real-life response of the device did not arise and therefore, the implementation of the devices in other case studies would bring new and meaningful results.

Drawing on the experience acquired during this project, the monitoring system would be modified so as to ensure a higher level of redundancy and differentiation. As it has been commented on the chapter on on-site validation, some phenomena were difficult to read and understand due to the lack of information that could be cross correlated. Conversely, the use of additional instruments such as, for instance, a set of accelerometers reading different rages of frequency so as to capture seismic tremors as much as environmental vibrations, or a set of LVDTs to cross check the strain measurements would allow a straightforward interpretation of records and improve the reliability of the system, thus allowing improvements and fine-tuning.

The refinement of the instrumentation to be installed on the dissipative devices would well serve the goal of “ease of monitoring, control and maintenance” stated by the ICOMOS (2005); indeed, the presence of reliable sensors would inform the refinement of the devices and allow studying how they respond to phenomena with different intensities, thus determining the level of damage experienced by the devices and whether this falls in line with the expected performance and whether substitution of the devices is required.

The concept of an instrumented anchor has also interesting potentials in terms of monitoring and early warning. Besides its use with the purpose of studying the response of anchor ties in general and of the anchoring devices in particular, an instrumented anchor could indeed be used to monitor a structural connection, when used in one single location, or even a whole structural system, when used in a more complex lay-out with several elements.

Whereas a standard monitoring system detects the response of a structure at a global level, an instrumented anchor offers the advantage of capturing localised phenomena,

such as the load experienced by the strengthening element or the stress transmitted to the parent material. Therefore, an instrumented anchor can cover two different functions at the time: on the one hand it works as strengthening element, as part of an emergency intervention or of a long-term seismic upgrade; on the other, it informs the decision-making process regarding the state of health of the structure and the need for interventions.

Furthermore, the monitoring anchor would be assembled in house so as to avoid the installation of a number of separate sensors, hence reducing the risks for contractors working on site.

Parallel to the development of the monitoring system with the purpose of achieving a robust performance and eventually minimising the number of sensors external to the anchor, the software for the data collection and conditioning can be refined, so as to serve as an early warning system.

8.2.1.4 Challenges of the Numerical Modelling

Similarly to experimental and on-site results, computational models would also benefit from exploring further scenarios and investigating different modelling techniques, so as to cover a broader range of case studies and refining the methodology developed so far. The analysis of a wider data set would allow complementing the design procedure; for instance, one could identify types of failures and include checks that have not been considered so far, as they were neither detected in the experimental campaigns nor through numerical modelling.

Furthermore, material mechanical properties of both the parent material and of the devices might be varied through new FEMs; this would allow exploring scenarios other than those already considered in this research project, which mainly aimed at calibrating the numerical models on the basis of experimental results, rather than carrying out a full parametric study. This would offer the advantage of assessing the potential for the application of the devices in other case studies as well as design variations of the devices before proceeding to the time consuming, more expensive real-life studies.

8.2.1.5 Study of the Long-Term Performance of the Devices

Finally, it is recommended that the issues of durability and reversibility are further investigated: these two features, which belong to the list of requirements for interventions on historic buildings reported by the ICOMOS/ISCARSAH 2015, have been only partly addressed in this research work by choosing stainless steel and by selecting an anchoring system where grouting is controlled. Nevertheless, it would be appropriate to study and trial test how the devices can be removed minimising the impact on the surrounding materials. The durability of anchors should also be tested in line with the long life cycles expected for historic buildings and considering different environmental situations, e.g. different compositions of the historic mortars that might affect the metal of the anchor and increase the deterioration rate of materials.

8.2.1.6 Final Remarks

In conclusion, despite the limitations and future challenges outlined above, this research has shown that the application of the concept of ductility and energy dissipation in the form of innovative anchors address the shortcomings of preceding capacity-based methods for the strengthening of structural connections, offering substantive promise for future improvements in the field of the seismic protection of heritage structures.

9 BIBLIOGRAPHY

ACI 318-11 (2011) Building Code Requirement for Structural Concrete. American Concrete Institute.

ACI 355.4-11 (2011) Qualification of Post-Installed Adhesive Anchors in Concrete. American Concrete Institute.

Aiello, M.A., Micelli, F., Valente, L. (2007) Structural Upgrading of Masonry Columns by Using Composite Reinforcements. *Journal of Composites for Construction*, 11(6): 650-658.

Aiken, I.D., Nims, D.K., Whittaker, A.S., Kelly, J.M. (1993) Testing of Passive Energy Dissipation Systems. *Earthquake Spectra*, 9(3): 335-370.

Al Shawa, O., Bellisario, M., Benedetti, S., de Felice, G., Mauro, A., Paolacci, F., Renieri, N., Roselli, I, Sorrentino, L. (2009) Prove sperimentali su tavola vibrante di pareti murarie sollecitate fuori piano. *ReLuis, progetto di ricerca n.1* (in Italian).

Anastasi, G., Lo Re, G., Ortolani, M. (2009) WSNs for Structural Health Monitoring of Historical Buildings. In Proc. of Human System Interactions. Catania, Italy.

Antinori, A.L. (1777). Annali degli Abruzzi dalle origini all'anno 1777. 24 volumes. Ristampa anastatica, Bologna: Forni, 1971-1973 (in Italian).

Antonini, O. (1993). Architettura religiosa aquilana. Vol 2. L'Aquila: Gallo Cedrone Ed. (in Italian).

Antunes, P., Lima, H., Varum, H., André, P. (2012) Optical Fiber Sensors for Static and Dynamic Health Monitoring of Civil Engineering Infrastructures: Abode Wall Case Study. *Measurement*, 45: 1695–1705

ASTM C1196 – 09 (2009) Standard Test Method for In Situ Compressive Stress within Solid Unit Masonry Estimated Using Flatjack Measurements. ASTM International, West Conshohocken, PA, USA.

ASTM C1197 - 09 (2009) Standard Test Method for In Situ Measurement of Masonry Deformability Properties Using the Flatjack Method. ASTM International, West Conshohocken, PA, USA.

Bajer, M., Barnat, J. (2012) The glue–concrete interface of bonded anchors. *Construction and Building Materials*, 34: 267-274

Baronio, G., Binda, L., Saisi, A. (1999). Mechanical and Physical Behaviour of Lime Mortars Reproduced after the Characterisation of Historic Mortar. In Proc. of *RILEM International Workshop Historic mortars: characteristic and tests*. Paisley, Scotland.

Benedetti, D. (2007) La risposta fuori piano di sistemi murari: progetto e valutazione sperimentale di assorbitori di energia. *Ingegneria Sismica*, No. 2 (in Italian).

Benedetti, D. (2004) Increasing Available Ductility in Masonry Buildings via Energy Absorbers. Shaking Table Tests. *European Earthquake Engineering*, No. 3.

Benedetti, D., Carydis, P., Pezzoli, P. (1998) Shaking Table Tests on 24 Simple Masonry Buildings. *Earthquake Engineering and Structural Dynamics*, 27(1): 57-90.

Binda, L., Modena, C., Casarin, F., Lorenzoni, F., Cantini, L., Munda, S. (2011) Emergency Actions and Investigations on Cultural Heritage after the L'Aquila Earthquake: the Case of the Spanish Fortress. *Bulletin of Earthquake Engineering*, 9(1): 105-138

Binda, L., Lualdi, M., Saisi, A. (2007). Non-Destructive Testing Techniques Applied for Diagnostic Investigation: Syracuse Cathedral in Sicily, Italy. *International Journal of Architectural Heritage, Conservation, Analysis and Restoration*, 1(4): 380-402.

Binda, L., Lualdi, M., Saisi, A., Zanzi, L., Gianinetto, M., Roche, G. (2003). NDT Applied to the Diagnosis of Historic Buildings: a Case History. In Proc. of *X International Conference of Structural Faults and Repair*. Edinburgh, UK.

Binda, L., Saisi, A., Tiraboschi, C. (2000). Investigation Procedures for the Diagnosis of Historic Masonries. *Construction and Building Materials*, 14(4): 199-233.

Binda, L., Anzani, A., Mirabella Roberti, G. (1997). The Failure of Ancient Towers: Problems for their Safety Assessment. In Proc. of International Conference on Composite Construction - Conventional and Innovative - IABSE, Zurich, pp. 699-704.

Black, C.J., Makris, N., Aiken, I.D. (2004) Component Testing, Seismic Evaluation and Characterization of Buckling-Restrained Braces. *Journal of Structural Engineering*, 130(6): 880-894.

Blasi C., Borri A., Di Pasquale S., Malesani P., Nigro G., Parducci A., Tampone G. (1999). *Manuale per la riabilitazione e la ricostruzione postsismica degli edifici*. Regione dell'Umbria, Gurrieri Editore, DEI Tipografia del Genio Civile, Rome, Italy (in Italian).

Blondet, M., Aguilar, R. (2007). Seismic Protection of Earthen Buildings. In Proc. of *International Symposium on Earthen Structures*, Indian Institute of Science. Bangalore, India.

BOCA (1993). Basic National Building Code. Building Officials & Code Administrators International.

Bonci, A., Carluccio, G., Castellano, M.G., Croci, G., Infanti, S., Viskovic, A. (2001) Use of Shock Transmission Units and Shape Memory Alloy Devices for the Seismic Protection of Monuments: the Case of the Upper Basilica of San Francesco in Assisi. In Proc. of *the International Millennium Congress Archi 2000*. Bethlehem, Palestinian Territories.

Borri A., Corradi M., Giannantoni A., Speranzini E. (2008) Consolidamento e rinforzo di murature storiche mediante un reticolato di ristilature armate. *Bollettino degli Ingegneri*, 7:11-19 (in Italian).

Borri, A., Castori, G., Grazini, A., Giannantoni, A. (2007) Performance of Masonry Elements Strengthened with Steel Reinforced Grout. In Proc. of *Fibre-Reinforced Polymer Reinforcement for Concrete Structures - FRPRCS-8,* Patras, Greece, 16-18 July.

Borri, A., Castori, G., Grazini, A. (2009) Retrofitting of Masonry Building with Reinforced Masonry Ring-Beam. *Construction and Building Materials*, 23(5): 1892-1901.

Bruneau, M. (1996) Performances of Steel Bridges during the 1995 Hyogoken-Nanbu (Kobe, Japan) Earthquake - A North American Perspective. In Proc. of *ICAS 96: Advances in Steel Structures*. Hong Kong, China.

California Historical Building Code (2007) California Code of Regulations, Title 24, Part 8, *California Building Standards Commission*. International Code Council.

Carocci C.F., Lagomarsino S. (2009). Masonry Buildings in the Historic Centres of the L'Aquila Area. *Progettazione sismica*, Special issue, 3: 115-129.

Carpinteri, A., Lacidogna, G. (2006) Structural Monitoring and Integrity Assessment of Medieval Towers. *Journal of Structural Engineering*, 132(11): 1681-1690.

Casarin, F., Lorenzoni, F., Islami, K., Modena, C. (2011) Dynamic Identification & Monitoring of the Churches of St. Biagio and St. Giuseppe in l'Aquila. In Proc. *of 4th International Conference on experimental Vibration Analysis for Civil Engineering Structures*. Varenna, Italy

Casarin, F., Valluzzi, M. R., da Porto, F. (2010) Relazione relativa all'esecuzione di indagini sperimentali propedeutiche agli interventi di restauro dell'oratorio di S. Giuseppe dei Minimi in L'Aquila. Padova, Italy (in Italian).

Castellano, M.G., Antonucci, R., Balducci, F., Ahmadi, H., Goodchild, I., Fuller, K. (2001) Viscoelastic Dampers for Seismic Protection of Buildings: an Application to an Existing Building. In Proc. of *Fifth World Congress on Joints, Bearings and Seismic Systems for Concrete Structures*. Rome, Italy.

Ceriotti, M., Mottola, L., Picco, G. P., Murphy, A. L., Guna, S., Corra, M., Pozzi, M., Zonta, D., Zanon, P. (2009) Monitoring Heritage Buildings with Wireless Sensor Networks: the Torre Aquila Deployment. In Proc. of the 2009 International Conference on Information Processing in Sensor Networks. San Francisco, USA.

Chandler, A.M., Lam, N.T.K. (2001) Performance-Based Design in Earthquake Engineering: a Multi-Disciplinary Review. *Engineering Structures*, 23(12): 1525-1543.

Chang, P. C., Flatau, A., Liu, S. C. (2003) Review Paper: Health Monitoring of Civil Infrastructure. *Structural Health Monitoring*, 2(3): 0257–267.

Chang, C.Y.L., Pall, A., Louie J.J.C. (2006) The Use of Friction Dampers for Seismic Retrofit of the Monterey County Government Center. In Proc. of *8th US National Conference on Earthquake Engineering*. Oakland, CA, USA.

Chioccarelli, E., De Luca, F., Iervolino, I. (2012) Preliminary Study of Emilia (May 20th 2012) Earthquake Ground Motion Records. V2.1, available at http://www.reluis.it (last accessed on 04/01/2015)

Christopoulos, C., Tremblay, R., Kim, H. J., Lacerte, M. (2008) Self-Centering Energy Dissipative Bracing System for the Seismic Resistance of Structures: Development and Validation. *Journal of. Structural Engineering,* Special Issue: Design and Analysis of Structures with Seismic Damping Systems, 134: 96–107.

Ciampi, V., De Angelis, M., Paolacci, F. (1995) Design of Yielding or Friction-Based Dissipative Bracings for Seismic Protection Of Buildings, Engineering Structures, 17(5): 381-391.

Circolare 02/02/2009 n. 617 (2009) Ministero delle Infrastrutture e dei Trasporti – Istruzioni per l'applicazione delle Nuove norme tecniche per le costruzioni di cui al decreto ministeriale 14 gennaio 2008 (Suppl. Ordinario n.27). Gazzetta Ufficiale 26/02/2009 n. 47.

Clemente, P., De Stefano, A., Zago, R. (2012) Seismic Isolation in Existing Complex Structures. In Proc. of *15th World Conference of Earthquake Engineering*, Lisbon, Portugal.

CNR-DT 200/2004 (2004) Guide for the Design and Construction of Externally Bonded FRP Systems for Strengthening Existing Structures. English version available on http://www.cnr.it/documenti/norme/IstruzioniCNR_DT200_2004_eng.pdf (last accessed on 04/07/2013).

CNR-DT 200 R1/2012 (2012) Istruzioni per la Progettazione, l'Esecuzione ed il Controllo di Interventi di Consolidamento Statico mediante l'utilizzo di Compositi Fibrorinforzati. (in Italian).

CNR-GNDT (1984) Norme Technique per le costruzioni in zoni sismiche. In Italian.

Coffman Engineers, Inc., Los Angeles (2005) Buckling Restrained Braced Frame (BRBF) Structures: Analysis, Design and Approvals Issues. *Nippon Steel News*.

Colajanni, P., Papia, M. (1997). Hysteretic Behavior Characterization of Friction-Damped Braced Frames. *Journal of Structural Engineering*, 123(8): 1020–1028.

Constantinou, M.C., Soong, T.T., Dargush, G.F. (1998) Passive Energy Dissipation Systems for Structural Design and Retrofit. Buffalo: MCEER.

Cook, R.A. (1993). Behaviour of Chemically Bonded Anchors. *Journal of Structural Engineering*, 119(9): 2744-2762.

Cook, R.A., Eligenhausen, R., Appl, J.J. (2007) Overview: Behaviour of Adhesive Bond Anchors. *Beton – und Stahlbetonbau. Supplement: Structural Concrete Special Edition 2007: Anchorage to Concrete*, 102 (Suppl. 2): 16-21.

Corradi, M., Grazini, A., Borri, A. (2007) Confinement of Brick Masonry Columns with CFRP Materials. *Composites Science and Technology*, 67(9): 1772-1783.

Cuomo, G., De Luca, A., Mele, E. (2006) Seismic Rehabilitation of Cultural Heritage through Timber Slabs and Ties. In Proc. Of *V International Seminar on Structural Analysis of Historical Constructions - SAHC06*. Delhi, India.

da Porto, F., Silva, B., Costa, C., Modena, C. (2012). Macro-Scale Analysis of Damage to Churches after Earthquake in Abruzzo (Italy) on April 6, 2009. *Journal of Earthquake Engineering*, 6(6): 739-758.

D'Ayala, D., Ansal, A., (2012) Non-Linear Push-Over Assessment of Heritage Buildings in Istanbul to Define Seismic Risk. *Bulletin of Earthquake Engineering*, 10 (1): 285-306.

D'Ayala, D., Benzoni, G. (2012) Historic and Traditional Structures during the 2010 Chile Earthquake: Observations, Codes, and Conservation Strategies. *Earthquake Spectra,* 28(S1): S425-S451.

D'Ayala, D., Paganoni, S. (2014) Testing and Design Protocol of Dissipative Anchor Devices for Out-of-Plane Damage. Strengthening of Structures under Seismic Loads, themed issue of *Structures and Buildings*, 167(1):26-40.

D'Ayala, D., Paganoni, S. (2011) Assessment and Analysis of Damage in L'Aquila Historic City Centre After 6th April 2009. *Bulletin of Earthquake Engineering*, 9(1): 81-104.

D'Ayala, D., Speranza, E. (2003) Definition of Collapse Mechanisms and Seismic Vulnerability of Historic Masonry Buildings. *Earthquake Spectra*, 19(3): 479–509.

DD CEN/TS 1992:2009 (2009) Design of Fastenings for Use in Concrete.

de Felice, G., and Giannini, R., 2001. Out-Of-Plane Seismic Resistance of Masonry Walls. *Journal of Earthquake Engineering*, 5 (2): 253–271.

DesRoches, R., Delemont, M. (2002) Seismic Retrofit of Simply Supported Bridges Using Shape Memory Alloys. *Engineering Structures*, 24(3): 325-332.

De Stefano, A., Clemente, P. (2006) S.H.M. on Historical Heritage: Robust Methods to Face Large Uncertainties. SAMCO Final Report 2006.

Di Croce, M., Ponzo, F. C., Dolce, M. (2010) Design of the Seismic Upgrading of the Tambour of the S. Nicola Church in Catania with the DIS-CAM System. In Proc. of *VII International Seminar on Structural Analysis of Historical Constructions – SAHC10*, Shanghai, China.

Di Ludovico, M., D'Ambra, C., Prota, A., Manfredi, G. (2010). FRP Confinement of Tuff and Clay Brick Columns: Experimental Study and Assessment of Analytical Models. *Journal of Composites for Construction*, 14(5), 583–596

Dimova, S., Meskouris, K. and Krätzig, W. B. (1995) Numerical Technique for Dynamic Analysis of Structures with Friction Devices. Earthquake Engineering Structural Dynamics, 24: 881–898.

DM 14-01-2008. Nuove Norme Tecniche per le Costruzioni. Gazzetta Ufficiale No 29, 4th February 2008 (in Italian).

S. W. Doebling, Charles R. Farrar, Michael B. Prime, Daniel W. Shevitz (1996) Damage Identification and Health Monitoring of Structural and Mechanical Systems from Changes in Their Vibration Characteristics: A Literature Review. Los Alamos National Laboratory Report No. LA-13070-MS.

Doğangün, A., İskender Tuluk,Ö., Livaoğlu, R., Acar, R. (2006). Traditional Wooden Buildings and Their Damages during Earthquakes in Turkey. *Failure Analysis*, 13(6): 981-996.

Doglioni, F., Moretti, A., Petrini, V. (1994) Le chiese e il terremoto. Dalla vulnerabilità constatata nel terremoto del Friuli al miglioramento antisismico nel restauro. Verso una politica di prevenzione. Lint Editoriale Associati (in Italian).

Dolce, M., Nigro, D., Ponzo F.C. (2001) The CAM System for the Retrofit of Masonry Structures. In Proc. of *7th International Seminar on Seismic Isolation, Passive Energy Dissipation and Active Control of Vibrations of Structures*. Assisi, Italy.

Dowling, D.M., Samali, B. (2006) Low-Cost, Low-Tech Means of Improving the Earthquake Resistance of Adobe-Mud Brick Houses. In Proc. of *International Conference on Earthquake Engineering - ICEE 2006*. Lahore, Pakistan.

DPCM (2011) Direttiva del Presidente del Consiglio dei Ministri 9 febbraio 2011. Valutazione e riduzione del rischio sismico del patrimonio culturale con riferimento alle Norme tecniche per le costruzioni di cui al D.M. 14/01/2008. Official Bulletin no. 47, 26/06/2011 (in Italian). Gazzetta Ufficiale n. 47 (Suppl. Ordinario n. 54).

Ehsani, M. R., and Saadatmanesh, H. (1996). Seismic Retrofitting of URM Walls with Fiber Composites. *The Masonry Society Journal*, 14(2): 63-72

Elingehausen, R., Mall, R., Silva, J. F. (2006). Anchorage in Concrete Construction. Ernst Sohn, Berlin, Germany.

EN 772:2000 – Methods of Test for Masonry Units, 2000.

EN 846-2:2000 - Methods of Test for Ancillary Components for Masonry, Part 2: Determination of Bond Strength of Prefabricated Bed Joint Reinforcement in Mortar Joints, 2000.

EN 1015:1999 – Methods of Test for Mortar for Masonry, 1999.

EN 1052:1999 – Methods of Test for Masonry, 1999.

EN 1881:2006 – Products and Systems for the Protection and Repair of Concrete Structures – Test Methods – Testing of Anchoring Products by Pull-Out Method.

EN 1993-1-1:2005. Eurocode 3 – Design of steel structures. Part 1-1: General rules and rules for buildings.

EN 1998:2005. Eurocode 8- Design of Structures for Earthquake Resistance.

EN 15129:2009: Anti-seismic devices.

EOTA European Organization for Technical Approvals (2006). ETAG 001 – Guideline for European Technical Approval of Metal Anchors for Use in Concrete. Amended November 2006.

FEMA 356 (2000) Prestandard and Commentary for the Seismic Rehabilitation of Buildings. ASCE, Washington, USA.

FEMA 450 (2003) NEHRP Recommended Provisions for Seismic Regulations for New Buildings and Other Structures.

Fidia (2014) FIDIA Technical Global Services, catalogue available on http://www.fidiaglobalservice.com/eng/home.php (last accessed on 10/07/14)

Filiatrault, A., Cherry, S. (1990) Seismic Design Spectra for Friction-Damped Structures. *Journal of Structural Engineering*, 116(5): 1334–1355.

Filiatrault, A., Tremblay, R., Kar R. (2000) Performance Evaluation of Friction Spring Seismic Damper. *Journal of Structural Engineering*, 126(4): 491-499.

Fip Industriale (2006) Report on "Adeguamento sismico del liceo Perticari di Senigallia, AN, Italy". http://www.fip-group.it/fip_ind/prodotti/dispositivi_antisismici/Scheda_Perticari.pdf (in Italian).

Gattulli, V., Antonacci, E., Vestroni, F. (2013) Field Observations and Failure Analysis of the Basilica S. Maria di Collemaggio after the 2009 L'Aquila Earthquake. *Engineering Failure Analysis*, 34: 715-734.

Gattulli, V., Graziosi, F., Federici, F., Potenza, F., Colarieti, A., Lepidi, M. (2013). Structural Health Monitoring of the Basilica S. Maria di Collemaggio. In Proc. of *The Fifth International Conference on Structural Engineering, Mechanics and Computation*.

Gentile, C., Saisi, A. (2006) Ambient Vibration Testing of Historic Masonry Towers for Structural Identification and Damage Assessment. *Construction and Building Materials*, 21: 1311–1321.

Giambanco, G., Rizzo, S., Spallino, R. (2001) Numerical Analysis of Masonry Structures via Interface Models. *Computer Methods in Applied Mechanics and Engineering*, 190 (49–50): 6493-6511.

Gigla, B. (2004). Bond Strength of Injection Anchors as Supplementary Reinforcement In Proc. *of XIII International Brick and Block Masonry Conference*. Amsterdam, Netherlands.

Gigla, B., Wenzel, F. (2000) Design Recommendations for Injection Anchors as Supplementary Reinforcement of Historic Masonry. In Proc. of *12th International Brick/Block Masonry Conference*, Madrid, Spain.

Giuffrè, A. (1993). Sicurezza e conservazione dei centri storici in area sismica, il caso Ortigia. Laterza, Bari (in Italian).

Griffith, A. A. (1921) The Phenomena of Rupture and Flow in Solids. Philosophical Transactions of the Royal Society of London, Series A, 221:163-198.

Hanson, R.D1993) Supplemental Damping for Improved Seismic Performance. *Earthquake Spectra,* 9(3): 319-334.

Ibrahim, Y., Marshall, J., Charneyb, F. A. (2007) Visco-Plastic Device for Seismic Protection of Structures. *Journal of Constructional Steel Research*, 63(11): 1515-1528.

ICOMOS (1964). International Charter for the Conservation and Restoration of Monuments and Sites (The Venice Charter 1964). Available at http://www.international.icomos.org/charters/venice_e.pdf (last accessed on 29/08/2014).

ICOMOS (2003) ICOMOS Charter- Principles for the Analysis, Conservation and Structural Restoration of Architectural Heritage. Ratified by the ICOMOS 14th General Assembly in Victoria Falls, Zimbabwe. Available at http://www.icomos.org/en/charters-and-other-doctrinal-texts (last accessed 18/10/2013).

ICOMOS/ISCARSAH Committee (2005) Recommendations for the Analysis, Conservation and Structural Restoration of Architectural Heritage.

Indirli, M., Castellano, M.G., Clemente, P., Martelli, A. (2001) Demo-Application of Shape Memory Alloy Devices: the Rehabilitation of S. Giorgio Church Bell-Tower. In Proc. of *SPIE International*. Newport Beach, CA, USA.

Indirli, M., Castellano, M.G. (2008) Shape Memory Alloy Device for the Structural Improvement of Masonry Heritage Structures. *International Journal of Architectural Heritage*, 2:93-119.

Ingham, J., Griffith, M. (2011) Performance of Unreinforced Masonry Buildings during the 2010 Darfield (Christchurch, NZ) Earthquake. *Australian Journal of Structural Engineering*, 11(3): 207-224.

ISO/TC 98/SC2 (2010), ISO/FDIS 13822 - Bases for Design of Structures – Assessment of Existing Structures. Available at https://www.iso.org/obp/ui/#iso:std:iso:13822:ed-2:v1:en (last accessed on 29/08/2014)

ITACA. L'Aquila mainshock (2009-04-06 01:32:39). Records of the station of L'Aquila - Valle Aterno - Centro Valle (AQV). http://itaca.mi.ingv.it/ItacaNet/CadmoDriver (last accessed on 05/05/2012).

James, P., Lee, D., D'Ayala, D., Paganoni, S. (2012). Improvements In and Relating To Building Anchor Systems. WO Patent 2,011,030,105.

Jaishi, B., Ren, W.-X., Zong, Z.-H., Maskey, P. N. (2003) Dynamic and Seismic Performance of Old Multi-Tiered Temples in Nepal. *Engineering Structures*, 25: 1827–1839.

Johnson, J. G. (2005) Modern Solutions to Historic Problems: The Utah State Capitol Building Seismic Retrofit Project. Utah Preservation, 9: 52-56. Utah State Historical Society. http://utahhistory.sdlhost.com/#item/000000011019786/view (last accessed on 10/07/14).

Lagomarsino, S. (2012) Damage assessment of churches after L'Aquila earthquake (2009). *Bulletin of Earthquake Engineering*, 10(1), 73–92.

Langenbach, R. (1990). Of Taq and Dhajji Dwari, the Earthquake Resistant Mud and Brick Architecture of Kashmir. In Proc. of *International Conference on Earthen Architecture - ADOBE 90*, Las Cruces, New Mexico.

Legge 64/74. Legge 2 febbraio 1974, n. 64: Provvedimenti per le costruzioni con particolari prescrizioni per le zone sismiche. Gazzetta Ufficiale n.76, 21-3-1974. In Italian.

Lowes, L. N. (1999) Finite Element Modelling of Reinforced Concrete Beam-Column Bridge Connections. *Ph.D. dissertation*, University of Berkeley, California, USA. http://faculty.washington.edu/lowes/dissertation/dissertation.htm (last accessed on 28/06/13).

Karantoni, F, Fardis, M (1992) Effectiveness of Seismic Strengthening Techniques for Masonry Buildings. *Journal of Structural Engineering*, 118(7): 1884-1902.

Lima, H. F., da Silva Vicente, R., Nogueira, R. N., Abe, I., de Brito André, P. S., Fernandes, C., Rodrigues, H., Varum, H., Kalinowski, H. J., Costa, A., de Lemos Pinto, J. (2008) Structural Health Monitoring of the Church of Santa Casa da Misericórdia of Aveiro Using FBG Sensors. IEEE Sensors Journal, 8(7): 1236:1242.

Lourenço, P., Rots, J. (1997). Multisurface Interface Model for Analysis of Masonry Structures. *Journal of Engineering Mechanics,* 123(7): 660-668.

Macabuag, J., Smith, A., Redman, T., Bhattacharya S. (2009). Investigating the Use of Polypropylene for Seismic Retrofitting of Masonry Buildings in Developing Countries. In Proc. of *XI International Conference on Non-Conventional Materials and Technologies - NOCMAT 2009*. Bath, UK.

McVay, M., Cook, R., Krishnamurthy, K. (1996) Pullout Simulation of Postinstalled Chemically Bonded Anchors. *Journal of Structural Engineering*, 122(9):1016–24.

Magenes, G., Penna, A., Senaldi, I., Rota, M., Galasco, A. (2014) Shaking Table Test of a Strengthened Full-Scale Stone Masonry Building with Flexible Diaphragms. *International Journal of Architectural Heritage: Conservation, Analysis, and Restoration*, 8(3): 349-375.

Malvar, L.J. (1991) Bond of Reinforcement under Controlled Confinement. *Naval Civil Engineering Laboratory technical note*. http://www.dtic.mil/cgi-bin/GetTRDoc?Location=U2&doc=GetTRDoc.pdf&AD=ADA240142 (last accessed on 12/04/13).

Mandara, A., Mazzolani, F.M. (1994) Seismic Upgrading of Churches by Means of Dissipative Devices. In Proc. of *Behaviour of Steel Structures in Seismic Areas, STESSA* 94. London, UK.

Mandara, A., Mazzolani, F.M. (2001) Energy Dissipation Devices in Seismic Upgrading of Monumental Buildings. In Proc. of *3rd Seminar on Historical Construction*. Guimarães, Portugal.

Marti, P. (1993) Anchoring of Concrete Reinforcement Using HIT-HY 150. Technical report, Hilti Development Corporation.

Mazzolani, F. M. Passive (2001) Control Technologies for Seismic-Resistant Buildings in Europe. *Progress in Structural Engineering and Materials*, 3(3): 277-287.

Mayorca, P., Meguro, K. (2004). Proposal of an Efficient Technique for Retrofitting Unreinforced Masonry Dwellings. In Proc. of *XIII World Conference on Earthquake Engineering*, Vancouver, Canada.

Miller, D.K. (1998) Lessons Learned from the Northridge Earthquake. *Engineering Structures*, 20(4-6): 249-260.

Milizia, F. (1781) Principii di architettura civile, Vol. 3, No. 2 (in Italian).

Modena, C., Casarin, F., da Porto, F., Munari, M. (2010) L'Aquila 6th April 2009 Earthquake: Emergency and Post-emergency Activities on Cultural Heritage Buildings. *Earthquake Engineering in Europe*. Series Geotechnical, Geological, and Earthquake Engineering 17: 495-521.

Modena, C., da Porto, F., Casarin, F., Munari, M., Simonato, E. (2010) Cultural Heritage Buildings and the Abruzzo Earthquake Performance and Post-Earthquake Actions. In Proc. of *VII International Seminar on Structural Analysis of Historical Constructions – SAHC10*, Shanghai, China.

Moreschi, L. M., Singh, M. P. (2003) Design of Yielding Metallic and Friction Dampers for Optimal Seismic Performance. Earthquake Engineering Structural Dynamics, 32: 1291–1311

Morgen, B.G., Kurama, Y.C. (2008) Characterization of Two Friction Interfaces for Use in Seismic Damper Applications. *Material and Structures*, 42(1): 35-49.

Mualla, I. H., Belev, B. (2002) Performance of Steel Frames with a New Friction Damper Device under Earthquake Excitation. *Engineering Structures*, 24(3): 365–371.

Müller, U., Weise, F. (2008). Condition Assessment of Ancient Architectural Monuments in the Pergamon Museum – Investigation of Paint and Stone Substitute Material by Micro Analytical Methods. *Berliner Beiträge zur Archäometrie*, 21: 13-22.

Nims, D.K., Richter, P.J., Bachman, R.E. (1993) The Use of the Energy Dissipating Restraint for Seismic Hazard Mitigation. *Earthquake Spectra*, 9(3): 467-489.

National Technical University of Athens NTUA/ Earthquake Protection and Planning Organization EPPO (2005) Investigation of Timber Reinforced Masonry. Research Rep., E. Vintzileou, P. Touliatos, and E. Tsakanika, eds. (in Greek).

P.C.M. (2003) Primi elementi in materia di criteri generali per la classificazione sismica del territorio nazionale e di normative tecniche per le costruzioni in zona sismica. (Ordinanza n. 3274)

Paganoni, S., D'Ayala, D. (2014) Testing and Design Procedure for Corner Connections of Masonry Heritage Buildings Strengthened by Metallic Grouted Anchors. *Engineering Structures*, 70: 278-293.

Paganoni, S. (2009) Dissipative Anchor Prototype for the Retrofit of Heritage Structures. Report for the Transfer to the Study of the Degree of Doctor of Philosophy. University of Bath.

Paganoni, S., D'Ayala, D. (2009) Development and Testing of Dissipative Anchor Devices for the Seismic Protection of Heritage Buildings. In Proc. of *ANCER Workshop 2009*. Urbana-Champaign, Illinois, USA.

Paganoni, S., D'Ayala, D. (2012) Numerical Simulations of Dissipative Anchor Devices in Historic Masonry. In Proc. of *15th World Conference of Earthquake Engineering*. Lisbon, Portugal.

Paikara, S., Rai, D.C. (2006) Confining Masonry Using Pre-Cast R.C. Element for Enhanced Earthquake Resistance. In Proc. of *VIII U.S. National Conference on Earthquake Engineering*, San Francisco, California, USA.

Pall, A., Marsh, C. (1982) Seismic Response of Friction Damped Braced Frames. *Journal of the Structural Division*, 108(6): 1313-1323

Pall, A., Pall, T. (2004) Performance-Based Design Using Pall Friction Dampers - An Economical Design Solution. In Proc. of *13th World Conference on Earthquake Engineering*. Vancouver, Canada.

Peng, P., Zamfirescu, D., Nakashima, M., Nakayasu, N., Kashiwa, H. (2005) Base-Isolation Design Practice in Japan: Introduction to the Post-Kobe Approach. *Journal of Structural Engineering*, 9(1): 147-171.

Pluijm, van der, R. (1997) Non-Linear Behaviour of Masonry under Tension. *HERON*, 42(1): 25-54.

Priestley, M.J.N., (2000) Performance Based Seismic Design. In Proc. of *12th World Conference of Earthquake Engineering*, paper No. 2831.

Rainieri, C., Fabbrocino, G., Cosenza E. (2011) Integrated Seismic Early Warning and Structural Health Monitoring of Critical Civil Infrastructures In Seismically Prone Areas. *Structural Health Monitoring*, 10:291–308.

Ramos, L. F., Marques, L., Lourenço, P.B., DeRoeck, G., Campos-Costa, A., Roque, J. (2010) Monitoring Historical Masonry Structures with Operational Modal Analysis: Two Case Studies. *Mechanical Systems and Signal Processing,* 24: 1291–1305.

Rice, J. A., Mechitov, K. A., Sim, S. H., Spencer Jr, B. F., Agha, G. A.(2011) Enabling Framework for Structural Health Monitoring Using Smart Sensors. Structural Control and Health Monitoring, 18: 574–587.

Robinson, W. H. (1982) Lead-Rubber Hysteretic Bearings Suitable for Protecting Structures during Earthquakes. *Earthquake Engineering and Structural Dynamics*, 10(4): 593-604.

Rodgers, G. W. , Mander, J. B., Chase , Dhakal, R. P., Leach, N. C., Denmead, C. S. (2007) Spectral Analysis and Design Approach for High Force-to-Volume Extrusion Damper-based Structural Energy Dissipation. *Earthquake Engineering and Structural Dynamics*, 37(2): 207-223.

Rojas, P., Ricles, J. M., Sause, R. (2005) Seismic Performance of Post-tensioned Steel Moment Resisting Frames with Friction Devices. *Journal of Structural Engineering*, 131(4): 529–540.

Russo, S. (2013) On the monitoring of Historic Anime Sante Church Damaged by Earthquake in L'aquila. *Structural Control and Health Monitoring*, 20: 1226–1239.

San Bartolomé, Á., Quiun, D., Zegarra, L. (2004). Effective System for Seismic Reinforcement of Adobe Houses. In Proc. of *XIII World Conference on Earthquake Engineering*. Vancouver, Canada.

San Bartolomé, Á., Quiun, D., Zegarra, L. (2008). Performance of Reinforced Adobe Houses in Pisco, Peru Earthquake. In Proc. of *XIV World Conference on Earthquake Engineering*, Beijing, China.

Schacher, T. (2007) Bhatar construction – Timber reinforced masonry. An Illustrated Guide for Craftsmen. *Guidebook prepared by the Swiss Agency for Development And Cooperation, French Red Cross in collaboration with Belgian Red Cross and UN Habitat*, Mansehra, NWFP, Pakistan.

Senaldi, I., Magenes, G., Penna, A., Galasco, A., Rota, M. (2014) The Effect of Stiffened Floor and Roof Diaphragms on the Experimental Seismic Response of a Full-Scale Unreinforced Stone Masonry Building. *Journal of Earthquake Engineering*, 18: 407-443.

Soong, T. T., Spencer, B. F. (2002) Supplemental energy dissipation: state-of-the-art and state-of-the-practice. Engineering Structures, 24(3): 243–259.

Sorrentino, L., Raglione, E., Liberatore, D., Decanini, L. D. (2010) Oratorio di S. Giuseppe dei Minimi a L'Aquila: Analisi Dinamica dei Meccanismi Locali di Collasso. In Proc. of Sicurezza e Conservazione nel Recupero dei Beni Culturali Colpiti da Sisma. Venezia, Italy (in Italian).

Spence, R., D'Ayala, D. (1999). Damage Assessment and Analysis of the 1997 Umbria-Marche Earthquakes. *Structural Engineering International*, 9(3): 229-233.

Symans, M. D., Charney, F. A., Whittaker, A. S., Constantinou, M. C., Kircher, C. A., Johnson, M. W., McNamara, R. J (2008) Energy Dissipation Systems for Seismic Applications: Current Practice and Recent Developments. Journal of Structural *Engineering*, 134(1): 3-21.

Subramanian, N., Cook, R.A. (2004) Behaviour of Grouted Anchors. *The Indian Concrete Journal*, 78: 25-33.

Tan, K. H., Patoary, M. K. H. (2004). Strengthening of Masonry Walls against Out-of-Plane Loads Using Fiber-Reinforced Polymer Reinforcement. *Journal of Composites for Construction*, 8(1), 79–87.

Tarchi, D., Rudolf, H., Pieraccini, M., Atzeni, C. (2000) Remote monitoring of buildings using a ground-based SAR: Application to cultural heritage survey. *International Journal of Remote Sensing*, 21(18): 3545-3551.

Tolles, E. L., Krawinkler, H. (1988) Seismic Testing on Small Scale Models of Adobe Houses. In Proc. of *Ninth World Conference on Earthquake Engineering*. Tokyo Kyoto, Japan.

Tolles, E. L., Kimbro, E. E., Ginell, W. S. (2002) Planning and Engineering Guidelines for the Seismic Retrofitting of Historic Adobe Structures. GCI scientific program reports, Getty Conservation Institute.

Tomaževič, M. (1999) Earthquake-Resistant Design of Masonry Buildings. Imperial College Press, London, UK.

Tomaževič, M., Klemenc, I. (1997a). Seismic Behaviour of Confined Masonry Walls. *Earthquake Engineering and Structural Dynamics*, 26: 1059-1071.

Tomaževič, M., Klemenc, I. (1997b). Verification of the Seismic Resistance of Confined Masonry Walls. *Earthquake Engineering and Structural Dynamics*, 26: 1073-1088.

Tomaževič, M., Lutman, M., Weiss, P. (1996) Seismic Upgrading of Old Brick-Masonry Urban Houses: Tying of Walls by Steel Ties. Earthquake Spectra, 12(3): 599-622.

Torrealva, D. (2009). Diseño Sismico de Muros de Adobe Reforzados con Geomallas. Departamento de Ingeñieria Civil, Universidad Pontificia del Peru. (In Spanish)

Torrealva, D., Cerrón, C., Espinoza, Y. (2005). Shear and Out of Plane Bending Strength of Adobe Walls Externally Reinforced with Polypropylene Grids. In Proc. of *XIV World Conference on Earthquake Engineering*. Beijing, China.

Torrealva, D., Vargas Neumann, J., Blondet, M. (2009). Earthquake Resistant Design Criteria and Testing of Adobe Buildings at Pontificia Universidad Catolica del Peru. In Proc. of *Getty Seismic Adobe Project Colloquium*, The Getty Conservation Institute.

Tsakanika, E. (2006) The Structural Role of Timber in the Masonry of Palace Type Buildings in the Minoan Crete. Ph.D. thesis, Faculty of Architecture, National Technical University of Athens (in Greek).

Valle, S., Zanzi, L., Saisi, A., Binda, L., Lenzi, G. (1998). Tomography for NDT Applied to Masonry Structures: Sonic and/or EM Methods. In Proc. of *II International Arch Bridge Conference*. Venezia, Italy.

Valluzzi, M. R., Cardani, G., Binda, L. Modena, C. (2004) Seismic Vulnerability Methods for Masonry Buildings in Historical Centres: Validation and Application for Prediction Analyses and Intervention Proposals. In Proc. of the 13th World Conference on Earthquake Engineering. Vancouver, B.C., Canada.

Vintzileou, E. (2008) Effect of Timber Ties on the Behaviour of Historic Masonry. Journal of Structural Engineering, 134(6): 961-972.

Vishay (2014) http://www.vishaypg.com/docs/11551/gageser.pdf (last accessed on 14/07/14)

Wen, Y.K. (2001) Reliability and Performance-Based Design. *Structural Safety*, 23(4): 407-428.

Wilkinson, S., Grant, D., Williams, E., Paganoni, S., Fraser, S., Mason, A., Boon, D., Free, M. (2013) Observations and Implications of Damage from the Magnitude Mw 6.3 Christchurch, New Zealand, Earthquake of 22 February 2011. *Bulleting of Earthquake Engineering*, 11:107-140.

Zhou, Z., Walker, P., D'Ayala, D. (2008) Strength Characteristics of Hydraulic Lime Mortared Brickwork. In Proc. of *the Institution of Civil Engineering – Construction Materials*, 161(4): 139-146.

Zuccarello, F.A., Milani, G., Olivito, R.S., Tralli, A. (2009) A Numerical and Experimental Analysis of Unbonded Brickwork Panels Laterally Loaded. *Construction and Building Materials*, 23(5):2093-2106.